Anglia Ruskin University

Faculty of Science and Engineering

Biomechanics of First Ray Hypermobility

Oliver J. Morgan

A thesis in partial fulfilment of the requirements of Anglia Ruskin University for the degree of Ph.D., Biomechanical Engineering

This research programme was carried out in collaboration with the Hospital for Special Surgery, New York, NY, USA

Submitted: November 2020

Acknowledgements

I wish to dedicate this thesis to my parents, Mary and Stephen Morgan. Without their unwavering support it would not have been possible to accomplish.

I would like to thank my supervisory team, Prof. Rajshree Hillstrom, Ph.D., MBA., Dr. Scott J. Ellis, MD, Mr. Roland Russell, MB,BS, FRCS, Howard J. Hillstrom, Ph.D., and Prof. Hassan Shirvani, Ph.D., for their guidance and encouragement over these past 4 years. I am truly grateful to Raj and Howard, for welcoming me into their home whenever I was in New York, showing me around the city, and providing lots of laughs along the way.

Additionally, I want to express my appreciation to the team at Hospital for Special Surgery for their support. In particular, Ibadete Thaqi, MBA., Mehnaz Shahid, BS., Jonathan Day, MS., Robert Turner, PT, OCS, MS, OM., and Daniel Sturnick, MS., for their roles in participant recruitment, data collection, and cadaveric specimen acquisition. I would also like to acknowledge my other collaborators Marian T. Hannan of Harvard University, Yvonne M. Golightly of University of North Carolina at Chapel Hill, and Jinsup Song of Temple University.

A special thanks to Jonathan T. Deland III, MD, who provided the initial idea for this research, Rogerio Bitar, MD, for the cadaveric dissections shown throughout the thesis, and Dan Jackson for help with manufacturing the cadaveric test-rig.

This research was gratefully funded by the British Orthopaedic Foot and Ankle Society, Chelmsford Medical Education and Research Trust, and Anglia Ruskin University Capital Research Fund.

Abstract

In 1887, Dr Joseph Cotterill identified a stiffening of the big toe he termed “hallux rigidus”; a manifestation of first metatarsophalangeal joint osteoarthritis. To date, 133 years after its discovery, we are no further in understanding how it occurs except for a higher-odds ratio among the planus foot type. The majority of clinical and basic-science research of osteoarthritis has concentrated on the hand, hip, and knee. Although large epidemiological studies are best able to identify at-risk populations, new studies need to focus on the unresolved questions related to biomechanical pathways. While many possible etiological factors of hallux rigidus have been dismissed due to a lack of convincing evidence, the role of first ray hypermobility remains enigmatic. However, there is limited understanding of first ray hypermobility and its relationship to foot structure and function. The purpose of this thesis was to provide insight into the biomechanics of first ray hypermobility as a potential etiological factor in hallux rigidus. Four distinct but related investigations were conducted to address current gaps in knowledge: (1) an epidemiology study of population-based trends in hallux rigidus compared to more frequently studied joints; (2) the design and testing of a novel device to standardise measurements of/and quantify first ray hypermobility; (3) investigation of the differences and relationships between foot structure and function caused by first ray hypermobility, and; (4) development, verification, and validation of a finite element model for predictions of cartilage contact mechanics in the hypermobile first ray. Incidence of hallux rigidus was found to be increasing at a rate comparable to the hip and knee. In contrast to other joints, a bimodal age-distribution was found for hallux rigidus, highlighting a subset of younger patients in whom hallux rigidus may be initiated by biomechanical factors other than wear and tear in old age. The novel device for measurements of first ray mobility was found to be substantially more reliable than the standard, clinical exam. Measurements may be performed in partial- and full-weightbearing conditions to facilitate investigation of aberrant foot mechanics resulting from first ray hypermobility. A study of healthy, asymptomatic subjects with planus and rectus foot types established that individuals with first ray hypermobility were predominantly planus in foot type. Subjects who were characterised as hypermobile exhibited increased maximum force beneath the hallux and greater first metatarsophalangeal joint rotational laxity, demonstrating an interaction with translational first ray mobility. Finite element simulations predicted

increased first MTP joint stress in the planus foot with first ray hypermobility which, at a magnitude of 6.5 MPa, was within the upper bound of a proposed 5-7 MPa failure limit of cartilage. Taken together, these interlinked studies may elucidate the role of first ray hypermobility in abnormal structure and function of the foot. In the presence of pes planus and hypermobility, an interaction between translational first ray mobility and rotational first metatarsophalangeal joint flexibility may reduce the mechanical advantage from the Windlass mechanism. Concomitant increased force beneath the hallux likely promotes a higher flexion moment arm between the hallucial load and first metatarsophalangeal joint, subjecting the cartilage to potentially harmful tensile and shear stress. Microtrauma to the first metatarsophalangeal joint's articular soft tissues, after repetitive excessive loading on a daily basis from first ray hypermobility, may initiate degenerative changes. The significance of this research rests on its potential to reveal the interaction between pes planus and first ray hypermobility as an etiological factor in hallux rigidus onset and progression.

Table of Contents

Author's Contributions

The topics of this thesis are original, and the author has been the primary contributor to the research design, methods, data analyses, and conclusions presented herein.

Book Chapters

i. Morgan OJ, Song J, Hillstrom R, Hillstrom HJ, 2020. Biomechanics of the Peroneal Tendon. In: Sobel M (eds.), The Peroneal Tendon – A Clinical Guide to Evaluation and Management. Springer Nature, Singapore.

Publications

i. Morgan OJ, Hillstrom HJ, Ellis SJ, Golightly YM, Russell R, Hannan MT, Deland III JT, Hillstrom R. 2019. Osteoarthritis in England: Incidence Trends from National Health Service Hospital Episode Statistics. ACR Open Rheumatology, 1(8):493-498.

ii. Morgan OJ, Hillstrom R, Turner R, Day J, Thaqi I, Caolo K, Song J, Russell R, Ellis SJ, Deland JT, Hillstrom HJ. 2021. Comparative Reliability of a Novel Electromechanical Device and Handheld Ruler for Measuring First Ray Mobility. Foot & Ankle International, In Press

Conference Abstracts

i. Morgan OJ, Hillstrom HJ, Turner R, Day J, Ellis S, Deland JT, Hillstrom R, 2020. Is First Ray Hypermobility Related to the Flat Foot? International Foot and Ankle Biomechanics Meeting 2020. São Paulo, Brazil (Oral Presentation).

ii. Morgan OJ, Hillstrom HJ, Turner R, Thaqi I, Day J, Caolo K, Ellis S, Deland JT, Hillstrom R, 2020. Intra- and Inter-Rater Reliability of a Hand-Held Device for Measuring First Ray Mobility. Expert Scientific Meeting 2020. Spitzensee, Germany (Oral Presentation).

iii. Morgan OJ, Hillstrom HJ, Turner R, Thaqi I, Day J, Caolo K, Ellis S, Deland JT, Hillstrom R, 2020. Role of First Ray Hypermobility in Plantar Loading of the Forefoot. Expert Scientific Meeting 2020. Spitzensee, Germany (Oral Presentation, *shortlisted for the Art in Science Award*®).

Patents

i. Foot structure and function assessment device and methods of using the same: Patent No. PCT/US21/22791, March 2021

List of Abbreviations

OA	Osteoarthritis
MTP	Metatarsophalangeal
MTC	Metatarsocuneiform
MLA	Medial Longitudinal Arch
ROM	Range of Motion
GRF	Ground Reaction Force
GJH	Generalised Joint Hypermobility
HCTD	Heritable Connective Tissue Disorder
FE	Finite element
RMSE	Root Mean Square Error
GDP	Gross Domestic Product
HA	Hemiarthroplasty
TJA	Total Joint Arthroplasty
NICE	National Institute for Health and Clinical Excellence
MDA	Medical Devices Agency
HV	Hallux Valgus
SI	Superior/Inferior
AP	Anterior/Posterior
ML	Medial/Lateral
IE	Internal/External
AA	Abduction/Adduction
PD	Plantarflexion/Dorsiflexion
MRI	Magnetic Resonance Imaging
CT	Computed Tomography
CAD	Computer Aided Design
FE	Finite Element Analysis
DOF	Degrees of Freedom
NHS	National Health Service
HES	Hospital Episode Statistics
CMC	Carpometacarpal
FL	Foot Length
TFL	Truncated Foot Length

FRMD	First Ray Mobility Device
STJN	Subtalar Joint Neutral
RCSP	Resting Calcaneal Stance Position
FRMI	First Ray Mobility Index
IRB	Institutional Review Board
AHMI	Arch Height Measurement Index
ICC	Intra/Interclass Correlation Coefficient
BMI	Body Mass Index
HSS	Hospital for Special Surgery
AHF	Arch Height Flexibility
MF	Maximum Force
PP	Peak Pressure
CPEI	Centre of Pressure Excursion Index
COP	Centre of Pressure
SD	Standard Deviation
SEM	Standard Error of Measurements
B&A	Bland-Altman
3D	Three-Dimensional
2D	Two-Dimensional
1D	One-Dimensional
PP	Peak Pressure
MF	Maximum Force
ARU	Anglia Ruskin University
SPGR	Spoiled Gradient Recalled Echo
FHB	Flexor Hallucis Brevis
PB	Peroneus Brevis
PL	Peroneus Longus
TP	Tibialis Posterior
FHL	Flexor Hallucis Longus
EHL	Extensor Hallucis Longus
FDL	Flexor Digitorum Longus
EDL	Extensor Digitorum Longus
TA	Tibialis Anterior

MTS Metatarsosesamoid

List of Figures

List of Tables

Chapter 1. Introduction

Osteoarthritis (OA) is the most frequent manifestation of arthritis in the human body. The pathology of OA involves the entire structure of a synovial joint, in a process that includes focal and progressive cartilage loss with concomitant changes in the bone beneath the cartilage, osteophytes, and gradual bony sclerosis (Dieppe & Lohmander, 2005). Osteoarthritis may be comprised of several factors including biomechanical stress, biochemical changes, nutrition, and genetics although the precise aetiology remains unknown. Onset and progression of OA is considered multifactorial, but it is evident that changes in the mechanical environment of a joint adversely influence load distribution and soft-tissue degeneration (Felson et al., 2000). Osteoarthritis represents a growing burden to the National Health Service (NHS) in England. The UK Chief Medical Officer has recommended better understanding of this disease, for which there is currently no cure (Davies SC, 2012). Previous estimates of hand, hip, and knee OA from a local database in North Staffordshire, England indicated rising diagnoses among 35-44-year-olds between 2003 and 2010 (Yu et al., 2015). However, there is limited up-to-date population-based data of temporal trends in patient demographics with respect to OA in England, particularly for the foot which represents a relatively understudied field (Roddy & Menz, 2018).

Although few investigations use the same definition to provide population prevalence estimates, first Metatarsophalangeal (MTP) joint OA appears to be the most common degenerative disease in the foot and ankle (Bremner et al., 1968; Van Saase et al., 1989; Roddy et al., 2015). Clinically referred to as hallux rigidus, this end-stage condition results in severely restricted joint motion and pain (McMaster MJ, 1978; Zammit et al., 2010). The frequency of hallux rigidus among middle-aged to older adults can vary greatly from 6 to 39%, largely due to differences in ages, populations, and case definitions (Trivedi et al., 2010; Roddy & Menz, 2018). It is unclear why the first MTP joint is more affected than others (Van Saase et al. 1989; Whittle, M.W., 1999). Many anatomical and biomechanical abnormalities of the foot have been proposed as the primary cause. Suggestions include pes planus, forefoot pronation,

metatarsus primus elevatus, and an abnormally long first metatarsal. (Bingold and Collins, 1950; McMaster, M.J., 1978; Viegas, G.V., 1998; Coughlin & Shurnas, 2003; Menz et al., 2015; Telfer et al., 2017). One of the only evidence-based findings from this body of research is that people with the planus foot type (Figure 1) have a higher-odds ratio of developing first MTP joint OA (Rao and Bell, 2013; Menz et al., 2015).

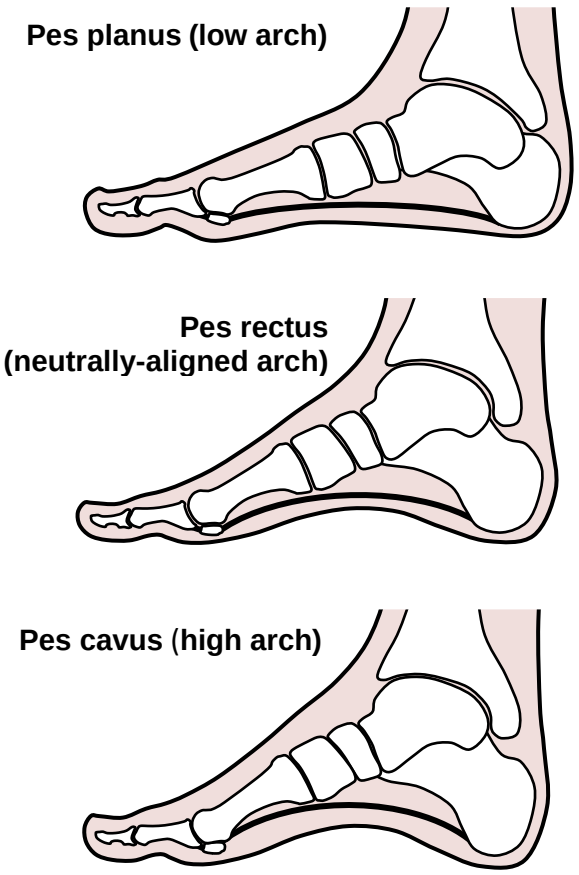

Figure 1. Three general classifications of foot type in the population. Feet are often categorised into three general structures: Planus (a low-arch with an everted calcaneus and/or varus forefoot); rectus (a moderate-arch with the posterior surface of the calcaneus close to perpendicular with the ground); and cavus (a high-arch with inverted calcaneus and/or valgus forefoot) (Ledoux et al., 2003).

Individuals with pes planus have demonstrated greater odds of developing foot injuries (Kaufman et al., 1999), increased first MTP joint flexibility (Rao et al., 2011; Buldt et al., 2015), lower first than second metatarsal head pressure (Ledoux & Hillstrom, 2002; Hillstrom et al., 2013; Buldt et al., 2018). In contrast, individuals with a rectus foot type, who may be considered “normal”, will exhibit higher peak pressures beneath the first metatarsal head than the second during gait. First ray hypermobility has been

suggested as the cause of aberrant function in the planus foot (Morton DJ, 1928; Root et al., 1977; Hillstrom et al., 2013) (Figure 2). Hypermobility of the first ray is a term that describes an inability of the medial forefoot to adequately support weightbearing load, causing excessive superior translation of the first metatarsal (Klaue et al., 1994; Lee & Young, 2001; Glasoe & Michaud, 2019; Munuera-Martinez et al., 2020). However, definitions of first ray hypermobility can vary from 7-10 mm based on differences in case definitions and methods of assessment (Klaue et al., 1994; Roukis et al., 1996; Lee & Young, 2001; Glasoe et al., 2005; Shirk et al., 2006; Tavara-Vidalon et al., 2018; Glasoe & Michaud, 2019; Munuera-Martinez et al., 2020) and understanding of this condition has been impeded by vague clinical definition. Roukis et al., (Roukis et al., 1996) observed a relationship between increased dorsal first ray translation and restricted first MTP joint dorsiflexion, suggesting a repetitive jamming mechanism leading to hallux rigidus. Many possible causative factors have been rejected due to a lack of convincing evidence, yet the role of first ray hypermobility in abnormal and potentially harmful mechanics of the foot remains enigmatic (Roukis et al., 1996; Bouaicha et al., 2010; Cacacae et al., 2013; Doty et al., 2014; Roddy & Menz, 2018).

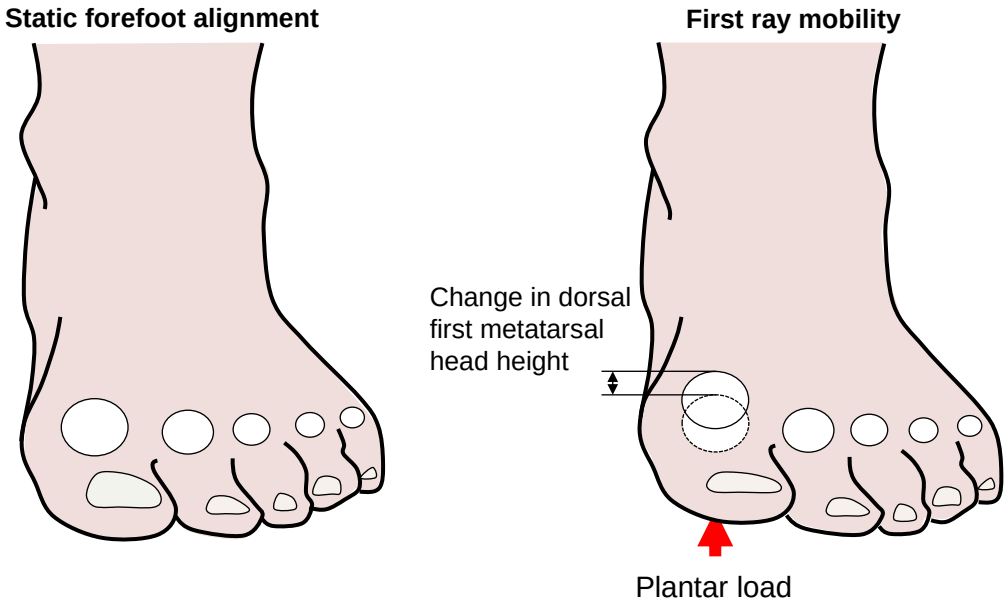

Figure 2. Illustration of first ray mobility where each white circle denotes the first through fifth metatarsal heads. A change form static forefoot alignment which illustrates the equilibrium position for the first ray to first ray mobility that occurs in response to first MTP joint plantar loading is shown.

1.1 Research Theory

It is proposed in this thesis that the planus foot type and first ray hypermobility are interrelated mechanisms, which may initiate hallux rigidus in the early stage. The research theorises that during gait, the first metatarsal of a hypermobile planus foot will translate excessively in the superior direction, causing the foot to pronate, and redistributing the body's weight. Once the first ray is at its maximum elevation and the medial band of the plantar fascia becomes maximally taught, the first MTP joint will undergo increased loading and dorsal articular impingement (Jack, E, 1940; Roukis et al., 1996). As a result of altered first MTP joint contact mechanics, excessive force between the dorsal articular surfaces of the joint will permit repetitive excessive loading to this region, which may initiate joint degeneration indicative of hallux rigidus.

1.2 Scope and Boundaries

Despite the frequency of hallux rigidus, there is limited population representative samples in contemporary research (Van Saase et al., 1989; Roddy & Menz, 2018). Although large epidemiological studies are best able to identify at-risk populations, new studies need to focus on unresolved questions related to biomechanical pathways. A significant barrier to the study of hallux rigidus has been insufficient understanding of abnormal medial forefoot loading, which could adversely affect the first MTP joint and influence early-stage degenerative changes. Initiation and progression of articular joint degeneration is still not fully understood, but excessive loading and cumulative stress in the cartilage play major roles. Modern data has revealed a higher-odds ratio of developing hallux rigidus among the planus foot type (Cacacae et al., 2013; Menz et al., 2015), yet the precise biomechanical explanation remains enigmatic. One theory which will be explored by this thesis is that first ray hypermobility, a condition which compromises the ability of the medial forefoot to adequately support weightbearing load, is interrelated with the planus foot type, causing abnormal and potentially harmful loading of the first ray and first MTP joint. However, little is known about first ray hypermobility and research in this area has been hindered by a lack of standardised measurement technique and conflicting

definitions for the condition. To bridge the present gaps in knowledge, the thesis was broken down into a number of smaller, incremental studies:

- Investigate population-based trends in hallux rigidus compared with osteoarthritis of the hand, hip, and knee.
- Design and test the reliability of a novel electromechanical device for reliable assessments of first ray hypermobility.
- Analyse the relationships between first ray hypermobility and structure and function of individuals with planus and rectus foot types.
- Predict the effects of first ray hypermobility on cartilage contact mechanics of the first metatarsophalangeal and first metatarsocuneiform joints.

The overarching objective of this thesis was to elucidate aberrant biomechanics of the foot, related to first ray hypermobility, as a pathway to early-stage degeneration of the first metatarsophalangeal joint. The information and tools generated from this research are expected to help guide the design of future clinical and basic-science research. A longitudinal, population-based investigation which could explore associations of first ray hypermobility and degenerative symptoms of hallux rigidus was considered beyond the scope of this thesis.

1.3 Specific Aims and Hypotheses

The central hypothesis is that the planus foot type and first ray hypermobility are interrelated, imposing aberrant contact mechanics within the joints of the first ray as an etiological factor in hallux rigidus. To examine these postulated relationships, the following specific aims and hypotheses were formulated:

Aim 1: Investigate the population prevalence and incidence of hallux rigidus compared with osteoarthritis of the hand, hip, and knee in England.

Hypothesis 1: Hallux rigidus will demonstrate increased population prevalence over time and comparable incidence to OA of the hand, hip, and knee.

Aim 2: Design and prototype a novel device for measuring first ray mobility.

Hypothesis not required for technical design and development.

Aim 3: Test the reliability of the novel device for measuring first ray mobility, compared with a commercially available, handheld ruler.

Hypothesis 3a: First ray mobility in ***non-weightbearing (prone) subjects*** with asymptomatic rectus and planus foot structures will exhibit test-retest and remove-replace reliability (ICC (2,1) >0.7) within and between raters using a commercially available handheld ruler.

Hypothesis 3b: First ray mobility in ***partial weightbearing (seated) subjects*** with asymptomatic rectus and planus foot structures will exhibit test-retest and remove-replace reliability (ICC (2,1) >0.7) within and between raters, using MAP1st.

Hypothesis 3c: First ray mobility in ***weightbearing (standing) subjects*** with asymptomatic rectus and planus foot structures will exhibit test-retest and remove-replace reliability (ICC (2,1) >0.7) within and between raters, using MAP1st.

Aim 4: Investigate the relationships between foot structure, first ray mobility, arch height flexibility (AHF), first MTP joint flexibility, and plantar loading.

Hypothesis 4a: First ray mobility will be negatively related with arch height and first MTP joint flexibility and positively related with arch height flexibility.

Hypothesis 4b: The ratio of peak plantar loading* beneath the first and second metatarsal heads will be higher across subjects with rectus versus planus foot types.

Hypothesis 4c: The ratio of peak plantar loading* beneath the first and second metatarsal heads will be higher across subjects with normal versus high levels of first ray mobility.

Aim 5: Verify the first MTP and MTC joint contact mechanics of a medial forefoot FE model simulating planus and rectus foot types.

Hypothesis 5: In vitro-measured and FE-predicted first MTP and MTC joint contact mechanics (force, contact pressure, and contact area) will be within 30% for the same boundary and loading conditions.

Aim 6: Predict the effects of first ray hypermobility on medial forefoot cartilage contact mechanics during stance phase of gait.

Hypothesis 6: First MTP and MTC joint stress will be higher in the presence of first ray hypermobility.

1.4 Thesis Structure and Objectives

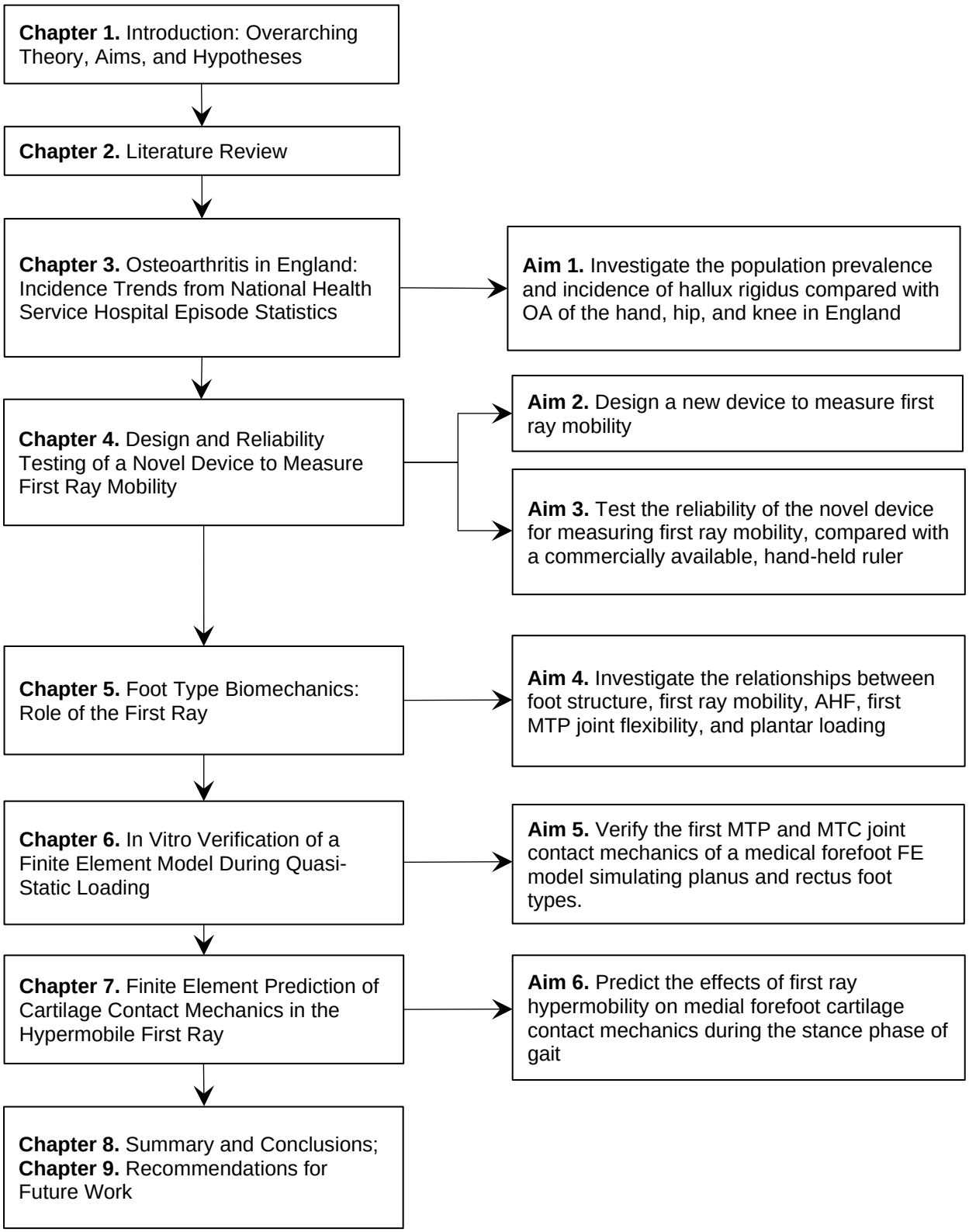

Figure 3. Thesis flow chart detailing the relationship between chapter structuring and research aims.

Chapter 2. Literature Review

The term biomechanics describes the study of mechanical laws governing the structure and function of a living organism. Many branches exist in the tree of biomechanics, but the topics of this thesis and following literature review relate closely to orthopaedic biomechanics: the study of human joints. Research in this field requires broad knowledge of interdisciplinary processes to understand function of the human musculoskeletal system and how it can fail. Hence, the following chapter will explore combinations of anatomical studies, cadaveric experiments, histology, pathology, gait assessments, engineering designs, and FE modelling, which encompass research in orthopaedic biomechanics of the foot and first ray.

2.1 Anatomy, Structure, and Function of the Foot and First Ray

The foot is a complex structure comprised of 28 bones, 33 joints, and 112 ligaments which are controlled by 13 extrinsic and 21 intrinsic muscles (Grant JCB, 1972). Anatomy of the foot can be subdivided into three segments: hindfoot (tibia, and fibula of the lower leg, calcaneus and talus); midfoot (cuboid, navicular, medial, intermediate and lateral cuneiform bones) and; forefoot (five metatarsals, numbered first to fifth, medially to laterally; 14 phalanges, three per toe, proximal, middle, and distal, excluding the hallux (big toe) which is composed of only two bones, the proximal and distal) (Grant JCB, 1972) (Figure 4A-B). The medial forefoot is the main weightbearing structure in early- to mid-stance, resisting the Ground Reaction Force (GRF) in healthy feet for stable and propulsive gait (Ledoux & Hillstrom, 2002; Hillstrom et al., 2013; Buldt et al., 2018).

2.1.1 Structure and Function of the Foot

Feet are often categorised into three general structures: Planus (a low-arch with an everted calcaneus and/or varus forefoot); rectus (a moderate-arch with the posterior surface of the calcaneus close to perpendicular with the ground); and cavus (a high-arch with inverted calcaneus and/or valgus forefoot) (Ledoux et al., 2003). These structural references describe common morphological and structural variations among the general population. It is generally accepted that foot function and structure are related to one another and that functional variations exist between these three distinct classifications (Ledoux and Hillstrom, 2002; Hagerdorn et al., 2013; Hillstrom et al., 2013; Song et al., 2018). A key feature of the MLA, and in general the foot, is its adaptability to different conditions, acting as a compliant interface between the body and the ground during weightbearing and as a powerful rigid lever arm at the propulsive stage of gait. The foot's two-fold purpose is enabled by the interlocking

composition of the bones, passive effect of the plantar fascia, and muscle-tendon stabilisers of the MLA (Fiolkowski, et al., 2003). Structure of the MLA and aberrant kinematics of the bones that comprise its construct have been suggested as major etiologic factors of foot injuries and pathologies (Kaufaman et al., 1999; Ogon, M., et al., 1999; Levy et al., 2006; Menz et al., 2010; Cacace et al., 2013; Song et al., 2018).

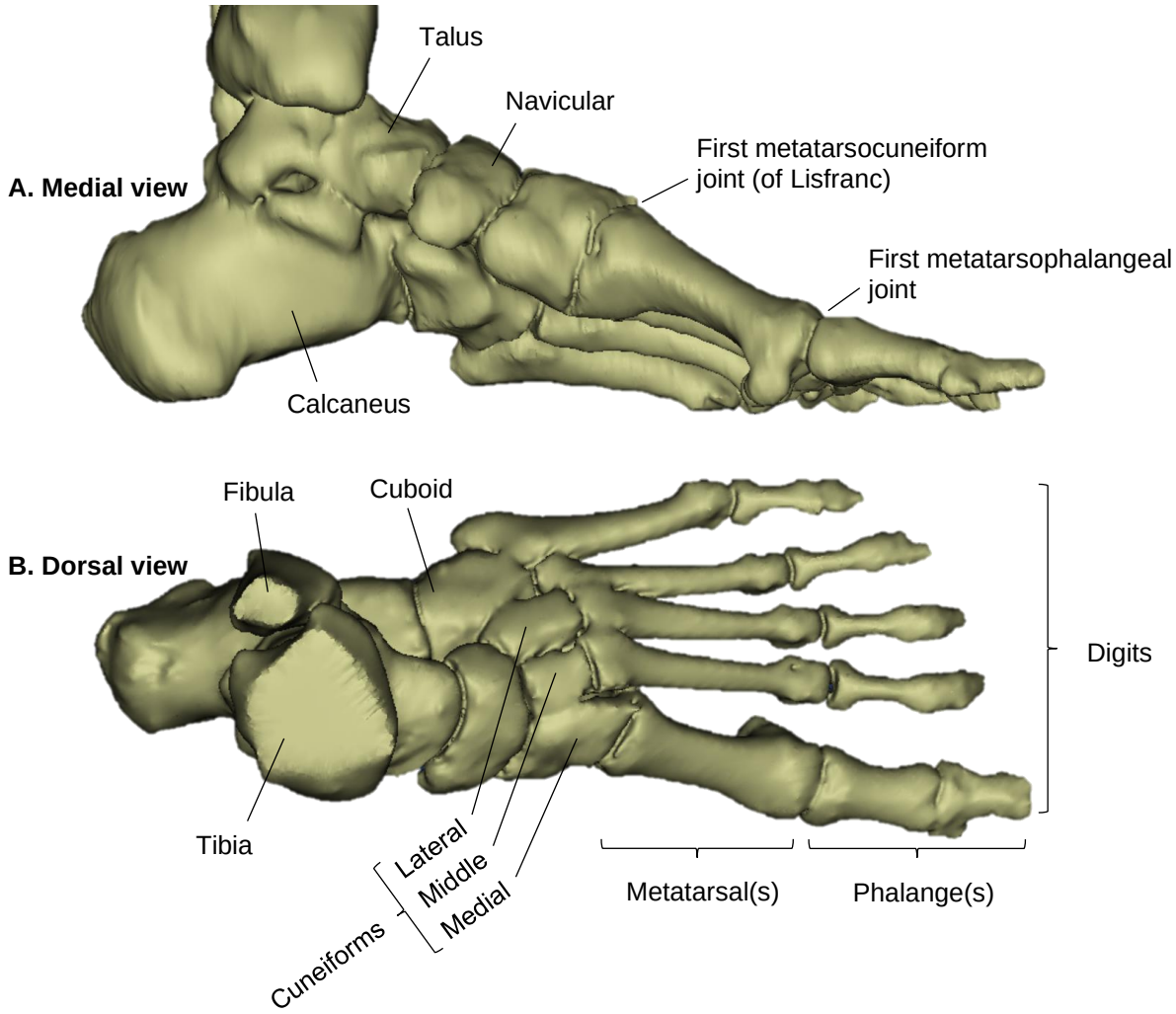

Figure 4A-B. A three-dimensional (3D) Computed Tomography (CT)-scan reconstruction of the foot's skeletal anatomy. The images are shown from the (A) medial and (B) dorsal aspects, including anatomical terminologies.

In 1953, Hicks (Hicks HJ, 1953) first postulated and proved that a rising of the MLA occurred when the MTP joints are flexed. Extension of toes pull the plantar pads, as well as the plantar fascia, forward and around the metatarsal heads causing the arch to rise and shorten the distance between the forefoot and rearfoot (Hicks HJ, 1954; Erdemir et al. 2004). The interaction between the plantar fascia and MLA is generally likened to the tightening of a rope or cable (i.e. Windlass mechanism), where the

passive mechanics of the plantar fascia arise from its connection to the calcaneus and phalanges, forming an arch-like truss.

Rupture of the plantar fascia has been cited as a mechanism of MLA collapse and thus, holds an important role in stabilising the bones of the foot (Sellman JR, 1994; Borton & Saxby, 1997; Sammarco et al., 2001; Kohls-Gatzoulis et al., 2004; Hicks HJ, 1953; Hicks HJ, 1954; Root et al., 1977; Deland et al., 1992; Huang et al., 1993; Fuller, EA, 2000). The diverse functions of the human foot are reflected by the complexity of its overall motion (Canesco et al., 2008; Buldt et al., 2015). The foot moves about three axes and on three planes. Plantarflexion-Dorsiflexion (PD) occurs in the sagittal plane, Abduction-Adduction (AA) in the transverse (horizontal) plane, and Inversion-Eversion (IE) in the coronal (frontal) plane (Buldt et al., 2015). The position of the foot is described either as supinated (i.e. laterally overloaded) or pronated (i.e. medially overloaded) (Root et al., 1977; Shirk et al., 2006; Hillstrom et al., 2013; Song et al., 2018). A supinated position represents the tri-planar effects of inversion, flexion, and adduction whereas, pronation is the tri-planar effects of eversion, extension, and abduction (Lundgren et al., 2008).

2.1.2 Structure and Function of the First Ray

The first ray is the primary weightbearing structure of the forefoot (Van Beek & Greisberg, 2011). Located at the medial border of the forefoot, the first ray segment is a single column comprised of four bones: distal and proximal phalanges of the hallux; first metatarsal; and medial cuneiform (Figure 5) (Root et al., 1977; Glasoe et al., 1999). As load is transferred from rearfoot to forefoot during locomotion, the flexibility of the MLA and orientation of the first ray play an important role in supporting bodyweight, absorbing shock, and maintaining a smooth and propulsive gait pattern. At midstance, the calcaneus and metatarsal heads are pressed to the ground, with the MLA of the foot functioning like a truss. Truss-and-beam mechanics of the healthy rectus foot rely on the first ray to support the MLA (Glasoe et al., 1999; Caravaggi et al., 2016).

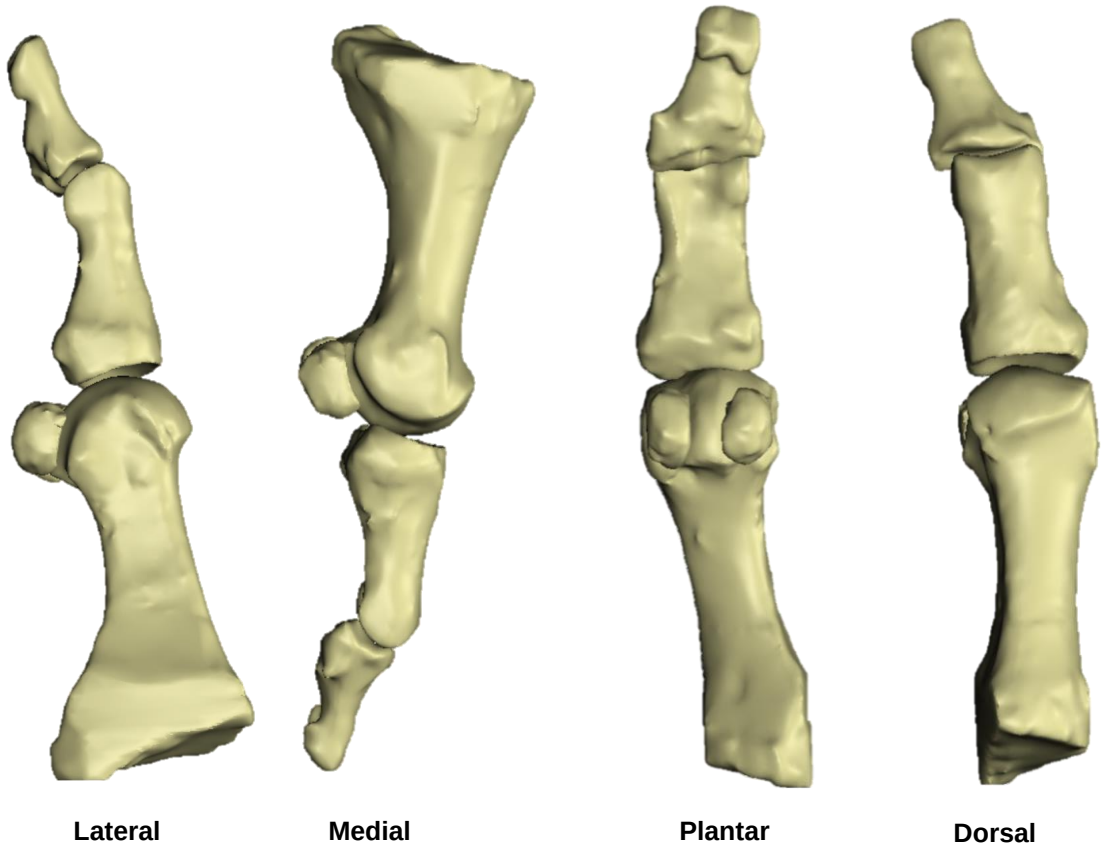

Figure 5. A 3D CT-scan reconstruction of the bones of a left sided first ray, shown from four anatomical aspects. The medial sesamoid, lateral sesamoid, distal phalanx, proximal phalanx, and first metatarsal are shown. The medial cuneiform is not included in these images.

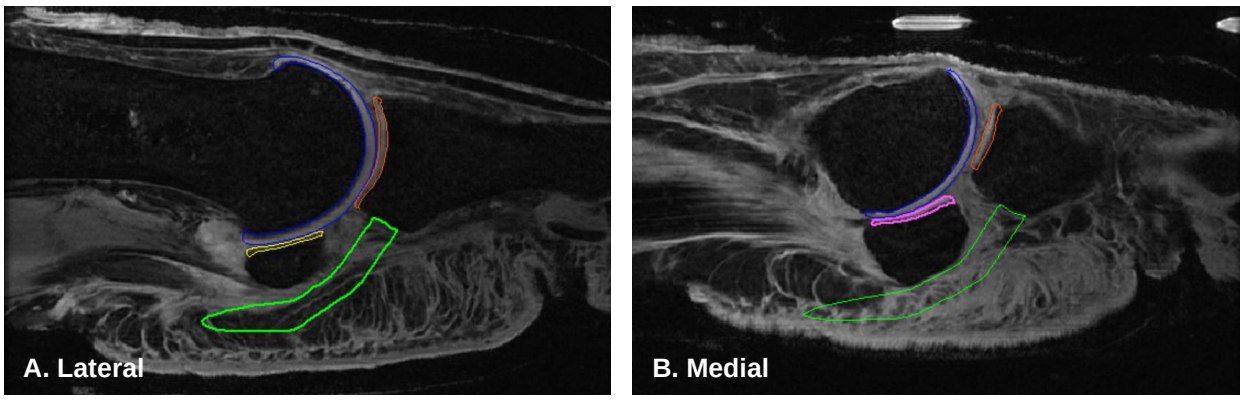

Figure 6A-B. Sagittal slices of a Magnetic Resonance Imaging (MRI)-scan of a left sided cadaveric first ray. The metatarsal head articular cartilage is outlined in blue, the proximal phalanx base articular cartilage in orange, and the lateral and medial sesamoid cartilage outlined in yellow and pink, respectively. These articulating surfaces form the first metatarsophalangeal joint. Additionally, the medial and lateral slips of the medial band of the plantar fascia are outlined in green.

2.1.3 The First Metatarsophalangeal Joint

The first MTP joint includes three articulations; the metatarsophalangeal joint which connects the first metatarsal head to the proximal phalanx while the metatarsosesamoid joints connect the first metatarsal head to the lateral and medial hallucial sesamoids (Figure 6A-B) (Grant JCB, 1972). The articular surfaces of the first MTP articulation are formed by the convex head of the first metatarsal and the shallow concave region of the proximal phalanx base (Athanasiou et al., 1998; Arbuthnot et al., 2008; Dietrich et al., 2015). At the plantar aspect of the first metatarsal head, the metatarsosesamoid articulations are formed by two longitudinal grooves running Anterior-Posterior (AP), separated by a middle crest (Athanasiou et al., 1998; Dietrich et al., 2015). Each individual groove articulates with a sesamoid bone embedded in the tendon of the flexor hallucis brevis muscle. Stability of the MTP joint is provided by collateral, suspensory, and plantar plate ligaments (Athanasiou et al., 1998).

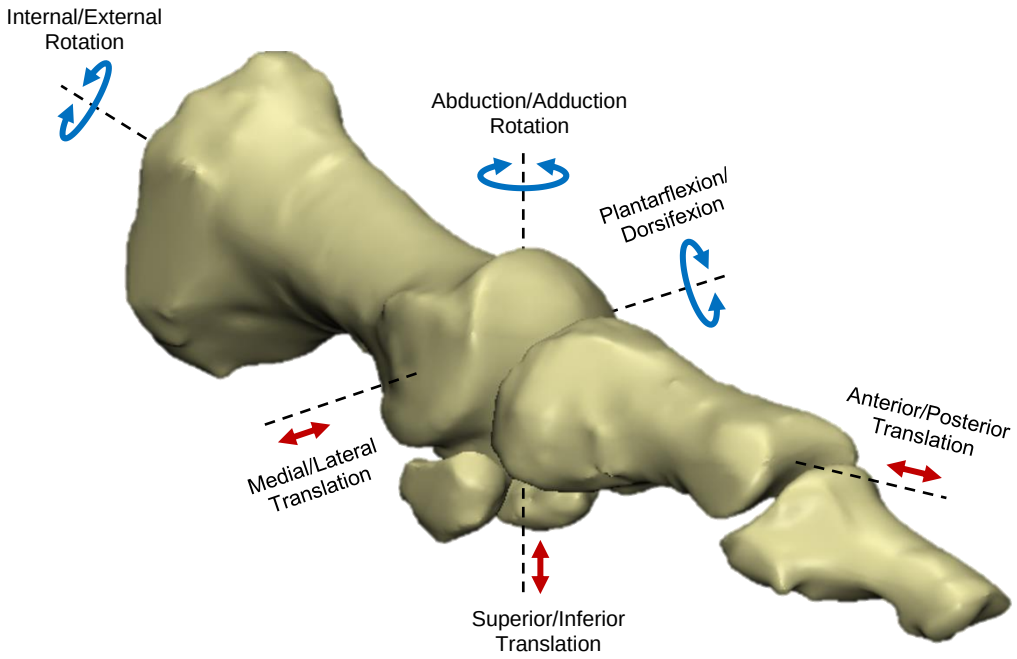

Figure 7. A 3D CT-scan reconstruction of a left sided first ray, showing the six Degrees of Freedom (DOF) of the metatarsophalangeal joint, looking from the anteriomedial aspect. There are three translational directions: medial-lateral (ML), AP, inferior-superior (IS). The primary rotation is PD. In addition, IE and AA (also referred to as (varus-valgus (VV)) rotationas occur to a lesser extent.

Articulation of the first MTP joint is constrained by two primary axes of motion. A vertical axis in the transverse plane enables AA while a horizontal axis in the sagittal plane enables PD (Figure 7) (Athanasiou et al., 1998). Approximately, 65° - 75° of dorsiflexion and 30°- 40° of plantarflexion are necessary for healthy locomotion (Shereff et al., 1986). Healthy first MTP joints exhibit a 'C-shaped' pattern of the instant centre of rotation, while pathologic joints exhibit altered and less regular patterns. Articular surface motion in healthy individuals can be described by tangential sliding, including marginal translations and compression of the joint at maximum dorsiflexion (Figure 8) (Nordin & Frankel, 2001).

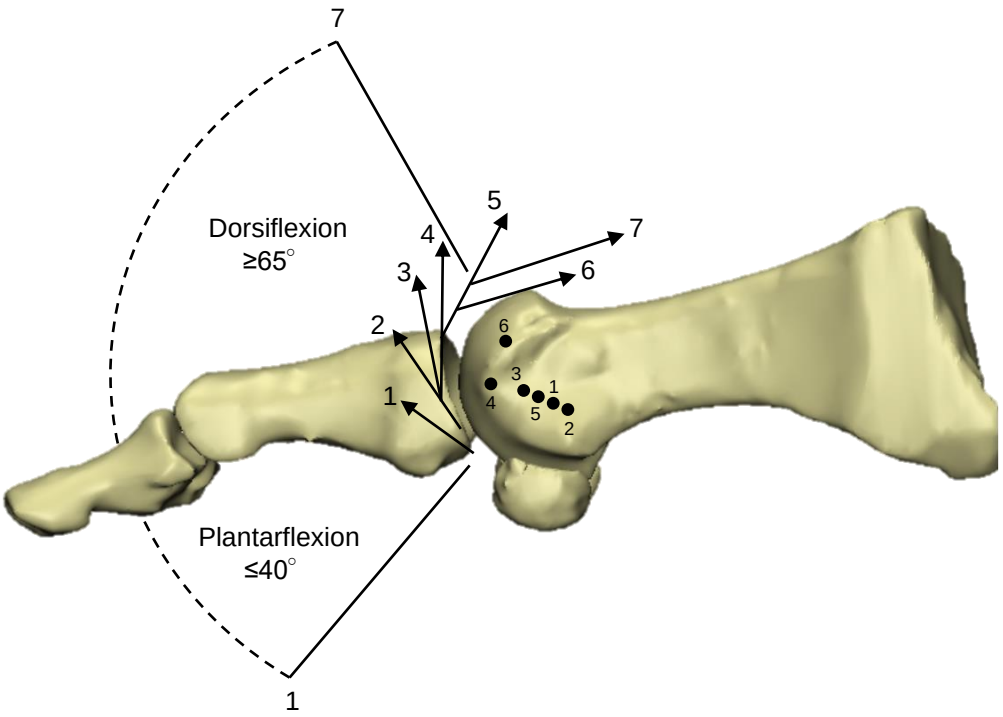

Figure 8. Adapted from Chapter 9 of Basic Biomechanics of the Musculoskeletal System by Nordin and Frankel (2001). Healthy metatarsophalangeal center of rotation in the sagittal plane. Each arrow denotes the direction of translation of the contact points which correspond to the instant centers of rotation. The Range of Motion (ROM) of the hallux is indicated by the arc (dashed line).

2.1.4 The First Metatarsocuneiform Joint

The head of the medial cuneiform articulates with the base of the first metatarsal to form the first MTC joint. This joint, in conjunction with the surrounding ligaments, forms

a stable segment with little mobility (Liu et al., 1997). It is one of the five articulations that make-up the transverse arch of the foot. Bodyweight is supported by this arch via the medial cuneiform which acts as a medial stabiliser of the midfoot (Min et al., 2019). Its structure is also an integral component of the medial forefoot, aiding in plantarflexion and dorsiflexion (Liu et al., 1997). Motion of the first MTC joint comprises 3.5° of PD and 1.5° of IE, with limited AA (Wanivenhaus & Pretterklieber, 1989).

2.2 Structure and Function of Osseous and Soft Tissues in the Foot

The musculoskeletal system of the foot, described in section 2.1, act as rigid segments that articulate in the form of joints and actuate via muscle contractions. Biological soft tissues, such as those which make up the human anatomy, are designed to withstand large deformations, and have a highly nonlinear behaviour to account for their complex mechanical functions. The capability of the foot's musculoskeletal system to withstand and transmit dynamic forces can serve as an indication of both health and disease. Indeed, the mechanical properties of different osseous and soft tissues, such as bone, cartilage, ligament, muscle, and tendon have evolved to support the various functional demands of the foot (Nordin & Frankel, 2001).

2.2.1 Bone

Bone is a complex material consisting of extracellular cortical, subchondral, and trabecular structures. It is a hard tissue and has a stress-strain relationship comparable to many engineering materials. The inhomogeneous, anisotropic composition of bone exhibits different moduli in tension and compression (Rho et al., 1998). The various structures of bone also exhibit different material properties. The material strength of bone is subject to these structural differences in architecture. Cortical bone is stiffer than trabecular bone and can withstand higher stress but less strain before fracture (Fung YC, 1993).

It is well known that mechanical stress of bone modulates change, growth, and resorption. An under-stressed bone can become weaker; an over-stressed bone can also become weakened (Ruff et al., 2006). There is an optimal range of stress for the bone. This phenomenon is known as Wolff's Law, which describes a bone cell's ability to adaptively realign itself in the direction of the maximum time averaged stress.

Evidence of these biological effects due to stress are prevalent in orthopaedic surgery and rehabilitation (Fung YC, 1993). For example, improper integration of a joint replacements stem can cause resorption, or even bone loss, over time.

Many small (arterioles, venioles, and capillaries) and large (arteries and veins) blood vessels traverse bone. Circulation of blood supplies oxygen and nutrients, regulates tissue growth, and removes metabolic waste. Bone receives approximately 10% of cardiac output, permitting greater capabilities of remodeling and repair than other parts of the anatomy. Reduction of vascular supply to the bone is related to bone loss. Decline in circulatory power with age is implicated in pathological changes associated with osteoporosis (Marenzana & Arnett, 2013).

2.2.2 Articular Cartilage

Human joints are classified into three categories: fibrous (e.g. immobile joints connected by dense fibrous tissue), cartilaginous (e.g. joints united by fibrocartilage with very little mobility) and diarthrodial (e.g. highly mobile joints joined by a fibrous capsule that is continuous with subchondral bone) (Archer et al., 1994; Fox et al., 2008). In healthy diarthrodial joints, cartilage serves as a deformable bearing with non-linear viscoelastic properties that, in conjunction with synovial fluid, present a low coefficient of friction (Eyre D, 2001; Krishnan et al., 2003). Analogous to a sponge, when subjected to load cartilage exudes synovial fluid into the joint space and when unloaded imbibes synovial fluid back into the extracellular matrix such that a dynamic ‘squeeze film’ lubrication occurs between the articular surfaces (Nordin & Frankel, 2001). The solid and fluid phases of this structure provide a unique multiphasic interface between opposing bones providing lubrication and shock absorption (Fung YC, 1993). Hence, articular cartilage provides a smooth, gliding surface, while simultaneously allowing some compressibility and elasticity (Reynaud & Quinn, 2006).

The high-water content of cartilage and the stiffness and permeability of its collagen-proteoglycan matrix ensures the adaptability of diarthrodial joints to different loading conditions (Shepard & Seedhom, 1999; Reynaud & Quinn, 2006). The primary function of the collagen fibrils is to provide tensile support to the extracellular matrix

while the proteoglycans aid in cartilage resistance to compression (Eyre D, 2001; Li et al., 2016). The collagen-proteoglycan matrix is shielded from excessive stress by interstitial fluid pressurisation during loading which, contributes more than 90% of the load support (Fox et al., 2008). Mature articular cartilage can be subdivided into three depth-dependent zones based on its characteristic collagen network architecture: superficial, middle, and deep. The material strength of articular cartilage is subject to the cross-linking of the collagen and the depth-dependent zonal differences in fibrillar architecture. In the superficial zone of cartilage, the fibrils are oriented tangential to the articular surface comprising 10%-20% of the depth, the middle zone forms an arcade like organisation randomly interlinking and comprising 40%-60% of the depth, and the fibrils in the deep zone are aligned in columns perpendicular to the calcified zone of cartilage comprising 30%-40% of the depth. The tidemark forms the transition from cartilage to subchondral bone (Fung YC, 1993; Nordin & Frankel, 2001).

Damage to the fibrillar network from mechanical stress is considered an important pathway to numerous disorders and particularly to degenerative disease such as OA (Brown et al., 1991; Archer et al., 1994; Bareither et al., 1998). Athanasiou et al., (Athanasiou et al., 1998) and Liu et al., (Liu et al., 1997) noted a more random chondrocyte arrangement in the deep zones of first MTP and second MTC joint cartilages. This contrasts with the organisation of chondrocytes in the hip, knee, and ankle, which exhibit a columnar arrangement in the deep zone of cartilage (Fox et al., 2008). The structures of MTP and MTC cartilage have likely adapted to these joints 90° orientation with respect to the remainder of the body, generating greater shear and bending as opposed to compressive forces during gait (Liu et al., 1997; Athanasiou et al., 1998).

2.2.3 The Plantar Fascia

The plantar fascia is a robust band of fibrous tissue that supports the MLA. It originates from the medial turbercle of the calcaneus and inserts into the phalanges (Figure 9) (Grant JCB, 1972; Erdemir et al., 2006). Arch-height deformation occurs when vertical forces from bodyweight are transmitted down the tibia or GRF’s are transmitted up through the calcaneus and the metatarsal heads (Gefen A, 2002; Gefen A, 2003).

Collapse of the MLA is therefore, prevented by the tensile strength and anatomical placement of the plantar fascia between the calcaneus and phalanges (Hicks JH, 1954; Sharkey et al., 1998; Fuller EA, 2000).

Plantar fasciectomy or rupture of the plantar fascia has been shown to reduce arch-height (Sharkey et al., 1998; Erdemir et al., 2006), confirming the passive support function first proposed by Hicks (Hicks HJ, 1954). Patients who received plantar fasciectomy exhibited postoperative flattening of the MLA and decreased GRF, particularly at the push-off phase of gait (Daly et al., 1992). The distal structure of the plantar fascia divides into five fibrous bands which insert into the five phalanges of the forefoot. Each band then splits into two slips, at each phalanx, which straddle the toe flexor tendons (Grant JCB, 1972). These slips articulate beneath the metatarsal head in the anterior and posterior directions as the phalanges become flexed or extended, respectively (Wright et al., 1964; Daly et al., 1992; Kitaoka et al., 1994).

Figure 9. Cadaveric photograph with the skin dissected to reveal the plantar fascia, comprised of three bands of fibrous connective tissue: medial, central, and lateral bands which radiate toward the bases of the toes from the posterior tubercle of the calcaneus. The plantar fascia appears to be turquoise/silver in colour.

2.2.4 The Ligament and Muscle-Tendon Systems

In order for the joints of the foot to maintain a smooth articulation they are stabilised by 112 ligaments. The functional ligamentous unit is bone-ligament-bone (Fung YC, 1993). The primary ligamentous structures of the first MTP joint are the fibrous capsule attached to its articular margins, collateral ligaments, deep transverse metatarsal ligaments, and the plantar plate (Altchek et al., 2013). Movement of these joints is actioned via forces transmitted to the bones through a complex system of 13 extrinsic and 21 intrinsic muscle-tendons (Nordin & Frankel, 2001). The functional unit of muscle is considered bone-tendon-muscle-tendon-bone (Fung YC, 1993). The extrinsic muscles are considered the primary active controllers of the foot during gait. Much like the cartilage, the material capacity and tensile strength of tendons and ligaments is derived from collagen (Fung YC, 1993).

Unlike the complex network of collagen fibers in the cartilage, the tendons and ligaments have a more simplistic structure, typically comprising parallel fibers. Insertion of ligament into bone is gradual. The network of collagen fiber remains constant as it inserts into the calcified tissue, gradually transitioning to bone from ligament (Nordin & Frankel, 2001). Whereas, tendon is anchored to bone and muscle less distinctly. The tendon inserts broadly into the main fibrous layer of the bone's periosteum and at the other end, transitions from tendon to muscle by a junction between the muscle fibers and many terminal indentations of the tendons collagenous fibers (Fung, Y.C., 1993).

The medial and lateral collateral ligaments attach to the dorsal turbercles of metatarsal head and proximal phalanx base. Adjacent to collaterals are the plantar ligaments, thick, dense structures which insert between the proximal phalanx base and hallucial sesamoids (Mkandawire et al., 2005). Finally, the deep transverse metatarsal ligaments are flat bands of soft tissue that connect to the first through fifth metatarsal heads (Altcheck et al., 2013). The plantar plate is a robust ligamentous structure that has three main functions to: 1) cushion and offload the compressive loads of the first ray as bodyweight is transferred from rearfoot to forefoot, 2) assist in first MTP joint stability via its attachments to the plantar fascia, intermetatarsal ligaments, and collateral ligaments, and 3) provide support to the function of the windlass mechanism (Deland et al., 1995; Sharkey et al., 1998).

A. Plantarmedial view **B. Medial view**

Figure 10A-B. Cadaveric photographs of a dissected foot showing (A) the Flexor Hallucis Longus (FHL) placed under tension, causing the hallux to plantarflex and (B) the insertion sites of the collateral, metatarsosesamoid, and plantar plate ligaments of the first MTP joint (marked by black dashes).

The first MTC joint ligaments can be categorised into the fibrous capsule, dorsal, plantar, intercuneiform, and interosseous ligaments (Mkandawire et al., 2005). Mizel MS, demonstrated that the plantar ligament of the first MTC joint is the primary restraint of dorsal angulation and displacement of the first metatarsal head (Mizel MS, 1993). Control of the first ray is facilitated by both the intrinsic and extrinsic muscles including flexors, extensors, abductors, and adductors (Figure 10A-B) (Altcheck et al., 2013). The sesamoid bones are integrated into the Flexor Hallucis Brevis (FHB) muscle, increasing the lever arm of muscular pull, and increasing first MTP joint flexion torque (Nordin & Frankel, 2001). Extensors of the toe fire eccentrically to control the foot's descent and prevent heavy ground impact (Figure 11) (Altcheck et al., 2013). The peroneal tendons originate in the lateral compartment of the leg, separating to form the Peroneus Brevis (PB) and PL (Johnson & Christensen, 1999). The PB tendon inserts into the base of the fifth metatarsal while the PL curves around the cuboid, obliquely crossing the sole of the foot to insert into the plantar-lateral aspect of the first metatarsal and medial cuneiform (Figure 11) (Duchenne GB, 1949; Clarke et al., 1998).

Lateral stabilisation of the forefoot is performed by the PB, where loss of its strength may cause varus of the hindfoot (Sammarco, GJ, 1995). The PL is the primary everter of the forefoot. The PL acts to combine eversion and plantarflexion motions to keep the first metatarsal head purchased to the ground, inserting into the base of the first metatarsal and medial cuneiform, depressing the metatarsal head, and acting to

control propulsion (Figure 11) (Bohne et al., 1997; Bierman et al., 2001). The Tibialis Posterior (TP) is a dynamic inverter of the foot which supports the MLA. Its inversion of the subtalar joint during mid- to late-stance locks the transverse tarsal joint, thus ensuring the foot acts as a rigid lever arm during toe-off (Duchenne GB, 1949). Loss of TP strength is known to result in acquired flatfoot (Altchek et al., 2013). The interosseous muscles stablise the forefoot during toe-off. Intrinsic and extrinsic muscular imbalances are thought to lead to several toe deformities (Garcia-Gonzalez et al., 2009; Isvilanonda et al., 2012)

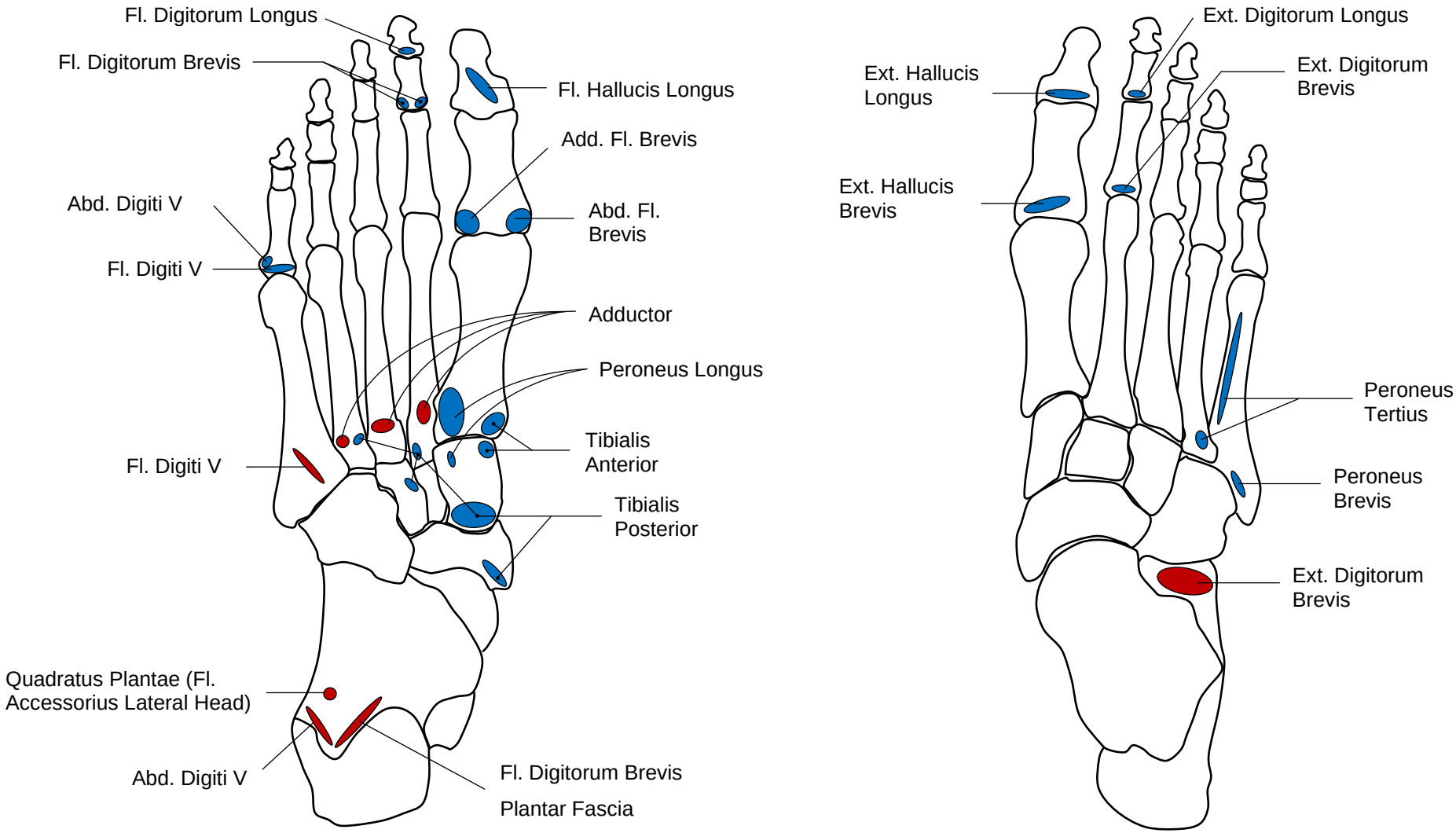

Figure 11. Insertion sites of the plantar and dorsal muscle/tendon systems. Adapted from Grant's Atlas of Anatomy (Grant JCB, 1972).

2.2.5 Plantar Fat Pads

The plantar fat pads are structures for distributing and cushioning load that cover the sole of the rearfoot (calcaneus) and forefoot (submetatarsal heads one through five and the hallux) (Fung YC, 1993). Comprising fibrous compartments of adipose tissue, plantar fat is divided into superficial microchamber and deep macrochamber layers (Hsu et al., 2009). During locomotion, plantar fat pads are subjected to considerable forces as the foot contacts the ground, absorbs shock, protects against excessive load transmission, and reduces plantar pressures. Such characteristics of the fat pads have evolved to cushion the remaining structures of the foot (Isvilanonda et al., 2016).

2.2.6 Plantar Skin

Plantar skin is a multi-layer (epidermis, dermis) barrier that provides a mechanical, infectious, and thermo-regulatory cover to the sole of the foot. Some studies have shown plantar skin can withstand greater abrasion and pain than skin along other body parts (Wang et al., 2011).

2.3 First Ray Hypermobility

While the different soft tissues of the foot have evolved to support complex function, they are also susceptible to aberrant mechanics and injury. Structure begets function and synergy of the osseous- and soft-tissues of the foot, characterised in section 2.2, rely upon normal biomechanics. Hypermobility, a condition in which the articular joints possess abnormally large ROM, results from ligamentous or muscular laxity (Grahame R, 1999). Clinically referred to as double-jointed or joint hyperlaxity, it can be inherited or acquired through years of training and stretching, as seen in athletes and gymnasts (Hakim & Grahame, 2003; Remvig et al., 2007). Hypermobility is a condition that encompasses a spectrum of disorders, where Generalised Joint Hypermobility (GJH) lies at the mild end of several Heritable Connective Tissue Disorders (HCTD) with Marfan's syndrome and Ehlers-Danlos syndrome at the severe end (Beighton and Horan, 1969; Gray et al. 1994; Judge and Dietz, 2005). The present work does not focus on GJH or other HCTD's, but rather explores traits related specifically to first ray hypermobility and its interactions with the surrounding musculoskeletal tissues of the foot.

2.3.1 Classifications of Hypermobility

Despite hypermobility being implicated in a number of orthopaedic and rheumatologic disorders (Bird and Tribe, 1978; Johnsson et a., 1996: Golightly et al., 2012; Golightly et al., 2018; Flowers et al., 2018), the role of joint laxity in pathologies of the foot and ankle remains understudied and poorly understood. Numerous methods exist to assess hypermobility of the human body: The Carter and Wilkinson Diagnostic criteria (Carter and Wilkinson, 1964), the Beighton criteria (which is a modification of the original Carter and Wilkinson method) (Beighton et al., 1973), the Contompasis method, the Bulbena criteria, and the Brighton criteria (Golightly et al., 2012). Though these assessments of diagnosing hypermobility differ by process, they present a universal deficiency: none assess hypermobility in structures below the knee.

Pes planus is a common occurrence, varying from mild-asymptomatic to severe malformation whereby, medial displacement of the hindfoot results in collapse of the MLA (Grahame R, 1999). Many patients with foot deformity develop Hallux Valgus (HV) but do not develop pain (Coughlin MJ, 1996; King & Toolan, 2004; Nguyen et al., 2010). Conversely, pes cavus is also present in a subset of individuals. Many authors have independently suggested that first ray hypermobility may be present in most individuals with planus feet (King and Toolan, 2004; Cooper et al., 2009; Rao and Bell, 2013; Doty et al., 2014). Although hypermobility is considered a risk factor for joint pain, the evidence of an association between hypermobility and symptomatic pain in the foot and ankle can differ in population-based studies (Bird and Tribe, 1978; Johnsson et a., 1996: Golightly et al., 2012; Golightly et al., 2018; Flowers et al., 2018). Tobias et al., (2013) reported an 82% higher odds-ratio of symptomatic foot/ankle pain among adolescents, as measured by the Beighton criteria, versus controls. In contrast, Golightly et al., (2018) did not find any significant relationships in the foot and ankle except for talonavicular joints and hypermobile knees. While the findings of these studies differed, both found an association with knee hypermobility and mild-to-moderate foot and ankle pain. Golightly et al., postulated that hypermobility may overload synovial joints during repetitive, abnormal motion and expose the soft tissues to microtrauma, resulting in increased joint pain.

2.3.2 Clinical Assessments of First Ray Hypermobility

First ray mobility is the collective motion between the medial cuneiform and first metatarsal (Morton DJ, 1928; Klaue et al., 1994; Glasoe et al., 1999; Glasoe & Michaud, 2019). Superior translation of this structure under load is typically used to quantify first ray mobility, where ≤5 mm is considered “normal” (Voellmicke & Deland, 2002; Coughlin and Shurnas, 2003; Jones et al., 2005; Coughlin & Jones, 2007; Glasoe & Michaud, 2019). Definitions of the “abnormal” first ray hypermobility can vary from 7-10 mm based on differences in case definitions and methods of assessment (Roukis et al., 1996; Root et al., 1997; Lee & Young, 2001; Tavara-Vidalon et al., 2018; Glasoe & Michaud, 2019; Munuera & Martinez, 2020). First ray hypermobility compromises the MLA’s ability to resist the GRF during ambulation (Glasoe et al., 2000; Grebing & Coughlin, 2004; Glasoe et al., 2006; Doty et al., 2014). Morton (1928)

first proposed the term “hypermobility of the first metatarsal segment”, but it wasn’t until later that Root et al., (1977) defined the term first ray hypermobility as “a state of abnormal first ray instability that occurs while the forefoot is bearing weight”. Currently, there is no standardised measurement for hypermobility of the first ray and, hence, no robust method of studying possible relationships between hypermobility of the first ray and symptoms of OA.

Clinical assessments of first ray hypermobility involve a qualitative judgment by the clinician (Voellmicke and Deland, 2002). They will grasp the first metatarsal head with their thumb and forefinger, translating the first ray superiorly and inferiorly (Figure 12). This measurement is typically performed with the patient prone, hence, non-weightbearing. Glasoe et al., (2002) found that such manual examinations were unreliable, demonstrating wide variations among experienced clinical staff. Nonetheless, this method of examination continues to be used today as it is easy to perform and requires no additional equipment. However, there is no agreement for this threshold amongst investigators.

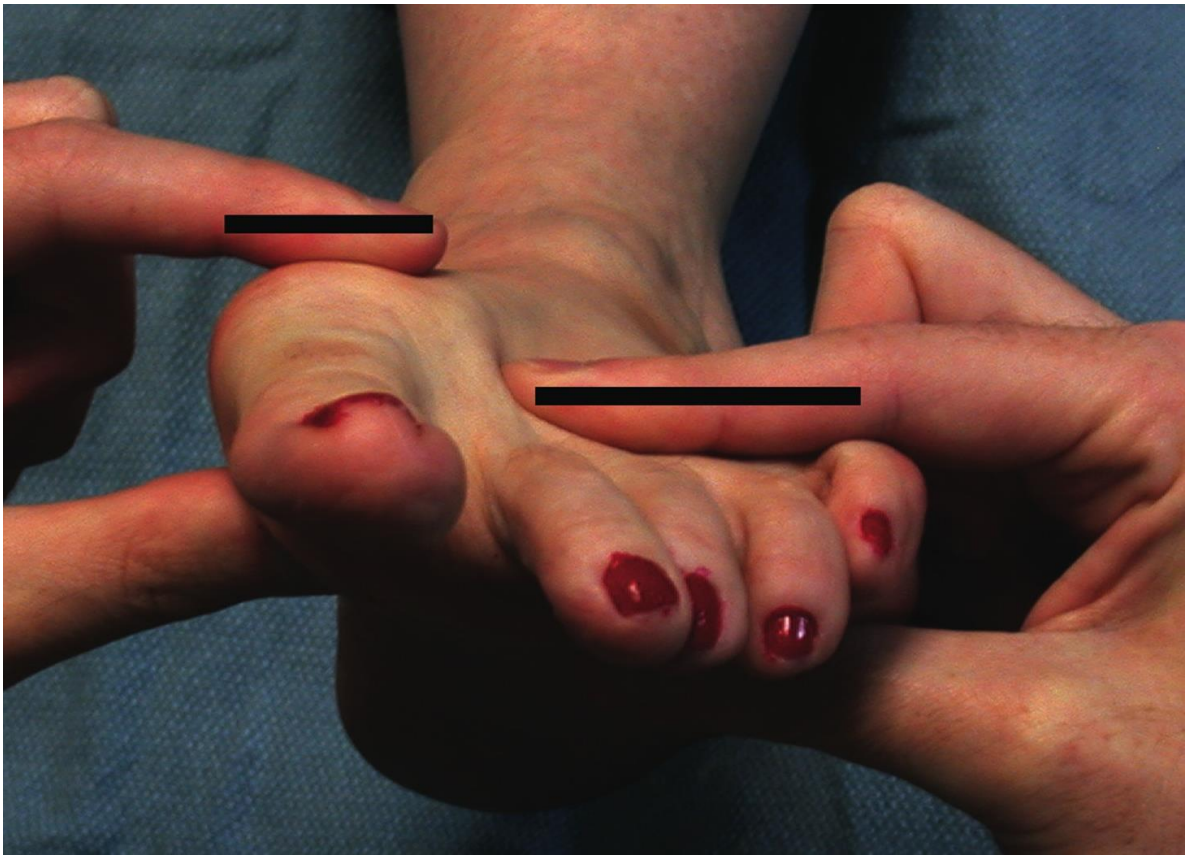

Figure 12. Standard clinical method of assessing first ray mobility, the surgeon will grasp the lesser metatarsals with one hand and apply a force to the first ray with their other.

Handheld rulers have also been developed, to more accurately measure dorsal first ray mobility (Lee & Young, 2001 Kim et al., 2008; Munuera-Martinez et al., 2020). Wallace and Kilmartin (1990), published such a device, made up of two moveable rulers. The measurements were made by placing the ruler at the dorsum of the forefoot, quantifying the first ray translation in 1-mm gradients. This method provided a simple and practical measurement, yet its reliability was never established. Reliability may be a function of foot position including, resting calcaneal stance position (RCSP), subtalar joint neutral (STJN), and a 90° lateral border of the foot with respect to shank but this is still to be determined. A similar device to those described above is commercially available but has not been tested for reliability or validity (www.HumanLocomotion.org).

2.3.3 Mechanical Assessments of First Ray Hypermobility

Over the past 40 years several investigators have developed mechanically driven devices to objectively quantify first ray mobility (Rodgers & Cavanagh, 1986; Klaue et al., 1994; Glasoe et al., 2000). While these devices differ in design, they are similar in that a plantar force is applied to the first ray and linear translation measured to quantify first ray mobility. In 1986, Rodgers and Cavanagh (1986), built the first-of-its-kind prototype which was prone to include fat pad compression in the measurement, yielding overestimates of the actual first ray mobility (Figure 13A). Klaue et al., (1994) constructed a smaller mechanical system in 1994 which was found to be reliable (2005), however, the measurement required a manual force, potentially adding variability to the result (Figure 13B). Finally, in 1999, Glasoe et al., (1999) produced a device that was reliable but overly complicated and bulky, thus limiting its use in a clinical setting (Figure 13C). A summary of device attributes can be found in Table 1.

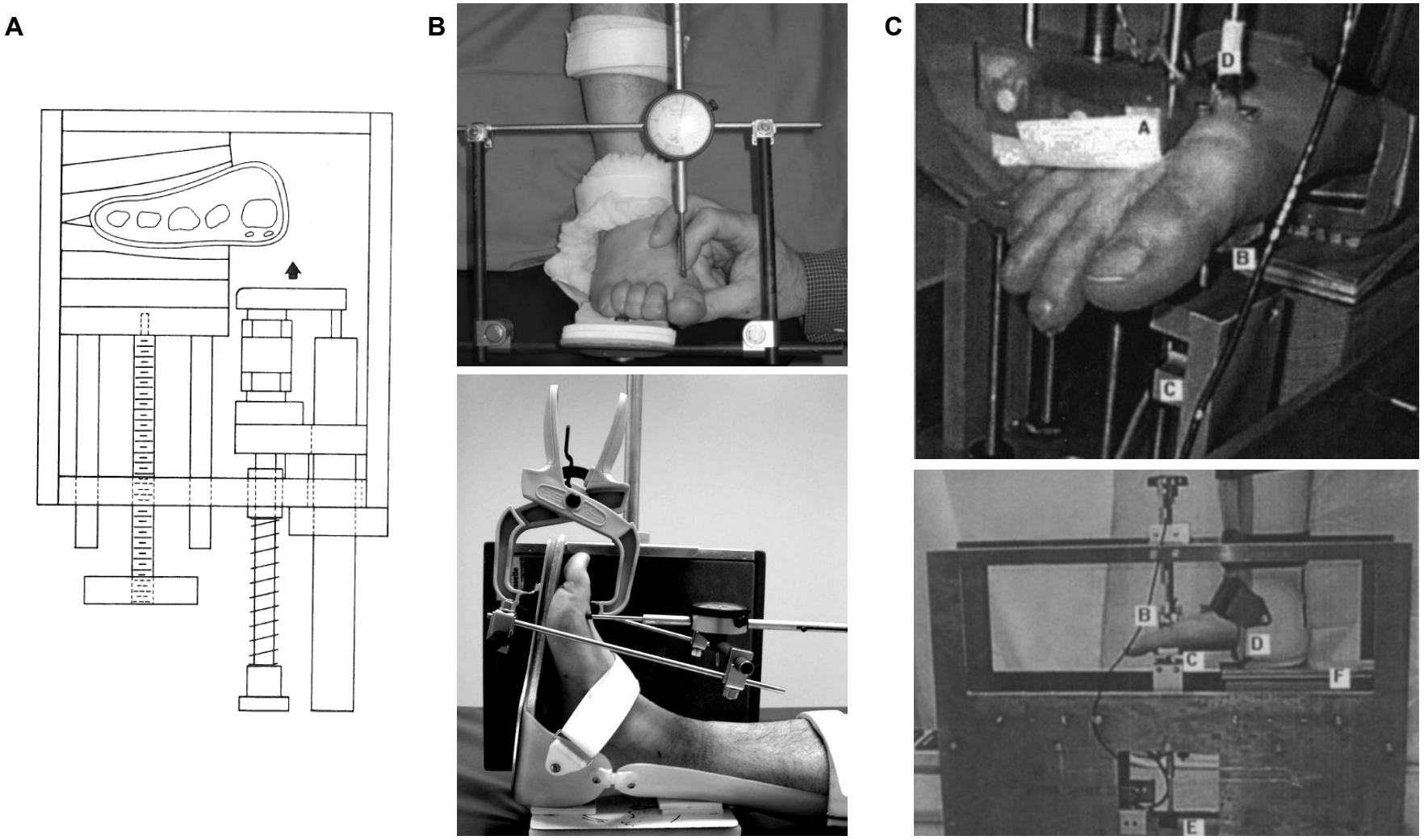

Figure 13A-C. (A) Rodgers and Cavanagh device, 1986 (Adapted from Rogers and Cavanagh, Rogers and Cavanagh, Proceedings of the North American Congress on Biomechanics, 1986); (B) Klaue et al., device, 1994 (Adapted from Klaue et al., Foot Ankle Int, 1994); (C) Glasoe et al., device, 1998 (Adapted from, Glasoe et al., Foot Ankle Int, 1998).

Table 1. First ray mobility and defined hypermobility using mechanical devices.

Mechanical Assessment				
Study	**Method**	**First Ray Mobility**	**Defined Hypermobility**	**Design Comments**
Rodgers and Cavanagh, 1986	Lateral foot immobilised by a clamp, and first metatarsal head displaced by a manually operated plunger containing a force transducer and Linear Variable Differential Transducer (LVDT). The applied force and displacement of the first ray, were simultaneously recorded at the plantar aspect of the metatarsal head. Subjects positioned in the jig such that the knee, hip and ankle joint angles were maintained at 90° of flexion. Maximum force of approximately 80 N applied.	Maximum displacement of 20 mm	N/A	Took measurements from plantar aspect of the foot, potentially leading to fat pad compression involved in the results. Large and bulky – not portable. Designed for partial weightbearing only.
Klaue et al., 1994	Ankle-foot orthosis cut to midfoot height, and a plantar aluminium rail fixed to the heel. The forefoot is placed plantigrade. A micrometer is fixed to an aluminium plate and can be positioned anywhere at the foot's dorsum. A manual force is applied to the metatarsal head. The first ray is mechanically free and the distance between the origin and extended location is measured directly from the skin of the dorsum of the foot.	HV group: 9.3 ± 1.9 mm; control group: 5.3 ± 1.4 mm	≥8 mm	No standardised force --- may result in variable measurements. Ankle-Foot Orthosis does not appear to change depending on foot size. Designed for supine (non-weight bearing) and partial weightbearing only.
Glasoe et al 1999	A platform for the hindfoot and immobilising boot preventing leg and rearfoot motion. Maintained 90° of flexion at the ankle joint. Adjustable clamp for the forefoot to immobilise the lesser metatarsals. Screw mechanism for loading forces (55 N applied to dorsal head of first metatarsal) to the first ray.	Right foot: 6.27 mm (4.40-9.45 mm), left foot: 6.62 mm (4.90-8.41 mm); HV group: 5.9 ± 1 mm; control group (Morton's neuroma): 4.2 ± 1 mm; normal: 5.5 mm (4.2-7.6mm)	≥10 mm	Large and bulky device, not portable, difficult to use in a clinical setting. Designed for partial weightbearing only.

2.3.4 First Ray Hypermobility and Foot Type Biomechanics

In an ideal rectus foot, the first ray purchases the ground and bears load through the first metatarsal head (Ledoux & Hillstrom, 2002; Hillstrom et al., 2013; Song et al., 2018). Peak plantar pressures are typically highest beneath the first metatarsal head followed by the second and lesser rays (Hillstrom et al., 2013). In pes planus, the first metatarsal head may not be able to remain purchased to the ground and share in forefoot loading causing a transfer of load to the second metatarsal head (Ledoux & Hillstrom, 2003; Olson et al., 2003; Hillstrom et al., 2013) (Figure 14A-B). Several authors have postulated an association between pes planus and first ray hypermobility to explain aberrant plantar loading of this foot type (Song et al., 1996; Ledoux & Hillstrom, 2003; Hillstrom et al., 2013). As described in a study of 61 asymptomatic feet, the peak pressures beneath the first metatarsal head decreased while those beneath the second metatarsal head increased in planus compared to rectus feet (Hillstrom et al., 2013). Paradoxically to this possible effect of hypermobility, the centre of pressure (origin of the ground reaction force vector) is reduced in concavity in the planus versus rectus foot as evidenced by the lower centre of pressure excursion index (Ledoux & Hillstrom, 2003; Hillstrom et al., 2013) (grey line extending from rearfoot to forefoot in Figure 14A-B).

The cause of this aberrant mechanics in the planus foot is unclear; however, from a structural perspective, the peroneus longus provides passive and active contributions to stabilising and “locking” the first metatarsal against the medial cuneiform (Bohne et al., 1997; Johnson & Christensen, 1999; Bierman et al., 2001). Torsion of the first metatarsal was suggested by Johnson and Christensen, (1999) to tighten the midfoot ligaments, stabilise the medial column, and maintain integrity of the transverse arch. Bohne et al., (1997) demonstrated a significant increase in medial displacement of the transverse arch after transecting the peroneus longus. Conceptually, the peroneus longus may help the first ray to resist excessive motion by drawing it into plantarflexion due to the tendon’s line of action across the lateral ankle (Bohne et al., 1997; Johnson & Christensen, 1999; Bierman et al., 2001; Denyer et al., 2013; Hamid et al., 2017). Hypermobility resulting from decreased peroneus longus function likely causes the first ray of a planus foot to excessive translate upon weightbearing. Kokubo et al., (2012) examined the influence of the posterior tibialis and peroneus longus on stiffness

of the foot's MLA. They hypothesised that foot shock absorption and arch stiffness would be affected by force transmitted through each tendon. The posterior tibialis was shown to have more effect on arch stiffness than the peroneus longus, indicating the peroneal tendon does not function to maintain the MLA. However, loading of this tendon was shown to improve first MTC joint sagittal plane subluxation (reduced translation) and intermetatarsal angle (reduced abduction) (Dullaert et al., 2016). This suggests the peroneus longus interacts with the orientation of the first ray under weightbearing load.

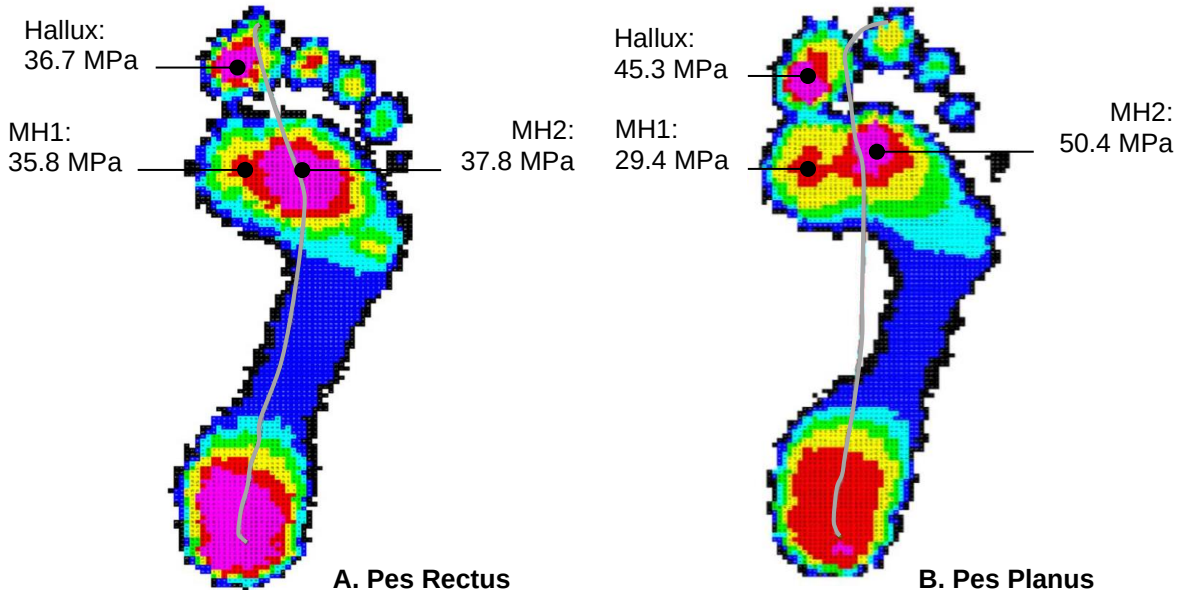

Figure 14A-B. Image of plantar pressure distributions during gait where the rectus and planus foot types exhibit different biomechanical functions. The planus plantar pressure distribution demonstrates lateral transfer of forefoot load from the first to the second metatarsal, in the presence of a more medially oriented centre of pressure.

Johnson and Christensen (1999) have shown the importance of the peroneus longus on forefoot stability in vitro. In a study of seven fresh frozen cadavers, they simulated static loads from bodyweight. Increased force in the peroneus longus caused the first metatarsal to evert and plantarflex, the first ray to lower, and the medial column to exhibit torsion while enhancing the transverse arch. Increasing tensile load in the peroneus longus caused a mean difference in first metatarsal motion of 8.1° ± 3.1° in the frontal plane and 3.8° ± 0.5° in the sagittal plane. Similarly, frontal plane motion of the medial cuneiform exhibited a mean increase of 7.4° ± 2.6°. Medial cuneiform motion in the sagittal (3° ± 0.6°) and transverse (2.1° ± 1.8°) planes also increased

due to peroneus longus loading. No significant differences in arch height were observed. Of the limited work performed in this area, Olson et al., (2003) also found the peroneus longus to be the primary muscle for increasing plantar pressures beneath the first metatarsal head. In patients with clawed hallux deformity, ulceration beneath the first metatarsal head may occur due to increased overpull of the peroneus longus.

2.4 Characteristics of Osteoarthritis and Hallux Rigidus

First ray hypermobility may adversely influence plantar loading of the foot, as conveyed in section 2.3. Aberrant loading of this kind may influence joint contact mechanics and initiate degenerative changes in the first MTP joint over time. Such adverse loading has been linked to onset and development of OA in the knee, hip, and ankle (Birde & Tribe, 1978; Golightly et al., 2012; Flowers et al., 2018; Golightly et al., 2018); however, the interaction between hypermobility and pathologic function in the foot remains unclear. The pathology of OA involves the entire joint in a process that includes focal and progressive cartilage defects with concomitant changes in subchondral bone, comprising marginal outgrowths, osteophytes, and gradual bony sclerosis (Dieppe & Lohmander, 2005). Structurally, bone marrow edema has been observed on MRI and is considered an important source of pain as these bone marrow lesions reside within innervated bone (Felson et al., 2000). Aberrant mechanics play an important role in disease pathogenesis (Sarzini-Puttini et al., 2005; Wyles et al., 2017). The study of mechanical factors is highly complicated due to the progressive nature (structurally, biomechanically, biologically and biochemically) of this disease (Felson et al., 2000). There is limited knowledge of the mechanistic pathway to hallux rigidus. Therefore, better understanding and prediction of the potential burden of this disease on healthcare institutions is required, particularly identification of causative factors which enable targeted intervention at an early stage. Several investigators have hypothesised that first ray hypermobility, plays a role in various pathologies of the foot including hallux rigidus (Bremner et al., 1968; Nguyen et al., 2010; Cacacae et al., 2013; Menz et al., 2015).

2.4.1 Aetiology, Epidemiology, and Clinical Features of Osteoarthritis

Osteoarhtirits is often categorised into two groups: primary and secondary (Felson et al., 2000). Primary OA normally occurs in older people due to wear and tear from repetitive use over time, whereas secondary OA is frequently caused by trauma (Van Saase et al., 1989). Sources of mechanical stress leading to OA can include acute (e.g. injury) or gradual joint overloading (e.g. repetitive stress from malalignment, incongruence, overuse, obesity, or neuromuscular dysfunction) (Dieppe & Lohmander, 2005). Degeneration of the cartilage matrix is associated with loss of proteoglycans, decorin and biglycan, which are directly related to the compressive strength of the solid cartilage matrix (Figure 15A-B). Loss of these molecules is associated with increased cleavage of type II collagen by collagenase, aggrecan cleavage and the degradation of small proteoglycans (Sarzi-Puttini et al., 2005).

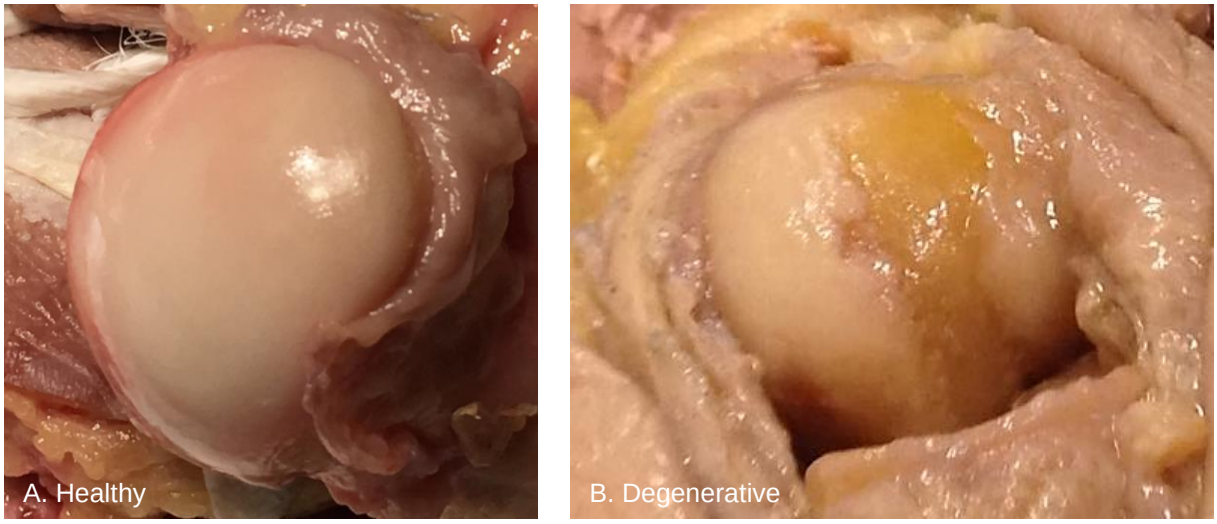

Figure 15A-B. Photographs of cadaveric specimens with: (A) healthy cartilage and (B) degenerative cartilage indicative of OA including severe degenerative changes in the cartilage extending down to the subchondral bone.

Excessive joint loading and cartilage deformation, in conjunction with altered biomechanical properties, leads to cartilage erosion overlaying the bone (Meachim G, 1972; Golightly et al., 2012; Carrol & Coleman, 2019). The clinical presentation includes pain, crepitus, and reduced mobility. Osteoarthritis is considered the leading cause of regional joint pain in older people (Dieppe and Lohmander, 2005). Due to the longevity of modern careers and the significant incidence of OA among middle-aged people, a considerable societal burden is placed on the global economy through

lost time at work and early retirement (Felson et al., 2000). Economic models forecast an exponential increase in the cost of OA in Europe, Australia, and the USA, accounting for between 1-2.5% of the Gross Domestic Product (GDP) (Chen et al., 2012).

2.4.2 Hallux Rigidus

Osteoarthritis of the first MTP joint is considered the most common degenerative pathology in the foot and ankle (Van Saase et al., 1989), clinically defined as hallux rigidus (Cotterill MJ, 1887). The frequency of first MTP joint OA among adults can vary from 6% to 39%, largely due to differences in ages, populations, and case definitions (Roddy and Menz, 2018). End stage OA in the first MTP joint manifests as severely restricted motion, pain, and disability (Dananberg et al., 1993; Canesco et al., 2008). Loss of cartilage is typically situated dorsal to the apex of the dome of the metatarsal head, and adjacent to the dorsal lip of the base of the proximal phalanx (McMaster MJ, 1978) (Figure 15A-B). Figure 15B is even more advanced than typical with cartilage degeneration extending to the central and plantar aspects of the joint. The disturbance in function when repeated on a daily basis, can alter foot and postural biomechanics, causing substantial disability at the end-stage (Dananberg et al., 1993).

Jack, E., (1940) was the first investigator to describe a jamming mechanism of the first MTP joint occurring when the first ray was excessively dorsiflexed or pushed abnormally into extension. Nearly 60 years later, Roukis et al., (1996) reinforced Jack's theory that rather than abnormal gait or anatomical variances, motion of the first MTP joint is influenced by first ray position. The authors found that 4 mm of first ray dorsal translation reduced first MTP joint dorsiflexion by 19.3%, and when dorsal translation reached 8-mm, dorsiflexion reduced by a further 34.7%. Some authors believe that a form of functional hallux limitus is present in most individuals with first ray hypermobility (Dananberg, H.J., 1993; Roukis et al., 1996; Durrant and Chockalingam, 2009) since hallux limitus is defined by a decrease of first MTP joint dorsiflexion. A progression from hallux limitus to hallux rigidus may depend on the actual amount of first ray mobility that occurs during gait, rather than the inherent properties of the first MTP joint (Roukis et al., 1996; Roukis et al., 2005).

2.4.3 Treatment Options

Following the exhaustion of conservative treatments such as, intra-articular injections and foot orthoses, options for treating hallux rigidus are limited to joint-destructive procedures (Brewster M, 2010; Gibson & Thomson, 2005; Titchener et al., 2015). For moderate OA that is recalcitrant to non-surgical therapy: cheilectomy, capsular interposition, osteochondral autogenous transplantation for focal defects, joint distraction, periarticular osteotomy, and excision arthroplasty have been utilised (Brewster M, 2010). Arthrodesis (i.e. fusing the joint) is the current gold-standard for end-stage intervention. The literature suggests that success rates are between 95%-100% (De Frino et al., 2002).

Among those treatments associated with hallux rigidus, joint replacement is considered the most controversial (NICE, 2005). Pain relief, functional restoration and maintenance of normal appearance are benefits of joint arthroplasty but the surgery has a marked effect on metatarsal length, reducing bone stock and thus, the ability for surgeons to perform effective revision surgeries (Shankar, N.S., 1995; Barwick and Talkhani, 2008; Kissel, C.G., 2008; Carpenter et al., 2010; Titchener et al., 2015). Aside from the functional benefits of first MTP joint arthroplasty, the UK National Institute for Health and Clinical Excellence (NICE) (2005) have emphasised the poor resilience of contemporary first MTP joint prostheses. Prior to the report published by NICE, the Medical Devices Agency (MDA) (2002) issued an alert for the first-generation ceramic screw-fit implant after 10 months of clinical use.

In contrast to the poor results of first MTP joint replacement, 6.2% and 2.5% of all primary knee and hip replacements were revised at approximately 20 years between 2014 and 2015 in the UK (National Joint Registry, 2015). While proven long-term results for certain joint types have been made available through the National Joint Registry (NJR), the inability to evaluate brand-specific implant outcomes and survival at the population level is an obvious disadvantage in performing first MTP joint replacement. Hence, patients exhibiting this condition do not experience the same level of functional restoration compared with other joints. This emphasises the need to identify etiological factors of hallux rigidus and research standards of care for underappreciated and unrecognised foot burdens.

2.5 Finite Element Modelling of Osseous and Soft Tissue Mechanics in the Foot

Aberrant mechanics play an important role in the pathomechanics of OA. Sections 2.3 and 2.4 showed there is limited understanding of forefoot mechanics and etiological factors in onset and development of hallux rigidus. Although physical testing is essential in the evaluation process, reliable computational predictions, such as those from finite element (FE) modelling, can augment in vivo experiments (Reggiani et al., 2006; Anderson et al., 2008; Wong et al., 2018). Finite element modelling refers to a method of computational simulation which virtually represents a physical problem (Viceconti M, 2005; Henninger et al., 2010). This process is performed by subdividing a geometry into many discretized regions, called finite elements. These regular small 3D elements are governed by constitutive relationships, which collectively represent the larger physical problem. Due to their capability of representing complex systems, FE models are used to simulate, study, and predict a diverse set of problems in biomechanics, ranging from classical structural analysis (e.g. crack propagation in fractures) to surgical outcomes (e.g. stress distribution in soft tissues) (ASME Committee, 2006; Henninger et al., 2010). Some scientists are sceptical of results from FE models. There are no perfect models and no perfect experiments but the real value of FE models in biomechanical applications is that they give the investigator the potential to estimate parameters, such as joint stress, that would not be possible to measure directly in vivo (Viceconti, M 2005).

To reduce scepticism, all models prior to being placed into practice should be verified and validated against physical data (Viceconti M, 2005; Henninger et al., 2010). It is for this reason that models and experiments are inextricably linked. When considering the applicability of FE models, it is important to remember that they are predictive tools that require assessment of validity which is comprised of accuracy and reliability (ASME Committee, 2006; Anderson et al., 2008; Biedokhti et al., 2016; Akrami et al.,

2018). The main challenge in biomechanics is the uncertainty relating to material properties and macro-geometry of biological tissues. Verification and validation of these tools are normally used; ensuring the output is correctly interpreted before its predictions can be considered clinically valuable (ASME Committee, 2006; Henninger et al., 2010).

2.5.1 Finite Element Modelling of the Foot and Ankle

Finite element investigations of the foot have predominantly involved healthy humans and cadaveric specimens (Cheung et al., 2005; Isvilanonda et al., 2012; Wong et al., 2014; Akrami et al., 2018; Wong et al., 2018; Peng et al., 2021). Validation of in vivo models can be obtained from comparisons of measured and predicted plantar pressure distributions (Wong et al., 2014; Akrami et al., 2018). Plantar pressure measurements of the subject are taken during gait, by a dynamic in-sole plantar pressure measuring system or plantar pressure plate (Behforootan et al., 2017). Such validations may be limited by the assumption that predictions of joint kinematics, and internal stress and strain are accurate, without validating for soft-tissue geometries or material properties. Such factors create inherent uncertainty regarding the clinical application of models validated against plantar pressures (Anderson et al., 2008).

Therefore, in vitro techniques are typically employed for physical validation of internal joint contact mechanics (Anderson et al., 2008; Henak et al., 2014; Biedokhti et al., 2016). While this method may provide better information regarding the internal joint contact mechanics, it may also be limited by assumptions associated with body loads, muscle forces, and the technology available to obtain such measurements (Viceconti M, 2005; Anderson et al., 2008; Henninger et al., 2010; Henak et al., 2014; Biedokhti et al., 2016). Thin-film pressure sensors are typically employed to measure joint contact mechanics but are inherently temperamental (Wu et al., 1998). Assumptions such as equilibration, calibration, insertion, and fixation can contribute to errors (Jansson et al., 2013). Moreover, these sensors are known to affect joint congruence and alter joint mechanics (Anderson et al., 2008; Beidokhti et al., 2017), leading to further errors between physical measurements and FE predictions. Table 2 presents an overview of several published foot and ankle FE models.

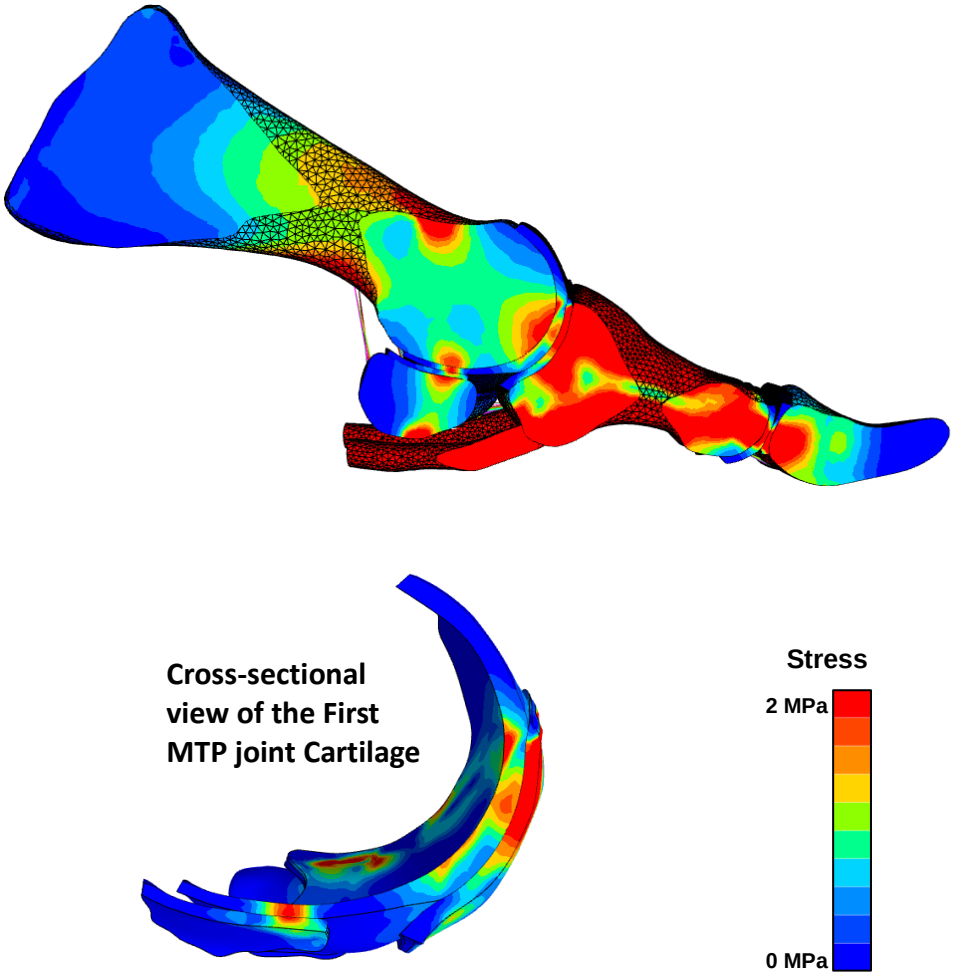

Figure 16. A finite element model of the first ray. The cross-sectional view illustrates the transmission of stress through the virtual first MTP joint articular cartilages, shown from the lateral aspect of a right foot. Predictions of stress are created through simulated physiological loading.

The primary difficulty with studying soft-tissue mechanics in vivo are the potential risks and ethical considerations associated with such invasive measurements (Behforootan et al., 2017). Patient- or specimen-specific models enable the researcher to circumvent these issues (Jacob & Patil, 1999; Gu et al., 2010). Force distributions are calculated to detect biomechanical stress by applying physiological loads (Figure 16) (Imhauser et al., 2008; Flavin et al., 2008). Detailed internal mechanical information provided by FE models enables researchers to non-invasively predict the mechanical behaviour of soft tissues, implants, and surgical outcomes (Cheung et al., 2005; Reggiani et al., 2006; Flavin et al., 2008; Tao et al., 2009). Furthermore, FE modelling has been used to predict excessive joint stress as a potential mechanism of osteoarthritis (Chegini et al., 2008; Mononen et al., 2012; Venäläinen et al., 2016).

Table 2. Overview of relevant, published finite element models of the foot and its associated structures.

Study	Purpose	Model Development		Material Assignment	Loading Conditions		Validation	
		Scan/Subject(s)	Element type(s)	Virtual tissue material model	Simulation	Reference	Type	Source
Nakamura et al., 1981	Predict stress within the plantar soft tissue for a variety of shoe conditions	1 subject (in vitro); 3D	Tetrahedral	Bone, linear elastic; soft tissue, nonlinear elastic	Standing	Bodyweight	None	-
Gefen et al., 2002	Analysis of the biomechanical effects of plantar fascia release on the foot	0.5T MRI; 1 woman (*in vivo*); age, 27; 3D	Hexahedral	Bone/cartilage, linear elastic; fascia/ligaments/soft tissue, nonlinear elastic	Standing	Bodyweight from literature	Indirect	Bone displacement measured during standing
Cheung et al., 2004	Investigate the effect of soft tissue stiffness on plantar pressure distributions	MRI; 1 man (*in vivo*); age, 26; height, 174 cm; weight, 70 kg; 3D	Tetrahedral	Bone/cartilage/ ligaments/fascia; soft tissue, hyperelastic	Standing	Bodyweight	Direct	Plantar pressure
Budhabhatti et al., 2007	Develop a FE model of the first ray as a tool for the design of therapeutic interventions	MRI; 1 man (*in vivo*); 3D	Hexahedral	Bone, rigid; soft tissue, Ogden; cartilage/ligaments/fascia, linear elastic	Toe off	Measured	Direct	Plantar pressure
Isvilanonda et al., 2012	Study the effect of muscle overpull on the formation of the clawed hallux deformity and its surgical treatments	CT & MRI; 1 man (*in vitro*); weight, 823 N; 3D	Tetrahedral & nonlinear, tension-only discrete elements	Bone, rigid body; cartilage, rigid body, ligaments/tendons/fascia, nonlinear elastic; fat pad, linear elastic.	Gait	Literature	Indirect	Plantar pressure

Indirect, derived from the literature or measured from a different specimen or subject from that used to build the model; Direct, measured from the same specimen or subject.

Table 2. (Cont'd) Overview of relevant, published finite element models of the foot and its associated structures.

Study	Purpose	Model Development		Material Assignment	Loading Conditions		Validation	
		Scan/Subject(s)	Element type(s)	Virtual tissue material model	Simulation	Reference	Type	Source
Sun et al., 2012	Analyse stress distributions in the foot resulting from different arch alignments.	CT; 1 man (*in vivo*); age, 24; height, 179 cm; weight, 79 kg; 3D	Tetrahedral & tension-only truss elements	Ligament/bone/soft tissue/cartilage/fascia, linear elastic; Skin/fat pad/muscle, hyperelastic	Standing	Bodyweight	Direct	Plantar pressure
Wong et al., 2014	Predict the effect of first ray hypermobility on foot forces	MRI; 1 woman (*in vivo*); age, 28; height, 165 cm; weight, 54 kg; 3D	Tetrahderal, quadrilateral & hexahedral	Ligament/Bone, linear elastic; soft tissue, hyperelastic	Gait	Gait analysis	Direct	Plantar pressure
Akrami et al., 2018	Development of a foot model, incorporating the cartilage, ligaments, muscle-tendon systems etc.	1.5T MRI; 1 man (*in vivo*); age, 27; weight, 75 kg; 3D	Tetrahedral	Bone/cartilage/plantar fascia/achillies tendon/encapsulated soft tissue, linear elastic; ligament, tension-only truss	Gait and muscle forces	Gait analysis and multi-body modelling	Direct	Plantar pressure
Guo et al., 2018	Evaluation of hallux valgus pre- and post-distal osteotomy	CT; 1 woman (*in vivo*); age, 26; weight, 54 kg; 3D	Tetrahedral	Bone/cartilage/plantar fascia/ligaments/skin, linear elastic; soft tissue, hyperelastic	Standing	Bodyweight	Direct	Plantar pressure

Indirect, derived from the literature or measured from a different specimen/subject from that used to build the model; Direct, measured from the same specimen or subject.

2.6 Gaps in Knowledge

Several gaps in knowledge were identified in the literature review relating to the study of hallux rigidus, first ray hypermobility, foot type biomechanics, and cartilage contact mechanics in the first ray. The subsequent studies conducted in this thesis were designed to address the following research gaps:

Hallux Rigidus

- Insufficient up-to-date population-based age- and sex-related trends in hallux rigidus including etiological factors and groups most at risk.

First Ray Hypermobility

- No standardised, reliable measurement of first ray hypermobility to facilitate robust clinical definition and investigation of associated biomechanical parameters.

Foot Type Biomechanics

- No objective evidence to prove or disprove a connection between foot type and first ray hypermobility.
- Lack of evaluation for relationships between first ray hypermobility, foot structure, and foot function as causes of altered weightbearing beneath the medial forefoot.

First Ray Contact Mechanics

- No study has applied FE modelling to the prediction of first ray contact mechanics in the presence of hypermobility, as a potential mechanism of excessive loading and pathway to hallux rigidus.

Chapter 3. Osteoarthritis in England: Incidence Trends from National Health Service Hospital Episode Statistics

Published in ACR Open Rheumatology: DOI 10.1002/acr2.11071

3.1 Chapter Overview

This first study explored hallux rigidus epidemiology in England compared to OA of the hand, hip, and knee. It examined the population prevalence and incidence trends in National Health Service (NHS) secondary-care records for hallux rigidus, compared with more OA of frequently studied sites in the body, including the first Carpometacarpal (CMC), knee, and hip joints. The objective of this section was to understand if hallux rigidus affects a subset of younger patients, thus emphasising the potential for conditions such as, first ray hypermobility to contribute to disease onset.

Aim 1: Investigate the population prevalence and incidence of hallux rigidus compared with osteoarthritis of the hand, hip, and knee in England.

Hypothesis 1: Hallux rigidus will demonstrate increased population prevalence over time and comparable incidence to osteoarthritis of the hand, hip, and knee.

3.2 Introduction

Osteoarthritis affecting the foot was included in early descriptions of the generalised disease, circa 1990, yet subsequent epidemiological research has focused on the hand, hip, and knee (Van Saase et al., 1989; Roddy and Menz, 2018). The public health needs related to hallux rigidus, which is considered the most common form of OA in the foot (Van Saase et al., 1989), are unclear due to a lack of population representative samples in contemporary research. Up-to-date population-based sources are needed to better approximate the sex-ratios and age-distributions of

patients with hallux rigidus in England and the potential burden posed to the NHS. To address these gaps in knowledge, the NHS Hospital Episode Statistics (HES) database was reviewed to ascertain population prevalence and incidence trends in hallux rigidus compared to first CMC, hip, and knee joint OA by sex and age between 2000/01 and 2017/18.

3.3 Materials and Methods

Aggregate data for English NHS patients were derived from HES between 2000/01 and 2017/18, made publicly available through the National Archives (http://www.webarchives.nationalarchives.gov.uk). The HES database (governed by the Department of Health and Social Care) stores records for all NHS England-related admissions within a given fiscal year. It covers care delivered in treatment centres (including the independent sectors) funded by NHS England, episodes of care in England for non-British residents, and privately funded patients treated within NHS England hospitals. Each record in the database is associated with a 'finished consultant episode'. This refers to the duration a patient has spent under the care of a hospital consultant (board certified specialist). The HES database was accredited as a national statistic in 2008 and has been validated for research purposes (Thorn et al., 2016). The HES records included were those with the International Classification of Disease (ICD-10) codes M16 (arthrosis of the hip), M17 (arthrosis of the knee), M18 (arthrosis of the first CMC joint), and M20.2 (hallux rigidus). The information associated with these ICD-10 codes included the total number of diagnoses, sex, and age. Age was calculated for all cases in the HES dataset, which did not discriminate between men and women. English population data for 2000/01-2017/18 were obtained from the Office for National Statistics UK (ONS UK) (www.ons.gov.uk).

3.3.1 Statistics

Descriptive statistics were used to report the distribution of hallux rigidus, first CMC, hip, and knee joint OA, including totals and percentages (%). Population prevalence

and incidence trends were computed in Joinpoint v4.7.0.0 (www.surveillance.cancer.gov/joinpoint). Joinpoint is a publicly available statistical software that uses regression functions to test whether a change in trend over time is statistically significant. The software provides a summary measure of trend over time by calculating the Average Annual Percent Change (AAPC), using the weighted average of the slope coefficients of the regression line with the weights equal to the length of each segment over a predetermined time-period. A 95% Confidence Interval (CI) is then computed, based on the normal distribution of AAPC.

Population prevalence and incidence trends in OA were estimated in Joinpoint per 100,000 population in England, stratified by sex and age. The numerator for estimates by sex included each finished consultant episode divided into groups for pooled, men, and women, while the denominator comprised the total English population in each calendar year. The numerator for estimates by age included each finished consultant episode within the defined age-groups while the denominator comprised the population of each age-group for the same calendar year. A *p*-value of <0.05 was used to indicate statistical significance. Sex-stratified incidence of OA were compiled for the entire 17-years reviewed in this study; however, calculations stratified by age were made using data from the most recent six-years due to limitations of the HES age classification system prior to 2012/13. Before this period, patient age was reported within a large range for example, patients aged 15-59-years-old were calculated as a single group. Such grouping would have biased the age-stratified incidence calculations of OA, therefore data before 2012/13 were excluded from the regression analyses. The concurrent age boundaries used were those provided in the HES database.

3.4 Results

3.4.1 Distribution of Osteoarthritis (2000/01-2017/18)

During 2000/01-2017/18, there were a total of 3,143,928 patients presenting with OA. Based on this data, knee OA represented the greatest proportion of patients. Distribution of OA was higher among women for all joints examined (Table 3).

Table 3. Total joint-specific OA diagnoses, 2000/01-2017/18.

	Joint			
	First MTP	**First CMC**	**Hip**	**Knee**
All (N)	60,986	88,178	1,222,446	1,772,318
Men	32%	24%	39%	43%
Women	68%	76%	61%	57%

3.4.2 Sex-Stratified Incidence of Osteoarthritis (2000/01-2017/18)

Estimated OA incidence increased significantly from 2000/01-2017/18 for every joint. Similar trends for hallux rigidus, hip, and knee OA were observed. The first CMC joint demonstrated comparatively higher increases (Table 4). Over more recent years, hallux rigidus and knee OA experienced a stabilisation in diagnoses. The incidence of hallux rigidus was significant from 2000/01-2010/11 [6.6% (5.5, 7.7)]. After this time, no significant change occurred [-0.1% (-1.5, 1.4)]. Knee OA demonstrated significant increases until 2007/08 [6.7% (5.1, 8.4)], after which time no significant change was estimated [0.3% (-0.3, 1.1)]. Incidence of hip OA continued to rise significantly until 2014/15 [4.5% (4.0, 5.1)]; this increase was not significant from 2015/16 [0.3% (-4.2, 5.1)] onwards. Estimated incidence of first CMC joint OA was significant throughout the 17 years reviewed (Figure 17).

Table 4. Incidence[a] of joint-specific OA stratified by sex, 2000/01-2017/18.

	Joint			
	First MTP	**First CMC**	**Hip**	**Knee**
All	3.8% (3.0, 4.6)*	10.9% (10.1, 11.7)*	3.8% (2.9, 4.7)*	2.9% (2.2, 3.6)*
Men	3.6% (2.8, 4.5)*	11.9% (10.7, 13.2)*	4.3% (3.2, 5.5)*	2.7% (2.0, 3.4)*
Women	3.9% (3.0, 4.7)*	10.7% (9.8, 11.7)*	3.8% (2.9, 4.7)*	3.1% (2.3, 3.8)*

Statistically significant results (p-value ≤0.05) are indicated by *.

[a]In the joinpoint regression analysis, AAPC (%) and 95% CI in crude rates per 100,000 population were used.

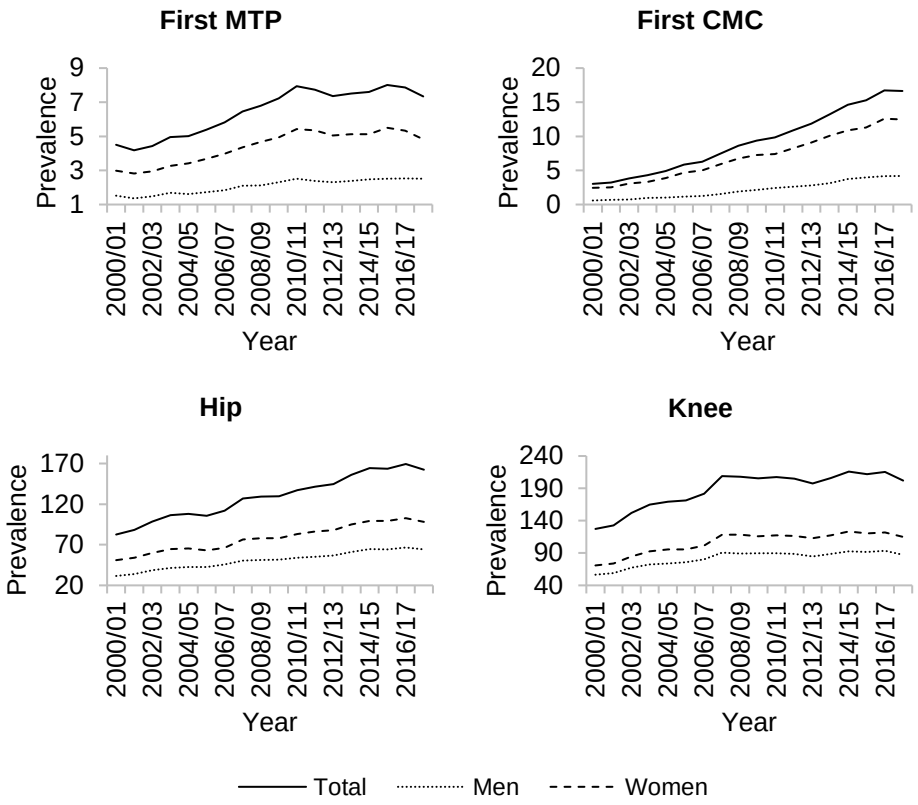

Figure 17. Population prevalence of joint-specific OA per 100,000 English population, 2000/01-2017/18.

Table 5. Incidence[a] of joint-specific OA stratified by age, 2012/13-2017/18.

	Joint			
	First MTP	**First CMC**	**Hip**	**Knee**
Age Group				
25-34	-0.6% (-11.4, 11.6)	6.7% (-9.1, 25.3)	2.3% (1.5, 3.2)*	-6.1% (-11.0, -0.9)*
35-44	-4.6% (-10.1, 1.2)	1.7% (-0.9, 4.5)	2.9% (1.1, 4.8)*	-7.4% (-12.1, -2.4)*
45-54	3.8% (-0.3, 8.0)	6.6% (2.2, 11.2)*	4.2% (1.8, 6.7)*	-2.1% (-5.0, 1.0)
55-64	-2.8% (-4.0, -1.7)*	5.8% (3.8, 7.8)*	1.9% (-0.1, 4.9)	-0.3% (-2.6, 2.2)
65-74	-0.2% (-2.8, 2.5)	5.2% (2.3, 8.0)*	-0.5% (-2.5, 1.6)	-0.8% (-2.8, 1.3)
75+	4.9% (1.0, 8.9)*	7.8% (4.4, 11.3)*	0.9% (-1.7, 3.6)	-0.7% (-1.7, 3.2)

Statistically significant results (p-value ≤0.05) are indicated by *.

[a]In the joinpoint regression analysis, AAPC (%) and 95% CI in crude rates per 100,000 population were used.

3.4.3 Age-Stratified Incidence of Osteoarthritis (2012/13-2017/18)

The distribution of knee and hip OA across age exhibited a single peak at the 70-74-year-old group. This distribution was bimodal for the first MTP and first CMC joints. Peaks at the 50-54- and 65-69-year-old groups were observed for the first MTP joint and 55-59- and 65-69-year-old groups for the first CMC joint (Figure 18). Between 2012/13 and 2017/18, a statistically significant decline in hallux rigidus was estimated in the 55-64-year-old group. There was a significant rise in the incidence of patients who were 75+-years-old. The 45-54-year-old group also exhibited an increasing trend of OA though this was not significant. The incidence of first CMC joint OA was significant in the 45-54-year-old group and older. There were also significant increases in the incidence of younger patients presenting with hip OA. Conversely, there were significant declines in the number of younger patients presenting with knee OA (Figure 18; Table 5).

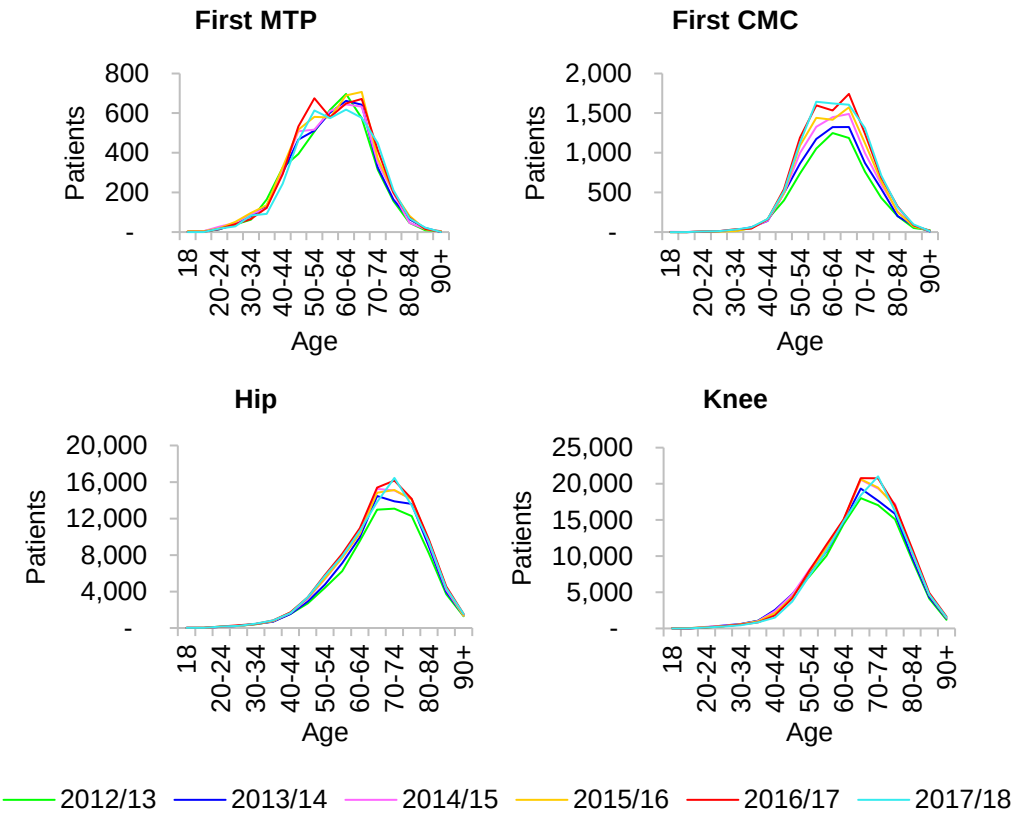

Figure 18. Distribution of joint-specific OA by age group, 2012/13-2017/18.

3.5 Discussion

The present study estimated significant increases in the incidence of hallux rigidus, first CMC, hip, and knee joint OA over a 17-year period in England. Consistent with the study hypothesis, the incidence rate of hallux rigidus was similar to that of the hip and knee. Although women comprised the largest proportion of diagnoses, greater incidence in first CMC and hip joint OA were estimated among men. Hip OA represented the highest growth among younger patients while the first CMC joint had the highest overall incidence. Older patients (75+-year-old group) with hallux rigidus and first CMC joint OA represented the fastest growing population. A significant rise in the total number of patients with knee OA was estimated from 2000/01-2017/18, however, there was a higher incidence of hallux rigidus over the same time-period. Moreover, the hip and knee presented unimodal age distributions at 70-years-old while hallux rigidus presented with bimodal peaks at 50 and 60-years-of-age. This suggests a pathway to hallux rigidus in younger years other than wear and tear that is typical of OA.

The current findings were within the range of UK-based estimates of OA (Yu et al., 2015; Yu et al., 2017). A large study by Yu et al., (2015) found a higher proportion of women were diagnosed with OA. The trend toward declined hip and knee OA later in life was also comparable to the current results, as was a plateau in diagnoses for the knee since 2008/09. However, previous estimates of increased knee OA among 35-44-year-olds were not in agreement with this study. This difference can be attributed to the prior analysis of local-level data from 1992-2013 compared with the present regression analyses of national-level data beginning 2012/13.

Incidence of OA in England was also consistent with global trends (Kurtz et al., 2009; Prieto et al., 2014; Kiadaliri et al., 2019). Analysis of a secondary-care database from Sweden found that population growth and ageing accounted for just one-third of patients presenting with OA, suggesting these factors do not fully explain increased incidence of the disease (Kiadaliri et al., 2019). Kiadaliri et al., (2019) postulated that while hip OA constituted the highest proportion of patients in Sweden, knee OA could surpass the hip in coming years. In contrast, the present data suggests that incidence of knee OA has stabilised in England and may be overtaken by the hip, if current trends are maintained.

An increasing trend toward younger patients diagnosed with hip OA may align with the adoption of a healthier lifestyle in modern society and the role this may play in femoroacetabular impingement, as a precursor to hip degeneration in young adults (Chegini et al., 2008; Tannast et al., 2008; Wyles et al., 2017). Highly active patients with features of femoroacetabular impingement may place greater than normal stress on their hips, leading to mechanical damage at an early age (Wyles et al., 2017). The potential for early onset OA in young adulthood can have serious implications on quality of life and the efficacy of conventional treatment strategies; thus, this finding warrants further investigation.

While population-level data for risk factors associated with hand, hip, and knee OA are well documented (Van Saase et al., 1989: Felson et al., 2000), there is sparse evidence with respect to the first MTP joint, which has largely been excluded from OA-based epidemiology research (Roddy & Menz, 2018). The frequency of hallux rigidus, which had equal numbers to first CMC joint OA and higher incidence than the knee, emphasises the need for well-conducted epidemiological studies of the first MTP joint to guide the design of future research. Though long-term results of joint replacement for the hip and knee have been made available through the National Joint Registry, the inability to evaluate brand-specific first MTP joint implant outcomes and survival at the population level is an obvious shortcoming in this data. Such information would be especially useful for the evaluation and design of next generation joint replacements. Current versions of the technology for this joint yield unpredictable results and unreliable longevity.

Most relevant to the present thesis was an observed bimodal age-distribution of hallux rigidus, which likely resulted from differences in primary and secondary pathways of disease. The specific reasons are unclear, but may reflect multiple factors, such as better diagnostics, improvements in referral to secondary care, a change in healthcare seeking behaviour among certain age groups, differences in joint injury/trauma, (Allen et al., 2015) occupation, longevity of modern careers (Felson et al., 2000), and aberrant biomechanics of the foot in younger patients. Additional studies of patient demographics and populations are required to explore these potential risk factors in more depth. The following chapters of this thesis will, however, investigate abnormal

biomechanical parameters of the foot which have been hypothesised as etiological factors in hallux rigidus onset and development.

3.5.1 Limitations

Some limitations must be considered when interpreting the results of this study. We were unable to account for body mass index (BMI), height, or other patient characteristics from the available data. Furthermore, utilisation of secondary-care data should be cautiously interpreted. While it reflects a large dataset, across extended time-periods, it may reflect biases due to under- or over-recording practices for conditions incentivised by the General Medical Services, as well as variable coding quality between different NHS trusts. However, the application of these large and population representative samples, which have been validated for use and maintained across recent timeframes, enabled comprehensive evaluation of temporal trends in OA.

3.6 Conclusion

In conclusion, the current study provided up-to-date population data for OA in England across 17 years. Highlighting the burden that hallux ridigus represents in England, with comparative data from the hand, hip, and knee, emphasises the urgent need for future research into causal factors, modes of diagnosis, surgical outcomes, and standards of care for under-appreciated and under-recognised foot burdens at the population-level. Identification of a younger subset of patients presenting with hallux rigidus underscores the importance of exploring biomechanical pathways which my initiate degenerative changes in the first MTP joint. As discussed in the literature review of this thesis, many possible etiological factors have been dismissed due to a lack of convincing evidence, yet the role of first ray hypermobility remains enigmatic. The following chapters will investigate the influence of first ray hypermobility on structural and functional parameters of the foot, which may be indicative of aberrant and potentially harmful biomechanics.

Chapter 4. Design and Reliability Testing of a Novel Device to Measure First Ray Mobility

Foot structure and function assessment device and methods of using the same: Patent No. PCT/US21/22791, March 2021

Published in Foot and Ankle International: DOI 10.1177/10711007211020345

4.1 Chapter Overview

This chapter describes the design and intra- and inter-rater reliability testing of a new device to measure first ray mobility, named MAP1st. The device was designed to be simple and efficient for use in clinic. The objectives of this chapter were to: 1) describe the design of MAP1st; 2) establish the intra- and inter-rater reliability (Intra- and Inter-Class Correlation (ICC) coefficients) of measuring first ray mobility with MAP1st, and; 3) compare the reliability of first ray mobility measurements made with MAP1st to those using a commercially-available, handheld device.

Aim 2: Design and prototype a novel device for measuring first ray mobility.

Hypothesis not required for technical design and development.

Aim 3: Test the reliability of the novel device for measuring first ray mobility, compared with a commercially available, handheld ruler.

Hypothesis 3a: First ray mobility in ***non-weightbearing (prone) subjects*** will exhibit test-retest and remove-replace reliability (ICC (2,1) > 0.7) within and between raters using a commercially available handheld ruler.

Hypothesis 3b: First ray mobility in ***partial weightbearing (seated) subjects*** will exhibit test-retest and remove-replace reliability (ICC (2,1) > 0.7) within and between raters, using MAP1st.

Hypothesis 3c: First ray mobility in ***weightbearing* (*standing) subjects*** will exhibit test-retest and remove-replace reliability (ICC (2,1) > 0.7) within and between raters, using MAP1st.

4.1.1 Design Contributions

MAP1st was developed by an interdisciplinary team of engineers, scientists, and clinicians. The thesis author was the primary contributor to the development process, iteratively designing concepts in CAD with feedback from the wider scientific and clinical team. Once finalised, the concept design was passed to an independent contractor for manufacture (Jaktool Engineered Solutions, Cranbury, NJ).

4.2 Introduction

Quantifying first ray mobility is crucial to understand aberrant foot biomechanics and first ray hypermobility as a potential correlate of hallux rigidus. Several investigators have hypothesised that first ray hypermobility, which refers to abnormal first ray mobility while the forefoot is bearing weight, (Root et al., 1977) plays a role in various pathologies of the foot (King & Toolan, 2004; Coughlin & Jones, 2007; Cooper et al., 2009; Rao & Bell, 2013; Golightly et al., 2018). While numerous clinical methods are used to assess mobility of different joints, none have been standardised for structures below the knee. The lack of a standardised and reliable technique for measuring first ray mobility has hindered research into aberrant foot biomechanics imposed by hypermobility.

Therefore, MAP1st was developed to objectively measure mobility of the first ray. Measurements of first ray mobility can be performed in either partial- or full-weightbearing conditions normalised to foot length. The study's aim was to test the intra- and inter-rater reliability of MAP1st compared with a commercially available handheld ruler. The handheld device (humanlocomotion.org) was selected to recreate the clinical exam reported by Voellmicke and Deland, (2002) with the addition of a ruler to quantify first ray displacement. MAP1st design specifications were to: (1) measure sagittal mobility of the first ray; (2) allow the foot to be placed in user specified

orientations; (3) be portable, and; (4) require no more than two minutes for examination. Establishing the reliability of this device for future clinical use was paramount and was established by performing assessments with two raters: a qualified physiotherapist and an experienced research scientist.

4.2.1 Description of the Device

The design was drafted in SolidWorks (SolidWorks version 2018, Dassault Systèmes, Vélizy-Villacoublay, France) (Figure 19). The finalised Computer Aided Design (CAD) model was prototyped by Jaktool. MAP1st was implemented as a pair (left and right). The base was configured from two upper and lower aluminium base plates, and four polycarbonate side panels which housed the electronic components and circuitry. The upper base plate acts as a platform for the foot. The head of the first metatarsal is placed against an aluminium block with a delve for repeatable positioning. A heel cup is used to accommodate the rearfoot, which is adjustable for foot length in the AP directions. Located at the medial border of the foot is a ruler used to quantify truncated foot length (TFL). This measurement enables normalisation of first ray mobility relative to the size of the subjects foot. The heel is not constrained, giving the user a choice to place the foot either in subtalar joint neutral (STJN) or resting calcaneal stance position (RCSP). At the anterior border of the device is an auto-adjustable toggle clamp (Bessey STC-HH, Bessey Tools, Bietigheim-Bissingen, Germany), to mechanically ground the second metatarsal head. The clamping force is set to 110 N. The toggle clamp includes a quick release handle, enabling the subject to remove their foot at any time during examination. The toggle clamp base is screwed to an aluminium block with a dove tail joint, allowing for ML translation to accommodate different foot widths. While using the device, the subject's foot is unconstrained to enable assessments in user-defined alignments of the foot-ankle complex. In addition, measurements of first ray mobility can be performed in either partial- or full-weightbearing conditions and be normalised to foot length.

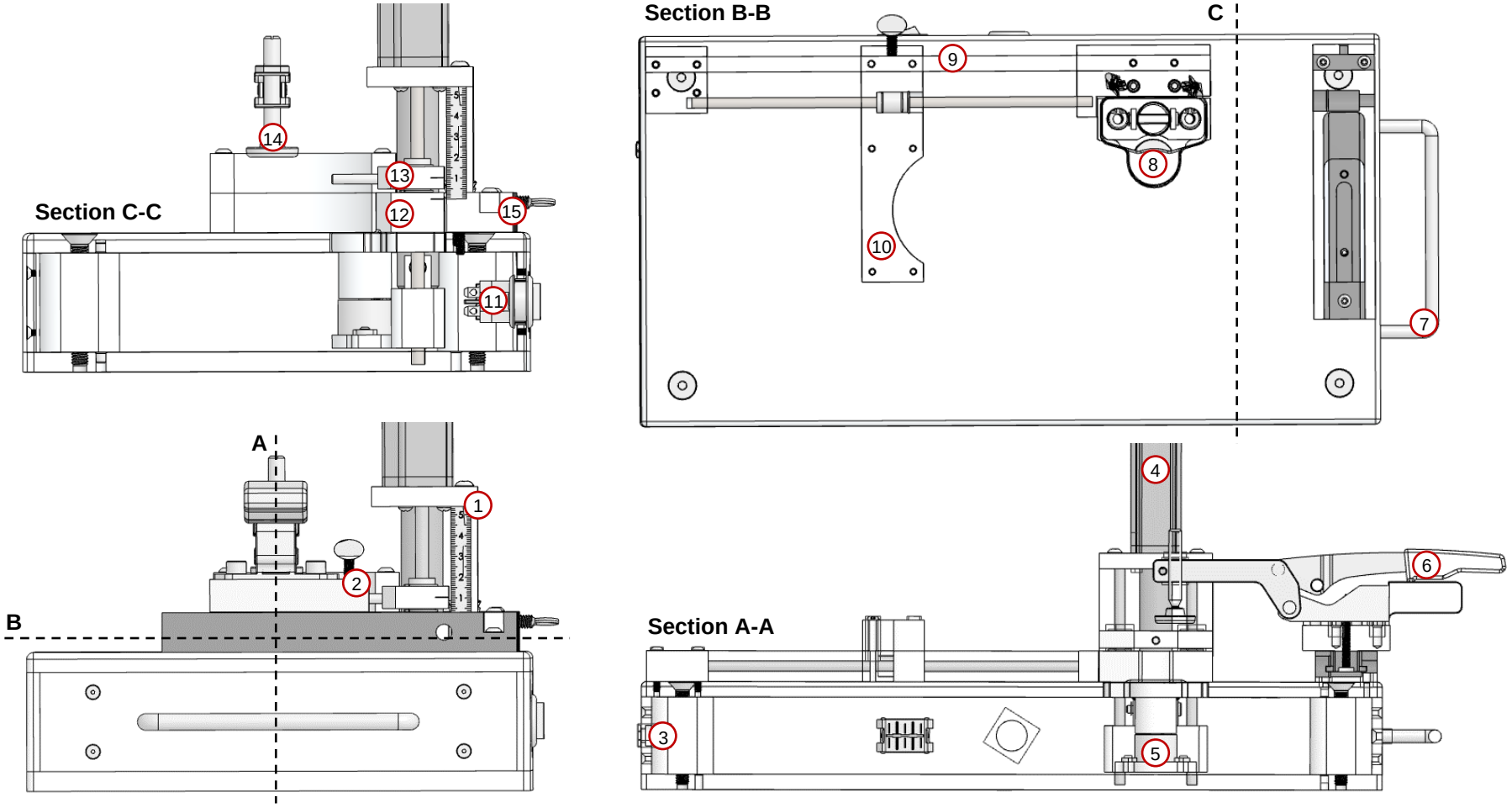

Figure 19. SolidWorks (Dassault Systèmes, Vélizy-Villacoublay, France) illustration of a right-sided MAP1st design. Illustrations showing a lateral view (Section A-A), superior view (Section B-B), and anterior view (Section C-C). Component labels include: (1) mobility graticule; (2) second metatarsal clamp locking screw; (3) charging port; (4) linear actuator; (5) load cell; (6) quick release handle of second metatarsal clamp; (7) handle; (8) first metatarsal plunger; (9) heel cup rail and foot length graticule (ruler markings not shown in this design); (10) heel cup; (11) DP-DT rocker switch; (12) first metatarsal plunger stock; (13) first ray mobility pointer; (14) second metatarsal clamp head, and: (15) heel cup locking screw.

Measurements of first ray mobility are driven by a linear actuator (Premium Linear Actuator, Firgelli Automations, Ferndale, Washington, USA) (Figure 20). The top of the linear actuator stroke is connected to a load cell beneath the first metatarsal head. This platform, which acts as a plunger, is attached to two cylindrical pillars fitted with linear bearings for frictionless SI translation. The force set point is controlled by a negative feedback servo using a compression load cell and amplifier (FC22 Compression Load Cell, TE Connectivity, Schaffhausen, Switzerland). An Arduino Uno microcontroller (Arduino Uno, Arduino, Somerville, Massachusetts, USA), powered by 12 volts dc, implements the force servo required for measurement of first ray mobility. Recharging is enabled by an AC-DC converter. Powering the circuitry and recharging are mutually exclusive by use of a double pole-double throw switch.

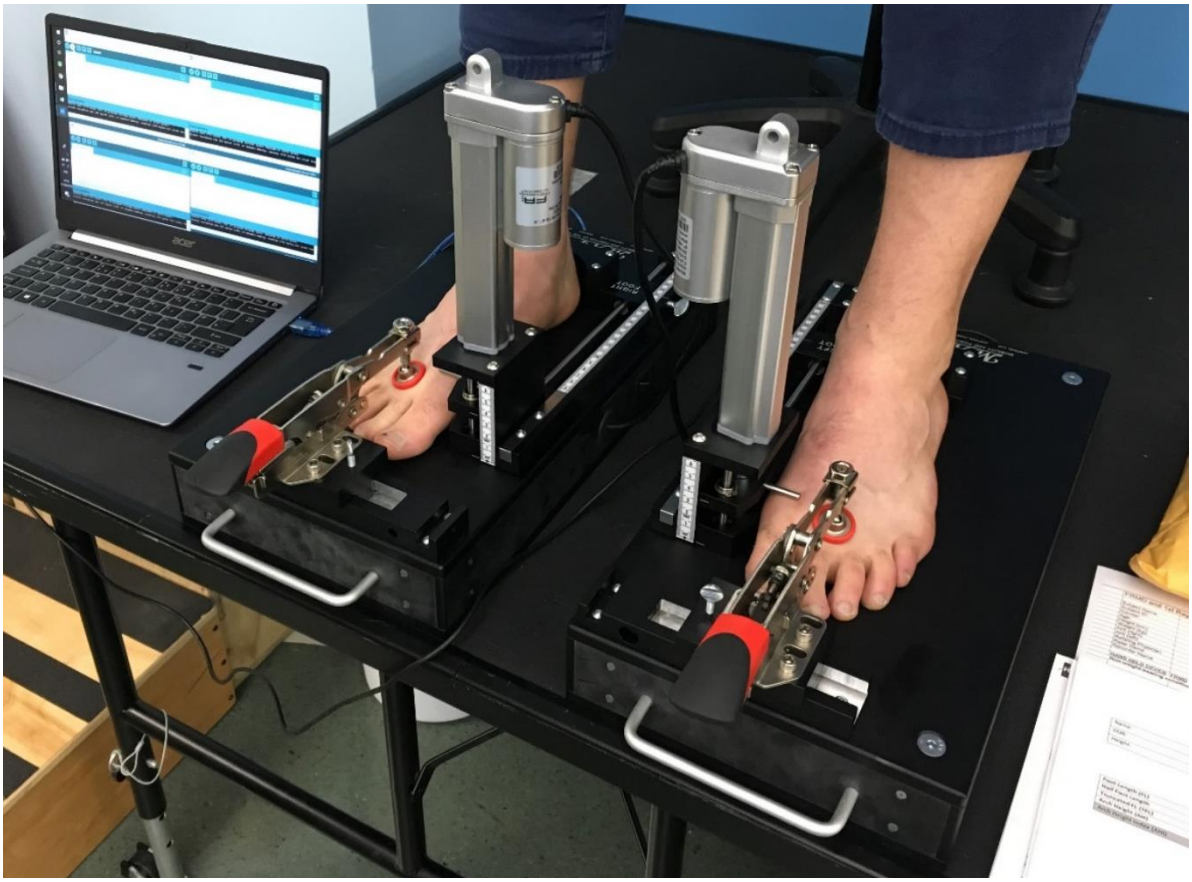

Figure 20. MAP1st (left and right) prepared for testing, with each of the subjects feet positioned and clamped in the device. The Arduino microcontrollers of each device are plugged into a laptop to interface the custom-written code for upload and testing. The programme was written to apply cyclic loads of 25 N to control for the recent strain history of the first ray soft tissues.

4.3 Materials and Methods

The study included 25 planus feet (N = 50 feet). Each participant was consented by the project research coordinator. Potential subjects were recruited from any willing individual who met the study inclusion/exclusion criteria in Table 6. Participant characteristics are shown in Table 7. All procedures were approved by the Hospital for Special Surgery (HSS) Institutional Review Board. Testing was performed at the Leon Root, MD, Motion Analysis Laboratory at HSS, where each subject was consented before testing.

Table 6. Inclusion/exclusion criteria for healthy and hallux rigidus subjects enrolled in the study.

Recruitment Criteria	
Inclusion	***Exclusion***
• Adults over the age of 21 years old	• Individuals without the capacity to consent and/or understand procedures of the study
• Male or female	• Hallux valgus
• No substantial pain within the lower extremity that could affect ability to walk	• Rheumatoid arthritis, osteoporosis, or any other degenerative disease of the lower limb
	• Significant cardiovascular disease or any pathology that would affect one's ability to walk independently
	• Limb length discrepancy greater than 1-cm

Table 7. Participant characteristics.

Characteristics	
Feet	50
Sex	
Male	15
Female	10
Mean age ± SD (years)	36 ± 13
Mean height ± SD (cm)	174 ± 12
Mean weight ± SD (kg)	76 ± 13
Mean BMI ± SD (kg/m^2)	25 ± 3

4.3.1 Measures of First Ray Mobility

Prior to first ray mobility measurements with MAP1st, ten successive 25-N loading cycles were used to control the soft tissue recent strain history (Woo et al., 1981). The procedure for recent strain history control spanned approximately, 60 seconds. First ray mobility measurements were taken from the dorsal aspect of the first metatarsal head. To quantify the first ray mobility, a vertical steel rod was positioned at the dorsal aspect of the first metatarsal head (Figure 21A). The measurement of first ray mobility was defined as the linear displacement of the first metatarsal head, on a graticule (Figure 21B), after 50-N of load. Glasoe et al., (2000) previously found that 50 N may fully translate the first metatarsal without causing discomfort to the test subject, showing that mobility measurements were only valid compared to x-ray-based measurements when first ray load did not exceed 55 N. Two methods of measurement were performed with MAP1st: 1) linear displacement of the first ray (FRM), given in mm, and; 2) linear displacement normalised by TFL to provide a first ray mobility Index (FRMI) for measurements relative to foot size, using the following equation:

$$\mathrm{FRMI} = \frac{\text{Dorsal First Metatarsal Height}_{50N} - \text{Dorsal First Metatarsal Height}_{0N}}{\text{TFL}} \quad (1)$$

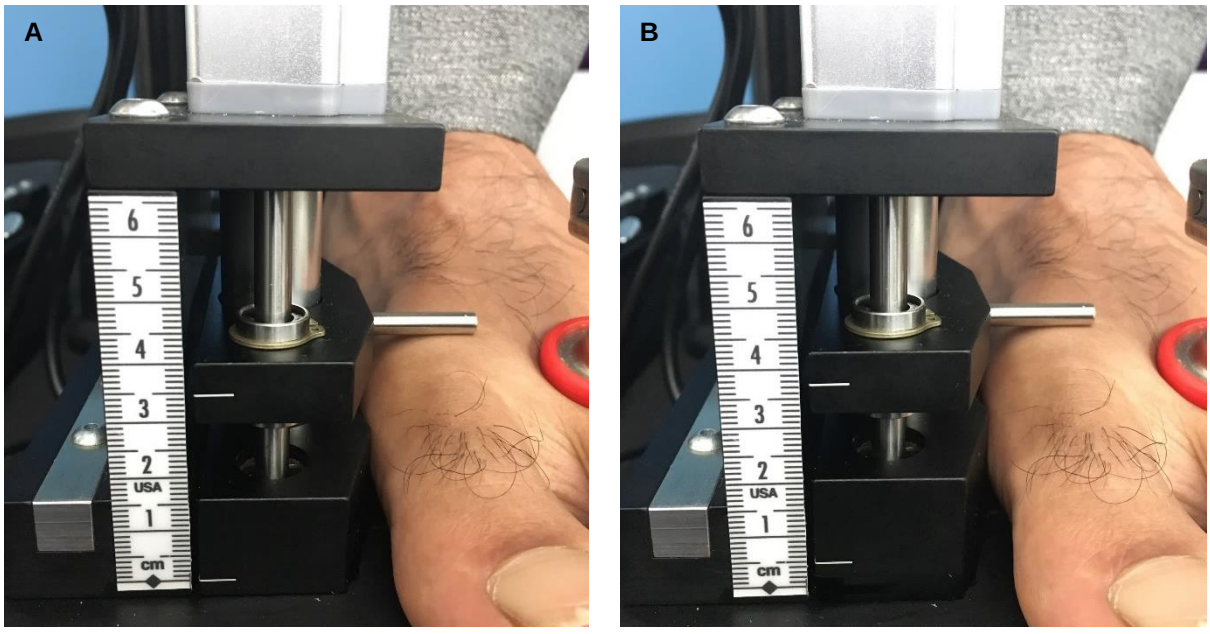

Figure 21A-B. Photographs of MAP1st: (A) Metatarsal head height with 0 N applied, and; (B) Metatarsal head height with 50 N applied to measure first ray mobility. The upper indicator (located at the dorsal aspect of the first metatarsal head) can be seen to displace by 2.5 mm from its initial position (A) to its loaded position (B).

First ray mobility, using MAP1st, was measured while the subjects were seated (i.e. lower extremity positioned in 90° of hip and knee flexion) and standing (i.e. hip-knee-ankle in 0° alignment) (Figure 22A). The ankle was placed in a neutral alignment for both partial- and full-weightbearing measurements (Grebing & Coughlin, 2004). The influence of foot placement was also assessed by taking measurements in Subtalar Joint Neutral (STJN) and Resting Calcaneal Stance Position (RCSP). Subtalar joint neutral may be defined as an alignment of the foot such that it is neither pronated nor supinated. Resting calcaneal stance position may be defined as a relaxed position of the foot with the medial longitudinal arch in its natural weightbearing alignment. To perform the measurements of first ray mobility, an independent recorder viewed MAP1st's graticule with their aiming eye, in a perpendicular orientation, to avoid parallax error and recorded dorsal displacement.

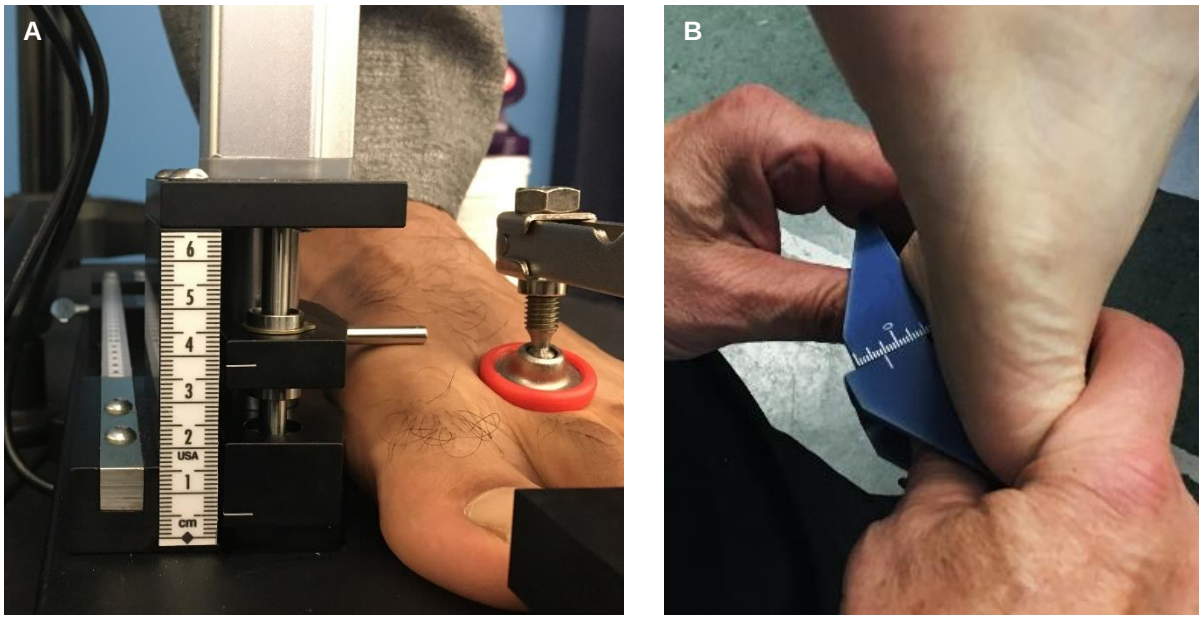

Figure 22A-B. (A) MAP1st measuring first ray mobility while the subject is seated (partial weightbearing) and standing (weightbearing); (B) The handheld ruler used to measure first ray mobility from the plantar aspect of the first metatarsal head while the subject is prone.

Measurements of first ray mobility using the handheld ruler were taken from the plantar aspect of the first metatarsal head, while the subjects were prone, on a flat treatment table. Their hip-knee-ankle was in a 0° alignment (Figure 22B). The ankle was neutrally positioned, which has been shown to produce more reliable measures of first ray mobility (Grebing & Coughlin, 2004). The subject's feet were placed in STJN during assessment with the handheld device. One side of the device was placed beneath the

second metatarsal head and the other side beneath the head of the first metatarsal, adjacent to the opposing components surface. Superior translation (mm) was then measured by applying a manual force to the first metatarsal head, viewing the ruler with respect to the second metatarsal head.

4.3.2 Statistics

Two independent raters (rater one, physiotherapist: Robert Turner, PT; rater two, biomedical engineer: Howard J Hillstrom, PhD), performed the measurements (baseline (first measurement), test-retest (measurement repeated twice), and remove-replace (initial measurement taken and repeated after the rater has removed and replaced the foot in the device), permitting estimation of intra- and inter-rater reliability for the test-retest and remove-replace assessments. Raters with both clinical and scientific backgrounds were selected to demonstrate the application of MAP1st in different research and clinical settings. Descriptive statistics were used to report means, Standard Deviations (SD), and Standard Error of Measurements (SEM). Intra- and inter-class correlation coefficients for test-retest and remove-replace reliability were computed for each rater in SPSS (SPSS version 26, IBM, Chicago IL, USA). This reliability study employed two raters, who were considered to be representative of the pool of all raters. Every subject was evaluated by each rater and hence, an ICC (2,1) model was employed as described by Shrout and Fleiss, (1979). The ICC (2,1) may be computed as:

$$\mathrm{ICC}\ (2,1) = \frac{\mathrm{BMS}-\mathrm{EMS}}{\mathrm{BMS}+(\mathrm{k}-1)\mathrm{EMS}+\mathrm{k}(\mathrm{JMS}-\mathrm{EMS})/\mathrm{n}} \quad (2)$$

where, n is the number of subjects, k is the number of raters evaluating each subject, BMS is between subject mean square error, EMS is the residual error, and JMS is the within subject between rater mean square error. All ICC parameter calculations were performed using the method of absolute agreement. Furthermore, 95% CI's for each ICC estimate were computed as well as the SEM. Data for reliability assessments were analysed for the intra- and inter-rater conditions. Bland-Altman (B&A) plots were constructed to determine if fixed biases or substantial outliers were present between the trials of each rater. This method compared the differences and 95% confidence

intervals (CI) (estimated as 1.96 times the standard deviation (SD)) for the inter-rater measurements of mobility (Bland and Altman, 1983). The 95% CI, which B&A termed the 'limits of agreement', assumes that the individual paired differences of the two raters are normally distributed.

4.4 Results

4.4.1 MAP1st

Linear regression of partial weightbearing RCSP measurements for FRM vs. FRMI with MAP1st demonstrated an R^2 of 0.95 for rater 1 and R^2 of 0.93 for rater 2 (Figure 23A-B). Full weightbearing measurements of FRM vs. FRMI exhibited an R^2 of 0.98 for both raters (Figure 23C-D). Excellent intra-rater ICC values (≥0.93) were obtained for test-retest conditions for FRM. Remove-replace conditions demonstrated lower intra-rater ICC values. The inter-rater reliability for the RCSP weightbearing condition yielded an ICC of 0.52 which was greater than the handheld device (Table 8). Sample B&A plots for inter-rater reliability exhibited biases of 2.88 mm for partial weightbearing STJN, 0.05 mm for weightbearing STJN, 0.28 mm for partial weightbearing RCSP, and -0.68 mm for weightbearing RCSP (Figure 24A-D). The limits of agreement were typically inclusive of 95% of the mean differences for all conditions. Good to excellent intra-rater ICC values (≥0.85) were obtained for test-retest conditions of FRMI. Remove-replace reliability demonstrated lower intra-rater ICC's for all but one condition. The inter-rater reliability for the RCSP partial weightbearing and weightbearing conditions yielded ICC values of 0.58 and 0.57, respectively (Table 9). Sample B&A plots for inter-rater reliability exhibited biases of -1.16 for partial weightbearing STJN, 0.01 for weightbearing STJN, 0.00 for partial weightbearing RCSP, and 0.04 for weightbearing RCSP (Figure 24E-H). Similar to FRM measurements, the limits of agreement were typically inclusive of 95% CI of the mean differences for all conditions.

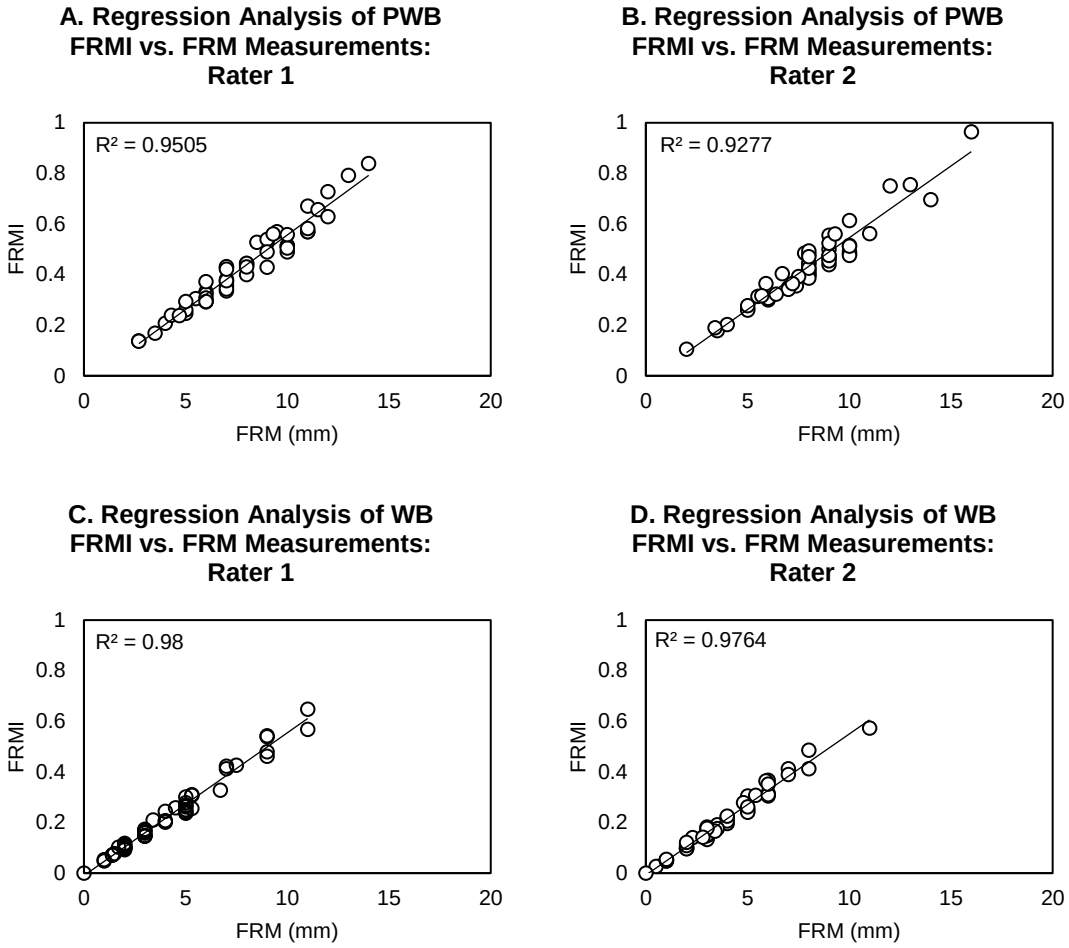

Figure 23A-B. Regression analyses of FRM versus FRMI measurements of first ray mobility for partial weightbearing (A) rater 1, (B) rater 2 and full weightbearing (C) rater 1, (D) rater 2.

4.4.2 Handheld Ruler

Despite good to excellent intra-rater ICC values for test-retest (≥0.88) and remove-replace (≥0.86), the inter-rater reliability was poor at 0.06, when using the handheld ruler (Table 8). The B&A plots for inter-rater reliability showed that the handheld ruler presented a bias of -1.26 mm with the limits of agreement spanning -5.54 mm to 3.49 mm (Figure 24I).

Table 8 Mean, standard deviation, SD, SEM, intra- and inter-rater reliability calculated using linear measurements of first ray mobility (FRM (mm)).

Measurement			Raw measurement		Intra-rater (test-retest)			Intra-rater (remove-replace)			Inter-rater		
			Rater 1	Rater 2	Rater	ICC (2,1)	95% CI	Rater	ICC (2,1)	95% CI	Trial	ICC (2,1)	95% CI
First Ray Mobility	FRMD NWB	Mean ± SD (mm)	5.9 ± 1.7	4.6 ± 1.5	1	0.91	0.84, 0.95	1	0.89	0.82, 0.94	1	0.06	-0.15, 0.28
		SEM	0.23	0.21	2	0.88	0.79, 0.93	2	0.86	0.77, 0.92			
	MAP1st PWB (STJN)	Mean ± SD (mm)	10.4 ± 3.3	8.0 ± 3.0	1	0.97	0.94, 0.98	1	0.82	0.71, 0.89	1	0.32	0.02, 0.56
		SEM	0.46	0.41	2	0.97	0.94, 0.98	2	0.88	0.79, 0.93			
	MAP1st PWB (RCSP)	Mean ± SD (mm)	7.8 ± 2.6	7.7 ± 2.3	1	0.93	0.88, 0.96	1	0.73	0.58, 0.84	1	0.33	0.06, 0.55
		SEM	0.37	0.31	2	0.96	0.93, 0.98	2	0.69	0.51, 0.81			
	MAP1st WB (STJN)	Mean ± SD (mm)	5.9 ± 3.3	6.3 ± 2.9	1	0.95	0.91, 0.97	1	0.79	0.66, 0.87	1	0.20	-0.07, 0.45
		SEM	0.46	0.40	2	0.95	0.92, 0.97	2	0.81	0.69, 0.89			
	MAP1st WB (RCSP)	Mean ± SD (mm)	4.2 ± 2.6	3.7 ± 2.2	1	0.94	0.90, 0.97	1	0.71	0.51, 0.83	1	0.52	0.30, 0.69
		SEM	0.37	0.31	2	0.97	0.95, 0.99	2	0.61	0.40, 0.76			

FRMD, first ray mobility device (handheld); MAP1st, first ray mobility (electromechanical); NWB, non-weightbearing; PWB, partial weightbearing; WB, weightbearing; RCSP, resting calcaneal stance position; STJN, subtalar joint neutral; ICC, intra/interclass correlation coefficient; CI, confidence interval; SEM, standard error of measurement: $SEM = SD * \sqrt{(1 - ICC)}$.

Table 9. Means, SD, SEM, intra- and inter-rater reliability using measurements normalised by truncated foot length (FRMI).

Measurement			Normalised measurements		Intra-rater (test-retest)			Intra-rater (remove-replace)			Inter-rater		
			Rater 1	Rater 2	Rater	ICC (2,1)	95% CI	Rater	ICC (2,1)	95% CI	Trial	ICC (2,1)	95% CI
First Ray Mobility	FRMD NWB	Mean ± SD	-	-	1	-	-	1	-	-	1	-	-
		SEM	-	-	2	-	-	2	-	-			
	MAP1st PWB (STJN)	Mean ± SD	0.532 ± 0.22	0.437 ± 0.175	1	0.85	0.71, 9.2	1	0.68	0.50, 0.80	1	0.41	0.15, 0.61
		SEM	0.030	0.024	2	0.97	0.95, 0.99	2	0.89	0.82, 0.94			
	MAP1st PWB (RCSP)	Mean ± SD	0.429 ± 0.159	0.434 ± 0.152	1	0.95	0.91, 0.97	1	0.79	0.67, 0.88	1	0.58	0.36, 0.73
		SEM	0.022	0.021	2	0.98	0.97, 0.99	2	0.81	0.69, 0.88			
	MAP1st WB (STJN)	Mean ± SD	0.318 ± 0.186	0.295 ± 0.163	1	0.94	0.91, 0.97	1	0.82	0.70, 0.89	1	0.30	0.03, 0.52
		SEM	0.026	0.023	2	0.96	0.92, 0.97	2	0.82	0.71, 0.89			
	MAP1st WB (RCSP)	Mean ± SD	0.228 ± 0.150	0.202 ± 0.125	1	0.95	0.92, 0.97	1	0.76	0.58, 0.86	1	0.57	0.35, 0.73
		SEM	0.021	0.017	2	0.97	0.96, 0.98	2	0.63	0.43, 0.77			

FRMD, first ray mobility device (handheld); MAP1st, first ray mobility (electromechanical); NWB, non-weightbearing; PWB, partial weightbearing; WB, weightbearing; RCSP, resting calcaneal stance position; STJN, subtalar joint neutral; ICC, intra/interclass correlation coefficient; CI, confidence interval; SEM, standard error of measurement: $SEM = SD * \sqrt{(1 - ICC)}$.

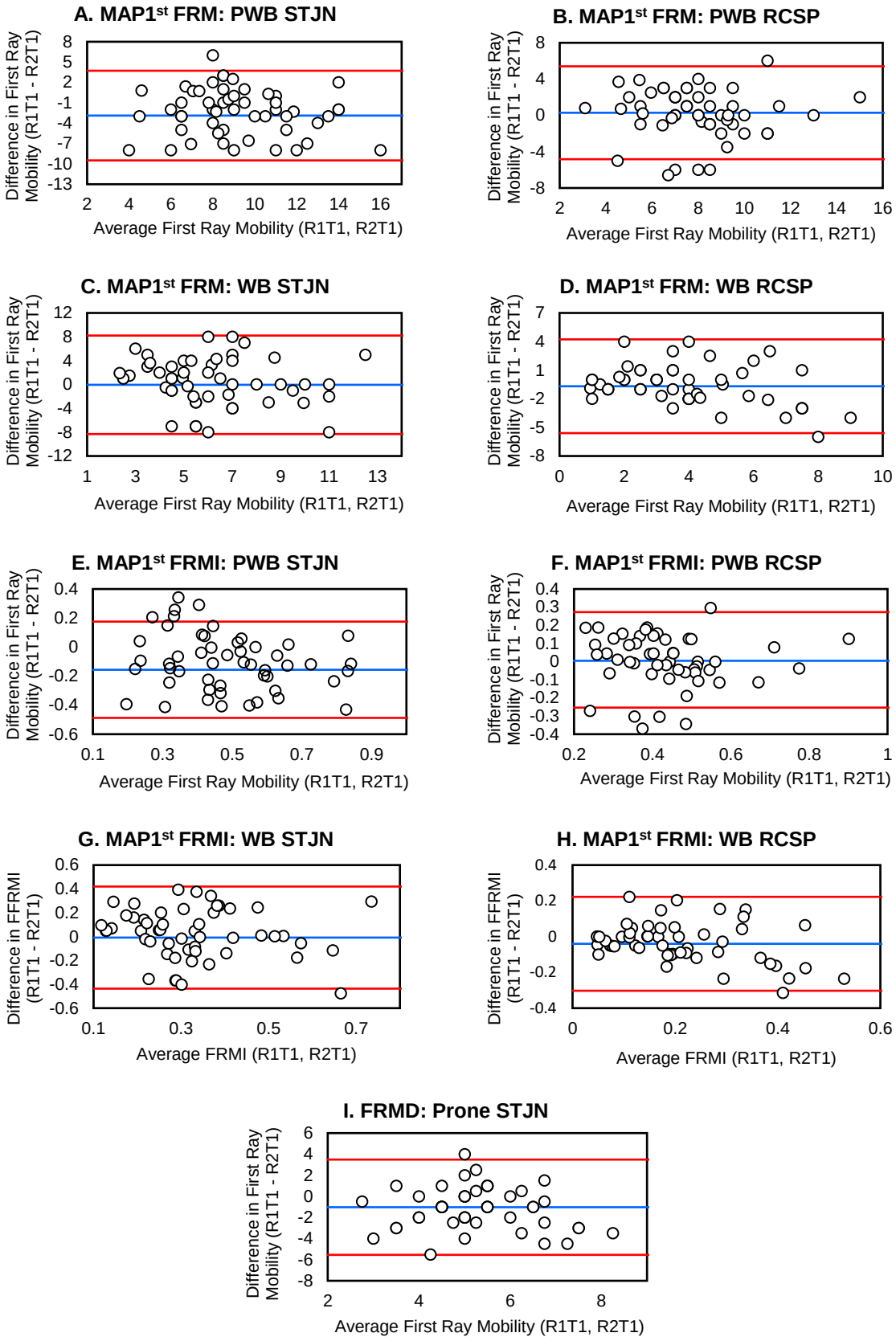

Figure 24A-I. Bland-Altman analysis plots of the inter-rater reliability of first ray mobility measurements made using: (A) FRMD; (B-E) MAP1st FRM, and; (F-I) MAP1st FRMI.

4.5 Discussion

Several studies have presented novel mechanical (Klaue et al., 1994; Glasoe et al., 2002; Glasoe et al., 2005) and handheld (Kim et al., 2008; Rao & Bell, 2013; Munuera-Martinez et al., 2020) devices for measuring first ray mobility. They reported measurements in non- or partial-weightbearing which did not account for the effect of foot size. Grebing and Coughlin (2004) studied the influence of ankle position on reliability of first ray mobility measurements, but the effect of foot position has not been examined in the literature. The present research investigated partial- and full-weightbearing, STJN and RCSP orientations of the foot, as well as measurement normalization to foot length. Future research or clinical use with the MAP1st may be conducted in partial- or full-weightbearing while the foot is in RCSP. Although measurements of FRMI presented superior reliability to FRM, linear regression of these parameters demonstrated a strong relationship which suggested foot length had no effect on first ray mobility. Despite good to excellent intra-rater reliability of the handheld device, poor inter-rater reliability was obtained. Consistent with previous research (Glasoe et al., 2002; Glasoe et al., 2005), this handheld device and the common clinical exam which it represented should not be applied in clinical care or research, where multiple individuals may compare or combine their measurements.

Of the mechanical devices used to quantify first ray mobility, the most widely published were designed by Klaue et al., (1994) and Glasoe et al., (2000) in the 1990's. Though different in design, neither device performed measurements in full weightbearing. The capability of MAP1st to reliably quantify partial- and full-weightbearing first ray mobility presents an advantage over these predicate devices. Roukis et al., (1996) demonstrated an interaction between increased translational mobility of the first ray and decreased rotational first MTP joint flexibility. Their findings indicated that, in weightbearing, first ray hypermobility may increase passive tension in the plantar fascia, placing the 'Windlass mechanism' at the end of its available motion and limit first MTP joint dorsiflexion. Several investigators have postulated that over time, repetitive overloading at the joints dorsal articular surfaces may occur, leading to onset and development of hallux rigidus (Jack E, 1940; Roukis et al., 1996; Golightly et al., 2018). Future weightbearing measurements may better represent underlying aberrant

structural and functional characteristics of the first ray, which may not be fully appreciated when the foot is unloaded.

Table 10. Design feature comparison of the Klaue device, Glasoe device, and MAP1st.

Design Features	Klaue	Glasoe	MAP1st
Measurements in nonweightbearing	✓	×	×
Measurements in partial weightbearing	×	✓	✓
Measurements in full weightbearing	×	×	✓
Mechanical grounding of the forefoot	✓	✓	✓
Mechanical grounding of the rearfoot	✓	✓	×
Controlled load	×	✓	✓
Measure of truncated foot length	×	×	✓
Measurement normalization	×	×	✓
Supported by in vitro reliability analysis	✓	✓	×
Supported by in vivo reliability analysis	✓	✓	✓

✓, design feature supported by the device; ×, design feature not supported by the device.

Prior assessments of first ray mobility were conducted with no reported foot position, (Rodgers & Cavanagh, 1986; Wallace & Kilmartin, 1990; Lee & Young, 2001; Kim et al., 2008) in STJN (Shirk et al., 2006; Munuera-Martinez et al., 2020) or mechanically constrained by an orthotic (Klaue et al., 1994; Glasoe et al., 2000). Root et al., (1977) advocated the use of STJN to characterise normal and abnormal foot function. Shirk et al., (2006) suggested that STJN combined with a neutral ankle alignment (Grebing & Coughlin, 2004) was necessary to reliably measure first ray mobility. In contrast, the present study found a STJN position diminished inter-rater reliability. Good to excellent intra- and inter-rater ICC's ≥0.85 and ~0.58, respectively, were achieved for RCSP measurements. The reliability of RCSP measurements demonstrated equivalent reliability to the Glasoe et al., (2000) and Klaue et al., (1994) devices. Furthermore, B&A plots demonstrated lower biases in RCSP compared to STJN for both FRMI (0.02 ± 0.03 vs. 0.59 ± 0.81) and FRM (0.5 ± 0.3 mm vs. 1.5 ± 2.0 mm). Feet are often categorized into three general structures: Planus (a low-arch with an everted calcaneus and/or varus forefoot); rectus (a moderate-arch with the posterior surface of the calcaneus close to perpendicular with the ground); and cavus (a high-arch with inverted calcaneus and/or valgus forefoot) (Ledoux et al., 2003). A STJN position may artificially reduce or increase first ray mobility measurements in planus and cavus feet, respectively, by forcing an inversion or eversion of the foot. As such,

neutralising the foot's arch alignment may affect the flexor and extensor muscle-tendon systems and passive tension in the plantar fascia, which are fundamental in foot type-specific kinematics and muscular activity (Murley et al., 2009; Buldt et al., 2015). Therefore, placement of the foot in RCSP may not only promote greater reliability but may also elucidate a potential interaction between foot type and first ray mobility not appreciated in STJN. Specifically, greater prevalence of first ray hypermobility has been theorised in planus individuals leading to greater odds of foot injuries, (Kaufman et al., 1999) increased first MTP joint flexibility, (Rao et al., 2011) and higher plantar loading of the medial forefoot (Hillstrom et al., 2013).

Many investigations of first ray mobility have presented linear translational (mm) measurements which did not account for foot size (Klaue et al., 1994; Glasoe et al., 2002; Glasoe et al., 2005; Glasoe et al., 2006; Tavara-Vidalon et al., 2018; Munuera-Martinez et al., 2020). In the present study, normalisation of first ray mobility by foot size, to provide a FRMI, demonstrated strong agreement with the traditional linear displacement of FRM. This finding indicated foot size had no effect on first ray mobility. While measurements of FRMI exhibited greater ICC reliability, FRM measurements presented a SEM of 0.1 mm, demonstrating near identical outcomes between raters. Furthermore, B&A analyses found a between-rater fixed bias of 0.5 mm. Based on these findings, FRM may be given in conjunction with FRMI for comparison with previous research. Prior work from Tavara-Vidalon et al., (2018) and Jones et al., (2005) reported mean FRM of 6.5 mm and 7.4 mm with radiographic measurements. In comparison to these data, mean FRM obtained with MAP1st was approximately, ± 1 mm in RCSP and ± 3 mm in STJN, further supporting RCSP assessments in future research as well as providing indirect validation of MAP1st. Direct validation testing, with radiographic data, is still required to fully understand the device accuracy.

Measurements using the handheld ruler can be considered analogous to the clinical exam (Voellmicke & Deland, 2002). Poor inter-rater ICC reliability of this method (0.06) suggests that, despite its simplicity, it is not an accurate method for measurements between raters. This finding was supported by Glasoe et al., (2002) who observed significant variability in the manual measurements made by three clinicians with different levels of clinical experience. Fat pad compression from plantar measurements has been shown to underestimate first ray mobility (Glasoe et al.,

1998). Several handheld devices which performed dorsal measures have been studied in the literature (Wallace & Kilmartin, 1990; Glasoe et al., 2000; Lee & Young, 2001; Kim et al., 2008; Munuera-Martinez et al., 2020). Glasoe et al., assessed the inter-rater reliability of dorsal mobility measurements using a handheld ruler advocated by Lee et al., (2001). Their findings demonstrated similar inter-rater ICC reliability (0.05) (Glasoe et al., 2005) to the handheld device used in the present work. In contrast, a later study of the same device found improved reliability comparable to the mechanical system developed by Klaue et al., (1994) More recently, a novel handheld device, which accounted for the arc of first ray dorsal motion, demonstrated excellent intra- and inter-rater ICC reliability of 0.89 and 0.93 (Munuera-Martinez et al., 2020). While the handheld method used in the present research was not performed at the dorsal aspect of the foot, the study aim was to recreate the clinical exam reported by Voellmicke and Deland (2002). The addition of the handheld ruler enabled first ray mobility to be quantified. Neither the Glasoe, Klaue, or handheld devices discussed are widely used in a clinical setting. While these devices represent the current state-of-the-art, they could not provide comparison as a method which represented the most common technique. The clinical examination, which is the most widely used technique to date, may not provide an objective, quantifiable method of studying first ray mobility in large, population-based research where multiple examiners are involved. The same concern would be reasonable in a group practice of multiple clinicians.

There are several potential clinical applications of MAP1st.The device may be used to evaluate the efficacy of conservative treatments including the prescription of orthotics and first ray stabilising surgeries such as bunion correction, Lapidus arthrodesis or distal crescentic osteotomy of the first metatarsal. To assess orthotics, arthrodesis, and osteotomy, measurements of first ray mobility may be taken before and after intervention to quantify the efficacy of these treatment modalities in stabilizing the medial forefoot. The potential to improve assessment procedures for the weightbearing mobility and elevation of the first ray in pathologic individuals may help to optimize contemporary treatment methods. Furthermore, MAP1st may be used to discriminate between the first ray mobility of planus, rectus, and cavus foot types, to identify structural and functional differences related to common conditions including, flatfoot deformity, hallux valgus, and hallux rigidus.

4.5.1 Limitations

There are several limitations in this chapter. Given the viscoelastic nature of soft-tissue, it was possible that a time-dependent stretch of the plantar fascia and ligaments could have occurred between trials. This phenomenon is difficult to measure and may have differed between subjects. Each subject began testing with 10 dorsiflexion excitations to control for the recent strain history. Furthermore, to make measurements of first ray mobility, it is necessary to record the height of the first metatarsal head, at baseline, before load-deformation testing. In the current protocol, first metatarsal head height was recorded just once for each subject at baseline. However, first metatarsal head height was not recorded during remove-replace. It is possible that the initial metatarsal head height changed upon replacing the foot into the device for the final trial. Therefore, remove-replace reliability of MAP1st may have been improved had a new baseline for metatarsal head height been recorded.

4.6 Conclusion

A novel device, for assessments of first ray mobility, was developed to address the limitations of current methods. Equivalent reliability was found compared to predicate mechanical devices, in addition to greater reliability than the standard clinical exam. Measurements may be performed in partial- and full-weightbearing RCSP which may facilitate investigation of aberrant foot mechanics not fully appreciated in nonweightbearing or STJN. Future research or clinical use of MAP1st should abide by recording measurements in RCSP that are normalised for FRMI. However, measurements of FRM may be given in conjunction with normalisation to provide comparison with previous research. In summary, the present method may provide reliable assessments of first ray mobility and will be used in the next chapter to elucidate the theoretical interaction between first ray hypermobility and foot type, as a cause of aberrant pedal mechanics.

Chapter 5. Foot Type Biomechanics: Role of First Ray Mobility

5.1 Chapter Overview

In chapter 5, the relationships between first ray mobility and foot type biomechanics (arch height, AHF, first MTP joint flexibility, and plantar loading) were examined. This work was performed using asymptomatic subjects with planus and rectus foot types, only. It was theorised that greater first ray mobility would be present in the planus compared to rectus subjects.

Aim 4: Investigate the relationships between foot structure, first ray mobility, AHF, first MTP joint flexibility, and plantar loading*.

Hypothesis 4a: First ray mobility will be negatively related with arch height and first MTP joint flexibility and positively related with arch height flexibility.

Hypothesis 4b: The ratio of peak plantar loading* beneath the first and second metatarsal heads will be higher across subjects with rectus versus planus foot types.

Hypothesis 4c: The ratio of peak plantar loading* beneath the first and second metatarsal heads will be higher across subjects with normal versus high levels of first ray mobility.

*Plantar loading refers to plantar pressure, maximum force, pressure-time-integral, and force-time integral.

5.2 Introduction

Hypermobility of the first ray is a term that describes excessive superior translation when subjected to plantar load. The etiology of first ray hypermobility is unclear, as is the threshold for excessive first ray mobility in the absence of an objective standard

for quantifying motion in the sagittal plane. Definitions of first ray hypermobility (Morton DJ, 1935) can vary from 7-10 mm based on differences in case definitions and methods of assessment (Roukis et al., 1996; Lee & Young, 2001; King & Toolan, 2004; Tavara-Vidalon et al., 2018; Glasoe et al., 2019; Munuera-Martinez et al. 2020). Hillstrom et al., (2013) postulated that first ray hypermobility may be present in most individuals with pes planus. Their research demonstrated lower peak pressures beneath the first MTP joint and higher peak pressures beneath the second MTP joint in planus compared to rectus feet. This finding indirectly suggested a transfer of load from the first to second metatarsal head in planus subjects may be caused by a varus forefoot in the presence of first ray hypermobility. These research findings were limited by indirect observations of hypermobility through plantar pressures rather than empirical measurements of first ray mobility. MAP1st, which was found to be reliable in Chapter 4, was used in the present study to explore differences and relationships between first ray mobility and foot type biomechanics. The objective of this study was to determine if an interaction exists between the planus foot type and first ray hypermobility, influencing aberrant structural and functional parameters of the foot.

5.3 Materials and Methods

The study included 23 asymptomatic planus feet and 17 asymptomatic rectus feet for a total of 20 participants (N = 40 feet). Potential subjects were recruited from any willing individual that met the study inclusion/exclusion criteria (Table 11). Participant characteristics are shown in Table 12. The method of subject recruitment and procedure for measuring first ray mobility were detailed in Chapter 4. Any subjects with a cavus foot type and patients with hallux rigidus were excluded from the analyses in this chapter. One asymptomatic rectus subject was also excluded due to presentation of GJH. All subjects were categorised according to their foot type (planus or rectus), and further assessed for AHF, first MTP joint flexibility, and plantar loading.

Table 11. Inclusion/exclusion criteria for subjects enrolled in the study.

Recruitment Criteria	
Inclusion	***Exclusion***
• Healthy adults over the age of 21 years old	• Individuals without the capacity to consent and/or understand procedures of the study
• No substantial pain within the lower extremity that could affect ability to walk	• Hallux valgus, hallux rigidus, rheumatoid arthritis, osteoporosis, or any other degenerative disease involving the lower limb
• Male or female	• Significant cardiovascular disease or any pathology that would affect one's ability to walk independently
• Planus: $AHI_{standing} < 0.345$	• Limb length discrepancy greater than 1 cm
• Rectus: $AHI_{standing} \geq 0.345 \leq 0.37$	• Cavus: $AHI_{standing} > 0.37$

Table 12. Participant characteristics.

Characteristics	**Planus (n = 23)**	**Rectus (n = 17)**	***p*-value**
Male:Female	16:7	12:5	0.946
Mean age ± SD (years)	29 ± 6	39 ± 15	**0.010***
Mean height ± SD (cm)	176 ± 9	177 ± 9	0.780
Mean weight ± SD (kg)	80 ± 12	78 ± 15	0.983
Mean BMI ± SD (kg/m^2)	25 ± 3	25 ± 4	0.782

Bold text* indicates statistically significant differences ($p \leq 0.05$).

5.3.1 Measures of Foot Structure

After consenting, the left and right feet of each participant were categorised according to their foot structure, using the AHI system (Figure 25A-C). Arch height index can reliably distinguish planus, rectus, and cavus foot structures in asymptomatic healthy individuals, according to thresholds previously established by Hillstrom et al (2013). Each of the subject's feet were positioned in the AHI device with the most anterior bar set to maximum Foot Length (FL). A small adjustable cup was positioned at the first MTP joint to denote TFL and a vertical bar, which was positioned at one half of FL, was lowered upon the dorsal aspect of the foot to measure arch-height. Linear rulers, scaled in centimetres (cm), were used to visually measure each parameter. The

graticule was viewed by the rater with their aiming eye, in a perpendicular orientation, to avoid parallax error. Arch height index was defined as the dorsal arch height at one-half of FL, normalised by TFL, while standing ($AHI_{standing}$) calculated according to the following formula:

$$AHI_{standing} = \frac{\text{Arch Height}_{standing}}{\text{TFL}} \quad (3)$$

Figure 25A-C. Assessment of arch height using the AHI system: (A) vertical graticule to measure arch height in standing; (B) left and right feet placed in corresponding device, and; (C) position of the TFL measurement, placed at the medial aspect of the first metatarsal head.

5.3.2 Arch Height Flexibility

The arch height of an individual can be calculated either in sitting or standing positions for partial- and full-weightbearing assessments, respectively. Arch height flexibility (mm/kN) is a measure of the change in arch height between the sitting (i.e. partial weightbearing) and standing (i.e. weightbearing) conditions using the AHI system described in section 5.3.1 (Figure 26). The measurement is normalised to the change in load (estimated to be 40% of bodyweight (Hillstrom et al., 2013)). Calculation of AHF can be made with the following formula:

$$\text{AHF}\left(\frac{\text{mm}}{\text{kN}}\right) = \frac{\left|\text{AH}_{standing}(mm) - \text{AH}_{sitting}(mm)\right|}{0.4 \times \text{bodyweight (kN)}} \text{ x } 100 \quad (4)$$

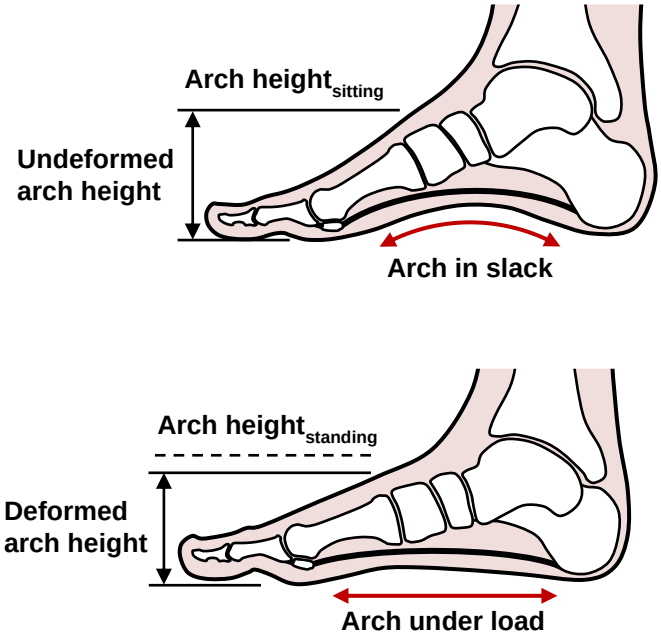

Figure 26. Illustration of AHF measured as the change in AHI from the seated to standing conditions.

5.3.3 First Metatarsophalangeal Joint Flexibility

The first MTP joint flexibility test-rig (Figure 27A-B) has previously been tested and found to be reliable (Rao et al., 2011; Cody et al., 2017). The left and right feet of every subject were tested to provide bilateral assessments of first MTP joint flexibility. During testing, each patient was seated in a chair with their knees flexed to 90° and thighs perpendicular to the floor. The flexibility test-rig was connected to a laptop running DAQami software (Measurement Computing Corporation, Norton, MA), which recorded the voltage signals for first MTP joint torque (N·cm) and dorsiflexion (°). Before recording, the first MTP joints of each patient were cyclically loaded ten times to control for the soft tissues recent strain history. Five trials were then performed while seated. The average of the five trials defined the final flexibility curve.

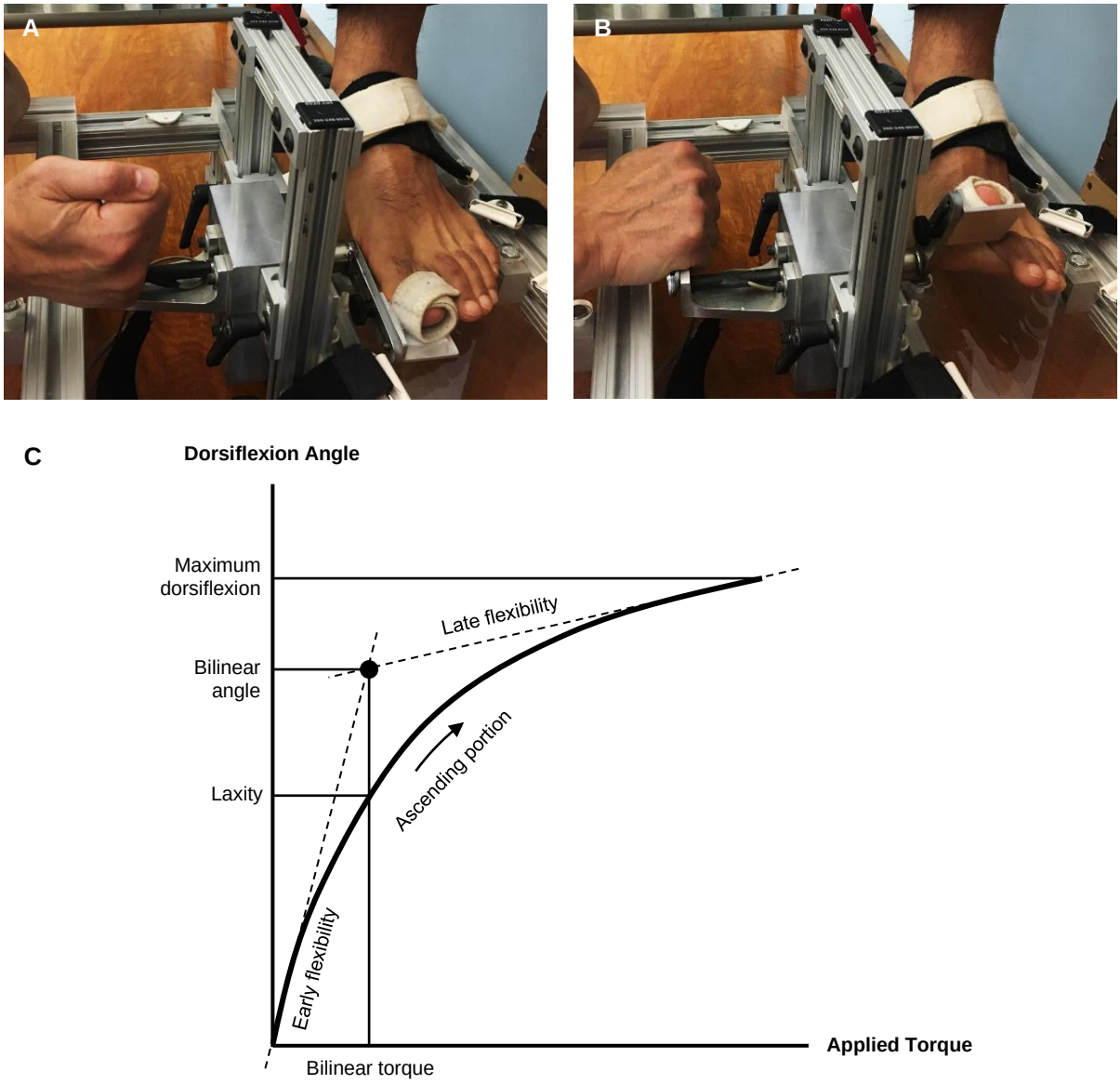

Figure 27A-C. (A) the subject's foot is placed in the test-rig, where their hallux is strapped to a pivot mechanism and the mid- and rear-foot are immobilised by Velcro straps; (B) the tester applies a torque to dorsiflex the hallux and measure the residual torque using a transducer integrated into the pivot mechanism. (C) Illustrated diagram of the first MTP joint flexibility curve. The intersection of the early and late flexibility slope lines is denoted by the reference point. The coordinates for this point, at the x- and y-axes, define the bilinear torque and bilinear angle, respectively. The bilinear angle is the y-axis at which the value for normal bilinear torque intersects the flexibility curve. Laxity is the amount of angular rotation observed for a standardised amount of applied torque.

The recordings were post-processed in Microsoft Excel (Redmond, WA, USA) using a 10-point moving average formula to smooth the voltage signals for torque and dorsiflexion (Siegler et al., 1985). Several characteristic parameters were obtained from testing. First, applied torque (X-axis) and first MTP joint dorsiflexion (Y-axis) were

plotted graphically to create a flexibility curve for each subject. Early flexibility was defined as the slope of the curve over the first 25% of the graph; late flexibility was the slope in the last 25% of the graph. The intersection point of the early and late flexibility lines was used to generate the bilinear torque and angle parameters. Maximum dorsiflexion of the first MTP joint was collected. Finally, the joint laxity was calculated, which represents the angle at which the average bilinear torque of controls (rectus) intersects each subject's flexibility curve. Five trials were collected for each foot (right and left) where the mean was used for final analysis.

5.3.4 Plantar Loading

Each subject walked across an emed-x (Novel, Munich, Germany) plantar pressure measurement device (Figure 28A). Dynamic loading data were collected using a mid-gait protocol. Centre of Pressure Excursion Index (CPEI (%)) (Figure 28B) and Initial Pronation Index (IPI (%)) were calculated as per standard methods (Hillstrom et al., 2013; Diaz et al., 2018). In addition, Peak Pressure (PP (MPa)), Maximum Force (MF (N)), Force-Time Integral (FTI (Ns)), Pressure-Time Integral (PTI (Ns/cm^2)), and Area (cm^2) were calculated for each masked region of the foot. A 12-segment mask was used that established regions of plantar loading as shown in Figure 28C. Each plantar loading parameter was computed from the data collected as the mean of five good walking trials per foot (right and left) to provide an unbiased estimate (Hafer et al., 2013).

5.3.5 Statistics

Descriptive statistics (frequency, median, mean, and SD) were computed for each group. Linear regressions were performed to test Hypotheses 4a-c. An R^2 value >0.7 implied a sufficient goodness of fit. Generalized Estimation Equation (GEE) analyses were performed across foot type and first ray mobility. A $p<0.05$ suggested a significant difference. Stepwise regression models were also employed to determine if first ray mobility was related to functional measures of the Windlass mechanism.

Significance levels for inclusion and exclusion within each stepwise model were set at $p<0.05$ and $p>0.10$, respectively. All analyses were performed using SPSS version 26.

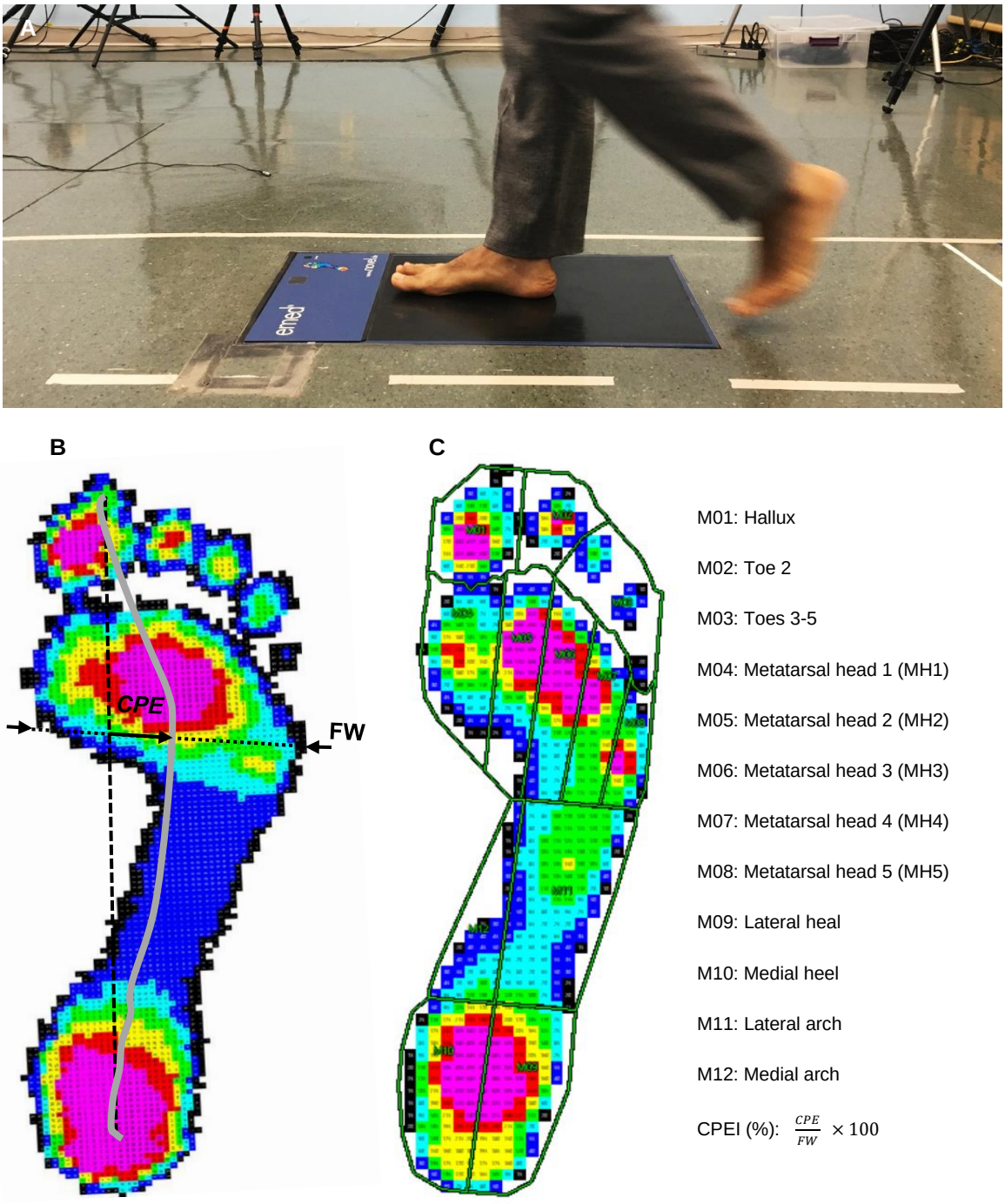

Figure 28A-C. (A) A subject walking across the emed-x plantar pressure measuring system during normal gait at a self-selected speed. This protocol was repeated five times, for the left and right feet; (B) visualisation of foot width (FW) and centre of pressure excursion (CPE) measurements for calculating the Centre of Pressure Excursion Index (CPEI); and (C) typical plantar pressure distribution showing the 12-segment foot mask employed.

5.4 Results

5.4.1 Foot Type

Measurements of AHF and first ray mobility (partial weightbearing) were significantly different across foot types. Normalised first ray mobility (FRMI) of the planus group was 0.418 (8 mm) compared to 0.335 (6 mm) in the rectus group. No significant difference in weightbearing first ray mobility was observed. Furthermore, no between-group differences were found for first MTP joint flexibility parameters. Results from the GEE analyses are summarised in Table 13.

Table 13. Means, SD, and results from Generalised Estimating Equations (GEE) for biomechanical parameters across the planus and rectus foot types.

Parameters	**Planus (n=23 feet)**		**Rectus (n=17 feet)**		**GEE Results**	
	Mean	**SD**	**Mean**	**SD**	X^2	***p*-value**
AHF (mm/kN)	145.4	13.1	92.3	18.7	**7.578**	**0.006***
FRMI (PWB)	0.418	0.033	0.335	0.032	**6.357**	**0.012***
FRMI (WB)	0.205	0.033	0.166	0.025	1.876	0.171
Early flexibility (°/Ncm)	0.47	0.08	0.51	0.06	0.460	0.497
Late flexibility (°/Ncm)	0.07	0.01	0.08	0.01	0.924	0.336
Bilinear angle (°)	56.0	2.4	63.4	4.7	1.840	0.175
Bilinear torque (N·cm)	184.1	30.4	148.4	15.7	1.222	0.269
Maximum Dorsiflexion (°)	74.4	2.9	82.9	6.0	1.577	0.209
Laxity (°)	47.5	2.0	53.3	4.8	1.166	0.280

AHF, arch height flexibility; FRM, first ray mobility; FRMI, first ray mobility index. Bold text with a * indicates statistically significant differences ($p \leq 0.05$).

5.4.2 First Ray Mobility

The mean normalised first ray mobility of all subjects was 0.383 (7.2 mm) which was used to stratify non-hypermobile (<0.383) and hypermobile (≥0.383) groups. $AHI_{standing}$ demonstrated significant between-group differences. Of the hypermobile subjects, 71% exhibited a planus foot type. However, this group was not exclusively planus, with 29% exhibiting a rectus foot type. The hypermobile group exhibited significantly higher normalised first ray mobility at 0.462 (9.5 mm) compared to 0.323 (5.5 mm) for those

who were not hypermobile, as expected. In contrast to the GEE analyses by foot type, AHF was not significantly different between the hypermobile and non-hypermobile groups. Of the parameters related to first MTP joint flexibility, laxity was significantly higher in the hypermobile individuals. The resulting differences in related parameters including AHF and first MTP joint flexibility can be found in Table 14.

Table 14. Means, SD, and results from Generalised Estimating Equations (GEE) for biomechanical parameters across first ray mobility.

Parameters	**Non-Hypermobile (n=23 feet)**		**Hypermobile (n=17 feet)**		**GEE Results**	
	Mean	**SD**	**Mean**	**SD**	***X²***	***p*-value**
Planus (%)	43.5 (n=10)	-	70.6 (n=12)	-	-	-
AHF (mm/kN)	131.1	18.6	111.6	13.5	0.989	0.320
FRMI (PWB)	0.323	0.027	0.462	0.024	**29.617**	**0.000***
FRMI (WB)	0.203	0.033	0.170	0.025	1.704	0.192
Early flexibility (°/Ncm)	0.49	0.09	0.48	0.07	0.037	0.848
Late flexibility (°/Ncm)	0.08	0.01	0.07	0.01	0.736	0.391
Bilinear angle (°)	56.2	3.0	60.8	2.5	2.195	0.138
Bilinear torque (N·cm)	155.1	15.2	189.4	38.4	0.815	0.367
Maximum Dorsiflexion	75.2	3.2	79.4	3.2	2.412	0.120
Laxity (°)	46.1	3.2	53.1	2.0	**4.271**	**0.039***

AHF, arch height flexibility; FRM, first ray mobility; FRMI, first ray mobility index; bold text with a * indicates statistically significant differences ($p \leq 0.05$).

Linear regression analyses were performed to test Hypothesis 4a which are shown in Figure 29A-C. No significant relationships were found between first ray mobility and $AHI_{standing}$ ($R^2 = 0.0005$, $p = 0.665$), AHF ($R^2 = 0.0015$, $p = 0.810$), and first MTP joint laxity ($R^2 = 0.1193$, $p = 0.066$). These findings did not support hypothesis 4a.

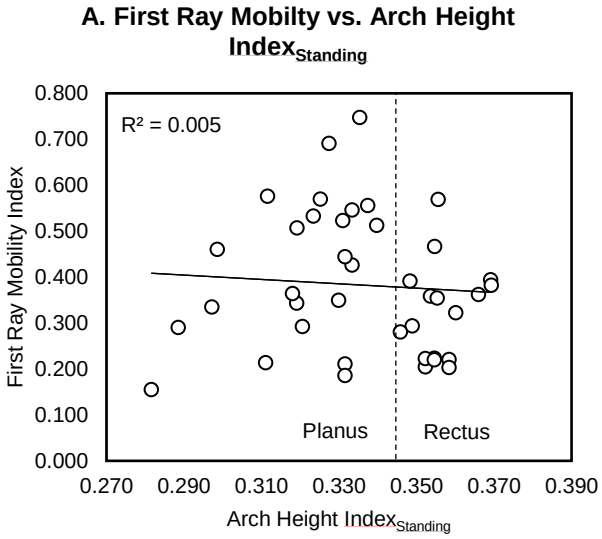

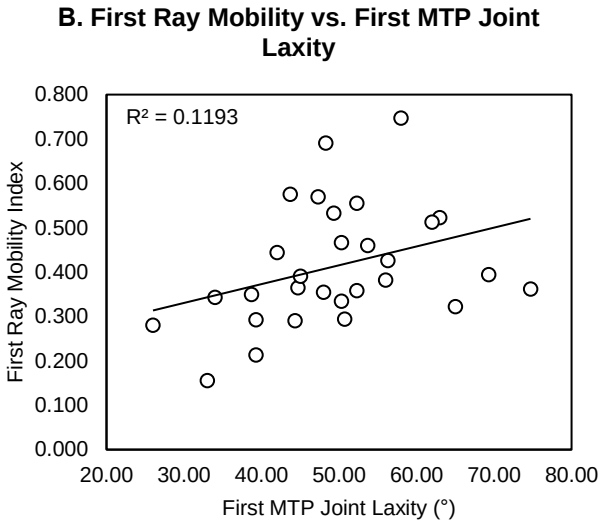

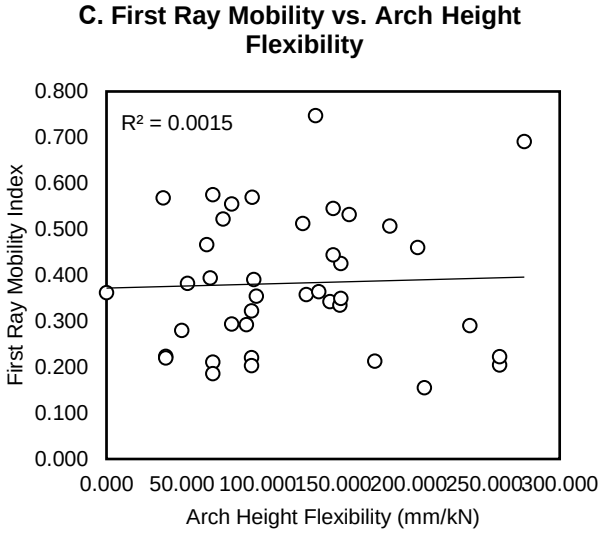

Figure 29A-C. Linear regression analyses of first ray mobility index vs. $AHI_{standing}$, first MTP joint laxity, and arch height flexibility.

5.4.3 Plantar Loading

Differences in the plantar pressure distributions between planus and rectus subjects are summarised in Tables 15A-B. Significant between-group differences were observed for the ratio of first to second metatarsal PP, MF, PTI, and FTI, hallucial MF, FTI and area, first metatarsal PTI, and CPEI. Based on these results, hypothesis 4b was accepted.

Table 15A. Means, SD, and results from Generalised Estimating Equations (GEE) for plantar peak pressure (PP) and maximum force (MF) across the planus and rectus foot types.

Parameters	**Planus (n=23 feet)**		**Rectus (n=17 feet)**		**GEE Results**	
	Mean	**SD**	**Mean**	**SD**	X^2	***p*-value**
PP (kPa)						
Hallux	468.3	48.6	365.0	70.4	1.976	0.160
Toe two	176.9	23.6	127.4	17.5	3.083	0.079
Toes three-five	109.1	15.0	77.2	12.3	3.668	0.055
First metatarsal	269.7	27.4	339.6	33.3	3.036	0.081
Second metatarsal	501.9	51.2	439.9	35.3	1.430	0.232
First-second ratio	0.55	0.03	0.87	0.09	**10.720**	**0.001***
Third metatarsal	430.5	26.5	422.6	28.3	0.058	0.810
Fourth metatarsal	293.9	22.1	331.3	42.7	0.627	0.428
Fifth metatarsal	268.7	36.4	257.5	37.3	0.122	0.727
Lateral arch	106.3	8.5	105.8	7.7	0.009	0.926
Medial arch	4.1	0.6	3.8	0.6	0.259	0.611
Lateral heel	326.7	19.0	322.4	23.1	0.024	0.878
Medial heel	353.1	26.5	330.9	26.5	0.373	0.541
Total PP	641.9	43.9	661.5	58.5	0.116	0.733
CPEI (%)	19.1	1.2	21.4	1.2	**5.366**	**0.021***
IPI (%)	7.1	1.0	7.4	0.9	0.045	0.832
MF (N)						
Hallux	139.8	11.9	96.1	11.1	**13.795**	**0.000***
Toe two	23.5	2.9	19.4	2.5	1.303	0.254
Toes three-five	30.0	4.0	17.4	3.5	1.077	0.299
First metatarsal	134.8	10.1	165.0	15.3	3.070	0.080
Second metatarsal	187.2	12.5	182.8	11.9	0.103	0.748
First-second ratio	0.72	0.05	0.96	0.06	**12.718**	**0.000***
Third metatarsal	201.7	8.4	199.0	10.9	0.070	0.791
Fourth metatarsal	118.1	9.8	135.9	13.2	1.063	0.303
Fifth metatarsal	60.4	5.9	66.4	7.6	0.628	0.428
Lateral arch	107.8	16.1	110.5	14.8	0.026	0.871
Medial arch	18.6	2.8	15.3	3.0	1.150	0.283
Lateral heel	242.5	10.8	247.7	9.6	0.359	0.549
Medial heel	283.5	15.6	278.3	15.6	0.070	0.792
Total MF	813.7	31.1	821.9	30.8	2.891	0.089

CPEI, Centre of Pressure Excursion Index; bold text with a * indicates statistically significant differences ($p \leq 0.05$).

Table 15B. Means, SD, and results from Generalised Estimating Equations (GEE) for Pressure-Time Integral (PTI), Force-Time Integral (FTI), and Area across the planus and rectus foot types.

Parameters	Planus (n=23 feet)		Rectus (n=17 feet)		GEE Results	
	Mean	SD	Mean	SD	X^2	*p*-value
PTI (kPa/s)						
Hallux	102.4	11.2	74.0	14.3	2.779	0.095
Toe two	36.0	4.8	26.5	3.8	3.144	0.076
Toes three-five	23.9	3.0	17.8	3.2	2.355	0.125
First metatarsal	76.0	6.5	96.1	9.2	**4.071**	**0.044***
First-second ratio	0.58	0.03	0.89	0.08	**12.888**	**0.000***
Second metatarsal	129.1	10.7	117.1	6.5	1.395	0.237
Third metatarsal	123.8	8.0	126.8	7.3	0.091	0.762
Fourth metatarsal	89.4	6.1	100.4	11.5	0.876	0.349
Fifth metatarsal	72.9	8.0	73.8	9.5	0.016	0.899
Lateral arch	35.4	3.2	36.5	2.9	0.306	0.580
Medial arch	22.6	2.0	24.3	2.2	0.527	0.468
Lateral heel	82.6	4.7	87.5	5.9	0.542	0.462
Medial heel	87.4	5.9	89.6	6.1	0.073	0.787
Total PTI	235.0	11.9	235.2	14.2	0.000	0.991
FTI (Ns)						
Hallux	28.3	2.8	19.2	2.7	**6.224**	**0.013***
Toe two	4.7	0.7	3.7	0.5	1.790	0.181
Toes three-five	4.3	0.8	3.4	0.8	0.562	0.454
First metatarsal	38.3	3.2	48.0	5.3	3.558	0.059
First-second ratio	0.65	0.05	0.93	0.06	**17.120**	**0.000***
Second metatarsal	58.5	4.6	54.3	4.3	0.622	0.430
Third metatarsal	64.5	3.0	63.5	3.5	0.141	0.707
Fourth metatarsal	40.0	3.3	45.1	4.1	1.017	0.313
Fifth metatarsal	18.7	1.9	20.6	2.4	0.669	0.413
Lateral arch	29.2	5.1	33.9	4.8	1.132	0.287
Medial arch	4.3	0.7	3.7	0.8	0.324	0.569
Lateral heel	62.2	3.4	65.3	3.7	1.037	0.309
Medial heel	71.7	4.2	73.3	3.9	0.126	0.722
Total FTI	429.4	18.4	427.0	18.4	1.094	0.296
Area (cm^2)						
Hallux	11.5	0.6	9.2	0.4	**27.298**	**0.000***
Toe two	3.6	2.0	3.5	0.2	0.111	0.739
Toes three-five	5.7	0.6	5.2	0.6	0.439	0.508
First metatarsal	13.0	0.5	13.4	0.5	0.645	0.422
Second metatarsal	10.2	0.4	10.9	0.4	**15.805**	**0.000***
Third metatarsal	11.8	0.4	12.4	0.4	**151.922**	**0.000***
Fourth metatarsal	9.9	0.3	10.4	0.3	**11.944**	**0.001***
Fifth metatarsal	6.2	0.2	6.7	0.2	**6.009**	**0.014***
Lateral arch	21.5	1.7	22.2	2.1	0.142	0.707
Medial arch	4.1	0.6	3.8	0.6	0.259	0.611
Lateral heel	18.3	0.5	17.6	0.5	**46.941**	**0.000***
Medial heel	18.2	0.5	17.7	0.5	**23.284**	**0.000***
Total Area	133.9	4.2	132.9	4.6	0.097	0.756

Bold text with a * indicates statistically significant differences ($p \leq 0.05$).

Plantar loading parameters of the hypermobile and non-hypermobile groups are shown in tables 16A-B. Significant between-group differences were observed for lateral heel PP, MF, PTI, and FTI, media heel PP, PTI, and FTI, hallucial MF, and first metatarsal FTI, and CPEI. No significant differences were found for the first to second metatarsal load ratio. Based on these results, hypothesis 4c was rejected.

Table 16A. Means, SD, and results from Generalised Estimating Equations (GEE) for plantar peak pressure (PP) and maximum force (MF) across non-hypermobile and hypermobile subjects.

Parameters (Normalised)	**Non-Hypermobile (n=23 feet)**		**Hypermobile (n=17 feet)**		**GEE Results**	
	Mean	**SD**	**Mean**	**SD**	X^2	***p*-value**
PP (kPa)						
Hallux	426.2	56.3	421.9	40.4	0.012	0.913
Toe two	172.5	22.3	133.3	18.6	3.017	0.082
Toes three-five	106.7	15.8	80.4	11.7	2.715	0.099
First metatarsal	281.0	21.1	324.3	37.2	1.669	0.196
First-second ratio	0.65	0.06	0.75	0.09	2.132	0.144
Second metatarsal	500.0	47.2	442.4	33.3	3.738	0.053
Third metatarsal	415.7	21.1	442.7	41.0	0.386	0.534
Fourth metatarsal	311.9	27.4	306.9	23.7	0.046	0.831
Fifth metatarsal	262.2	32.9	266.2	38.9	0.024	0.876
Lateral arch	104.6	6.8	108.0	9.5	0.589	0.443
Medial arch	86.7	6.9	88.1	5.9	0.088	0.767
Lateral heel	341.5	18.5	302.4	13.5	**7.379**	**0.007***
Medial heel	352.8	19.7	331.3	17.4	**5.911**	**0.015***
Total PP	677.9	50.5	612.7	36.7	2.634	0.105
CPEI (%)	21.1	1.2	18.7	1.3	**4.289**	**0.038***
IPI (%)	7.5	0.8	6.9	0.8	0.922	0.337
MF (N)						
Hallux	114.8	10.8	129.9	9.9	**7.805**	**0.005***
Toe two	23.8	2.5	18.9	2.1	**5.420**	**0.020***
Toes three-five	22.5	3.3	18.1	2.6	3.533	0.060
First metatarsal	145.8	8.9	150.1	12.7	0.299	0.585
First-second ratio	0.84	0.05	0.82	0.06	0.270	0.603
Second metatarsal	185.1	10.2	185.7	11.3	0.015	0.904
Third metatarsal	200.3	9.4	200.8	11.8	0.001	0.971
Fourth metatarsal	126.6	8.8	124.3	7.2	0.170	0.680
Fifth metatarsal	62.7	6.0	63.4	6.0	0.030	0.863
Lateral arch	111.6	13.3	105.4	13.9	0.650	0.420
Medial arch	17.8	3.1	16.4	2.1	0.442	0.506
Lateral heel	251.2	10.0	236.0	9.5	**4.045**	**0.044***
Medial heel	281.3	11.8	281.3	14.4	0.000	0.997
Total MF	817.0	30.9	817.3	31.4	0.002	0.965

CPEI, Centre of Pressure Excursion Index; bold text with a * indicates statistically significant differences ($p \leq 0.05$).

Table 16B. Means, SD, and results from Generalised Estimating Equations (GEE) for Pressure-Time Integral (PTI), Force-Time Integral (FTI), and Area across non-hypermobile and hypermobile subjects.

Parameters (Normalised)	**Non-Hypermobile (n=23 feet)**		**Hypermobile (n=17 feet)**		**GEE Results**	
	Mean	**SD**	**Mean**	**SD**	X^2	***p*-value**
PTI (kPa/s)						
Hallux	89.6	10.8	91.4	8.7	0.072	0.789
Toe two	36.1	4.5	26.4	3.7	**6.766**	**0.009***
Toes three-five	23.2	2.8	18.7	2.9	2.090	0.148
First metatarsal	77.4	6.1	94.2	9.2	**5.710**	**0.017***
First-second ratio	0.69	0.05	0.75	0.07	1.271	0.260
Second metatarsal	124.1	8.5	123.8	7.9	0.002	0.961
Third metatarsal	120.3	6.5	131.4	10.7	0.838	0.360
Fourth metatarsal	91.6	8.2	97.4	7.5	0.713	0.398
Fifth metatarsal	71.6	7.9	75.6	9.2	0.531	0.466
Lateral arch	37.0	3.1	34.2	2.9	2.542	0.111
Medial arch	24.0	2.2	22.5	1.5	0.748	0.387
Lateral heel	88.5	4.3	79.5	4.7	**6.388**	**0.011***
Medial heel	91.1	4.4	84.5	4.9	**6.570**	**0.010***
Total PTI	231.9	11.6	239.4	14.7	0.396	0.529
FTI (Ns)						
Hallux	23.5	2.3	25.7	1.9	3.774	0.052
Toe two	4.8	0.6	3.5	0.6	**5.516**	**0.019***
Toes three-five	4.2	0.6	3.4	0.6	2.021	0.155
First metatarsal	40.9	3.6	44.5	4.5	1.271	0.260
First-second ratio	0.77	0.05	0.76	0.06	0.044	0.834
Second metatarsal	55.7	3.4	58.0	4.1	1.164	0.281
Third metatarsal	63.0	3.4	65.5	3.8	0.331	0.565
Fourth metatarsal	41.9	3.2	42.5	2.5	0.128	0.720
Fifth metatarsal	19.4	2.0	19.7	1.9	0.033	0.857
Lateral arch	32.8	4.7	29.0	4.4	2.139	0.144
Medial arch	4.3	0.8	3.6	0.5	1.723	0.189
Lateral heel	65.8	3.3	60.3	3.6	**3.833**	**0.050***
Medial heel	74.2	3.6	69.9	3.5	**3.921**	**0.048***
Total FTI	429.3	19.5	427.2	17.1	0.127	0.721
Area (cm^2)						
Hallux	10.3	0.4	10.9	0.4	**4.594**	**0.032***
Toe two	3.6	0.2	3.4	0.2	1.001	0.317
Toes three-five	5.7	0.4	5.2	0.5	2.189	0.139
First metatarsal	13.2	0.5	13.1	0.5	0.026	0.871
Second metatarsal	10.6	0.4	10.4	0.4	0.460	0.497
Third metatarsal	12.2	0.4	11.9	0.4	2.017	0.155
Fourth metatarsal	10.1	0.3	10.1	0.3	0.264	0.607
Fifth metatarsal	6.4	0.2	6.5	0.2	0.862	0.353
Lateral arch	22.2	1.6	21.2	1.7	0.988	0.320
Medial arch	4.2	0.7	3.7	0.5	2.810	0.94
Lateral heel	18.1	0.5	17.9	0.5	2.417	0.120
Medial heel	18.1	0.5	17.9	0.5	0.835	0.361
Total Area	134.7	4.3	131.9	4.1	**4.440**	**0.035***

Bold text with a * indicates statistically significant differences ($p \leq 0.05$). Pressure-Time Integral (PTI); Force-Time Integral (FTI).

Stepwise linear regression models were created to estimate functional parameters of first MTP joint laxity and MF beneath the hallux and first metatarsal (Table 17). Of the parameters predictive of first MTP joint laxity, first ray mobility explained some of the model variance. Exclusion of first ray mobility from this parameter reduced the R value from 0.853 to 0.821 and the adjusted R^2 value from 68% to 63% of the model variance. Early flexibility of the first MTP joint was related to MF beneath the hallux, with an R value of 0.649 and an R^2 value accounting for 40% of the model variance. This was increased to 57% with the inclusion of arch height $index_{standing}$. Weightbearing first ray mobility was predictive of MF beneath the first metatarsal head, with an R value of 0.538 and adjusted R^2 value which explained 26% of the model variance. Inclusion of maximum dorsiflexion and partial weightbearing first ray mobility increased the R value to 0.807 and adjusted R^2 value to 61% of the model variance.

Table 17. Model summary from the stepwise linear regression analyses.

Dependent Variable	Stepwise Linear Regression Model	R	R^2	Adj. R^2	Sig. F Change
Laxity (°)	Maximum dorsiflexion, early flexibility, late flexibility, first ray mobility (partial weightbearing)	0.853	0.727	0.682	**0.041***
MF (N) hallux	Early flexibility, arch height $index_{standing}$	0.776	0.603	0.572	**0.002***
MF (N) first metatarsal	First ray mobility (weightbearing), maximum dorsiflexion	0.807	0.652	0.610	**0.031***

MF, Maximum Force. Bold text with a * indicates statistically significant differences ($p \leq 0.05$).

5.5 Discussion

The present research hypothesised that upon weightbearing gait, flattening of the MLA in the planus foot would be accompanied by greater first ray mobility and a reduction in plantar load beneath the first metatarsal (Ledoux & Hillstrom, 2002; Hillstrom et al., 2013; Zifchock et al., 2017; Song et al., 2018). This theory was confirmed by greater prevalence of first ray hypermobility among planus individuals. Approximately, 71% of subjects with first ray hypermobility were classified as pes planus compared to 43% in the non-hypermobile group. Furthermore, this interaction between foot type and first ray mobility was found to alter the weightbearing mechanics of the foot. Upon

weightbearing gait, a lowering of the arch in the hypermobile planus foot was accompanied by a reduction in plantar load beneath the first metatarsal and increased plantar load beneath the hallux. Stepwise linear regression analyses indicated that first ray mobility explained 24% of the variance in MF sustained under the first metatarsal. Additionally, significantly greater first MTP joint laxity was present in individuals with first ray hypermobility where stepwise linear regression found first ray mobility to be predictive of first MTP joint laxity. Thus, an interaction was also demonstrated between translational first ray mobility and rotational first MTP joint flexibility. No relationships were observed between first ray mobility vs. arch height index, arch height flexibility, and first MTP joint dorsiflexion.

It has been well-established that pes planus exhibits a more flexible arch than pes rectus (Hillstrom et al., 2013; Zifchock et al., 2017; Song et al., 2018). Consistent with previous research, the current study observed significantly more arch height flexibility in planus subjects. As such, flexibility of the arch was expected in hypermobile participants due to dominance of the planus foot type yet arch height flexibility and first ray mobility were not related, rejecting the hypothesised negative relationship between these variables. Conversely, the non-hypermobile group exhibited greater arch height flexibility. While this difference was not statistically significant, it contrasted with conventional belief that flexibility of the MLA may be associated with hypermobility of the first ray.

Mean first ray mobility of pooled subjects was consistent with previously published data (Table 18). While prior research has postulated an association between planus feet and first ray hypermobility, (Ledoux & Hillstrom et al., 2002; Hillstrom et al., 2013) few investigations have provided objective measures of foot type alongside first ray mobility (Glasoe et al., 2005; Glasoe et al., 2005; Jones et al., 2005; Song et al., 2018; Tavara-Vidalon et al., 2018). Glasoe et al., (2000) and Coughlin and Jones, (2007) found no significant differences or correlation between increased first ray mobility and foot type or arch height, respectively. While the current research also found no linear relationship between arch height index and first ray mobility, there was a predominant distribution of hypermobile individuals classified as pes planus, confirming the overarching study hypothesis. Additional research comparing different classification systems of foot type/foot posture, (Ledoux & Hillstrom, 2002; Ledoux et al., 2003;

Redomond et al., 2006) in addition to larger sample sizes, would be useful in understanding these contrasting outcomes.

Table 18. Means and SD for first ray mobility of previous research compared to the present study.

Study	Year	Mean Mobility	Load (N)	Method
Jones et al.	2005	7.4 ± 2.0	N/A	Mechanical
Glasoe et al.	2005	6.1 ± 1.1	45	Electromechanical
Glasoe et al.	2005	5.5 ± 1.0	55	Electromechanical
Tavara-Vidalon et al.	2018	6.5 ± 2.6	N/A	Radiographic
Munuera-Martinez et al.	2020	6.5 ± 1.1	N/A	Handheld Ruler
Present Study	2021	7.2 ± 2.6	50	Electromechanical

In the rectus foot, the first ray will remain purchased to the ground, bearing a similar amount of load compared with the second ray (Ledoux & Hillstrom, 2002; Ledoux et al., 2003; Hillstrom et al., 2013; Buldt et al., 2018; Song et al., 2018). During midstance, the rectus foot will establish equilibrium between the plantar fascia and toe flexor muscles (Erdemir et al., 2006; Murley et al., 2009). In the planus foot, where the first ray is more likely to be hypermobile, the first metatarsal head may be unable to resist the ground reaction force and share the burden of forefoot loading with the second metatarsal. As a result, lowering of the MLA is likely to leave the plantar soft tissues in a maximally elongated position. Increased load observed under the hallux, in the present study, may be explained by first ray hypermobility due to reduced mechanical advantage of the Windlass mechanism (Jack E, 1940; Roukis et al., 1996; Rao et al., 2011). Consistent with this theory, rotational laxity of the first MTP joint, in partial-weightbearing, was related by stepwise linear regression to first ray hypermobility. Restricted first MTP joint rotational flexibility and concomitant increased load beneath the hallux may promote a higher flexion moment arm between the hallucial load and first MTP joint. This enlarged moment arm about the first MTP joint, and increased hallucial load, may subject the cartilage to higher contact forces and stress, ultimately resulting in cartilage failure: A theory which will be explored in the following chapters of this thesis.

Roukis et al., (1996) found that motion of the first MTP joint was influenced by first ray “position”. They reported that 4 mm of first ray dorsal translation reduced first MTP joint dorsiflexion by 19.3%, and when dorsal translation reached 8 mm, dorsiflexion reduced by an additional 34.7%. The rotational component of first MTP joint kinematics has typically been defined by dorsiflexion (Allen et al., 2004; Rao et al., 2013; Buldt et

al., 2015). Research in this area has provided conflicting evidence. Buldt et al., (2015) reported lower first MTP joint dorsiflexion in planus compared to rectus individuals during gait whereas, Rao et al., (2013) found no difference with the foot in static weightbearing. Furthermore, Allen et al., (2004) compared the first MTP joint dorsiflexion of subjects with “stiff” and “lax” first rays during gait, finding a weak relationship between first ray mobility and first MTP joint dorsiflexion. In the current work, rotational laxity of the first MTP joint, which is the amount of angular rotation for a standardised amount of torque, was assessed. It was found that hypermobile subjects exhibited significantly greater first MTP joint rotational laxity than non-hypermobile subjects. As shown by Roukis et al., (1996) position of the first ray is likely to influence “stiffness” of the first MTP joint during gait. Lowering of the MLA in pes planus may limit the first MTP joints mechanical advantage afforded by the Windlass mechanism through increased passive tension of the plantar fascia.

The mechanism of first ray hypermobility is not fully understood, and several pathways have been suggested including, posterior tibial tendinopathy (Wong et al., 2018), insufficiency of the deep transverse metatarsal ligament (Coughlin MJ, 1996), and a weak PL (Roukis et al., 1996; Johnson & Christensen, 1999; Murley et al., 2009; Kokubo et al., 2012). Several investigators have pointed to the sagittal plane effects of the PL as a likely mechanism of first ray mobility and its role in assisting the Windlass mechanism (Hick HJ, 1954) and enhancing dorsiflexion of the first MTP joint (Roukis et al., 1996; Johnson & Christensen, 1999). The PL tendon’s primary role is to evert the hindfoot and secondarily keep the first MTP joint purchased to the ground (Johnson & Christensen, 1999). From a structural perspective, the PL may provide passive and active contributions to stabilisation of the first metatarsal against the medial cuneiform. Conceptually, the PL in a rectus foot may help the first ray to resist excessive motion by drawing it into plantarflexion due to the tendons line of action across the lateral ankle (Johnson and Christensen, 1999). However, there is conflicting evidence for a relationship between foot type and PL function. Murley et al., (2009) observed a reduction of PL activation in planus feet during gait. Compared with a rectus group, planus subjects exhibited a mean decrease in peak PL Electromyographic (EMG) amplitude of 12.8% during the contact phase of gait and 13.7% during midstance (Murley et al., 2009). Conversely, Gray and Basmajian. (1968) found the PL to be more active in planus versus rectus individuals during level

walking. It is possible that these differences may be explained by the level of first ray mobility which was not measured in either study. Root et al., (1977) were some of the earliest researchers to theorise that the PL played a stabilising role in forefoot kinematics and first ray mobility during gait. The investigators suggested that pronation of the planus foot may reduce the mechanical advantage of the PL and transfer load from the first ray to lesser metatarsals. Of the limited work performed in this area, Olson et al., (2003) found the PL to be the primary muscle for increasing plantar pressures beneath the first metatarsal head, demonstrating the stability it provides to the first ray.

5.5.1 Limitations

There were several limitations of this research that should be considered. Firstly, a small sample size was presented. However, the current data could be used for power analysis to design future investigations. Secondly, first MTP joint flexibility was not assessed in weightbearing. Though the present information provides a novel understanding of the interaction between flexibility and foot structure, analyses in weightbearing would provide a more complete description of first ray mechanics in the presence of hypermobility. It is likely that weightbearing first MTP joint laxity is negatively related to first ray mobility due to maximal elongation of the plantar fascia, limiting the Windlass mechanism. Thirdly, the cavus foot type was not included in this study. It has previously been reported that pes cavus is protective against foot injuries and that individuals who exhibited this foot type were less likely to develop OA of the midfoot and forefoot (Kaufman et al., 1999; Rao & Bell, 2013). Finally, plantar pressure measurement platforms are valuable in assessing the interactions between weightbearing foot structure and functional mechanics. However, while the ability to measure vertical components of the GRF inform loading patterns of the foot, the reliability of such devices and effect of the supporting surface characteristics must be considered. Plantar loading measurements from the emed-x platform have found moderate to high reliability (Hughes et al., 1991; Hafer et al., 2013). Consistent with the present study's methodology, Hafer et al., (2013) found that an average of three to five walking trials were required to achieve reliable data. Surface flexibility of plantar pressure platforms have been suggested as a limitation of the technology; however,

Giacomozzi C, (2010) found Novel platforms to have high linearity, low creep, low hysteresis, and low variability in performance.

5.6 Conclusion

Many structural and functional abnormalities of the first ray have been linked to pes planus, in pursuit of explaining why this foot type is disproportionately affected by certain orthopaedic conditions such as, hallux rigidus. This study of healthy, asymptomatic subjects with planus and rectus feet established that individuals with first ray hypermobility were predominantly planus in foot type. The first metatarsal of planus individuals, presenting with first ray hypermobility, will translate excessively in the superior direction, causing foot pronation and a transfer of load to the second metatarsal and hallux. Furthermore, an interaction between rotational first MTP joint flexibility and translational first ray mobility was demonstrated. Stepwise linear regression analyses found that first ray mobility was predictive of MF beneath the first metatarsal and laxity of the first MTP joint. These findings provide objective evidence of first ray hypermobility's role in abnormal structure and function of the medial forefoot. It is the postulate of this research, that interactions between translational first ray hypermobility, rotational first MTP joint flexibility, and concomitant increased load beneath the hallux may be causative of aberrant first MTP joint loading. To explore this theory, the following chapters utilised FE modelling to predict the effect of first ray hypermobility, in the planus foot type, on cartilage contact mechanics of the first ray.

Chapter 6. In Vitro Verification of a Finite Element Model During Quasi-Static Loading

6.1 Chapter Overview

Chapter 6 describes the design of a cadaveric mechanical test-rig, cadaveric experimentation, and the development of a quasi-static force-controlled FE model of the medial forefoot. The study objective was to calibrate and verify the FE model first MTP and MTC joint contact mechanics against intracapsular TekScan pressure sensor measurements.

Aim 5: Verify the first MTP and MTC joint contact mechanics of a medial forefoot FE model simulating planus and rectus foot types.

Hypothesis 5: In vitro-measured and FE-predicted first MTP and MTC joint contact mechanics (force, contact pressure, contact area, and contact pattern) will be within 30% for the same boundary and loading conditions.

6.2 Introduction

In chapter 5 of this thesis, individuals with first ray hypermobility were linked with the planus foot type, increased hallucial loading, and greater first MTP joint flexibility. Although multi-factorial in nature, these three structural and functional parameters were indicative of aberrant pedal mechanics. Commensurate excessive loads across the first ray's articulating soft tissues may lead to cartilage matrix breakdown and degeneration (Jack E, 1940; Roukis et al., 1996; Golightly et al., 2018). Despite the frequency of degenerative disease at the first MTP and first MTC joints (Rao & Bell, 2013 Menz et al., 2015; Morgan et al., 2019), little is known about their loading environments (McBride et al., 1991; Liu et al., 1997; Athanasiou et al., 1998; Wong et al., 2018; Peng et al., 2021). Although physical testing is essential in the evaluation process, methods like intracapsular pressure sensors are limited to measurements of

contact force, pressure, and area (Wu et al., 1998). Computational modelling can augment these experiments by non-invasive predictions of cartilage failure modes including stress and strain (Sasazaki et al., 2006; Mononen et al., 2012; Venäläinen et al., 2016).

Finite element modelling of the foot has been used to predict plantar pressures (Budhabhatti et al., 2009; Cheung et al., 2004; Isvilanonda et al., 2012; Sun et al., 2012; Wong et al., 2014; Guo et al., 2018), visualise internal soft tissue stress distributions (Gefen et al., 2003; Wong et al., 2014; Wong et al., 2018), and perform parametric studies (Budhabhatti et al., 2009; Isvilanonda et al., 2012). The perceived reliability of such models is governed by verification and validation against experimental data (Viceconti M, 2005; Henninger et al., 2010). Verification acts as a precursor to validation and determines if "a computational model accurately represents its solution" (i.e. geometric reconstruction and mesh convergence) (ASME Committee (PT60) on Verification and Validation in Computational Solid Mechanics, 2006; Henninger et al., 2010). Validation is conducted to determine "the degree to which a computational model is an accurate representation of the real world" (i.e. kinetics and kinematics) (ASME Committee (PT60) on Verification and Validation in Computational Solid Mechanics, 2006; Henninger et al., 2010). Prior models of the foot have either excluded the geometries of forefoot cartilage (Budhabhatti et al., 2007; Flavin et al., 2008; Garcia-Gonzalez et al., 2009; Akrami et al., 2018; Wong et al., 2018) or been verified or validated using plantar pressures (Isvilanonda et al., 2012; Wong et al., 2014; Akrami et al., 2018) and kinematics (Gefen et al., 2002; Morales-Orcajo et al., 2017), not accounting for the accuracy of joint contact mechanics. This presents inherent ambiguity of the first ray's articular soft tissue properties and resulting contact mechanics.

Therefore, the purpose of this study was to build and verify a FE model of the medial forefoot by: (1) designing a custom force-controlled cadaveric test-rig for physiological loading of the medial forefoot and intracapsular TekScan (TekScan Inc, Boston, MA, USA) pressure sensor measurements of first MTP and first MTC joint contact mechanics; (2) conducting specimen-specific FE model calibrations of first MTP and first MTC joint articular cartilage moduli against the experimental data, and; (3) performing verification of the FE-predicted first MTP and first MTC joint contact forces, contact areas, and contact pressures from the corresponding TekScan pressure

sensor measurements. The limit of verification between the experimental measurements and FE-predictions was considered less than 30%.

6.3 Materials and Methods

The methodology in this chapter comprises two sections: (1) the design and testing of a custom-built cadaveric test-rig for measuring medial forefoot joint contact mechanics and (2) the 3D reconstruction, calibration, and verification of a medial forefoot FE model.

6.3.1 Design of a Cadaveric Test-Rig

The following design specifications were applied to the test-rig: (1) accommodate the first and second rays of any specimen; (2) emulate different arch-alignments of the foot; (3) allow the first metatarsal and phalanges of the first and second rays to move in all six DOF; (4) enable the application of forces beneath the first and second metatarsals, first and second distal phalanges, and medial band of the plantar fascia to achieve static equilibrium; (5) allow sagittal rotation of the medial cuneiform to emulate declination of the foot's arch during weightbearing. Since the test-rig would be transported from Anglia Ruskin University (ARU) in the UK, to HSS in the USA, its material selection required high yielding but to be lightweight. The test-rig components were therefore manufactured from aluminium alloy.

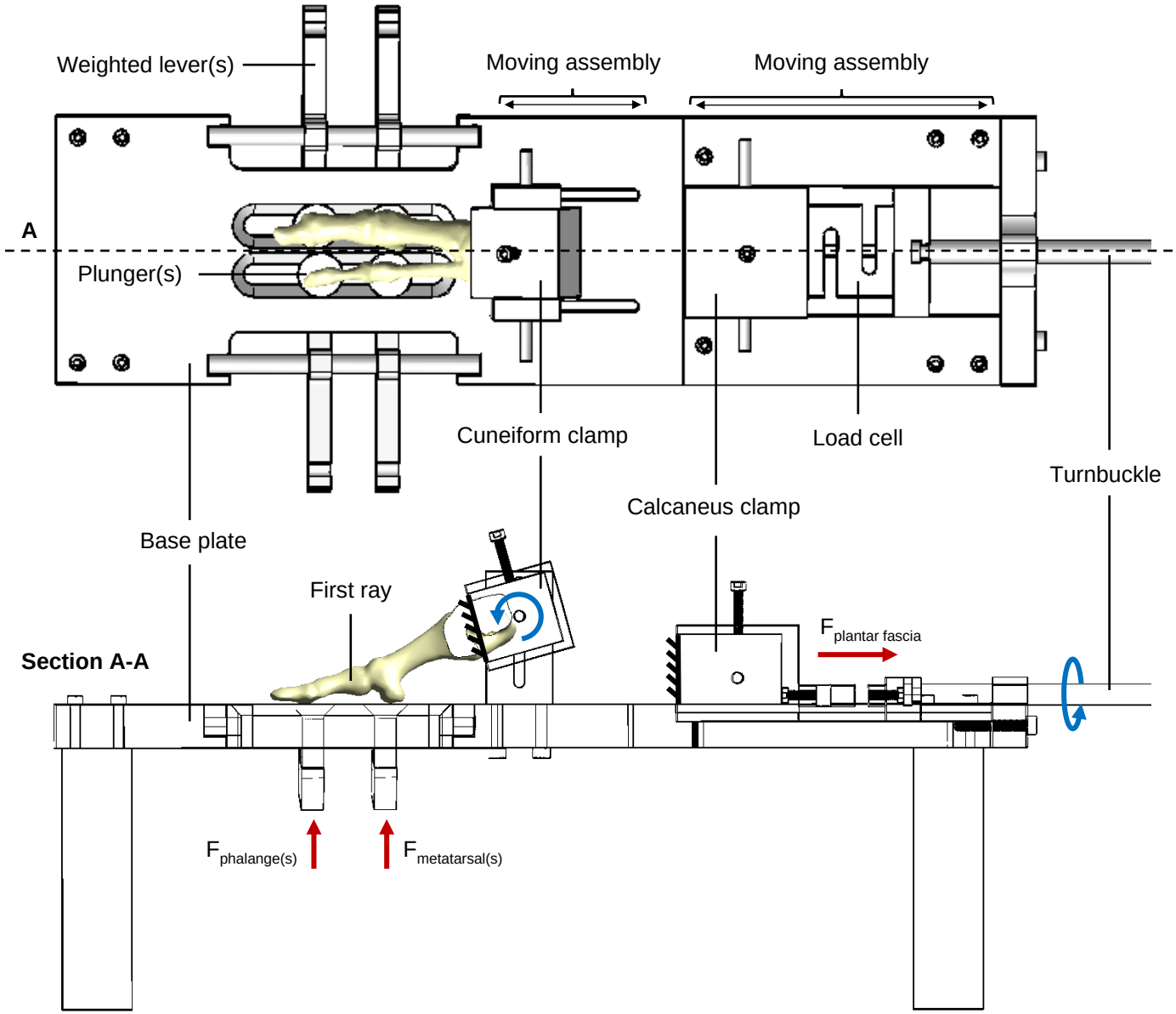

Figure 30. A SolidWorks illustration of the initial design concept for the cadaveric medial forefoot test-rig, shown from the superior view (top) and lateral cross-sectional view (bottom). The forces acting on the system are denoted using red arrows while rotating components are denoted using blue arrows. The medial forefoot placement is shown in the illustration; however, the location of the calcaneus and the plantar fascia path of insertion is not shown.

The custom-made test-rig was designed in SolidWorks (SolidWorks 2018, Dassault Systèmes, Vélizy-Villacoublay, France) by the author of this thesis (Figure 30). It was manufactured by an experienced technician (Dan Jackson) at ARU's mechanical engineering workshop. The test-rig included a clamp for the cuneiform and second metatarsal which allowed rotation in the sagittal plane. This clamp also translated in the SI directions, enabling the declination angle of the metatarsals to change, representing different arch heights. The metatarsals and phalanges of the first and second rays were free to move naturally, in all six DOF. The calcaneus was fixed to a mechanism that translated in the AP directions. This took advantage of the windlass mechanism to emulate tension in the plantar fascia upon weightbearing. Tensile load was applied to the plantar fascia using a turnbuckle. An S-shaped load cell was fixed between the calcaneus and turnbuckle to record the tensile force. Plantar loading was applied through a series of four levers, which distributed loads beneath distal phalanges and metatarsal heads in a physiological manner. Upon initial testing, the distance between the calcaneus clamp and end range of the cuneiform clamp was too large for the cadaveric specimen. A polymer extender for the calcaneus was designed and 3D printed (MakerBot Replicator 2, Brooklyn, NY, USA) to reduce this distance.

6.3.2 Cadaveric Testing

One fresh-frozen cadaveric specimen was tested which included the anatomical structures of the first ray (distal phalanx; proximal phalanx; hallucial sesamoids; first metatarsal; medial cuneiform) and the second ray (distal phalanx; middle phalanx; proximal phalanx, second metatarsal, and; medial band of the plantar fascia). The cadaveric specimen was a right foot from a male, 26 years of age, weighing 270 lbs at a height of 71 inches. There was no history of surgery, trauma, cartilage damage, or osteophytes. Preparation of the specimen was performed by a HSS clinical fellow assigned to the study (Rogerio Bitar, MD). A whole foot was dissected with the first, second, and third rays disarticulated from the surrounding soft tissues. The medial band of the plantar fascia was separated from the central band while retaining its insertion into the base of the first and second metatarsals and calcaneus (Figure 31A). To maintain the integrity of the transverse arch and cuneiform mortise the lateral cuneiform and base of the third metatarsal were preserved (Figure 31B).

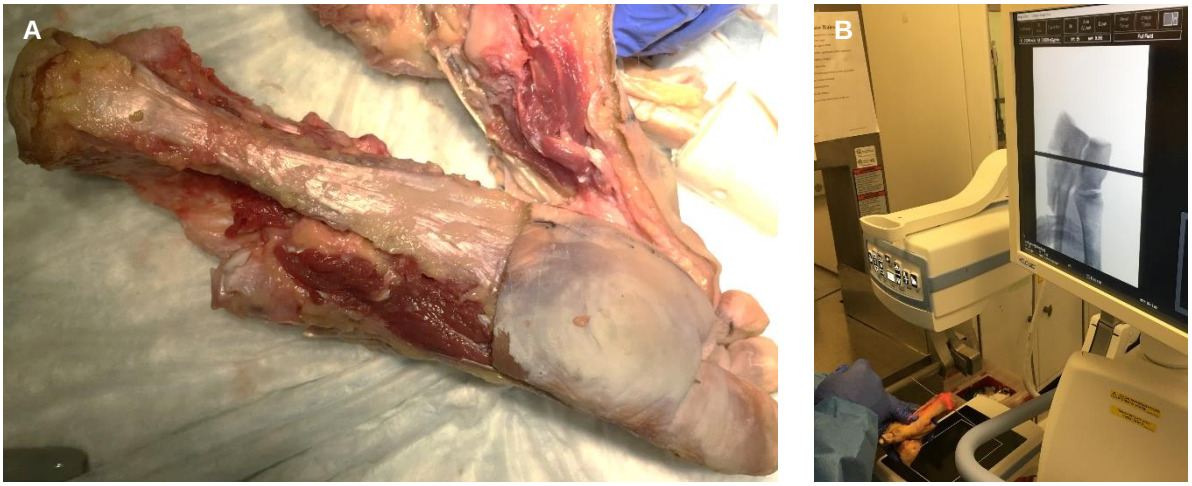

Figure 31A-B. Photographs of the cadaveric medial forefoot specimen being prepared for testing: (A) the medial band of the plantar fascia separated from the central band while retaining its insertion into the base of the first and second metatarsals and calcaneus, and; (B) Siemens C-Arm x-ray machine (Siemens, Munich, Germany) used to visualise the axis of sagittal rotation for the cuneiforms.

Two conditions were evaluated: (1) a planus arch-alignment, and (2) a rectus arch-alignment. The activity of midstance was simulated at ¼ of the maximum plantar force parameters of individuals with planus and rectus foot types (Hillstrom et al., 2013). Pes planus loading was set to 34 N at the first metatarsal head, 34 N at the hallux, 43 N at the second metatarsal head, and 6 N at the second distal phalanx. Pes rectus loading was set to 40 N at the first metatarsal head, 28 N at the hallux, 38 N at the second metatarsal head, and 5 N at the second distal phalanx. Pretension in the plantar fascia was calculated in order to achieve static equilibrium. This was based upon the arch-specific metatarsal declination angles; a pes planus pretension of 428 N and a pes rectus pretension of 343 N were applied.

During testing, thin pressure sensors (TekScan K-Scan 6900, TekScan Inc, Boston, MA, USA) were preconditioned, equilibrated, and calibrated to acquire measurements of first MTP and first MTC joint contact mechanics (force, area, pressure, and pattern) (Figure 32B). The pressure sensors were sutured to the plantar cortices of each joint to prevent ejection during testing (Figure 32C). The specimen was then mounted in the test-rig, which positioned the first metatarsal in 10° and 20° of declination in the sagittal plane, emulating planus and rectus arch-alignments, respectively (Buldt et al., 2015). A goniometer was used to measure the first metatarsal angle with respect to the base of the test-rig (Figure 32D). These conditions were selected based on the final aim of this thesis: to investigate arch specific variances in joint contact mechanics.

Insertion of the TekScan pressure sensors into the first MTP and MTC joints were performed by excising the capsules and inserting the sensor films into the joint cavities, from the superior aspect.

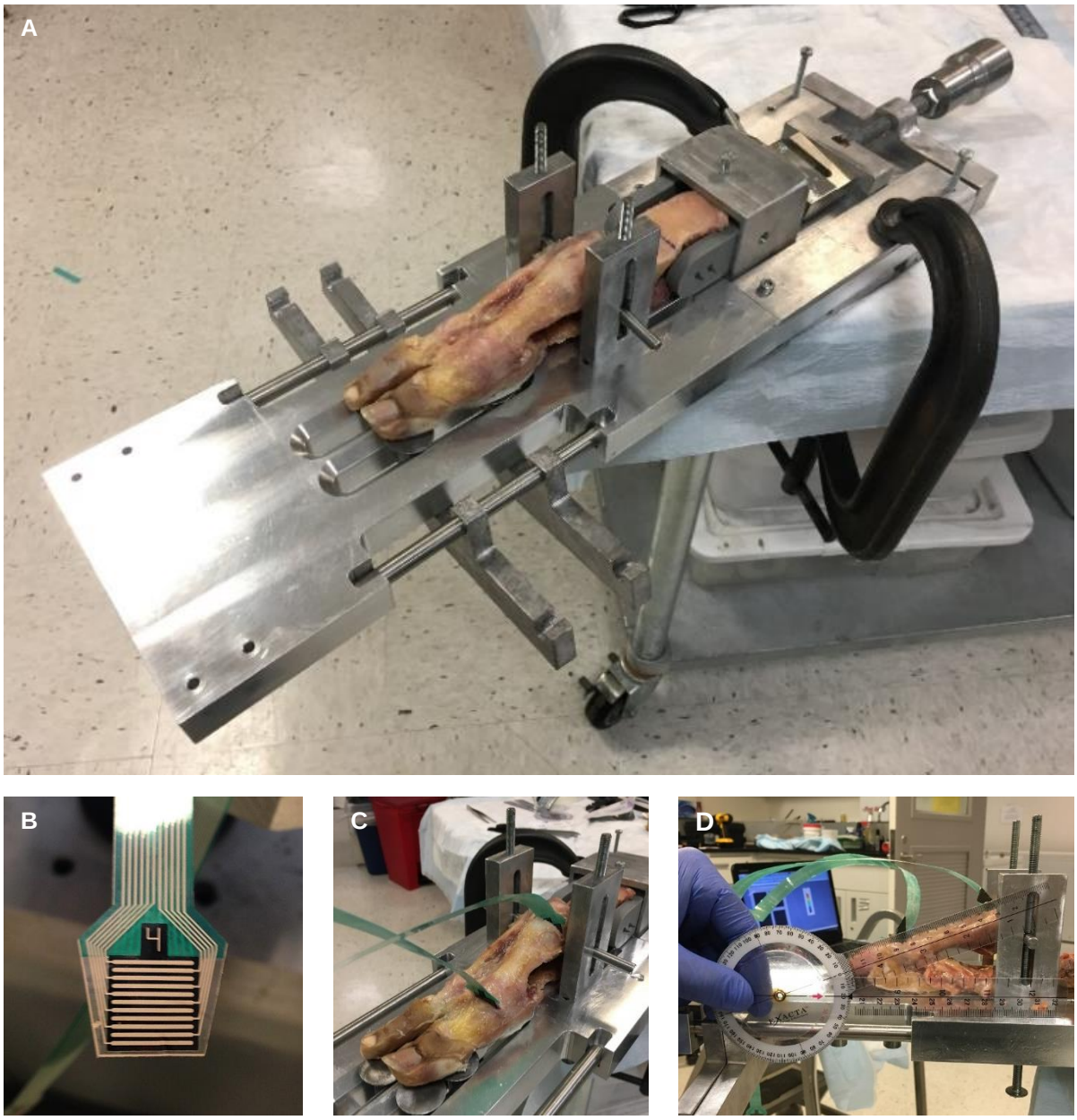

Figure 32A-D. A series of photographs showing a right cadaveric medial forefoot: (A) isometric view of the test-rig with the cadaveric foot ready for testing. The medial, middle, and lateral cuneiforms are fixed to a pivot mechanism at the anterior portion of the device which allows sagittal rotation, while the calcaneus has been fixed to a posterior component, with all DOF constrained. (B) the TekScan K-Scan 6900 intracapsular pressure sensor; (C) insertion of the pressure sensor into the first MTP and MTC joints, sutured to the plantar cortices of each joint to prevent ejection of each sensor during testing; and (D) measurements of the metatarsal angle using a goniometer to define the arch-alignments of the rectus and planus foot types.

6.3.3 Three-Dimensional Reconstruction

A 3T magnetic resonance imaging (MRI) scan (GE Healthcare, Waukesha, WI, USA) protocol was used to derive the three-dimensional (3D) geometries of the specimen (Figure 33). A CUBE sequence (echo time (TE) = 26.4 ms; repetition time (TR) = 2500 ms; echo train length: 20; voxel size: 0.31 mm x 0.31 mm x 0.8 mm, slice thickness) was used to create 3D representations of the plantar fascia. A frequency selective fat-suppressed spoiled gradient recalled echo (SPGR) sequence (TE = 3 ms; TR = 10 ms; echo train length: 1; voxel size: 0.2 mm x 0.25 mm x 1 mm, slice thickness) was used to define the geometries of the bones and articular cartilages. The anatomic geometries were manually segmented in Mimics (Mimics v21, Materialise, Leuven, Belgium). Intersecting segmented geometries were then eliminated using the non-manifold tool in 3-matic (3-matic v14.0, Materialise, Leuven Belgium).

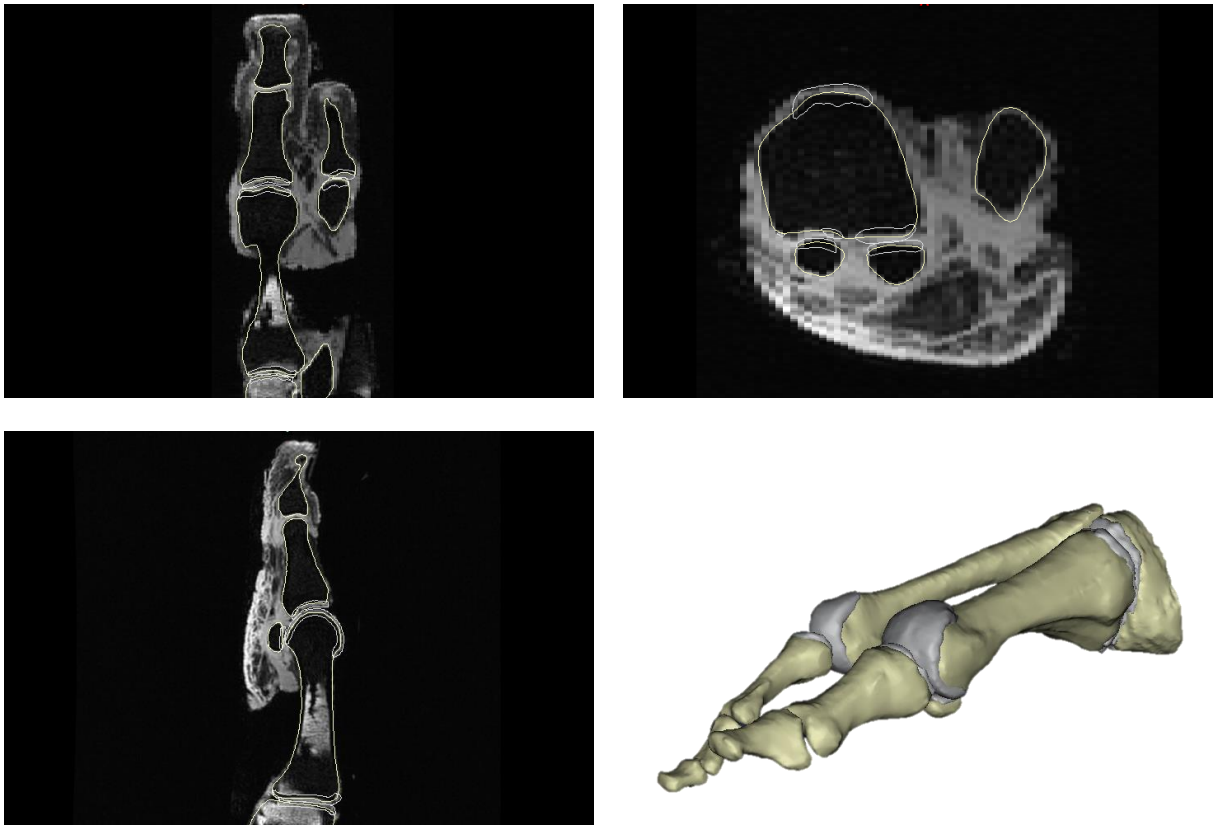

Figure 33. Image of the segmented geometries of the medial forefoot in Mimics. A 3T MRI-scan was used to image the soft tissues, enabling 3D reconstruction in preparation for FE model development.

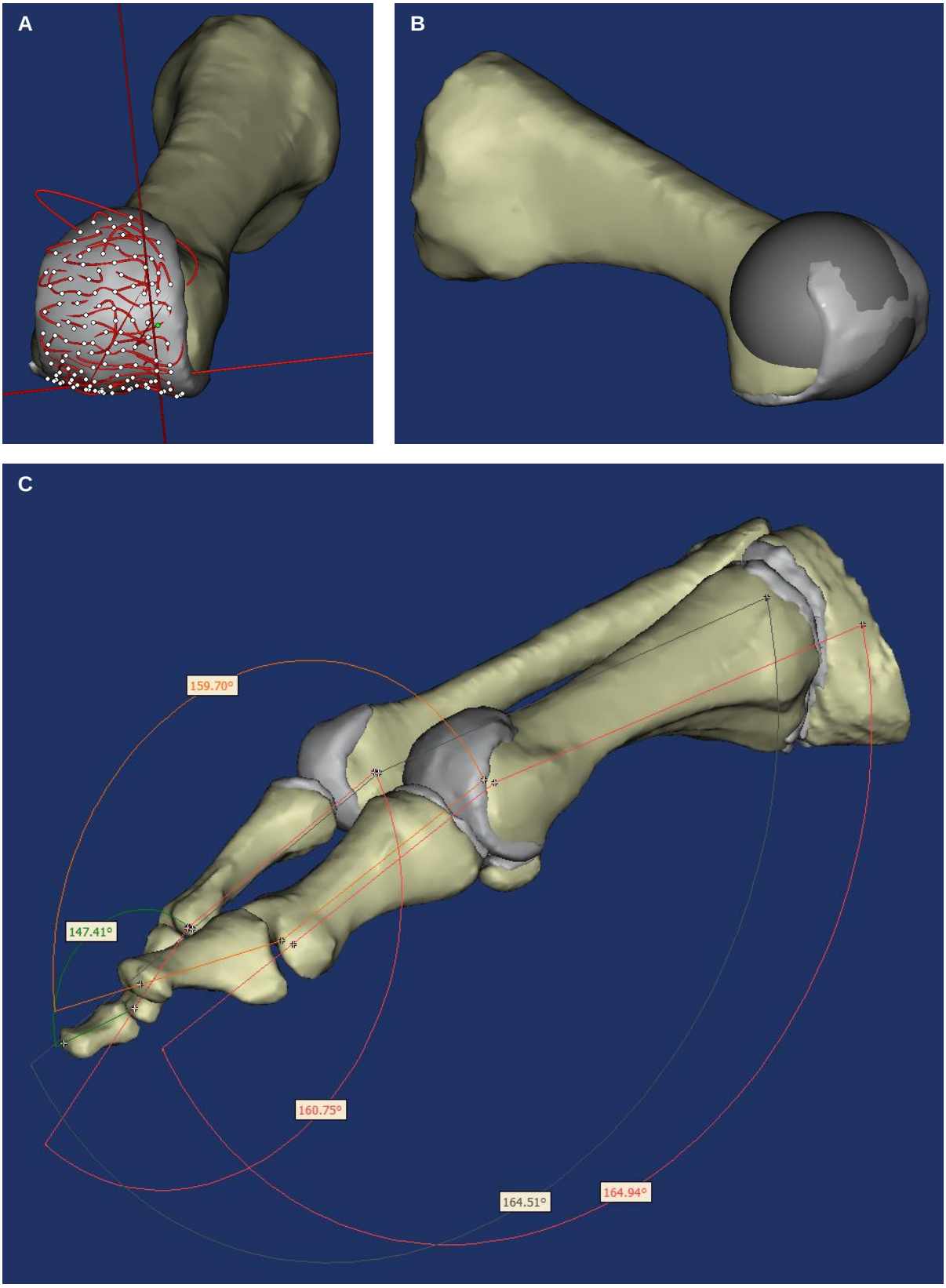

Figure 34A-C. Process for calculating the initial joint angles of the medial forefoot in Mimics. (A) Creation of an array of digitised points on the articular surface of the first metatarsal head; (B) virtual ball generated from the digitised points representing the first MTP joint's inertial axis; and, (C) the centre of the first MTP joint, calculated as the midpoint of the virtual ball.

The size and shape of the MRI-coil meant that the cadaver was unnaturally aligned during image acquisition. This necessitated a step prior to the FE-loading simulations, which realigned the sagittal joint angles of the model to match the cadaver during experimental testing. The initial joint angles were calculated in Mimics for the specimen (Figure 34C; Table 19). Digitised points were made at the joint rotation centres with which to calculate the angles (Figure 34A). The rotational axes of the first and second MTP joints were determined using a custom-written MATLAB code (MATLAB R2014a, Natwick, USA), which created a sphere to find the inertial axis of a joint (Figure 34B). To find the inertial axis, an array of points was created on the surfaces of the metatarsal and phalange heads in Mimics. Once the points were made, the MATLAB script was executed to create a virtual ball representing the inertial axis of the joint. The midpoint of the ball was used to define the anatomical axis for referencing the joint centre coordinates.

Table 19. Initial joint angles and realigned joint angles for the planus and rectus models.

Angle (°)	Initial	Planus	Rectus
First MTP joint	-15.06	-5.06	5.06
First IP joint	20.3	0	0
Second MTP joint	-15.49	-5.49	5.49
Second PIP joint	-19.25	0	0
Second DIP joint	32.59	0	0
IMA	10.10	10.10	10.10
First metatarsal declination	-3.49	10	20
Second metatarsal declination	-3.02	9.53	19.53

IP, interphalangeal; PIP, proximal interphalangeal; DIP, distal interphalangeal; IMA, intermetatarsal angle

6.3.4 Finite Element Modelling

The FE model was constructed in Abaqus (Abaqus 6.14-1, Dassault Systèmes, Vélizy-Villacoublay, France) (Figure 35), where the soft-tissues were meshed, and the metatarsals, and phalanges assigned prescribed sagittal rotations for realignment. Bone and plantar fascia were meshed as 4-noded linear tetrahedrons (C3D4) and cartilage as 8-noded linear hexahedrons (C3D8R). Athanasiou et al., (Athanasiou et al., 1998) measured MTP cartilage thickness through the superficial zone of 5%,

middle zone of 25%, deep zone of 60%, and calcified layer of 10%. Liu et al., (Liu et al., 1997) measured MTC cartilage thickness through the superficial zone of 6%, middle zone of 28%, deep zone of 60%, and calcified layer of 6%. Therefore, cartilage was meshed using 10 layers in a non-linear distribution of hexagonal elements with a double bias ratio (> = 1) of 5 towards the articular and osteochondral surfaces (Figure 35). Superficial zone: two elements equal to 8%; middle zone: two elements equal to 26%; deep zone: four elements equal to 58%; calcified layer; two elements equal to 8%. This was done in order to differentiate between the zonal distributions of the articular and osteochondral surfaces, which is in line with recent computational modelling techniques (Henak et al., 2014; Todd et al., 2018). This will enable the analysis of depth-dependent stress-strain distributions in future research.

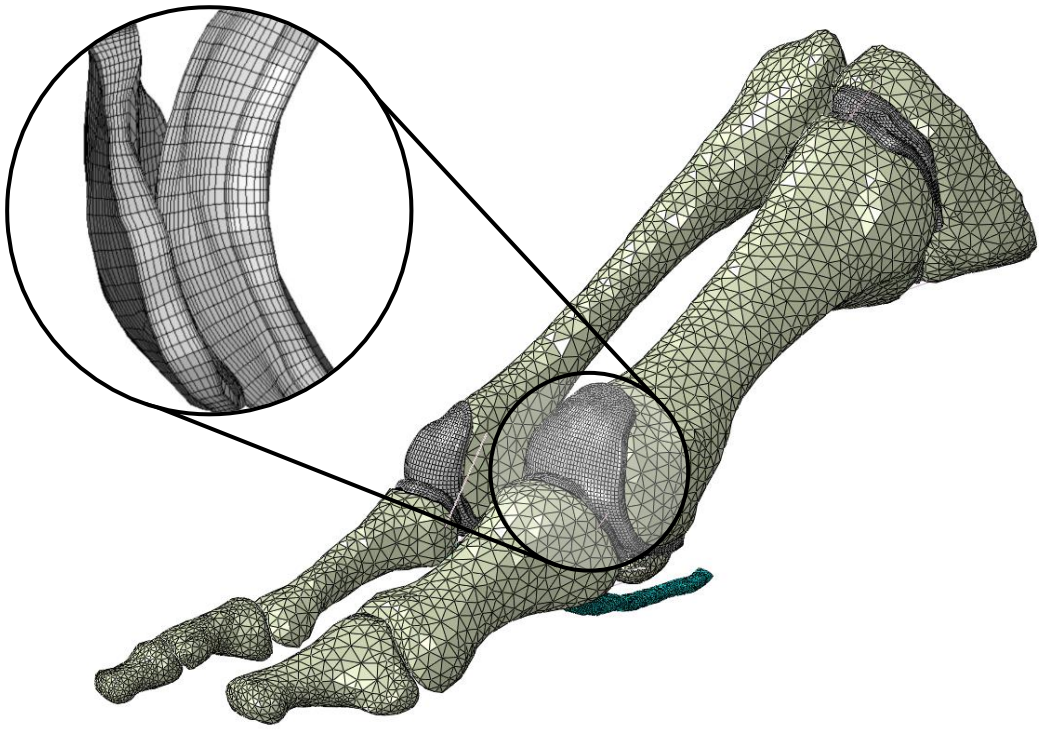

Figure 35. The medial forefoot FE model, showing the meshed geometries of bone, plantar fascia, and cartilage. Alignment angles were set to be the same as those of the cadaver during testing, for the corresponding planus and rectus conditions. A magnified image of the first metatarsal head and proximal phalanx base cartilage is shown. The method of double bias ratio meshing can be seen, with the layers of mesh becoming finer toward the articular and osteochondral surfaces.

The ground and bone were modelled as homogeneous isotropic, linear elastic materials (E = 7300 MPa; v = 0.3) (Nakamura et al., 1981). The simplest form of isotropic, linear elasticity and its stress (σ)-strain (ε) relationship can be defined as:

$$\begin{bmatrix} \varepsilon 11 \\ \varepsilon 22 \\ \varepsilon 33 \\ \varepsilon 12 \\ \varepsilon 13 \\ \varepsilon 23 \end{bmatrix} = \begin{bmatrix} 1/E & -v/E & -v/E & 0 & 0 & 0 \\ -v/E & 1/E & -v/E & 0 & 0 & 0 \\ -v/E & -v/E & 1/E & 0 & 0 & 0 \\ 0 & 0 & 0 & 1/G & 0 & 0 \\ 0 & 0 & 0 & 0 & 1/G & 0 \\ 0 & 0 & 0 & 0 & 0 & 1/G \end{bmatrix} \begin{bmatrix} \sigma 11 \\ \sigma 22 \\ \sigma 33 \\ \sigma 12 \\ \sigma 13 \\ \sigma 23 \end{bmatrix} \quad (5)$$

where, the elastic properties are the same in all directions and are defined by providing the Young's modulus (E), and the Poisson's ration (v). The shear modulus (G) can be expressed in terms of E and v as:.

$$G = \frac{E}{2}(1 + v) \quad (6)$$

The initial material properties for hyaline cartilage were derived from literature-based experimental compressive tests on talus cartilage (Shepard & Seedhom, 1999). A Poisson's ratio of 0.46 was set as constant (Klets et al., 2016) while the Young's modulus was calibrated to find a best-fit between the FE and experimental results. The material parameters were represented by a homogeneous isotropic, neo-Hookean material. The strain energy density function (Ψ) for the hyperelastic constitutive relations may be given as:

$$\Psi = C_{10}(I_1 - 3) + \frac{1}{2D}(J - 1)^2 \quad (7)$$

where, I_1 is the invariant of the Cauchy-Green deformation tensor and J is the elastic volume ratio. C_{10} and D are the neo-Hookean constant and inverse of the bulk modulus, respectively. The bulk (K_0) and shear (μ_0) moduli were acquired from the modulus of elasticity and Poisson's ratio. The neo-Hookean coefficients D and $C_{10,}$ were then calculated from the bulk and shear moduli and entered into the energy density function within Abaqus to define the cartilage properties. In addition, a homogeneous isotropic, neo-Hookean material was used to model the plantar fascia (E = 200 MPa; v = 0.4) (Kitaoka et al., 1994) and calcified zone of cartilage (E = 320 MPa; v = 0.3) (Mente & Lewis, 1994).

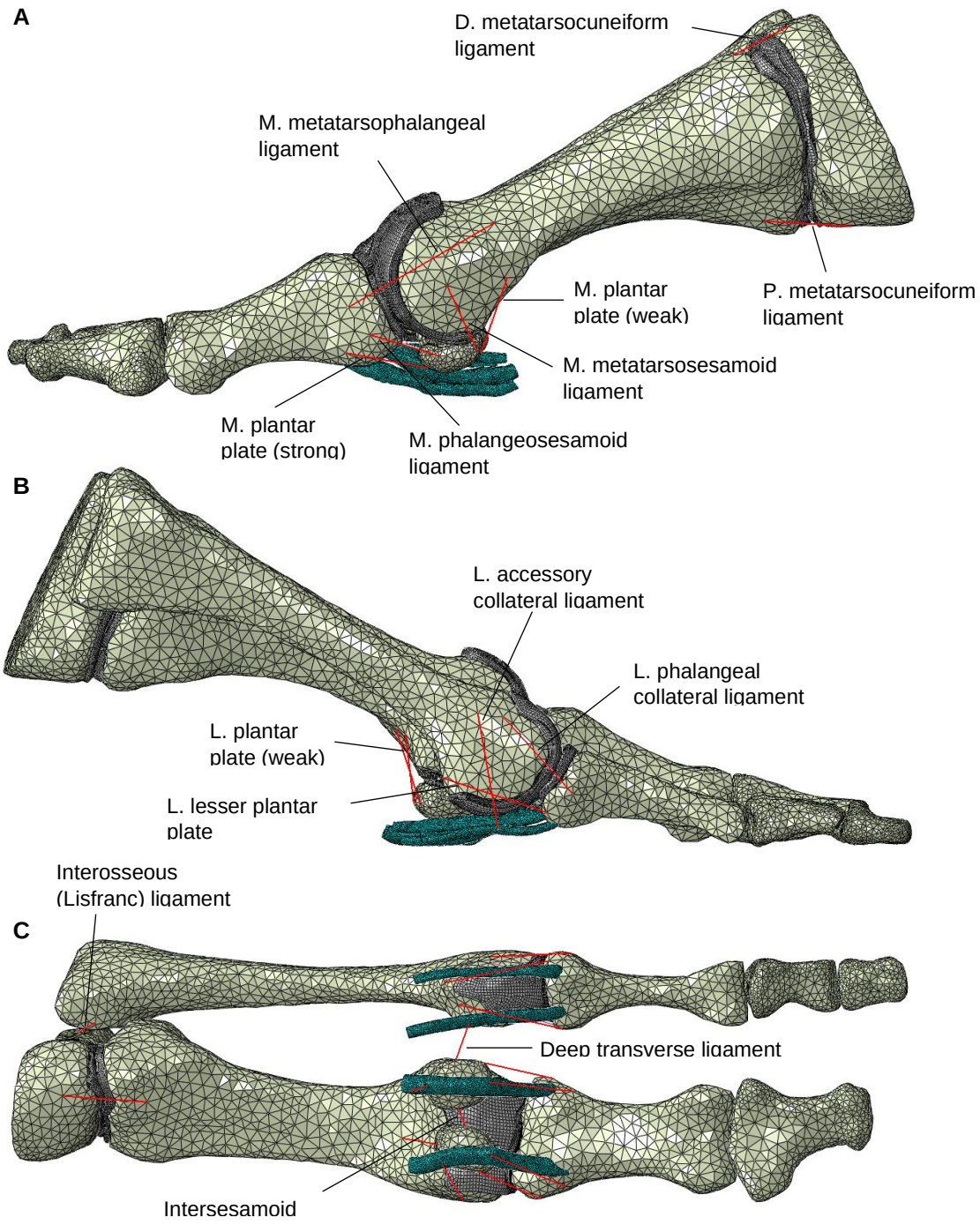

Figure 36A-C. Ligament insertion sites and positions within the Abaqus medial forefoot FE model shown from the: (A) medial; (B) lateral, and; (C) plantar aspects. The 2D connectors used to idealise the ligaments are highlighted in red.

The ligaments of the first and second rays were modelled as linear elastic 1D tension-only connector elements (T3D2), which characterised their functional contributions (Figure 36A-C). Due to difficulty in identifying the ligament insertion sites from the MRI datasets, positions were based upon guidance from the foot and ankle surgeons

involved in this study, (Scott J Ellis, MD and Jonathan T Deland III, MD) in addition to anatomic diagrams and literature descriptions. Ligament cross-sectional areas and material properties were derived from the literature (Table 20).

Table 20. Ligament properties.

Joint	Cross-sectional area (mm^2)	Young's modulus (E (MPa)), Poisson's ratio (ν)	Reference
First MTC Ligaments	28.8	264, 0.4	Mkandawire et al., 2005; Seigler et al., 1988
Interosseous (Lisfranc) Ligament	68.6	264, 0.4	Kura et al., 2001; Seigler et al., 1988
First MTP Ligaments	12.6	264, 0.4	Dietrich et al., 2015; Seigler et al., 1988
Deep Transverse Ligament	64.5	264, 0.4	Mkandawire et al., 2005; Seigler et al., 1988
Second MTP Ligaments	8	264, 0.4	Deland et al., 1995; Seigler et al., 1988

MTC, metatarsocuneiform; MTP, metatarsophalangeal;

Model boundary and loading conditions replicated the quasi-static activity performed during the experimental testing, detailed in section 6.3.2. Nodes proximal to the cuneiform and second metatarsal were free to rotate in the sagittal plane and constrained in all other DOF, according to the mechanical boundaries prescribed experimentally. The nodes of the first metatarsal, hallux, sesamoids, and second toe were free to move in all 6 DOF. The proximal surfaces of the medial band of the plantar fascia were constrained to a sagittal translation such that their displacement emulated the path of insertion into the calcaneus. These loading parameters matched the cadaveric testing protocol and ensured that both the experimental and FE results were obtained during a state of static-equilibrium, over the same time-period, and under the same boundary and loading conditions.

Frictionless surface-to-surface contact was defined for the articulations which formed the first MTP, lateral and medial metatarsosesamoid (MTS), second MTP, and first MTC joints. Contact between these surfaces was enforced using a "Hard" Penalty method. The interphalangeal articulations of the hallux and second toe were not included in the model, where the opposing nodes were tied together to form rigid bodies. The bone-cartilage and bone-fascia interfaces were also tied to represent the

osteochondral transition from soft tissue to bone. All analyses were computed using Abaqus 6.14-1.

Table 21. Mesh sensitivity analyses showing the resultant percentage change in the proximal phalanx base cartilage of the first MTP joint and metatarsal base cartilage of the first MTC joint (planus condition) for peak contact pressure, peak von Mises, and peak maximum principal stress from increasing mesh densities.

Mesh Size	First MTP Joint		First MTC Joint	
	Value	Percentage Change (%)	Value	Percentage Change (%)
Contact Pressure (MPa)				
0.1 mm	7.5	-	4.4	-
0.3 mm	7.6	1	4.6	4
0.5 mm	7.7	2	4.6	4
0.7 mm	7.9	6	4.7	7
1.0 mm	8.0	6	4.7	7
von Mises Stress (MPa)				
0.1 mm	8.6	-	4.0	-
0.3 mm	9.0	4	4.1	2
0.5 mm	9.0	4	4.4	11
0.7 mm	9.3	7	4.7	17
1.0 mm	9.4	8	4.7	17
Max. Principal Stress (MPa)				
0.1 mm	6.2	-	3.9	-
0.3 mm	6.8	8	4.2	8
0.5 mm	6.8	9	4.4	11
0.7 mm	7.0	12	4.4	11
1.0 mm	6.9	11	4.3	10
Mean Percentage Change (%)				
0.3 mm	4 ± 4		5 ± 3	
0.5 mm	***5 ± 4***		***9 ± 3***	
0.7 mm	8 ± 3		11 ± 5	
1.0 mm	8 ± 2		11 ± 5	

MTP, metatarsophalangeal; MTC, metatarsocuneiform

6.3.5 Mesh Convergence

Mesh convergence analyses were performed to determine the effects on FE model joint contact mechanics (Table 21). The mesh convergence identified the appropriate number of elements to achieve converged predictions within a 10% change of contact pressure, von Mises, and maximum principal stress. For these variables, the optimum mesh density for first MTP and first MTC joint cartilages was 0.5 mm. This density

obtained a mean 5% ± 4% change from 0.1 mm for the first MTP joint while the first MTC joint exhibited a mean 9% ± 3% change.

6.3.6 Calibration and Verification

The physical measurements of first MTP and MTC joint contact were compared to the computational measurements to provide a verification framework. Model outcomes included peak contact pressure, contact force, and contact area. These variables were extracted from Abaqus and compared to measurements from the K-Scan 6900 sensor.

6.4 Results

6.4.1 Calibration

The calibration procedure explored trends in contact pressure, contact force, and contact area for the first MTP and first MTC joint articular cartilages for both the planus and rectus simulations (Figure 37A-F). The articular cartilage was calibrated representing the lower (10 MPa), middle (15 MPa), and upper (20 MPa) bounds of human ankle cartilage compressive modulus (Shepard & Seedhom, 1999). Calibration of the cartilage Young's modulus resulted in a 7% ± 6% change in peak contact force, 28% ± 5% change in peak contact pressure, and 15% ± 11% change in contact area. A modulus of 10 MPa was found to be most appropriate for the first MTP joint while 20 MPa was most appropriate for the first MTC joint.

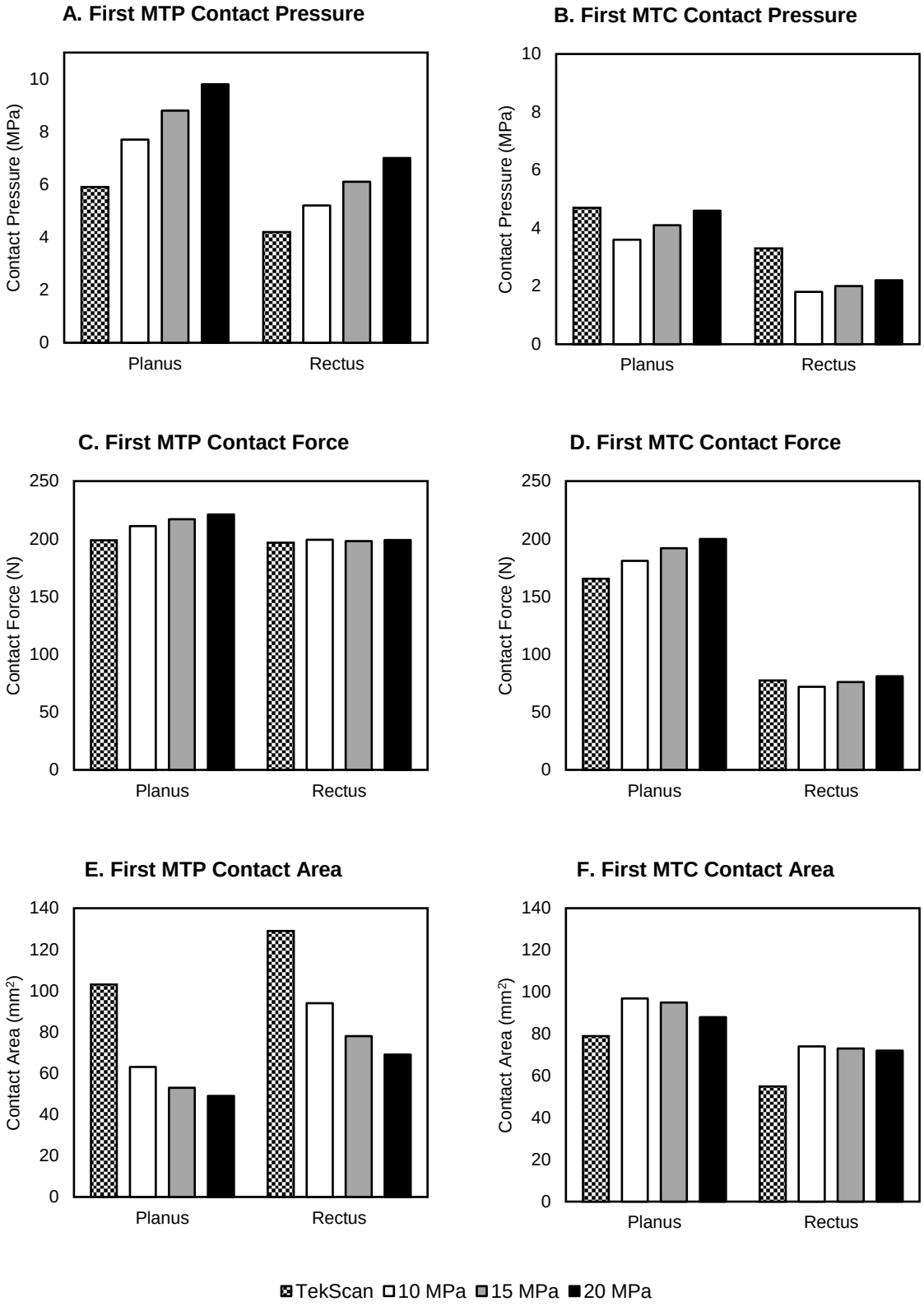

Figure 37A-F. Calibration outcomes of the FE model cartilage Young's modulus. The graph shows the change in contact variables by increasing cartilage elastic moduli from 10-20 MPa, compared to the TekScan measurements.

Table 22. Full-scale differences between the experimentally measured and FE predicted contact pressure, contact force, and contact area, for the planus and rectus models, during quasi-static loading.

Parameters	Planus			Rectus			Mean
	EXP	FE	% Diff	EXP	FE	% Diff	% Diff
First MTP Joint (10 MPa)							
Contact Pressure (MPa)	5.9	7.7	26	4.2	5.2	21	24
Contact Force (N)	198.8	211	6	196.8	200	2	4
Contact Area (mm^2)	103	63	48	129	94	31	40
First MTC Joint (20 MPa)							
Contact Pressure (MPa)	4.7	4.6	2	3.3	2.1	44	24
Contact Force (N)	165.4	200	19	77.5	81	4	12
Contact Area (mm^2)	79	88	11	55	72	27	19

EXP, experimental; FE, finite element; % Diff, percent difference; MTP, metatarsophalangeal; MTC, metatarsocuneiform.

6.4.2 Contact Pressure

Experimental peak contact pressures were decreased in the first MTP and first MTC joints from the planus to rectus conditions. While the absolute error remained <30% for most predictions, the rectus first MTC joint presented a 44% error (Table 22). Despite this finding, model predicted first MTC joint contact pressure showed agreement with experimental data in trend (Figure 37A-F). The experimental and model pressure distributions are shown in Figures 38.

6.4.3 Contact Force

When comparing model contact forces to the experimental measurements, the planus and rectus conditions had average errors of 12% ± 9% and 3% ± 2%, respectively (Table 22). The predicted reduction in first MTP and first MTC joint contact forces, from the planus to rectus conditions, were consistent with the trends demonstrated during experimental testing.

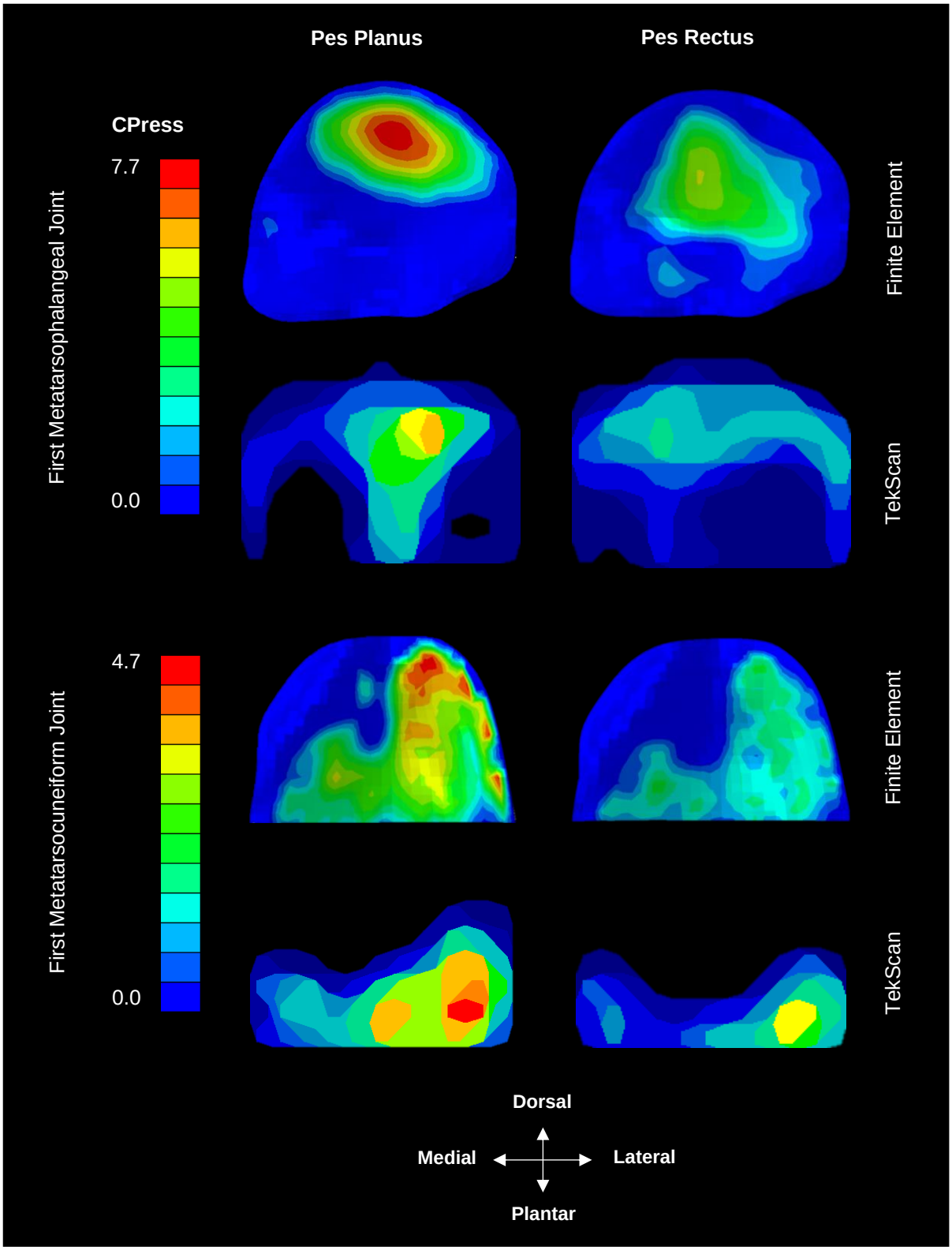

Figure 38. TekScan-measured and finite element-predicted contact pressure distributions shown at the proximal phalanx base (first metatarsophalangeal joint) and first metatarsal base (first metatarsocuneiform joint) for simulations of pes planus ad pes rectus arch-alignments.

6.4.4 Contact Area

First MTP joint contact area increased, from the planus to rectus condition, for both the experiment and model. However, the first MTP joint demonstrated a mean difference of 40% ± 12%. The first MTC joint exhibited a trend toward decreased contact area between planus and rectus conditions for the experiment and model, with a mean difference of 19% ± 11% (Table 22).

6.5 Discussion

Computational models can serve as effective tools in parametric analyses of musculoskeletal loading as well as indicate mechanisms of soft tissue failure. However, due to the complexity and time required to develop such models, their assumptions and anatomical detail are dependent on the research motivation and application. Many prior models of the foot have not included sufficient anatomical detail of the forefoot (Gefen A, 2002; Cheung et al., 2005; Budhabhatti et al., 2007; Flavin et al., 2008; Wong et al., 2014; Akrami et al., 2018; Peng et al., 2021) to explore cartilage mechanics of the first MTP and first MTC joints, which are common sites of orthopaedic disorders (Van Saase et al., 1989; Cacace et al., 103; Menz et al., 2015). The motivation for this study was to develop a reliable computational tool that could be used to predict physiological loading of the medial forefoot in planus and rectus foot types. To this aim, the model was successful in predicting trends and magnitudes of foot-type specific first MTP and first MTC joint contact forces and pressures, defined as less than 30% error of the experimental measurements.

Substantial uncertainty may be present when predicting joint contact mechanics, especially with consideration to the manual reconstruction of 3D geometries and the assignment of soft-tissue material properties. In the present study, calibration and verification of the FE model against cadaveric data acted to reinforce its accuracy where peak experimental contact forces were matched by the FE model across foot type, in both trend and magnitude, with an average difference of 8% ± 8%. However, TekScan pressure sensors have been found to affect joint congruence and alter joint mechanics (Anderson et al., 2008; Beidokhti et al., 2017). According to Wu et al.,

measured joint contact pressures may contain errors between 14-28% (Wu et al., 1998) and for this reason, the present limit of verification was considered less than 30%. Mean errors for first MTP and first MTC joint contact pressures and contact forces were within 24% of the experimental data but exceeded 30% for first MTP joint contact area. TekScan pressure sensors are approximately, 0.2 mm thick and intracapsular insertion of the pressure film likely disturbed the natural pattern of articular contact (Wu et al., 1998; Jansson et al., 2013). Drewniak et al., reported that TekScan measurements were increased by smaller surface contact areas (Drewniak et al., 2007) and hence, the higher relative error for predicted first MTP joint contact area may have resulted from its small concave surface, compared to larger, more frequently studies joints.

It is generally accepted that foot structure and function are related (Ledoux & Hillstrom, 2002; Hillstrom et al., 2013; Buldt et al., 2015; Buldt et al., 2018), where the planus foot exhibits higher plantar loads beneath the second metatarsal and hallux (Ledoux & Hillstrom, 2002; Hillstrom et al., 2013; Buldt et al., 2018; Chapter 5). These structural and functional characteristics of the planus foot have been theorised to initiate degenerative changes in the first MTP joint (Zammit et al., 2008; Cacace et al., 2013; Menz et al., 2015). To date, the literature has not explored medial forefoot contact mechanics in the presence of foot type. In the current study, simulations of pes planus and rectus revealed that medial forefoot joint contact mechanics may be dependent upon foot type. The cadaver model utilised a simplified set of quasi-static loads during a single phase of midstance. The flexor hallucis longus and brevis tendons were not included because static equilibrium was achieved from tension in the plantar fascia. This suggested the passive effect from the Windlass mechanism was sufficient to counteract plantar loads at the hallux and metatarsals. The medial band of the plantar fascia has been shown to be critical for transmission of forces to the forefoot (Sharkey et al., 1998; Erdermir et al., 2004). While the simulated GRF's of the first metatarsal and hallux were vertical, a large horizontal load was present from the line-of-action of the medial band of the plantar fascia. To achieve static equilibrium in the planus model, greater tension in the plantar fascia was required to resist the combined effects of a lower first metatarsal declination angle and increased hallucial loading. These structural and functional characteristics of the planus foot promoted increased first MTP and MTC joint contact forces and pressures. From a biomechanical perspective,

aberrant contact mechanics resulting from pes planus may provide insight into why this foot type is more affected by degenerative changes at the first MTP joint. However, further investigation of full-scale loading across different timepoints of gait, which will be explored in the next chapter, is required to fully understand these implications.

Cartilage Young's modulus, *E* and Poisson's ratio, *v* were derived from the literature (Shepard & Seedhom, 1999). However, calibration of the Young's modulus was performed to optimise the quality of predicted contact mechanics. Thus, a range of values were chosen to span the instantaneous compressive modulus of articular cartilage (Shepared & Seedhom, 1999) and found to influence joint-specific contact forces, pressures, and areas. While predictions of peak contact force were not overly sensitive to cartilage modulus, changes in peak contact pressures and contact areas of 28% ± 5% and 15% ± 11% occurred, respectively, from calibration. There have been few prior studies which evaluated the properties of articular cartilage in the forefoot (Liu et al., 1997; Athanasiou et al., 1998). Articular cartilage of the first MTP joint may be thicker and larger than the first MTC joint but exhibit a lower compressive modulus (Liu et al., 1997). These observations from the literature supported the present calibrations of first MTC and first MTP joint cartilage moduli. Previous studies have suggested that regional variations in cartilage properties result from adaptation to loading, where modulus may be proportional to loadbearing. In contrast to this theory, greater magnitudes of contact force and pressure were found for the first MTP joint; a finding which may provide insight into the frequency of degenerative changes at this site in the foot and ankle (Van Saase et al., 1989; Morgan et al., 2019)

A neo-Hookean constitutive model was used to represent the mechanical properties of articular cartilage in the present work. Henak et al. (Henak et al., 2014) investigated the effects of neo-Hookean versus Veronda Westmann hyperelastic constitutive models on predictions of contact stress, strain, and area in articular cartilage of the hip. They found that the results were "indistinguishable" between cartilage representation and advocated that a neo-Hookean constitutive model was sufficient to provide predictions of articular cartilage contact mechanics. While cartilage material behaviour is time- and rate-dependent, nearly incompressible elastic constitutive parameters, such as those used in the present study, are appropriate under fast loading rates which replicate physiological loading. Ateshian et al., found an equivalent

response between biphasic and incompressible elastic constitutive models of cartilage over short-term loading (≤0.5 seconds) (Ateshian et al., 2007). Furthermore, a recent study of the hip found minor differences in the predictive outputs between isotropic elastic and anisotropic biphasic constitutive models of cartilage. Therefore, it may be concluded that the isotropic, hyperelastic representation of articular cartilage used in the current work can provide meaningful results without loss of accuracy and greater computational efficiency (Todd et al., 2018).

6.5.1 Limitations

Only one FE model was developed. The bundles of 1D tension-only connectors which represented the ligaments were a necessary assumption to idealise their functional contributions. The resolution of our imaging protocol coupled with the small size of the forefoot ligaments meant that accurate segmentation of these structures was not feasible. The assumptions associated with the position and insertion sites of each ligament may have contributed to predictive errors (Beidokhti et al., 2017). Although individual muscles were not represented in the model, the study aim was to determine the accuracy of geometric reconstruction and cartilage properties. Hence, the muscular forces were not necessary to obtain verification metrics for the model. Cartilage is known to exhibit biphasic behaviour (Ateshian et al., 2007; Todd et al., 2018) where the present model may not account for variables such as fluid pressure. Finally, the FE model represented a reduced anatomical model of the foot (first and second rays). It is possible that further discrepancies occurred due to the simplified geometry, yet the predicted results were consistent with corresponding in vitro data. Thus, the modelling protocol provided accurate and robust predictions of magnitudes and trends of the experimental data. While the simplified anatomical geometry must be considered a limitation, the complexity of the overall development process and computational time required to perform the analyses were subsequently reduced as a result.

6.6 Conclusion

In summary, the present method for specimen-specific FE modelling of the medial forefoot, simulating planus and rectus foot types, produced accurate predictions of magnitudes and trends in first MTP and first MTC joint contact mechanics. Calibration of first MTP and MTC joint cartilage material properties were vital in obtaining best-fit data to intracapsular pressure sensor measurements. The results from calibration were consistent with prior experimental observations of regional differences in cartilage moduli. This verified FE model offers a platform to investigate understudied disorders and surgical techniques of the medial forefoot and provides a basis for the creation of a larger dataset. In the next chapter, the verified FE model will be further validated and used to simulate physiologically realistic loading of the medial forefoot to understand the role of hypermobility in contact mechanics of the first ray.

Chapter 7. Finite Element Prediction of Cartilage Contact Mechanics in the Hypermobile First Ray

7.1 Chapter Overview

This chapter describes the prediction of cartilage contact mechanics in the planus foot with first ray hypermobility. The study integrated the plantar force parameters of hypermobile planus and non-hypermobile rectus subjects, measured in Chapter 5, with the verified FE model from Chapter 6. Simulations of late stance phase during gait were conducted, utilising foot type-specific plantar fascia (Erdemir et al., 2004) and muscle (Murley et al, 2009; Aubin et al., 2012) forces obtained from the literature. The overarching goal of this final study was to elucidate the potential for elevated cartilage stress in the first MTP joint of planus individuals with first ray hypermobility, as a potential pathway to hallux rigidus.

Aim 6: Predict the effects of first ray hypermobility on medial forefoot cartilage contact mechanics during stance phase of gait.

Hypothesis 6: First MTP and MTC joint stress will be higher in the presence of first ray hypermobility.

7.2 Introduction

A higher odds-ratio of developing hallux rigidus has been reported among individuals with the planus foot type (Menz et al., 2015). In Chapter 3 of this thesis, a younger subset of patients presenting with hallux rigidus were identified, which may be indicative of aberrant medial forefoot biomechanics. Furthermore, an interaction between the planus foot type and first ray hypermobility was identified, in Chapter 5, as a potential cause of increased first MTP joint flexibility and hallucial plantar loading. In hypermobile feet, abnormal biomechanics affecting the first ray's kinetic chain may

be an etiological factor in hallux rigidus; a theory supported by several other investigators (Jack E, 1940; Roukis et al., 1996; Murley et al., 2009; Menz et al., 2015; Golightly et al., 2018). However, analysis of pathologic joint contact mechanics can be difficult to investigate in vivo. Finite element modelling may generate functional information of cartilage failure modes including excessive shear and tensile stress (Sasazaki et al., 2006). Golightly et al., (Golightly et al., 2018) postulated that repetitive trauma to first MTP joint articular cartilage, from first ray hypermobility due to altered kinematics and increased joint stress, may predispose an individual to degenerative changes. To date, the biomechanical implications of first ray hypermobility are unknown. Therefore, the purpose of this study was to: (1) validate the FE model described in Chapter 6 for simulations of hypermobile planus and non-hypermobile rectus foot types during late stance, and; (2) examine first MTP, first MTC, and second MTP joint stress in the presence of first ray hypermobility. The quasi-static simulations were driven with foot-type specific physiological plantar loading and muscular forces obtained from Chapter 5 and the literature, respectively. Validation was assessed through comparisons of FE model first MTP joint kinematics with foot type-specific in vivo data (Buldt et al., 2015). Kinematic errors within 10% of the in vivo data were considered valid.

7.3 Materials and Methods

The geometry reconstruction, mesh generation, choice of constitutive parameters, boundary conditions, calibration, and verification for the FE model were detailed in Chapter 6. The PL, FHL, FDL, EHL, and EDL tendons were added to the model for physiological simulation of muscle forces during gait. The properties of each tendon are shown in Table 23. Each tendon was modelled as a linear elastic 1D tension-only connector element (T3D2) (Figure 39). Insertion sites and positions were based upon guidance from the foot and ankle surgeons involved in this study, (Scott J Ellis, MD and Jonathan T Deland III, MD) in addition to anatomic diagrams and literature descriptions.

Table 23. Properties of the medial forefoot tendons.

Tendon	Cross-sectional area (mm^2)	Young's modulus (*E* (MPa)), Poisson's ratio (*v*)	Reference
Peroneus Longus	16.6	227, 0.3	
Flexor Hallucis Longus	15.7	440, 0.3	
Flexor Digitorum Longus	4.9	337, 0.3	Morales-Orcajo et al., 2016
Extensor Hallucis Longus	8.5	448, 0.3	
Extensor Digitorum Longus	4.8	395, 0.3	

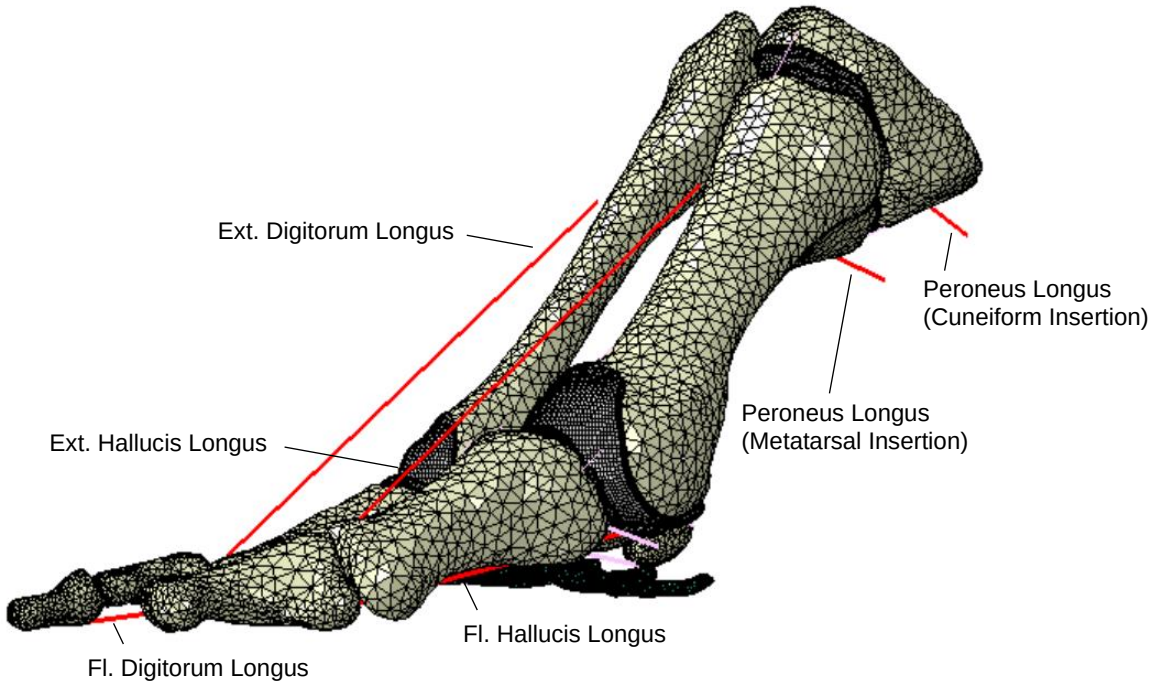

Figure 39. Tendon positions within the Abaqus medial forefoot FE model. The 2D connectors used to idealise the tendons are highlighted in red. Ext, extensor; Fl, flexor.

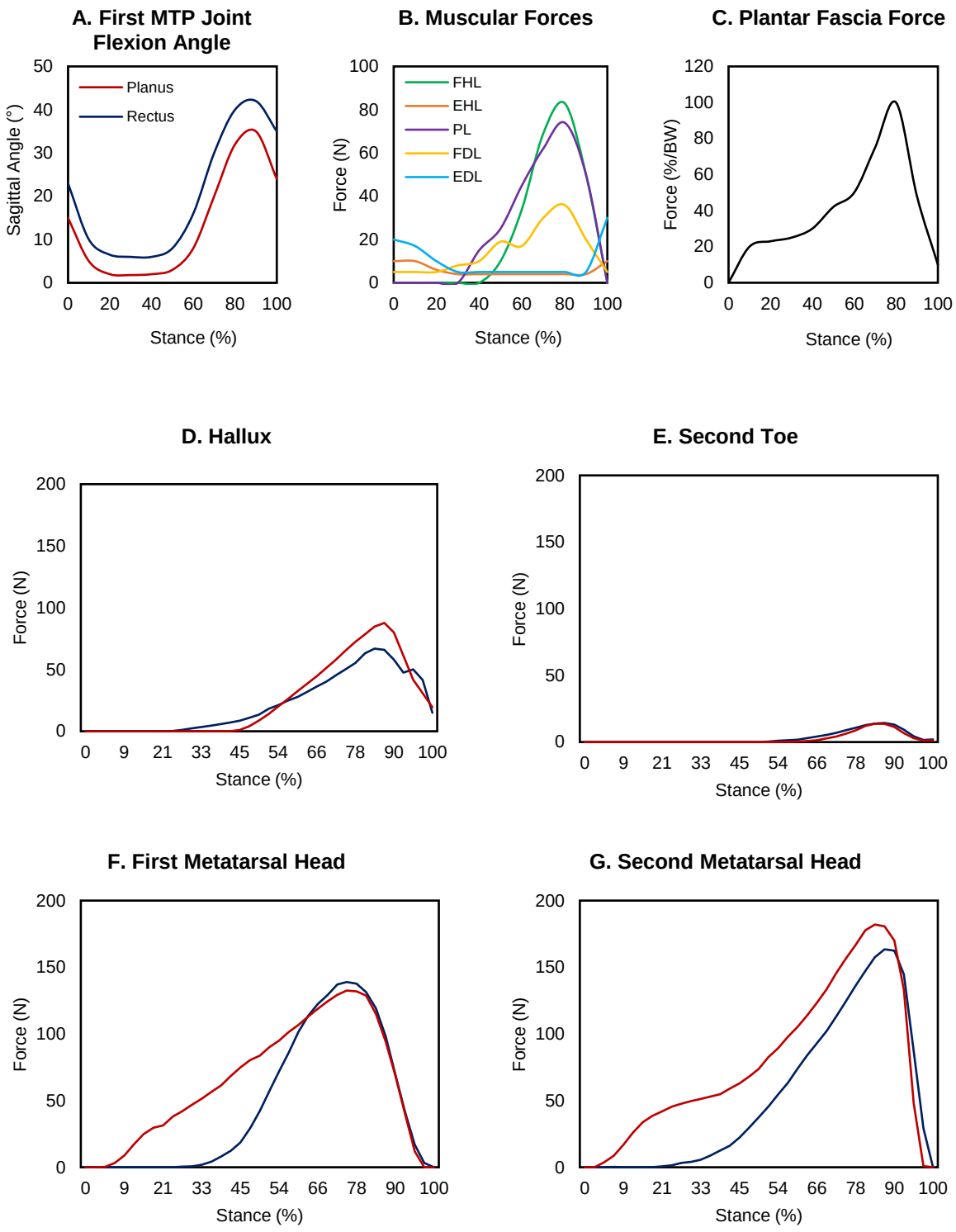

Figure 40A-G. (A) Sagittal kinematics of planus and rectus feet (adapted from Buldt et al., 2015) used to define the angles of the first and second MTP joints during stance; (B) muscle (adapted from Aubin et al., 2012) and; (C) plantar fascia forces (adapted from Erdemir et al., 2004) used to drive the model. Plantar forces (N) derived from the planus and rectus subjects in vivo (Chapter 5), for the (D) hallux; (E) second toe; (F) first metatarsal head, and; (G) second metatarsal head.

Table 24. The percentage of force applied to the plantar fascia were determined by the subject-specific percentage of loads beneath each toe, relative to the total forefoot load at 70%, 80%, and 90% of stance**.**

		Phase of Stance					
		70%		**80%**		**90%**	
		Ray 1	Ray 2	Ray 1	Ray 2	Ray 1	Ray 2
Planus	(%)	22.9	18.9	25.9	25.6	26.5	37.9
	(N)	122.1	100.0	184.1	182.0	90.4	129.3
Rectus	(%)	23.4	13.9	26.3	20.0	25.7	30.0
	(N)	132.5	78.7	198.5	151.0	93.1	108.7

7.3.1 Simulation of First Ray Hypermobility

The model simulations explored three loading scenarios: 70%, 80%, and 90% of the stance phase of gait. These components corresponded to the peak plantar forces in the medial forefoot and peak loading of the PL (Figure 40A-G). Two subjects of similar heights and weights were selected for the hypermobile planus and non-hypermobile rectus conditions. The hypermobile planus subject ($AHI_{standing}$, 0.312) was male, 27 years old, 72.6 kg, 185.4 cm tall, and exhibited a first ray mobility of 10 mm. The non-hypermobile rectus subject ($AHI_{standing}$, 0.353) was also male, 26 years old, 77.1 kg, 182.9 cm tall, and exhibited a first ray mobility of 2 mm. The sagittal angles of the first and second rays at each phase of stance, for the planus and rectus simulations, were based on in vivo kinematics data from the literature (Buldt et al., 2015) (Figure 40A). Muscle forces for the PL, FHL, EHL, FDL, and EDL were selected from cadaveric simulator data (Aubin et al., 2012) (Figure 40B). Subject-specific plantar loading parameters of the planus and rectus feet, measured in Chapter 5, were utilised. Forces averaged across five walking trials were used. Simulation of first ray hypermobility in the planus foot was defined by a reduction in PL force by 13.7%, as reported by Murley et al (2009). Force parameters for the plantar fascia were derived from cadaveric assessments in the literature and scaled to the weight of each subject (Erdemir et al., 2004) (Figure 40C). The percentage of force applied to the plantar fascia were determined by the subject-specific percentage of loads beneath each toe, relative to the total forefoot load at 70%, 80%, and 90% of stance (Table 24). The increased

passive tension that occurs in the plantar fascia of the planus hypermobile individual was represented by adding an initial strain of 5%.

7.3.2 Kinematic Validation

Kinematic accuracy of the FE model was assessed in comparison to an in vivo study which incorporated $n_p = 30$ planus and $n_r = 37$ rectus subjects (Buldt et al., 2015). In vivo measurements of first MTP joint frontal and transverse rotations for the planus and rectus foot types were compared to the FE predictions to provide a kinematic validation.

7.3.3 Contact Mechanics

Contact areas and forces were calculated at the articulating surfaces of each joint as absolute values. Peak values for von Mises and maximum principal stress were calculated at the articular and osteochondral Interfaces of the first and second MTP joints, and first MTC joint. The von Mises magnitudes were selected to account for the von Mises failure criterion, which may be applied to predict the failure limit of a material undergoing high shear stress. Maximum principal stress was also selected to assess tensile stress in the cartilage tissue.

7.4 Results

7.4.1 Kinematic Validation

The in vivo first MTP joint angle had a mean difference in the transverse plane of 10% for the planus simulation and 7% for the rectus simulation. The mean difference of the frontal plane first MTP joint angle was 4% and 6% for the planus and rectus models, respectively (Figure 41A-B).

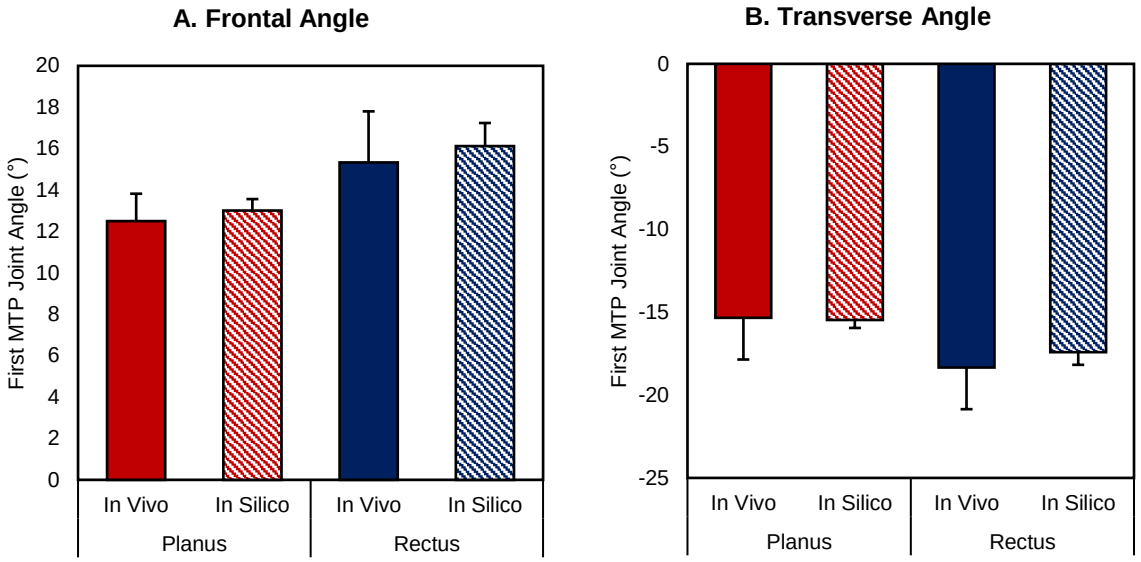

Figure 41A-B. (A) frontal and (B) transverse angles of the first MTP joint. Mean in vivo data (Buldt et al., 2015) compared with predicted FE results. In vivo results are denoted by solid blocks while FE outcomes are shown with striped blocks of the same colour. These results represent a kinematic validation of the computational model for simulated late stance.

7.4.2 Contact Forces

The mean and SD of contact force can be seen graphically in Figure 42. These results indicated minimal differences in the magnitudes of contact forces between foot type. The first MTP joint was predicted to have the highest compressive forces, peaking at 80% of stance. Compressive force in the first MTP joint was ~16% higher than the first MTC joint and ~41% higher than the second MTP joint. Shear forces in the SI directions were greatest in the first MTC joint by ~122% compared to the first MTP joint and ~117% compared to the second MTP joint. Peak SI shear force occurred at 80% of stance. There were no substantial differences in ML forces for any of the joints across foot type. The first MTC joint underwent medially directed shear forces while the first and second MTP joints demonstrated laterally oriented shear forces.

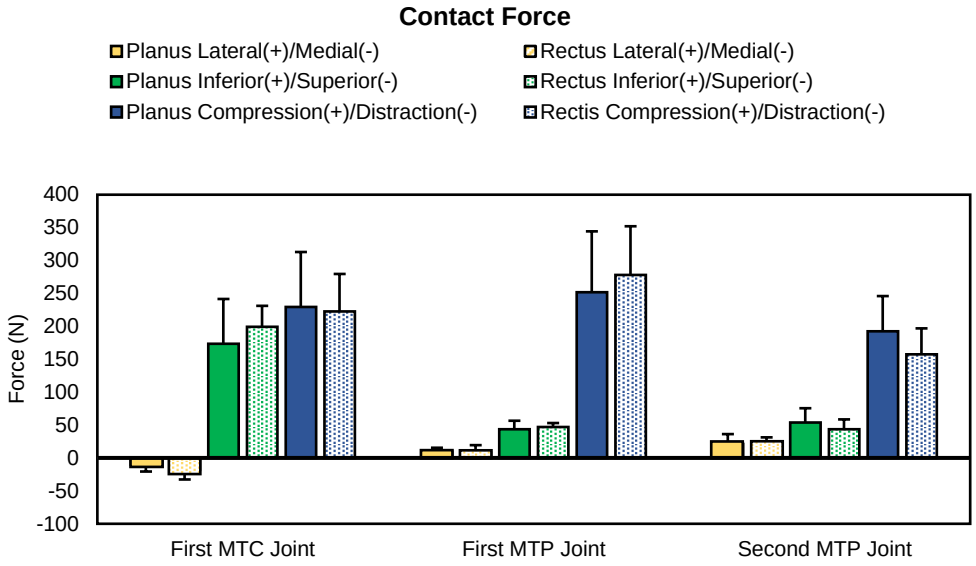

Figure 42. Means and SD of predicted contact forces for each of the three joints across the planus and rectus foot types.

7.4.3 Contact Areas

The mean and SD of contact areas can be seen in Figure 43. The trend in contact area was relative to joint size where the first MTC joint exhibited the greatest area of contact and the second MTP joint had the smallest. The data did not indicate substantial differences in the contact areas between foot type.

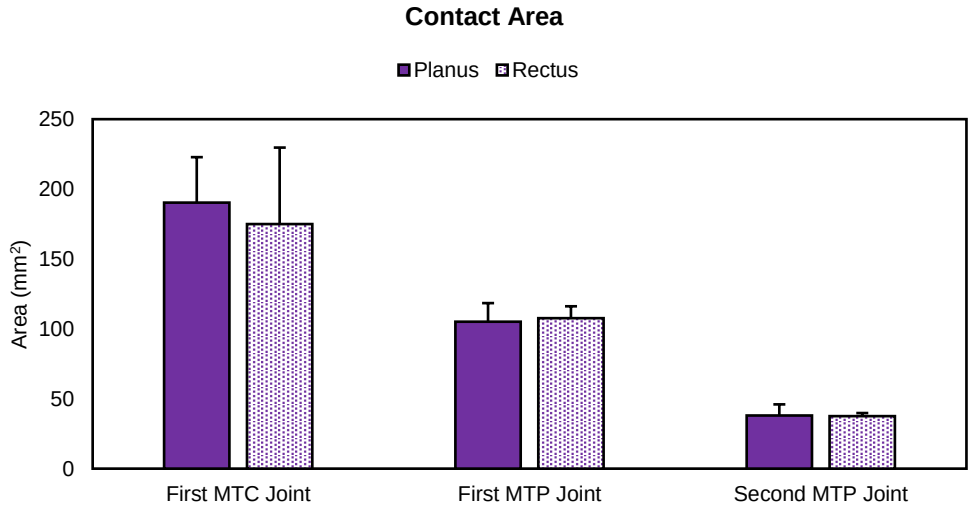

Figure 43. Means and SD of predicted contact area across the planus and rectus foot types.

7.4.4 von Mises and Maximum Principal Stress

Images of von Mises stress distributions at the articular interface of the first metatarsal head cartilage are shown in Figure 44. The mean and SD of von Mises and maximum principal stress can be seen graphically in Figure 45A-F. In the first MTC joint, peak stress at the articular and osteochondral interfaces occurred at 90% of stance. Peak von Mises stress in the first MTC joint cartilage was found to be higher in the rectus than planus foot, by ~8%, at the articular and osteochondral interfaces. The opposite trend was observed for maximum principal stress, where the first MTC joint of the planus foot exhibited higher stress at the articular and osteochondral interfaces.

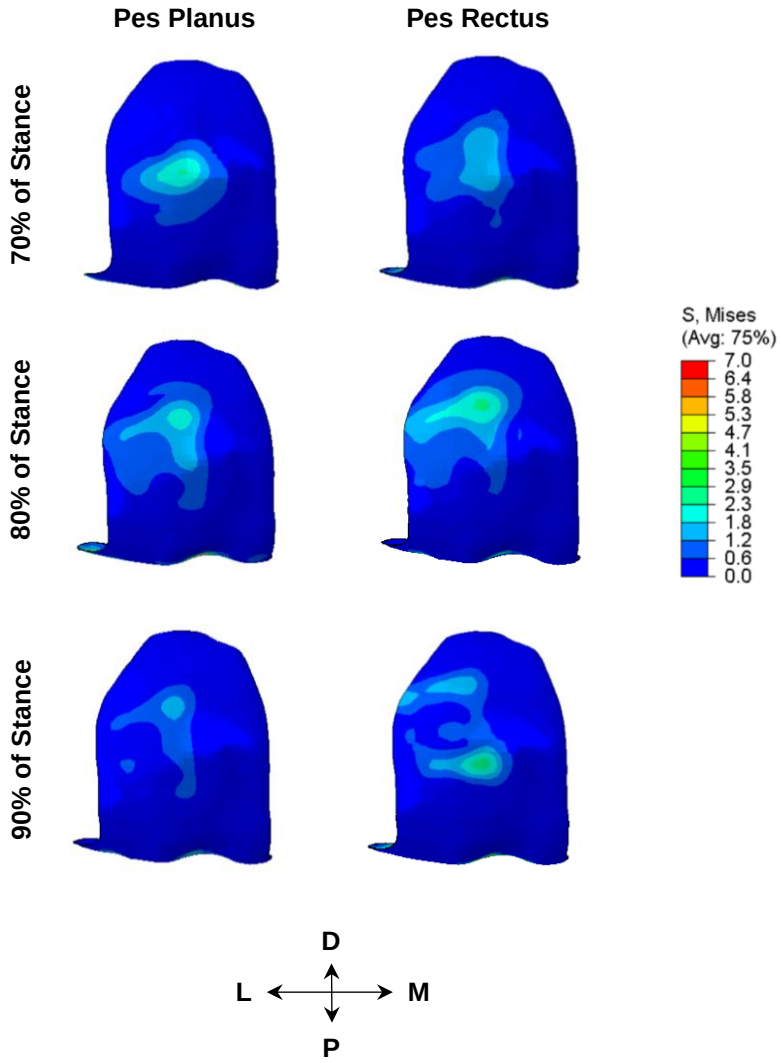

Figure 44. Predicted von Mises stress distributions at the articular surface of the first metatarsal head. The FE images are separated by planus and rectus simulations across late stance.

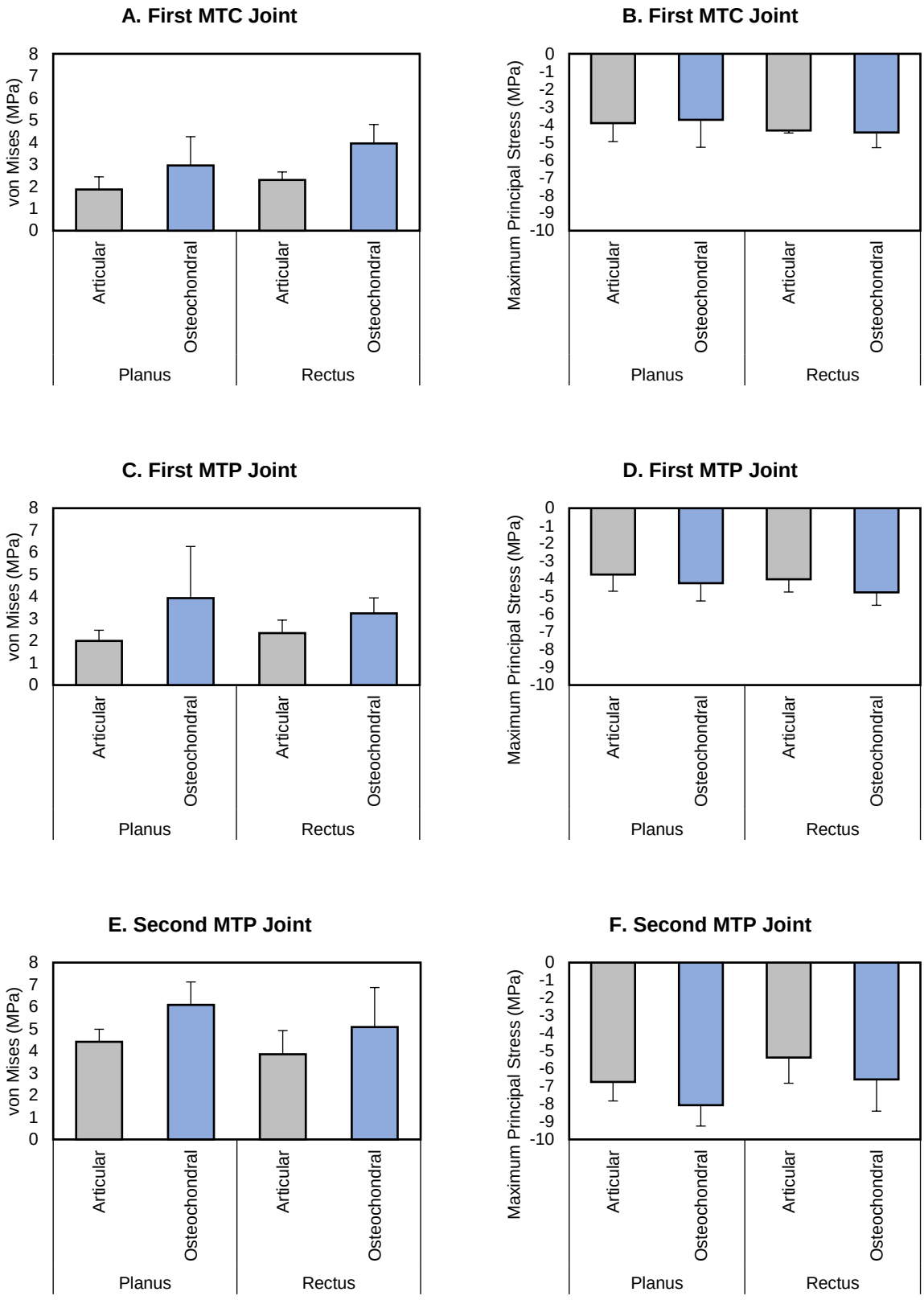

Figure 45A-F. Graphs showing predicted mean von Mises and mean maximum principal stress distributions in the first MTC joint (A-B); first MTP joint (C-D), and; second MTP joint (E-F). The stress distributions were computed at the articular and osteochondral interfaces of cartilage.

The highest von Mises stress in the first MTP joint was predicted to occur during 80% of stance, at the osteochondral interface of the planus foot. This magnitude was ~39% higher for the planus compared to rectus simulation and reached 6.5 MPa. At the articular interface, peak von Mises stress was ~66% greater in the rectus foot yet this magnitude did not exceed 5 MPa. Peak maximum principal stress at the osteochondral interface was ~13% higher in the rectus compared to planus foot. Different stress patterns were observed at the articular surface of the first metatarsal head, between foot type, but were distributed at the dorsal aspect of the joint for both simulations (Figure 44).

Peak von Mises stress in the second MTP joint occurred at 70% of stance for the planus foot and 90% of stance for the rectus foot. The greatest magnitudes were observed at the osteochondral interface of the second metatarsal head for each foot type. In the planus compared to rectus foot, peak von Mises stress at the osteochondral interface was ~5% higher while peak maximum principal stress was ~14% higher. For the articular interface, these differences were smaller; peak von Mises stress was ~6% and peak maximum principal stress was ~13% higher in the planus than rectus foot.

7.5 Discussion

The majority of clinical and basic-science research of OA has concentrated on the hand, hip, and knee (Roddy & Menz 2018). Despite a lack of focus, the first MTP joint has been identified as the most common site of OA in the foot and ankle (manifesting as hallux rigidus) (Van Saase et al., 1989; Roddy & Menz, 2018; Morgan et al., 2019). Many possible causative factors have been rejected due to a lack of convincing evidence (Bremner et al., 1968; Roukis et al., 1996; Bouachia et al., 2010; Nguyen et al., 2010; Roddy et al., 2015) and yet the role of first ray hypermobility in abnormal and potentially harmful pedal mechanics remains enigmatic (Morton DJ, 1935; King & Toolan, 2004). In the present study, the verified FE model, described in Chapter 6 of this thesis, was further validated to provide a computational tool for the evaluation of first MTP and first MTC joint contact mechanics in the presence of first ray hypermobility. Prior computational studies which have simulated pes planus (Wong et

al., 2018) or first ray hypermobility (Wong et al., 2014) did not account for differences in foot-type specific plantar loading or the relationship between foot type and first ray mobility. Furthermore, to the authors knowledge, this was the first study to investigate the role of first ray hypermobility in contact mechanics of the articular cartilage. The FE simulations of planus and rectus foot types successfully matched in vivo first MTP joint kinematics, demonstrating errors within 10% of the population-based data reported by Buldt et al. (2015). The hypermobile planus foot was predicted to increase first MTP joint stress by ~39% which, at a magnitude of 6.5 MPa, was within the upper bound of a proposed 5-7 MPa failure limit of cartilage (Sasazaki et al., 2006; Venäläinen et al., 2016). Microtrauma to the first MTP joint's articular soft tissues, after repetitive excessive loading from first ray hypermobility on a daily basis, may initiate degenerative changes and cartilage matrix breakdown. The significance of this finding rests with its potential to reveal first ray hypermobility as an etiological factor in hallux rigidus onset and progression.

The present study focused on late stance phase since peak plantar loading has been shown to occur in the medial forefoot, at this timepoint of gait, when the PL is maximally loaded (Murley et al., 2009). It is clear from the literature that the PL plays an important role in stabilising the first ray (Duchenne GB, 1949; Johnson and Christensen, 1999; Kokubo et al., 2012) and exhibits reduced activity in the planus foot type (Murley et al., 2009). Duchenne suggested that without the PL to counteract the TA, the first ray would elevate upon weightbearing gait (Duchenne GB, 1949). Cadaveric studies have shown the PL may contribute to stabilising and "locking" the first metatarsal against the medial cuneiform, causing the first ray to evert and plantarflex (Johnson and Christensen, 1999). The sagittal plane effects of the PL may assist the windlass mechanism during gait, enhancing dorsiflexion of the first MTP joint. Balanced forces in the PL, TA, FHL, and EHL likely provides equilibrium in the structure of the first ray during single limb support. As predicted in the present study, loss of PL strength in the planus foot, and commensurate first ray hypermobility, may affect the kinetic chain of the first ray and alter the pattern and magnitude of first MTP joint articular contact.

Quantifying foot type-specific joint contact mechanics of the medial forefoot serves not only to describe normal biomechanics but also further understanding of the

relationship between foot structure and function. While it has been demonstrated that the planus foot type exhibits greater incidence of hallux rigidus (Menz et al., 2015), the relationship between foot type and cartilage contact mechanics has not been explored in the literature. Comparing data for hypermobile planus and non-hypermobile rectus foot types could help to elucidate the roles foot structure and function play in determining aberrant first MTP and first MTC joint mechanics. Pathologic examination of hallux rigidus has shown chondral defects to frequently occur at the dorsal apex of the dome of the first metatarsal head and adjacent to the dorsal lip of the base of the proximal phalanx (McMaster, M.J., 1978). The present simulations demonstrated focal areas of stress at the dorsal aspect of first metatarsal head cartilage in the hypermobile planus simulation. Furthermore, peak first MTP joint stress occurred at the osteochondral interface of the first metatarsal head, which would suggest that degenerative changes may be initiated at the chondral surface. Several investigators have found chondral surface damage to be present in the early stages of cartilage injury mechanisms (Hughston et al. 1984; Schenck et al., 1994; Flachsman et al., 1995; Messner and Maletius, 1996; McCarty and Lee, 2002; Brown et al., 1991; Guettler et al., 2004; Tannast et al., 2008). Increased stress at the first MTP joint in the hypermobile planus simulation may be the effect of decreased plantar load beneath the first metatarsal head and increased load beneath the hallux. A higher flexion moment arm between the hallucial load and first MTP joint likely produced focal areas of articular contact, exposing the first MTP joint to higher magnitudes of tensile and shear stress. While the current data may provide a biomechanical explanation for first ray hypermobility as a potential pathway to onset and development of hallux rigidus, future research with a longitudinal dataset is required.

In the previous chapter, the moduli of first MTP and first MTC joint cartilage were best fit to the lowest range (10 MPa) and highest range (20 MPa) of experimentally tested human cadavera, respectively (Shepared & Seedhom, 1999). These differences should indicate the mechanical environment and functional requirements of each joint, where a low weightbearing region would exhibit a compressive modulus less than that of a high weightbearing region. In contrast to this theory, the first MTP and first MTC joints were predicted to undergo similar magnitudes of contact force. It is unclear why the first MTC joint exhibits a lower prevalence of OA compared to the first MTP joint. Therefore, it may be the combination of a low compressive modulus and increased

stress from first ray hypermobility that renders the first MTP joint to more susceptible to OA.

In a Dutch population, Van Saase et al., (1989) found 34.3% of men and 48.4% of women exhibited symptoms of hallux rigidus at 60 years of age, which was the highest prevalence of any joint in the foot and ankle. Additionally, within the same age-group, they observed 5.6% of men and 5.9% of woman presented with first MTC joint OA while 6.2% of men and 22.6% of women were affected by OA of the lesser MTP joints (second-fifth). In the present study, second MTP joint stress exceeded both the first MTC and first MTP joints, in both the planus and rectus foot types. Although high stress was present in the second MTP joint, this region is uncommon for developing OA. The explanation remains enigmatic. Future research exploring the mechanical properties of second MTP joint cartilage may be useful in understanding this phenomena.

7.5.1 Limitations

Some assumptions and limitations in the modelling process must be considered when interpreting the present results. First, cartilage was assumed to be isotropic, nearly incompressible and hyperelastic. While cartilage exhibits biphasic properties, computational predictions of stress are equivalent for nearly incompressible and hyperelastic and biphasic constitutive models during instantaneous loading (Ateshian et al., 2007; Todd et al., 2018). Second, sagittal joint angles and muscle forces used to drive the model were derived from the literature. Decreased loading of the PL in pes planus was assumed from in vivo EMG research. Furthermore, increased initial strain in the plantar fascia of pes planus was based on theoretical maximal elongation and reduced elasticity of its structure. Thirdly, the same specimen was used to simulate pes planus and pes rectus. Morphological differences in bone exist between foot types in addition to declination of the medial longitudinal arch (Moore et al, 2019). Fourthly, the current work utilised a quasi-static model which did not account for mass or acceleration during gait. However, since the cartilage was not modelled with a biphasic constitutive relationship, across cyclical loading, this may be considered reasonable. Finally, perhaps the fundamental limitation of this work was the utilisation of a single specimen which did not reflect the diverse geometries, material properties, and loading

conditions of different people. Commensurate changes to the joint kinetics and kinematics of an individual would lead to different contact mechanics.

7.6 Conclusion

This investigation may be considered significant by providing a biomechanical basis for first ray hypermobility as a potential etiologic factor in first MTP joint degeneration. Research in this area is particularly valuable since the first MTP joint exhibits high OA prevalence but is relatively understudied compared to the hand, hip, and knee (Chapter 3). The present work demonstrated that the interaction between first ray hypermobility and pes planus increased first MTP joint stress to a magnitude of 6.5 MPa, which was within the upper bound of a proposed 5-7 MPa failure limit of cartilage (Sasazaki et al., 2006; Venäläinen et al., 2016). This finding highlights the potential for first ray hypermobility to initiate microtrauma at the first MTP joint's articular soft tissues. More research is needed to fully understand the risk factors for OA development in the first MTP joint including a longitudinal dataset. However, the present study may act as a theoretical framework for the design of future research which addresses the biomechanics of first ray hypermobility and its relationship to hallux rigidus.

Chapter 8. Summary and Conclusions

Four distinct but related concepts were explored to address current gaps in knowledge:

1. Up-to-date population-based age- and sex-related trends in hallux rigidus.
2. The design of a standardised and reliable device for assessment of first ray hypermobility, to facilitate robust clinical definition and investigation of related biomechanical parameters.
3. Investigation of the relationships and differences between first ray hypermobility, foot type, foot structure, and foot function.
4. Calibration, verification, and validation of a FE model to predict cartilage contact mechanics of the hypermobile first ray, as a mechanism of excessive first MTP joint loading and cartilage damage.

This work provides evidence in several key areas for which there is limited or no data, including:

1. Incidence of hallux rigidus in England is increasing at a rate similar to the hip and knee. Age-related data for hallux rigidus was bimodal with a peak in younger patients, compared to unimodal distributions for the knee and hip at 70 years-of-age. This finding suggests an additional risk profile for hallux rigidus, other than wear and tear of the articular soft tissues in old age, which may be biomechanical in origin.
2. A novel electromechanical device (MAP1st) designed for assessments of first ray mobility was found to be more reliable than the standard clinical exam and equivalent in reliability to predicate devices. This new device provides an advantage over predicate methods by performing measurements in different weightbearing conditions, foot alignments, and normalisation to foot length.
3. Individuals with first ray hypermobility were predominantly planus in foot type. The first ray's translational mobility plays an important role in foot structure and function,

influencing first MTP joint rotational laxity and directing a forward transfer of plantar load to the hallux.

4. First ray hypermobility in the planus foot increased stress in first MTP joint cartilage which, at a magnitude of 6.5 MPa, was within the upper bound of a proposed 5-7 MPa failure limit.

The significance of these interlinked studies provides a foundation that first ray hypermobility as a possible etiological factor in hallux rigidus onset and progression. While this research does not identify a definitive relationship between first ray hypermobility and hallux rigidus, it offers a biomechanical basis for disease aetiology and provides the tools for future research on this subject.

8.1 Contributions to Knowledge

Each study resulted in novel information to support future research into the interaction between foot type biomechanics and first ray hypermobility as a potential pathway to hallux rigidus. The following section summarises the main contributions to knowledge from this thesis:

1. ***The results from Chapter 3 supported acceptance hypothesis 1: hallux rigidus would demonstrate increased population prevalence over time and comparable incidence to OA of the hand, hip, and knee***. Osteoarthritis of the foot has been neglected for many years in epidemiological research. Evidence of the sex ratios and age distributions are sparse compared to other frequently affected joints but hallux rigidus appears to be a common problem. Secondary care records for 3.1 million patients with OA in England, across 17 years, revealed statistically significant increases in the incidence rate of hallux rigidus which was similar to the hip and knee. Most interestingly, a peak in younger patients presenting with hallux rigidus may distinguish itself by biomechanical factors. Based on the findings from this thesis, these population-representative data provide a compelling basis for first ray hypermobility as a pathway to hallux rigidus in younger age. Nonetheless, further longitudinal research which utilises the tools developed in this thesis is required.

2. No standardised measurement for first ray mobility exists. Most methods have performed measurements in either nonweightbearing or partial weightbearing, with a fixed position of the foot. The design and reliability testing of a novel electromechanical device (MAP1st) was conducted, in Chapter 4, to address the limitations of prior methods. Several design features were built into MAP1st including, controlled application of load, measurement normalisation, assessments in partial- and full-weightbearing, and different foot alignments. The reliability of MAP1st was tested in comparison to a handheld ruler considered analogous of the standard clinical exam. ***The intra-rater reliability of MAP1st was >0.7, supporting acceptance of hypotheses 3a-b***. Although inter-rater reliability of MAP1st was ~0.6 (<0.7) rejecting hypothesis 3c, it was superior to the standard clinical exam (~0.06). Based on these novel design features, a patent application was submitted.

3. Many structural and functional abnormalities of the first ray have been linked to pes planus, in pursuit of explaining why this foot type is disproportionately affected by hallux rigidus. This was the first investigation to provide objective evidence of a link between the planus foot and first ray hypermobility. In Chapter 5, significantly higher first ray mobility was observed in the planus compared to rectus group, accounting for 71% of individuals with first ray hypermobility. No relationships were observed between first ray mobility vs. arch height index, arch height flexibility, and first MTP joint dorsiflexion, rejecting hypotheses 4a. ***Supporting acceptance of hypothesis 4b, planus individuals presented with significantly lower ratios of first-second metatarsal head PP and MF.*** Hypothesis 4c was rejected due to no significant differences in the ratios of first-second metatarsal plantar loading across subjects with normal vs. high levels of first ray mobility. However, significantly higher load beneath the hallux was observed for subjects with first ray hypermobility. Stepwise linear regression analyses found that first ray mobility was predictive of both MF beneath the first metatarsal and first MTP joint rotational laxity, providing evidence of first ray hypermobility's role in abnormal structure and function of the medial forefoot.

4. Cartilage stress plays a key role in the degradation of diarthrodial joint soft tissues. To predict these biomechanical effects from first ray hypermobility, a FE model of

the medial forefoot was calibrated, verified, and validated. ***The model predictions of contact forces and pressures were within 30% of intracapsular pressure sensor measurements, accepting hypothesis 5 and providing verification. In Supporting hypothesis 6, abnormal plantar and muscular loading resulted from the first ray hypermobility and was predicted to increase first MTP joint stress by ~39%.*** The magnitude of stress reached 6.5 MPa which was within previous reports of a 5-7 MPa failure limit of cartilage. Microtrauma to the first MTP joint's articular soft tissues, in the hypermobile planus foot, may initiate degenerative changes resulting hallux rigidus. This segment of research may act as a theoretical framework for the design of future investigations which address the biomechanics of first ray hypermobility and its potential relationship to hallux rigidus.

8.2 Clinical Relevance

In light of the findings presented by this thesis, early detection of pathologic first ray function with MAP1st or similar devices could reduce the prescription of unnecessary surgical interventions and associated complications. Thus, considering the population prevalence and incidence rate of hallux rigidus, early prescription of conservative treatments for patients with first ray hypermobility may act to decrease the number of people seeking secondary-care services, contributing to a reduction in treatment costs for the NHS and time lost at work for the individual. Specifically, MAP1st may be used to evaluate the efficacy of conservative treatments including the prescription of orthotics and first ray stabilising surgeries such as Lapidus arthrodesis or distal crescentic osteotomy of the first metatarsal. To assess orthotics, arthrodesis, and osteotomy, measurements of first ray mobility may be taken before and after intervention, to quantify whether surgical realignment of the first ray results in stabilisation of the medial forefoot. The clinical relevance relates to improved treatment options for people who have common, painful disorders of the first ray.

8.3 Overall Conclusions

The overarching theory of this thesis stated that the planus foot type and first ray hypermobility are interrelated mechanisms, which may alter weightbearing of the foot and initiate excessive loading of first MTP joint cartilage. In prior research, individuals with planus feet have demonstrated greater prevalence of foot injuries (Kaufman et al, 1999), increased first MTP joint flexibility (Rao et al., 2011; Buldt et al., 2015), load transfer from the first to second metatarsal and hallux (Ledoux & Hillstrom, 2002; Hillstrom et al., 2013; Buldt et al., 2018), and a higher-odds ratio of hallux rigidus (Menz et al., 2015). The present work found a subset of younger patients who presented with hallux rigidus. In-keeping with the theory of this thesis, the peak in younger patients may suggest an unidentified biomechanical pathway to early degeneration of the first MTP joint. To explore aberrant biomechanics of the foot resulting from first ray hypermobility, MAP1st was designed and tested to quantify first ray mobility in partial- and full-weightbearing. Using this device, a study of healthy, asymptomatic subjects with planus and rectus feet established that individuals with first ray hypermobility were predominantly planus in foot type. The first metatarsal of planus individuals will translate excessively in the superior direction, causing foot pronation and a transfer of load to the second metatarsal and hallux. From a biomechanical perspective, an interaction between translational first ray mobility and rotational first MTP joint flexibility may be causative of increased load beneath the hallux and promote a higher flexion moment arm between the hallucial load and first MTP joint. Finite element modelling of these unique structural and functional characteristics predicted excessive stress magnitudes at the first MTP joint of the planus foot presenting with first ray hypermobility. Taken together, these interlinked studies provide evidence of first ray hypermobility's role in aberrant weightbearing of the foot and its potential to initiate microtrauma at the first MTP joint's articular soft tissues leading to degenerative changes. Further longitudinal investigations, which adopt the tools developed in this thesis, are required to fully understand these biomechanical implications in onset and development of hallux rigidus.

Chapter 9. Recommendations for Future Work

The following section provides recommendations for future work which may utilise the tools and data presented in this thesis. These recommendations include improvements to MAP1st's design, as well as several potential basic science and clinical applications of the research:

- Develop MAP1st into a more clinically friendly tool for researchers and clinicians by integrating measurement recordings via electronic sensor, smartphone-Bluetooth functionality, and data storage.

- Evaluate the efficacy of conservative treatments and first ray stabilising surgeries including the prescription of orthotics, Lapidus arthrodesis, and distal crescentic osteotomy of the first metatarsal.

- Conduct longitudinal research of cohorts with normal and hypermobile first rays to examine changes in structural and functional parameters of the foot over time, and potential relationships to onset and progression of hallux limitus/hallux rigidus.

- Create a larger dataset of FE models, using the framework established by this thesis, to predict the effects of first ray hypermobility on first MTP and first MTC joint contact mechanics across a sample more representative of the general population.

Bibliography

Allen MK, Cuddeford TY, Glasoe WM, DeKam LM, Lee PJ, Wagner KJ, Yack HJ. 2004. Relationship between static mobility of the first ray and first ray, midfoot, and hindfoot motion during gait. Foot Anke Int 25:391-396.

Allen KD, Golightly YM. 2015. Epidemiology of osteoarthritis: State of the evidence. Curr Opin Rheumatol 27:276-283.

Altchek DW, DiGiovanni CW, Dines JS, Positano RG. 2013 Foot and ankle - Sports medicine. Wolters Kluwer - Lippincot Williams & Wilkins.

Akrami M, Qian Z, Zou Z, Howard D, Nester CJ, Ren L. 2018. Subject-specific finite element modelling of the human foot complex during walking: Sensitivity analysis of material properties, boundary and loading conditons. Biomch Model Mech 17:559-576.

Anderson AE, Ellis BJ, Maas SA, Peters CL, Weiss JA. 2008. Validation of finite element predictions of cartilage contact pressure in the human hip joint. J Biomech Eng 130:051008.

Arbuthnot JE, Cheung G, Balain B, Denehey T, Higgins G, Trevett MC. 2008. Replacement arthroplasty of the first metatarsophalangeal joint using a ceramic-coated endoprosthesis for the treatment of hallux rigidus. J Foot Ankle Surg 47:500-504.

Archer CW, Morrison H, Pitsillides AA. 1994. Cellular aspects of the development of diarthrodial joints and articular cartilage. J Anat 184:447-456.

ASME Committee (PT60) on Verification and Validation in Computational Solid Mechanics. 2006. Guide for verification and validation in computational solid mechanics, American Society of Mechanical Engineers, New York.

Ateshian GA, Ellis BJ, Weiss JA. 2007. Equivalence between short-time biphasic and incompressible elastic material responses. J Biomech Eng 129:405-412.

Athanasiou KA, Liu GT, Lavery LA, Lanctot DR, Schenck RC. 1998. Biomechanical topography of human articular cartilage in the first metatarsophalangeal joint. Clin Orthop Relat Res 348:269-281.

Aubin PM, Whittaker EC, Ledoux WR. 2012. A robotic cadaveric gait simulator with fuzzy logic vertical ground reaction force control. IEEE T Robot 28:246-255.

Bareither D, Manion BL, Sumner DR, Berzins A, Albright TB, Rottier F, Muehleman, C. 1998. Relationship between articular cartilage damage and bone density in the first metatarsal. Foot Ankle Surg 37:401-409.

Barwick TW, Talkhani IS. 2008. The MOJE total joint arthroplasty for 1st metatarsophalangeal osteoarthritis: A short-term retrospective outcome study. Foot 18:150-155

Beck M, Kalhor M, Leunig M, Ganz R. 2005. Hip morphology influences the pattern of damage to the acetabular cartilage: femeroacetabular impingement as a cause of early osteoarthritis of the hip. J Bone Joint Surg Br 87:1012-1018.

Behforootan S, Chatzistergos P, Naemi R, Chockalingham N. 2017. Finite element modelling of the foot for clinical application: A systematic review. Med Eng Phys 39:1-11.

Beidokhti HN, Janssen D, van de Groes S, Hazrati J, Van den Boogaard T, Verdenschot N. 2017. The influence of ligament modelling strategies on the predictive capability of finite element models of the human knee joint. J. Biomech 65:1-11.

Beighton P, Horan F. 1969. Orthopaedic aspects of the ehlers-danlos syndrome. J Bone Joint Surg Br 51B:444-453.

Beighton P, Solomon L, Soskolne CL. 1973. Articular mobility in an african populations. Ann Rheum Dis 32:413-418.

Bierman RA, Christensen JC, Johnson CH. 2004. Biomechanics of the first ray. Part III. Consequences of Lapidus arthrodesis on peroneus longus function: A three-dimensional kinematic analysis in a cadaver model. J Foot Ankle Surg 40:125-131.

Bird HC, Tribe P. 1978. Joint hypermobility leading to osteoarthritis and chondrocalcinosis. Ann Rheum Dis 37:203-11.

Bingold AC, Collins DH. 1950. Hallux Rigidus. Bone Joint J 32-B:214-222.

Bland JM, Altman DG. 1983. Measurement in medicine: The analysis of method comparison studies. Statistician 32: 307-317.

Bohne WHO, Lee KT, Peterson MGE. 1997. Action of the peroneus longus tendon on the first metatarsal against metatarsus primus varus forces. Foot Ank Int 18:510-512.

Borton DC, Saxby TS. 1997. Tear of the plantar calcaneonavicular (spring) ligament causing flatfoot. Bone Joint J 79-B:641-643.

Bouaicha S, Ehrmann C, Moor BK, Maquieria GJ, Espinosa N. 2010. Radiographic analysis of metatarsus primus elevatus and hallux rigidus. Foot Ank Int 31:807-814.

Bremner JM, Lawrence JS, Miall WE. 1968. Degenerative joint disease in a Jamaican rural population. Ann Rheum Dis 27:326-332

Brewster M. 2010. Does total joint replacement or arthrodesis of the first metatarsophalangeal joint yield better functional results? A systematic review of the literature. J Foot Ankle Surg 49:546-552.

Brown TD, Pope DF, Hale JE, Buckwalter JA, Brand RA, 1991. Effects of osteochondral defect size on cartilage contact stress. J Orthop Res 9:559-567.

Budhabhatti SP, Erdemir A, Petre M, Sferra J, Donley B, Cavanagh PR. 2007. Finite element modeling of the first ray of the foot: A tool for the design of interventions. J Biomech Eng 129:750-756.

Buell T, Green D, Risser J. 1988. Measurement of the first metatarsophalangeal joint range of motion. J Am Podiat Med Assoc 78:1665-1669.

Buldt AK, Forghany S, Landorf KB, Levinger P, Murley GS, Menz HB. 2018. Foot posture is associated with planar pressure during gait: A comparison of normal, planus and cavus feet. Gait Posture 62:235-240.

Buldt AK, Levinger P, Murley GS, Menz HB, Nester CJ, Landorf KB. 2015. Foot posture is associated with kinematics of the foot during gait: A comparison of normal, planus and cavus feet. Gait Posture 42:42-48.

Cacace LA, Hillstrom HJ, Dufour AB, Hannan MT. 2013. The association between pes planus foot type and the prevalence of foot disorders: The framingham foot study. Osteoarthritis Cartilage 21:166-167.

Canesco K, Long J, Marks R, Khazzam M, Harris G. 2008. Quantitative characterization of gait kinematics in patients with hallux rigidus using the milwaukee foot model. J Orthop Res 26:419-427.

Caravaggi P, Leardini A, Giacomozzi C. 2016. Multiple linear regression approach for the analysis of the relationship between joints mobility and regional pressure-based parameters in the normal arched foot. J Biomech 49:3485-3491.

Carpenter B, Smith J, Motley T, Garrett A. 2010. Surgical treatment of hallux rigidus using a metatarsal head resurfacing implant. J Foot Ankle Surg 49:321-325.

Carrol G, Coleman S. 2019. CMC1 osteoarthritis and erosive osteoarthritis in the hand are associated with hypermobility, in contrast to type 1 and type 2 polyarticular osteoarthritis phenotypes and rheumatoid arthritis. Osteoarthritis Cartilage 27:237-238.

Carter C, Wilkinson J. 1964. Persistent Joint Laxity and Congenital Dislocation of the Hip. J Bone Joint Surg Br 46:67-76.

Chegini S, Beck M, Ferguson SJ. 2008. The effect of impingement and dysplasia on stress distributions in the hip joint during sitting and walking: A finite element analysis. J Orthop Res 27:195-201.

Chen A, Gupte C, Akhtar K, Smith P, Cobb J. 2012. The global economic cost of osteoarthritis: How the UK compares. Arthritis 698709:101155.

Cheung JTM, Zhang M, Leung, AKL, Fan YB. 2005. Three-dimensional finite element analysis of the foot during standing—a material sensitivity study. J Biomech 38:1045-1054.

Christman RA, Flanigan KP, Sorrento DL, Stanich CC. 2001. Radiographic analysis of metatarsus primus elevatus: A preliminary study. J Am Pod Med Assoc 91:294-299.

Clarke HD, Kitaoka HB, Ehman RL. 1998. Peroneal tendon injuries. Foot Ank Int 19:280-288.

Cody EA, Kraszewski AP, Marinescu A, Kunas GC, Mani SB, Rao S, Hillstrom HJ, Ellis SJ. 2017. Measuring joint flexibility in hallux rigidus using a novel flexibility jig. Foot Ank Int 38:885-892.

Cook E, Cook J, Rosenblum B, Landsman A, Giurini J, Basile P. 2008. Meta-analysis of first metatarsophalangeal joint implant arthroplasty. J Foot Ankle Surg 48:180-190.

Cooper AJ, Clifford PD, Parikh VK, Steinmentz ND, Mizel MS. 2009. Instability of the First Metatarsal-Cuneiform Joint: Diagnosis and Discussion of an Independent Pain Generator in the Foot. Foot Ank Int 30:928-932.

Cotterill JM. 1887. Stiffness of the great toe in adolescents. Br Med J 1:1158.

Coughlin MJ. 1996. Hallux Valgus. J Bone Joint Surg Am 78:932-966.

Coughlin MJ, Shurnas PS. 2003. Hallux rigidus: Demographics, etiology, and radiographic assessment. Foot Ank Int 24:731-743.

Cowie S, Parsons S, Scammell B, McKenzie J. 2012. Hypermobility of the first ray in patients with planovalgus feet and tarsometatarsal osteoarthritis. Foot Ankle Surg 18:237-240.

Daly PJ Kitaoka HB, Chao EY. 1992. Plantar fasciectomy for intractable plantar fasciitis: clinical results and biomechanical evaluation. Foot Ank Int 13:188-195.

Dananberg HJ. 1993. Gait style as an etiology to chronic postural pain. Part I. Functional hallux limitus. J Am Podiatr Med Assoc 83:433-441.

Davies SC. 2012. Annual report of the chief medical officer: Volume One, 2011 – On the state of the public's health. London; Department of health.

Davies-Colley N. 1887. Contraction of the metatarsophalangeal joint of the great toe. Br Med J 1:728.

De Frino PF, Brodsky JW, Pollo FE, Crenshaw SJ, Beischer AD. 2002 First metatarsophalangeal arthrodesis: A clinical, pedobarographic and gait analysis study. Foot Ank Int 23:496-502.

Denyer JR, Hewitt NLA, Mitchell ACS. 2013. Foot structure and muscle reaction time to a simulated ankle sprain. J Athlet Train 48:326–330.

Dieppe PA, Lohmander LS. 2005. Pathogenesis and management of pain in osteoarthritis. The Lancet 365:965-973.

Dietrich TJ, da Silva FLF, de Abreu MR, Klammer G, Pfirrmann CWA, 2015. First metatarsophalangeal joint – MRI findings in asymptomatic volunteers. Eur Radiol 25:970-979.

Deland JT, Arnoczky SP, Thompson FM. 1992. Adult acquired flatfoot deformity at the talonavicular joint: Reconstruction of the spring ligament in an in vitro model. Foot Ank Int 13:327-332.

Deland JT, Lee K-T, Sobel M, DiCarlo EF. 1995. Anatomy of the Planar Plate and its Attachments in the Lesser Metatarsal Phalangeal Joint. Foot Ank Int 16:480-486.

Doty JF, Coughlin MJ, Hirose C, Stevens F, Schutt S, Kennedy M, Grebing B, Smith B, Cooper T, Golano P, Viladot R, Remington R. 2014. First metatarsocuneiform joint mobility: Radiographic anatomic, and clinical characteristics of the articular surface. Foot Ank Int 35:504-511.

Drewniak EI, Crisco JJ, Spenciner DB, Fleming BC. 2007. Accuracy of circular contact area measurements with thin-film pressure sensors. J Biomech 40:2569-2572.

Duchenne GB. Physiologie de mouvements. 1949. Translated and edited to physiology of motion. In: Saunders WB. (eds.) Bailliere 205-439.

Durrant B, Chockalingam N. 2009. Functional hallux limitus: A review. J Am Podiat Med Assoc 99:236-243.

Erdemir A, Hamel AJ, Fauth AR, Piazza SJ, Sharkey NA. 2004. Dynamic loading of the plantar aponeurosis in walking. J Bone Joint Surg 86:546-552.

Erdil M, Elmadag NM, Polat G, Tunçer N, Bilsel K, Ucan V, Erkocak OF, Sen C. 2013. Comparison of arthrodesis, resurfacing hemiarthroplasty, and total joint replacement in the treatment of advanced hallux rigidus. J Foot Ankle Surg 52:588-593.

Eyre D. 2001. Articular cartilage and changes in arthritis: Collagen of articular cartilage. Arth Res Therap 4:30-35.

Felson DT, Lawrence RC, Dieppe PA, Hirsch R, Helmick CG, Jordan JM, Kington RS, Lane NE, Nevitt MC, Zhang Y, Sowers M, McAlindon T, Spector TD, Poole RA, Yanovski SZ, Ateshian G, Sharma L, Buckwalter JA, Brandt KD, Fries JF. 2000. Osteoarthritis: New insights. Part 1: The disease and its risk factors. Ann Intern Med 133:635-646.

Flachsmann ER, Broom ND, Oloyede A. 1995. A biomechanical investigation of unconstrained shear failure of the osteochondral region under impact loading. Clin Biomech 10:156-165

Fiolkowski R, Brunt D, Bishop M, Woo R, Horodyski M. 2003. Intrinsic pedal musculature support of the medial longitudinal arch: An electromyography study. Foot Ank Int 42:327-333.

Flavin R, Halpin T, O'Sullivan D, FitzPatrick D, Ivankovic K, Stephens MM. 2008. A finite-element analysis study of the metatarsophalangeal joint of the hallux rigidus. J Bone Joint Surg Br 90-B:1334-1340.

Flowers PPE, Cleveland RJ, Nelson AE, Kraus VB, Hillstrom HJ, Goode AP, Hannan MT, Renner JB, Hordan JM, Golightly YM. 2018. Association between general joint hypermobility and knee, hip, and lumbar spine osteoarthritis by race: a cross-sectional study. Arth Res Ther, 20:76.

Fox AJS, Bedi A, Rodeo SA. 2008. The basic science of articular cartilage: Structure, composition, and function. Sports Health 1:461-468.

Fritz GR, Prieskorn D. 1995. First metatarsocuneiform motion: A radiographic and statistical analysis. Foot Ank Int 16:117-128.

Fuller EA. 2000. The windlass mechanism of the foot. A mechanical model to explain pathology. J Am Podiatr Med Assoc 90:35-46.

Fung YC. 1993. Bone and cartilage. In: Biomechanics: Mechanical properties of living tissue. 2nd ed. United States of America: Springer-Verlag New York. 500-538.

Garcia-Gonzalez A, Bayod J, Prados-Frutos JC, Losa-Iglesias M, Jules KT, de Bengoa-Vallejo RB, Doblare M. 2009. Finite-element simulation of flexor digitorum longus or flexor digitorum brevis tendon transfer for the treatment of claw toe deformity. J. Biomech. 42:1697-1704.

Gefen A. 2002. Stress analysis of the standing foot following surgical plantar fascia release. J Biomech 35:629-637.

Gefen A, 2003. The in vivo elastic properties of the plantar fascia during the contact phase of walking. Foot Ank Int 24:238-244.

Giacomozzi C. 2010. Appropriateness of plantar pressure measurement devices: A comparative technical assessment. Gait Posture 32:141-144.

Gibson JN, Thomson CE. 2005. Arthrodesis or total replacement arthroplasty for hallux rigidus: A randomized controlled trial. Foot Ank Int 26:680-690.

Glasoe WM, Allen MK, Saltzman CL, Ludewig PM, Sublett SH. 2002. Comparison of two methods used to assess first-ray mobility. Foot Ank Int 23:248-262.

Glasoe WM, Allen MK, Yack HJ. 1998. Measurement of dorsal mobility in the first ray: Elimination of fat pad compression as a variable. Foot Ank Int 19:542-546.

Glasoe WM, Coughlin MJ. 2006. A critical analysis of Dudley Morton's concept of disordered foot function. J Foot Ankle Surg 45:147-155.

Glasoe WM, Getsoian S, Myers M, Komnick M, Kolkebeck D, Oswald W, Liakos P. 2005. Criterion-related validity of a clinical measure of dorsal first ray mobility. J Orthop Sports Phys Therap 35:589-593.

Glasoe WM, Grebing BR, Beck S, Coughlin MJ, Saltzman CL. 2005. A comparison of device measures of dorsal first ray mobility. Foot Ankle Int 26:957-961

Glasoe WM, Michaud TM. 2019. Measurement of doral first ray mobility: A topical historical review and commentary. Foot Ank Int 40:603-610.

Glasoe WM, Yack HJ, Saltzman CL. 1999. Anatomy and biomechanics of the first ray. Phys Therap Rehab J 21:240-246.

Glasoe WM, Yack HJ, Saltzman CL. 2000. The reliability and validity of a first ray measurement device. Foot Ank Int 21:240-246.

Golightly, YM, Hannan, MT, Nelson, AE, Hillstrom, HJ, Cleveland, RJ, Kraus, VB, Schwartz, TA, Goode, AP, Flowers, P, Renner, JB, Jordan, JM. 2018. Relationship of joint hypermobility with ankle and foot radiographic osteoarthritis and symptoms in a community-based cohort. Arthritis Care Res 71:538-544.

Golightly YM, Nelson AE, Kraus VB, Renner JB, Jordan JM. 2012. General joint hypermobility and hip osteoarthritis: The johnston county osteoarthritis project. Osteoarthritis Cartilage 20:S182.

Grahame R. 1999. Joint hypermobility and genetic collagen disorders: are they related? Arch Dis Child 80:188-189.

Grant JCB. 1972. Lower Limb. In: Grant's Atlas of Anatomy. 6th ed. Baltimore: The Williams and Wilkins Co. 242-356.

Gray EG, Basmajian JV. 1968. Electromyography and cinematography of leg and foot (“normal” and flat) during walking. Anat Rec 161:1-15.

Gray JR, Bridges AB, Faed MJ, Pringle T, Baines P, Dean J, Boxer M. 1994. Ascertainment and severity of marfan syndrome in a scottish population. J Med Genet 31:51-54.

Grebing BR, Coughlin MJ. 2004. The effect of ankle position on the exam for first ray mobility. Foot Ank Int 25:467-475.

Gu YD, Ren XJ, Li JS, Lake MJ, Zhang QY, Zeng YJ. 2010. Computer simulation of stress distribution in the metatarsals at different inversion landing angles using finite element method. Int Orthop 34:669-676.

Guettler JH, Demetropoulos CK, Yang KH, Jurist KA. 2004. Osteochondral defects in the human knee: influence of defect size on cartilage rim stress and load redistribution to surrounding cartilage. Am J Sport Med 32:1451-1458.

Guo J, Wang L, Mao R, Chang C, Wen J, Fan Y. 2018. Biomechanical evaluation of the first ray in pre-/post-operative hallux valgus: A comparative study. Clin Biomech 60:1-8.

Hafer JF, Lenhoff MW, Song J, Jordan JM, Hannan MT, Hillstrom HJ. 2013. Reliability of plantar pressure platforms. Gait Posture 38:544-548.

Hagedorn TJ, Dufour AB, Riskowski JL, Hillstrom HJ, Menz HB, Casey VA, Hannan MT. 2013. Foot disorders, foot posture, and foot function: The Framingham foot study. Plos One 8:e74364. https://doi.org/10.1371/journal.pone.0074364

Hakim A, Grahame R. 2003. Joint hypermobility. Best Pract Res Clin Rheumatol 17:989-1004.

Halloran JP, Clary CW, Maletsky LP, Taylor M, Petrella AJ, Rullkoetter PJ. 2010. Verification of predicted knee replacement kinematics during simulated gait in the Kansas knee simulator. J Biomech Eng 132:081010-1

Henak CR, Abraham CL, Anderson AE, Maas SA, Ellis BJ, Peters CL, Weiss JA. 2014. Patient-specific analysis of cartilage and labrum mechanics in human hip with acetabular dysplasia. Osteoarthritis Cartilage 22:210-217.

Henninger HB, Reese SP, Anderson AE, Weiss JA. 2010. Validation of computational models in biomechanics. Pro Inst Mech Eng H 224:801-812.

Hamid KS, Amendola A. 2017. Chronic rupture of the peroneal tendons. Foot Ank Clin North Am 22:843–850.

Hicks JH. 1953. The mechanics of the foot I. The joints. J Anat 87:345-357.

Hicks JH. 1954. The mechanics of the foot II. The plantar aponeurosis and the arch. J Anat 88:25-30.

Hillstrom HJ, Song J, Kraszewski AP, Hafer JF, Mootanah R, Dufour AB, Chow BS, Deland III JT. 2013. Foot type biomechanics part 1: Structure and function of the asymptomatic foot. Gait Posture 37:445-451.

Holmes MH, Mow VC. 1990. The nonlinear characteristics of soft gels and hydrated connective tissues in ultrafiltration. J Biomech 23:1145-1156.

Horton GA, Park Y-W, Myerson MS. 1999. Role of metatarsus primus elevatus in the pathogenesis of hallux rigidus. Foot Ank Int 20:777-780.

Hsu C-C, Tsai W-C, Hsiao T-Y, Tseng F-Y, Shau Y-W, Wang C-L, Lin S-C. 2009. Diabetic effects on microchambers and macro chambers tissue properties in human heel pads. Clin Biomech 24:682-686.

Huang K, Hollevoet N, Giddins G. 2015. Thumb carpometacarpal joint total arthroplasty: a systematic review. J Hand Surg 40:338-350.

Hughes J, Pratt L, Linge K, Clark P, Klenerman L. 1991. Reliability of pressure measurements: the E-MED F System. Clin Biomech 6:14-18.

Hughston JC, Hergenroeder PT, Courtenay BG, 1984. Osteochondritis dissecans of the femoral condyles. J Bone Joint Surg Am 66:1340-1348.

Imhauser CW, Siegler S, Udupa JK, Toy JR. 2008. Subject-specific models of the hindfoot reveal a relationship between morphology and passive mechanical properties. J Biomech 41:1341-1349.

Isvilanonda V, Dengler E, Iaquinto JM, Sangeorzan BJ, Ledoux WR. 2012. Finite element analysis of the foot: Model validation and comparison between two common treatments of the clawed hallux deformity. Clin Biomech 27:837-844.

Isvilanonda V, Iaquinto MJ, Pai S, Mackenzie-Helwein P, Ledoux WR. 2016. Hyperelastic compressive mechanical properties of the subcalcaneal soft tissue: An inverse finite element analysis. J Biomech 49:1186-1191.

Jack E. 1940. The aetiology of hallux rigidus. Br J Surg 27:492-497.

Jacob S, Patil MK. 1999. Stress analysis in three-dimensional foot models of normal and diabetic neuropathy. Front Med Biol Eng 9:211-227.

Jansson KS, Michalski MP, Smith SD, LaPrade RF, Wijdicks CA. 2013. Tekscan pressure sensor output changes in the presence of liquid exposure. J Biomech 46:612-614.

Johnson CH, Christensen JC. 1999. Biomechanics of the first ray part I. The effects of peroneus longus function: A three-dimensional kinematic study on a cadaver model. J Foot Ankle Surg 38:313-321.

Jones BK, Hug CT, Ateshian GA. 2016. Biphasic Analysis of Cartilage Stresses in the Patellofemoral Joint. J Biomech Eng 29:92-98.

Jones CP, Coughlin MJ, Pierce-Villadot R, Golano P, Kennedy MP, Shurnas PS, Grebing BR, Teachout L. 2005. The validity and reliability of the klaue device. Foot Ank Int 26:951-956.

Jones MT, Sanders AE, DaChunha RJ, Cody EA, Sofka CM, Nguyen J, Deland JT, Ellis SJ. 2019. Assessment of various measurement methods to assess first metatarsal elevation in hallux rigidus. Foot Ank Ortho 4(3):1-9.

Jonsson H, Vlatysdottir ST, Kjartasson O, Brekkan A, 1996. Hypermobility associated with osteoarthritis of the thumb base: a clinical and radiological subset of hand osteoarthritis. Ann Rheum Dis 55:540-543.

Judge DP, Dietz HC. 2005. Marfan’s syndrome. Lancet 366:1965-1976.

Kaufman KR, Brodine SK, Shaffer RA, Johnson CW, Cullison TR. 1999. The effect of foot structure and range of motion of musculoskeletal overuse injuries. Am J Sports Med 27:585-593.

Key JA. 1927. Hypermobility of joints as a sex linked hereditary characteristic. J Am Med Assoc 88:1710-1712.

Kiadaliri AA, Rinaldi G, Lohmander LS, Ingemar FP, Englund M. 2019. Temporal trend and regional disparity in osteoarthritis hospitalisations in Sweden 1998-2015. Scand J Pub Health 47:53-60

King DM, Toolan BC. 2004. Associated deformities and hypermobility in hallux valgus: An investigation with weightbearing radiographs. Foot Ank Int 25:251-255.

Kissel CG, Husain ZS, Wooley PH, Kruger M, Schumaker MA, Sullivan M, Snoeyink T. 2008. A prospective investigation of the biopro® hemi-arthroplasty for the first metatarsophalangeal joint. J Foot Ankle Surg 47:505-509.

Kitaoka HB, Luo ZP, Growney ES, Berglund LJ, An KN 1994. Material properties of the plantar aponeurosis. Foot Ank Int 15:557-560.

Klaue K, Hansen ST, Masquelet AC. 1994. Clinical, quantitative assessment of first tarsometatarsal mobility in the sagittal plane and its relation to hallux valgus deformity. Foot Ank Int 15:9-13.

Klemp P, Williams SM, Stansfield SA. 2002. Articular mobility in maori and european new zealanders. Rhematol 41:554-557.

Klennert BJ, Ellis BJ, Maak TG, Kapron AL, Weiss JA. 2017. The mechanics of focal chondral defects in the hip. J Biomech 52:31-37.

Klets O, Mononen ME, Tanska P, Nieminen MT, Korhonen RK, Saarakkala S. 2016. Comparison of different material models of articular cartilage in 3D computational modelling of the knee: Data from the osteoarthritis initiative (OAI). J Biomech 49:3891-3900.

Kohls-Gatzoulis J, John C, Singh D, Haddad F, Livingstone J, Berry G. 2004. Tibialis posterior dysfunction: A common and treatable cause of adult acquired flatfoot. Br Med J 329:1328-1332.

Kokubo T, Hashimoto T, Nagura T, Nakamura T, Suda Y, Matsumoto H, Toyama Y. 2012. Effect of the posterior tibial and peroneal longus on the mechanical properties of the foot arch. Foot Ank Int 33:320-325.

Krishnan R, Park S, Eckstein F, Ateshian GA. 2003. Inhomogeneous cartilage properties enhance superficial interstitial fluid support and frictional properties, but do not provide a homogenous state of stress. J Biomech Eng 125:569-577.

Kura H, Luo Z-P, Kitaoka HB, Smutz WP, An K-N. 2001. Mechanical behaviour of the Lisfranc and dorsal cuneometatarsal ligaments: In vitro biomechanical study. J Orthop Trauma 15:107-110.

Kurtz S, Lau E, Ong K, Zhao K, Kelly M, Bozic KJ. 2009. Future young patient demand for primary and revision joint replacement: National projections from 2010 to 2030. Clin Orthop Relat Res 467:2606-2612.

Lambrinudi C. 1938. Metatarsus primus elevatus. Proc R Soc Med 31:1273.

Ledoux WR, Hillstrom HJ. 2002. The distributed plantar vertical force of neutrally aligned and pes planus feet. Gait Posture 15:1-9.

Ledoux WR, Shofer JB, Ahroni JH, Smith DG, Sangeorzan BJ, Boyko EJ. 2003. Biomechanical differences among pes cavus, neutrally aligned, and pes planus feet in subjects with diabetes. Foot Ank Int 24:846-860.

Lee, KT, Young, K. 2001. Measurement of first-ray mobility vs. hallux valgus patients. Foot Ank Int 22:960-964.

Levy JC, Mizel MS, Wilson Jr LS, Fox W, McHale K. Taylor DC, temple HT. 2006. Incidence of foot and ankle injuries in West Point cadets with pes planus compared to the general cadet population. Foot Ank Int 27:1060–1064.

Li J, Hua X, Jones AC, Williams S, Jin Z, Fisher J, Wilcox RK. 2016. The influence of the representation of collagen fibre organisation on the cartilage contact mechanics of the hip joint. J Biomech 49:1679-1685.

Liu GT, Lavery LA, Schenck Jr RC, Lanctot DR, Zhu CF, Athanasiou KA. 1997. Human articular cartilage biomechanics of the second metatarsal intermediate cuneiform joint. J Foot Ankle Surg 36:367-374.

Lundgren P, Nester C, Liu A, Arndt A, Jones R, Stacoff A, Wolf P, Lundberg A. 2008. Invasive in vivo measurements of rear-, mid- and forefoot motion during walking. Gait Posture 28:93-100.

Manzano S., Armengol M, Price AJ, Hulley PA, Gill HS, Dolabré M, Doweidar MH. 2016. Inhomogeneous response of articular cartilage: A three-dimensional multiphasic heterogeneous study. PLoS One 11:e0157,967

Marenzana M, Arnett TR. 2013. The key role of blood supply to bone. Bone Res 1:203-215.

Massie WK, Howorth MB. 1951. Congenital dislocation of the hip: Part II. Results of open reduction as seen in early adult period. J Bone Joint Surg Br 33:171-190.

McBride ID, Wyss UP, Cooke TDV, Murphy L, Phillips J, Olney SJ, 1991. First metatarsophalangeal joint reaction forces during high-heel gait. Foot Ank Int, pp. 282-288.

McCarty JC, Lee JA. 2002. Acetabular dysplasia: a paradigm of arthroscopic examination of chondral injuries. Clin Orthop Relat Res 405:122-128.

McMaster MJ. 1978. The pathogenesis of hallux rigidus. Bone Joint J 60:82-87.

Meachim G. 1972. Articular cartilage lesions in osteoarthritis of the femoral head. J Pathol 107:199-210.

Mente PL, Lewis JL. 1994. Elastic modulus of calcified cartilage is an order of magnitude less than that of subchondral bone. J Orthop Res 12:637-647.

Menz HB, Munteanu SE, Zammit GV, Landorf KB. 2010. Foot structure and function in older people with radiographic osteoarthritis of the medial midfoot. Osteoarthritis Cartilage 18:317-322.

Menz HB, Roddy E, Marshall M, Thomas MJ, Rathod T, Myers H, Thomas E, Peat GM. 2015. Demographic and clinical factors associated with radiographic severity of first metatarsophalangeal joint osteoarthritis: Cross-sectional findings from the clinical assessment study of the foot. Osteoarthritis Cartilage 23:77-82.

Messner K, Maletius W. 1996. The long-term prognosis of severe damage to weight-bearing cartilage in the knee. Acta Orthop Scand 67:629-643.

Min BC, Chung CY, Park MS, Choi Y, Koo S, Jang S, Lee KM. 2019. Dynamic first tarsometatarsal instability during gait evaluated by pedobarographic examination in patients with hallux valgus. Foot Ank Int 40:1104-1109.

Mizel MS. 1993. The role of the plantar first metatarsal cuneiform ligament in weightbearing on the first metatarsal. Foot Ank Int 14:82.

Mkandawire C, Ledoux WR, Sangeorzan BJ, Ching RP. 2005. Foot and ankle ligament morphometry. J Rehab Res Dev 42:809-820.

Mononen ME, Mikkola MT, Julkenen P, Ojala R, Nieminen MT, Jurvelin JS, Korhonen RK. 2012. Effect of superficial collage patterns and fibrillation of femoral articular cartilage on knee joint mechanics-a 3D finite element analysis. J Biomech 45:579-587.

Moore ES, Kindig MW, McKearney DA, Telfer S, Sangeorzan BJ, Ledoux WR. 2018. Hind – and midfoot bone morphology varies with foot type and sex. J Orthop Res 37:744-759.

Morales-Orcajo E, Becerro de Benoga Vallejo R, Iglesias ML, Bayod J. 2016. Structural and material properties of human foot tendons. Clin Biomech 37:1-6.

Morales-Orcajo E, Souza TR, Bayod J, de Las Cases EB. 2017. Non-linear finite element model to assess the effect of tendon forces on the foot-ankle complex. Med Eng Phys 49:71-78.

Morton D. 1928. Hypermobility of the first metatarsal bone: The interlinking factor between metatarsalgia and longitudinal arch strains. J Bone Joint Surg Br 10:187-196.

Morgan OJ, Hillstrom HJ, Ellis SJ, Golightly YM, Russell R, Hannan MT, Deland JT, Hillstrom R. 2019. Osteoarthritis in England: Incidence trends from national health service hospital episode statistics. ACR Open Rheum 1: 493-498

Munuera-Martinez PV, Tavara-Vidalon P, Monge-Vera, MA, Saez-Diaz A, Lafuente-Sotillos G. 2020. The validity and reliability of a new simple instrument for the measurement of first ray mobility. Sensor 20:2207

Murley GS, Menz HB, Landorf KB. 2009. Foot posture influences the electromyographic activity of selected lower limb muscles during gait. J Foot Ankle Res 26:35.

Nakamura S, Crowninshield RD, Cooper RR. 1981. An analysis of soft tissue loading in the foot – a preliminary report. Bull Pros Res 10:27-34.

No authors. National Institute for Health and Care Excellence. Metatarsophalangeal joint replacement of the hallux (Interventional Procedure Guidance 140). Available at: http:// guidance.nice.org.uk/IPG140/Guidance/pdf/English. Accessed February 16, 2019.

No authors. National Joint Registry for England and Wales: 15th Annual Report 2018. http://www.njrreports.org.uk/Portals/0/PDFdownloads/NJR%2015th%20Annual%20Report%202018.pdf. Accessed February 16, 2019.

No Authors. Medical Devices Agency. Screw-fit ceramic toe joint (metatarsophalangeal) replacement prosthesis (alert). 2002; 1-4.

Nordin M, Frankel VH. 2001. Biomechanics of the foot and ankle. In: Butler, J. Basic Biomechanics of the Musculoskeletal System. 3rd ed. United States of America: Lippincott Williams and Wilkins. 222-255.

Nguyen U-SDT, Hillstrom HJ, Li W, Dufour AB, Kiel DP, Procter-Gray E, Gagnon MM, Hannan MT. 2010. Factors associated with hallux valgus in a population-based study of older women and men: the MOBILIZE Boston study, Osteoarthritis Cartilage 18:41-46.

Ogon M, Aleksiev AR, Pope MH, Wimmer C, Saltzman CL. 1999. Does arch height affect impact loading at the lower back level in running? Foot Ank Int 20:263-266.

Ohara K, Tanaka Y, Taniguchi A, Kurokawa H, Kumai T, Yamada H. 2019. Is metatarsus primus elevatus truly observed in hallux rigidus? Radiographic study using mapping methods. J Orthop Sci 24:312-219.

Olson SL, Ledoux WR, Ching RP, Sangeorzan BJ. 2003. Muscular imbalances resulting in a clawed hallux. Foot Ank Int 6:477-485.

Peng Y, Wong DWC, Chen TLW, Wan Y, Zhang G, Yan F, Zhang M. 2021. Influence of arch support heights on the internal foot mechanics of flatfoot during walking: A muscle-driven finite element analysis. Comp Bio Med 132:104355.

Prieto-Alhambra D, Judge A, Javaid MK, Cooper C, Diez-Perez A, Arden NK. 2014. Incidence and risk factors for clinically diagnosed knee, hip, and hand osteoarthritis: influences of age, gender and osteoarthritis affecting other joint. Ann Rheum Dis 73:1659-1664.

Sinha S, Mcnamara P, Bhatia M, Louette L, Stephens I. 2010. Survivorship of the bio-action metatarsophalangeal joint arthroplasty for hallux rigidus: 5-Year follow-up. Foot Ankle Surg 16:25-27.

Raikin SM, Ahmed J, Pour AE, Abidi N. 2008. Comparison of arthrodesis and metallic hemiarthroplasty of the hallux metatarsophalangeal joint. J Bone Joint Surg 89:1979-1985.

Rao S, Bell K. 2013. Reliability and prevelance of radiographic measures of metatarsus primus elevatus and arch alignment in individuals with midfoot arthritis and controls. J Am Podiat Med Assoc 103:47-354.

Rao S, Song J, Kraszewski A, Backus S, Ellis SJ, Deland JT, Hillstrom HJ. 2011. The effect of foot structure on 1st metatarsophalangeal joint flexibility and hallucial loading. Gait Posture 34:131-137.

Redmond AC, Crosbie J, Ouvrier RA. 2006. Development and validation of a novel rating system for scoring standing foot posture: the foot posture index. Clin Biomech 21:89-98.

Reggiani B, Leardini A, Corazza F, Taylor M. 2006. Finite element analysis of a total ankle replacement during the stance phase of gait. J Biomech 39:1435-1443.

Remvig L, Jensen DV, Ward RC. 2007. Epidemiology of general joint hypermobility and basis for the proposed criteria for benign joint hypermobility syndrome: review of the literature. J Rheumatol 34:804-809.

Reynaud B, Quinn TM. 2006. Anisotropic hydraulic permeability in compressed articular cartilage. J Biomech 39:131-137.

Rho J-Y, Kuhn-Spearing L, Zioupos P. 1998. Mechanical properties and the hierarchical structure of bone. Med Eng Phys 20:92-102.

Rodgers MM, Cavanagh PR. 1986. A device for the measurement of first ray Mobility. In: Proceedings of the North American Congress on Biomechanics. Montreal. Montreal: North American Congress on Biomechanics 205-206.

Roddy E, Menz HB. 2018. Foot osteoarthritis: Latest evidence and developments. Ther Adv Musculoskelet Dis 10:91-103.

Roddy E, Thomas MJ, Marshall M, Rathod T, Myers H, Menz HB, Thomas E, Peat G. 2015. The population prevalence of symptomatic radiographic foot osteoarthritis in community-dwelling older adults: cross-sectional findings from the clinical assessment study of the foot. Ann Rheum Dis 74:156-163.

Root ML, Orien WP, Weed JH. 1977. Motion of the joints of the foot: The first ray. S.A. Root (Ed), Clinical Biomechanics. Volume IIP: Normal and Abnormal Function of the Foot, Clinical Biomechanics, Los Angeles 46-51 350-354.

Roukis TS. 2005. Metatarsus primus elevatus in hallux rigidus: Fact or fiction? J Am Podiat Med Assoc 95:221-228.

Roukis TS, Jacobs PM, Dawson D, Erdmann BB, Ringstrom JB. 2002. A prospective comparison of clinical radiographic, and intraoperative features of hallux rigidus. J Foot Ankle Surg 41:76-95.

Roukis TS, Scherer PR, Anderson CF. 1996. Position of the first ray and motion of the first metatarsophalangeal joint. J Am Podiat Med Assoc 8:538-546.

Ruff C, Holt B, Trinkaus E. 2006. Who's afraid of the big bad Wolff?: "Wolff's law" and bone functional adaptation. Am J Phys Anthropol 129:484-498.

Sammarco GJ. 1995. Peroneus longus tendon tears: Acute and chronic. Foot Ank Int 16:245-253.

Sammarco GJ, Hockenbury RT. 2001. Treatment of stage II posterior tibial tendon dysfunction with flexor hallucis longus transfer and medical displacement calcaneal osteotomy. Foot Ank Int 22:305-312.

Sarzi-Puttini P, Cimmino MA, Scarpa R, Caporali R, Parazzini F, Zaninelli A, Atzeni F, Canesi B. 2005. Osteoarthritis: An overview of the disease and its treatment strategies. Sem Arthritis Rheum 35:1-10.

Sasazaki Y, Shore R, Seedhom BB. 2006. Deformation and failure of cartilage in the tensile mode. J Anat 208:681-694.

Schenck RC, Athanasiou KA, Constantinides G, Gomez E. 1994. A biomechanical analysis of articular cartilage of human elbow and a potential relationship to oteochondritis dissecans. Clin Orthop 299:305-312.

Seiberg M, Felson S, Colson JP, Barth AH, Green RM, Green DR.1994. Closing base wedge versus austin bunionectomies for metatarsus primus adductus. J Am Podiat Med Assoc 84:548-563.

Shepard DE, Seedhom BB. 1999. The 'instantaneous' compressive modulus of human articular cartilage in joint of the lower limb. Rheumatol 38:124-132.

Siegler S, Hillstrom HJ, Freedman W, Moskowitz G. 1985. Effect of myoelectric signal processing on the relationship between muscle force and processed EMG. Am J Phys Med 64:130-149.

Sellman JR. 1994. Plantar fascia rupture associated with corticosteroid injection. Foot Ank Int 15:376-381.

Shankar NS. 1995. Silastic single-stem implants in the treatment of hallux rigidus. Foot Ank Int 16:487-491.

Sharkey NA, Ferris L, Donahue SW. 1998. Biomechanical consequences of plantar fascia release or rupture during gait: part I-disruption in longitudinal arch confirmation. Foot Ank Int 8:12-20.

Shereff MJ, Bejjani FJ, Kummer FJ. 1986. Kinematics of the first metatarsophalangeal joint. J Bone Joint Surg Am 68:392-398.

Shirk C, Sandrey MA, Erickson M. 2006. Reliability of first ray position and measurements in experienced and inexperienced examiners. J Athlet Train 41:93-101.

Shrout PC, Fleiss JL. 1979. Intraclass correlations: uses in assessing rater reliability. Psy Bull 86:420-428.

Siegler S, Block J, Schenck. 1988. The mechanical characteristics of the collateral ligaments of the human ankle joint. Foot Ank Int 8:234-242.

Song J, Choe K, Neary M, Zifchock RA, Cameron KL, Trepa M, Hannan MT, Hillstrom H. 2018. Comprehensive biomechanical characterization of feet in USMA cadets: Comparison across race, gender, arch flexibility, and foot types. Gait Posture 60:175-180.

Sturkie PD. 1941. Hypermobile joints in all descendants for two generations. J Hered 32:232-234.

Sullivan MR. 2009. Hallux rigidus: MTP implant arthroplasty. Foot Ankle Clin 14:33-42.

Sun P-C, S S-L, Chen Y-L, Hsu Y-C, Yan R-C, Chen, C-S. 2012. Biomechanical analysis of foot with different foot arch heights: a finite element analysis. Comp Method Biomech Biomed Eng 15:563-569.

Sutro CJ. 1947. Hypermobility of bones due to overlengthened capsular and ligamentous tissue; a cause for recurrent intra-articular effusions. Surgery 21:67-76.

Tannast M, Goricki D, Beck M, Murphy SB, Siebenrock KA. 2008. Hip damage occurs at the zone of femoroacetabular impingement. Clin Orthop Relat Res 466:273-280.

Tao K, Wang D, Wang C, Wang X, Liu A, Nester CJ, Howard D. 2009. An in vivo experimental validation of a computational model of human foot J Bionic Eng 6:387-397.

Tavara-Vidalon SP, Monge-Vera MA, Lafuente-Sotillos G, Dominguez-Maldonado G, Munuera-Martinez PV. Static range of motion of the first metatarsal in the sagittal and frontal planes. J Clin Med. 2018;7(11):1-12.

Telfer T, Kindig MW, Sangeorzan BJ, Ledoux WR. 2017. Metatarsal shape and foot type: A geometric morphometric analysis. J Biomech Eng 139:031008.

Thorn JC, Turner E, Hounsome L, Walsh E, Donovan JL, Verne J, Neal D, Hamdy F, Martin RM, Noble S. 2014 Validation of the hospital episode statistics outpatient dataset in England. Pharmacoeconomics 34:161-168.

Titchener AG, Duncan NS, Rajan RA. 2015. Outcome following first metatarsophalangeal joint replacement using toefit-plus™: A mid term alert. Foot Ankle Surg 21:119-124.

Tobias JH, Deere K, Palmer S, Clark EM, Clinch J. 2013. Joint hypermobility is a risk factor for musculoskeletal pain during adolescence. Arthritis Rheumatism 65:1107-1115.

Todd JN, Maak TG, Ateshian GA, Maas SA, Weiss JA. 2018. Hip chondrolabral mechanics during activities of daily living: Role of the labrum and interstitial fluid pressurization. J Biomech 69:113-120.

Trivedi B, Marshall M, Belcher J, Roddy E. 2010. A systematic review of radiographic definitions of foot osteoarthritis in population-based studies. Osteoarthritis Cartilage 18:1027-1035.

Usuelli F, Palmucci M, Montrasio UA, Malerba F. 2011. Radiographic considerations of hallux valgus versus hallux rigidus. Foot Ank Int 32:782-788.

Van Beek C, Greisberg J. 2011. Mobility of the first ray: Review article. Foot and Ankle International 32:917-922.

Van Saase JL, van Romunde LK, Cats A, Vandenbroucke JP, Valkenburg HA. 1989. Epidemiology of osteoarthritis; zoetermeer survey. Comparison of radiological osteoarthritis in a dutch population with that of 10 other populations. Ann Rheum DIs 48:271-280.

Venäläinen MS, Mononen ME, Salo J, Räsänen LP, Jurvelin JS, Toyräs J, Viren T, Korhonen RK. 2016. Quantitative evaluation of the mechanical risks caused by focal cartilage defects in the knee. Sci Rep 6:37538.

Viceconti M. 2005. Extracting clinically relevant data from finite element simulations. Clin Biomech 20:451-454.

Voellmicke KV, Deland JT. 2002. Manual examination technique to assess dorsal instability of the first ray. Foot Ank Int. 23:1040-1041.

Voskuijl T, Onstenk R. 2015. Operative treatment for osteoarthritis of the first metatarsophalangeal joint: Arthrodesis versus hemiarthroplasty. J Foot Ankle Surg 54:1085-1088.

Viegas GV. 1998. Reconstruction of hallux limitus deformity using a first metatarsal sagittal-z osteotomy. J Foot Ankle Surg 37:204-211.

Wallace WA, Kilmartin TE. 1990. Predicting hallux abducto valgus. J Am Podiat Med Assoc 80:509-510.

Wang YN, Lee K, Ledoux WR. 2011. Histomorphological evaluation of diabetic and non-diabetic plantar soft tissue. Foot Ank Int 32:802-810.

Wanivenhaus A, Pretterklieber M. 1989. First tarsometatarsal joint: Anatomical and biomechanical study. Foot Ank Int 9:153-157.

W-Dahl A, Robertsson O, Lars L. 2010. Surgery for knee osteoarthritis in younger patients. Acta Orthop 81:161-164.

Whittle MW. 1999. Generation and attenuation of transient impulsive forces beneath the foot: Review. Gait Posture 10:264-275.

Wang Z, Kido M, Imai K, Ikoma K, Hirai S. 2018. Towards patient-specific medializing calcaneal osteotomy for adult flatfoot: a finite element study. Comp Method Biomech Biomed Eng 21:332-343.

Wong DCW, Zhang M, Yu J, Leung, AK. 2014. Biomechanics of first ray hypermobility: An investigation on joint force during walking using finite element analysis. J Biomech 36:1388-1393.

Wong DCW, Wang Y, Leung AK-L, Yang M, Zhang M. 2018. Finite element simulation on posterior tibial tendinopathy: Load transfer alteration and implications to the onset of pes planus. Clin Biomech 51:10-16.

Woo SL-Y, Gomez MA, Akeson WH. 1981. The time and history-dependent viscoelastic properties of the canine medial collateral ligament. J Biomech Eng 103:293-298.

Wright DG, Rennels DC. 1964. A study of the elastic properties of plantar fascia. J Bone Joint. Surg Am 46:482-492.

Wu JZ, Herzog W. 2000. Finite element simulation of location- and time-dependent mechanical behaviour of chondrocytes in unconfined compression tests. Ann Biomed Eng 28:318-330.

Wu JZ, Herzog W, Epstein M. 1998. Effects of inserting a pressensor film into articular joints on the actual contact mechanics. J Biomech Eng 120:655-659.

Wyles CC, Heidenreich MJ, Jeng J, Larson DR, Trousdale RT, Sierra RJ. 2017. The John Charnley Award: Redefining the natural history of osteoarthritis in patients with hip dysplasia and impingement. Clin Orthop Relat Res 475:336-350.

Yu D, Jordan KP, Bedson J, Englund M, Blyth F, Turkiewicz A, Prieto-Alhambra D, Peat G. 2017. Population trends in the incidence and initial management of osteoarthritis: age-period-cohort analysis of the clinical practice research datalink, 1992-2013. Rheumatology 56:1902-1917.

Yu D, Peat G, Bedson J, Jordan KP. 2015. Annual consultation incidence of osteoarthritis estimated from population-based health care data in England. Rheumatology 54:2051-2060.

Zammit GV, Menz HB, Munteanu SE, Landorf KB. 2008. Plantar pressure distribution in older people with osteoarthritis of the first metatarsophalangeal joint (hallux limitus/hallux rigidus). J Orthop Res 26:1665-1669.

Zifchock RA, Theriot C, Hillstrom HJ, Song J, Neary M. 2017. The relationship between arch height and arch flexibility. J Am Podiat Med Assoc 107:119-123.

Appendix A. Additional Data for Epidemiology of Osteoarthritis

This appendix contains raw datasets from the HES and ONS databases, used to analyse trends in OA in Chapter 3.

Table A-1. Raw HES data for joint-specific OA diagnoses, 2000/01-2001/02.

Primary Diagnosis	Finished Consultant Episodes	Admissions	Male	Mean Age	Age 0-14	Age 15-59	Age 60-74	Age 75+
M20.2 Hallux rigidus	2,228	2,220	747	56	3	1,431	706	88
M17 Gonarthrosis [arthrosis of knee]	62,669	61,381	27,820	66	10	17,613	27,715	17,318
M16 Coxarthrosis [arthrosis of hip]	40,665	39,607	15,541	69	4	7,807	19,376	13,471
M18 Arthrosis of first carpometacarpal joint	1,493	1,485	288	60	0	754	614	125

Table A-2. Raw HES data for joint-specific OA diagnoses, 2001/02-2002/03.

Primary Diagnosis	Finished Consultant Episodes	Admissions	Male	Mean Age	Age 0-14	Age 15-59	Age 60-74	Age 75+
M20.2 Hallux rigidus	2,073	2,069	673	56	4	1,316	646	104
M17 Gonarthrosis [arthrosis of knee]	65,660	64,120	29,237	65	6	18,649	28,809	18,147
M16 Coxarthrosis [arthrosis of hip]	43,577	42,120	16,857	68	2	8,592	20,747	14,184
M18 Arthrosis of first carpometacarpal joint	1,584	1,583	343	60	-	801	644	139

Table A-3. Raw HES data for joint-specific OA diagnoses, 2002/03-2003/04.

Primary Diagnosis	Finished Consultant Episodes	Admissions	Male	Mean Age	Age 0-14	Age 15-59	Age 60-74	Age 75+
M20.2 Hallux rigidus	2,207	2,201	738	56	2	1,406	723	75
M17 Gonarthrosis [arthrosis of knee]	75,545	73,688	33,415	66	10	20,758	32,935	21,820
M16 Coxarthrosis [arthrosis of hip]	48,925	47,172	19,117	68	3	9,624	23,283	15,994
M18 Arthrosis of first carpometacarpal joint	1,908	1,903	368	61	-	930	806	171

Table A-4. Raw HES data for joint-specific OA diagnoses, 2003/04-2004/05.

Primary Diagnosis	Finished Consultant Episodes	Admissions	Male	Mean Age	Age 0-14	Age 15-59	Age 60-74	Age 75+
M20.2 Hallux rigidus	2,486	2,477	845	56	3	1,486	879	117
M17 Gonarthrosis [arthrosis of knee]	82,299	80,479	36,138	67	6	21,356	36,874	24,058
M16 Coxarthrosis [arthrosis of hip]	53,080	51,495	20,716	69	3	10,564	25,504	17,004
M18 Arthrosis of first carpometacarpal joint	2,140	2,134	491	61	0	1,017	932	191

Table A-5. Raw HES data for joint-specific OA diagnoses, 2004/05-2005/06.

Primary Diagnosis	Finished Consultant Episodes	Admissions	Male	Mean Age	Age 0-14	Age 15-59	Age 60-74	Age 75+
M20.2 Hallux rigidus	2,526	2,517	806	56	1	1,542	878	105
M17 Gonarthrosis [arthrosis of knee]	85,034	82,912	37,049	67	18	21,994	38,150	24,865
M16 Coxarthrosis [arthrosis of hip]	54,184	52,481	21,376	69	3	11,047	25,529	17,597
M18 Arthrosis of first carpometacarpal joint	2,456	2,453	503	61	0	1,112	1,120	224

Table A-6. Raw HES data for joint-specific OA diagnoses, 2005/06-2006/07.

Primary Diagnosis	Finished Consultant Episodes	Admissions	Male	Mean Age	Age 0-14	Age 15-59	Age 60-74	Age 75+
M20.2 Hallux rigidus	2,736	2,728	873	57	2	1,630	978	126
M17 Gonarthrosis [arthrosis of knee]	89,187	86,749	38,249	67	11	23,099	39,851	26,222
M16 Coxarthrosis [arthrosis of hip]	55,406	53,494	21,622	68	7	11,722	25,602	18,075
M18 Arthrosis of first carpometacarpal joint	2,972	2,966	590	61	0	1,293	1,460	219

Table A-7. Raw HES data for joint-specific OA diagnoses, 2006/07-2007/08.

Primary Diagnosis	Finished Consultant Episodes	Admissions	Male	Mean Age	Age 0-14	Age 15-59	Age 60-74	Age 75+
M20.2 Hallux rigidus	2,964	2,960	935	57	1	1,731	1,071	161
M17 Gonarthrosis [arthrosis of knee]	95,226	92,553	40,796	67	9	24,923	43,082	27,191
M16 Coxarthrosis [arthrosis of hip]	59,221	57,013	23,216	68	2	12,370	27,737	19,091
M18 Arthrosis of first carpometacarpal joint	3,219	3,205	648	61	0	1,382	1,554	283

Table A-8. Raw HES data for joint-specific OA diagnoses, 2007/08-2008/09.

Primary Diagnosis	Finished consultant episodes	Admissions	Male	Mean age	Age 0-14	Age 15-59	Age 60-74	Age 75+
M20.2 Hallux rigidus	3,321	3,311	1,082	57	0	1,864	1,285	171
M17 Gonarthrosis [arthrosis of knee]	107,329	104,432	46,566	66	12	28,311	49,114	29,816
M16 Coxarthrosis [arthrosis of hip]	65,291	62,947	25,931	68	5	13,811	30,787	20,665
M18 Arthrosis of first carpometacarpal joint	3,827	3,807	785	62	1	1,534	1,938	353

Table A-9. Raw HES data for joint-specific OA diagnoses, 2008/09-2009/10.

Primary Diagnosis	Finished consultant episodes	Admissions	Male	Mean age	Age 0-14	Age 15-59	Age 60-74	Age 75+
M20.2 Hallux rigidus	3,530	3,520	1,099	57	0	1,975	1,372	183
M17 Gonarthrosis [arthrosis of knee]	107,716	104,746	46,326	66	5	28,882	49,547	29,174
M16 Coxarthrosis [arthrosis of hip]	67,002	64,455	26,462	68	6	13,987	31,106	21,838
M18 Arthrosis of first carpometacarpal joint	4,472	4,454	982	62	0	1,810	2,226	433

Table A-10. Raw HES data for joint-specific OA diagnoses, 2009/10-2010/11.

Primary Diagnosis	Finished Consultant Episodes	Admissions	Male	Mean Age	Age 0-14	Age 15-59	Age 60-74	Age 75+
M20.2 Hallux rigidus	3,785	3,775	1,198	57	2	2,061	1,533	188
M17 Gonarthrosis [arthrosis of knee]	107,315	104,208	46,925	66	12	28,324	49,312	29,644
M16 Coxarthrosis [arthrosis of hip]	67,707	65,141	26,907	68	5	13,859	31,632	22,179
M18 Arthrosis of first carpometacarpal joint	4,898	4,890	1,116	62	0	1,935	2,467	496

Table A-11. Raw HES data for joint-specific OA diagnoses, 2010/11-2011/12.

Primary Diagnosis	Finished consultant episodes	Admissions	Male	Mean Age	Age 0-14	Age 15-59	Age 60-74	Age 75+
M20.2 Hallux rigidus	4,195	4,182	1,327	57	8	2,238	1,702	245
M17 Gonarthrosis [arthrosis of knee]	109,102	106,138	47,225	66	9	28,688	50,212	30,161
M16 Coxarthrosis [arthrosis of hip]	72,248	69,814	28,380	68	9	14,882	33,634	23,689
M18 Arthrosis of first carpometacarpal joint	5,171	5,155	1,276	62	-	2,032	2,617	519

Table A-12. Raw HES data for joint-specific OA diagnoses, 2011/12-2012/13.

Primary Diagnosis	Finished Consultant Episodes	Admissions	Male	Mean Age	Age 0-14	Age 15-59	Age 60-74	Age 75+
M20.2 Hallux rigidus	4,111	4,096	1,265	57	2	2,204	1,669	233
M17 Gonarthrosis [arthrosis of knee]	108,714	105,515	46,976	67	12	27,090	50,908	30,669
M16 Coxarthrosis [arthrosis of hip]	75,059	72,658	29,331	68	9	15,524	34,985	24,497
M18 Arthrosis of first carpometacarpal joint	5,756	5,729	1,382	62	-	2,153	2,992	610

Table A-13. Raw HES data for joint-specific OA diagnoses, 2012/13-2013/14.

Primary Diagnosis	Finished Consultant Episodes	Admissions	Male	Mean Age	Age 0	Age 1-4	Age 5-9	Age 10-14	Age 15	Age 16	Age 17	Age 18	Age 19	Age 20-24	Age 25-29	Age 30-34	Age 35-39	Age 40-44	Age 45-49	Age 50-54	Age 55-59	Age 60-64	Age 65-69	Age 70-74	Age 75-79	Age 80-84	Age 85-89	Age 90+
M20.2 Hallux rigidus	3,939	3,930	1,228	57	-	-	-	4	1	2	-	2	3	14	39	62	165	324	394	507	616	697	575	315	157	47	10	4
M17 Gonarthrosis [arthrosis of knee]	105,753	102,668	45,238	67	-	6	3	4	5	4	12	19	24	147	328	595	1,068	2,399	4,614	7,179	10,027	14,384	18,020	17,022	15,084	9,419	4,132	1,198
M16 Coxarthrosis [arthrosis of hip]	77,411	75,037	30,388	68	-	2	1	4	3	6	4	12	21	120	226	406	723	1,535	2,696	4,398	6,226	9,524	12,977	13,077	12,250	8,151	3,702	1,288
M18 Arthrosis of first carpometacarpal joint	6,344	6,326	1,485	62	-	-	-	1	-	1	-	1	-	4	10	15	52	159	400	739	1,055	1,249	1,188	761	430	200	53	23

Table A-14. Raw HES data for joint-specific OA diagnoses, 2013/14-2014/15.

Primary Diagnosis	Finished consultant episodes	Admissions	Male	Mean age	Age 0	Age 1-4	Age 5-9	Age 10-14	Age 15	Age 16	Age 17	Age 18	Age 19	Age 20-24	Age 25-29	Age 30-34	Age 35-39	Age 40-44	Age 45-49	Age 50-54	Age 55-59	Age 60-64	Age 65-69	Age 70-74	Age 75-79	Age 80-84	Age 85-89	Age 90+
M20.2 Hallux rigidus	4,051	4,043	1,285	57	-	-	-	-	4	4	-	2	5	15	42	81	132	299	467	512	603	662	643	326	165	64	20	-
M17 Gonarthrosis [arthrosis of knee]	110,964	107,561	47,664	67	-	9	2	7	3	12	11	15	21	178	379	609	1,071	2,578	4,755	7,516	10,652	14,737	19,339	17,656	15,857	9,774	4,347	1,358
M16 Coxarthrosis [arthrosis of hip]	84,050	81,431	32,960	68	-	1	1	5	-	2	8	13	11	130	237	427	703	1,536	2,886	4,756	7,095	9,955	14,464	13,873	13,606	8,913	3,947	1,390
M18 Arthrosis of first carpometacarpal joint	7,134	7,115	1,697	62	-	-	-	-	-	-	-	-	1	5	13	24	58	141	491	865	1,175	1,322	1,325	873	546	201	81	8

Table A-15. Raw HES data for joint-specific OA diagnoses, 2014/15-2015/16.

Primary Diagnosis	Finished consultant episodes	Admissions	Male	Mean age	Age 0	Age 1-4	Age 5-9	Age 10-14	Age 15	Age 16	Age 17	Age 18	Age 19	Age 20-24	Age 25-29	Age 30-34	Age 35-39	Age 40-44	Age 45-49	Age 50-54	Age 55-59	Age 60-64	Age 65-69	Age 70-74	Age 75-79	Age 80-84	Age 85-89	Age 90+
M20.2 Hallux rigidus	4,144	4,131	1,342	57	-	-	1	2	2	2	6	2	4	27	47	90	121	310	508	517	611	644	633	351	197	46	16	4
M17 Gonarthrosis [arthrosis of knee]	117,289	113,699	50,274	67	3	6	4	3	4	10	13	23	22	200	373	594	1,008	2,392	4,706	8,093	11,258	14,968	20,556	19,323	17,203	10,297	4,684	1,482
M16 Coxarthrosis [arthrosis of hip]	89,226	86,477	35,171	68	-	-	1	5	5	7	12	14	14	128	239	435	761	1,623	3,174	5,346	7,711	10,349	15,242	15,084	14,138	9,291	4,202	1,370
M18 Arthrosis of first carpometacarpal joint	7,952	7,927	2,045	63	-	-	1	-	-	-	-	2	1	11	11	23	51	145	488	996	1,327	1,448	1,490	996	603	260	79	16

Table A-16. Raw HES data for joint-specific OA diagnoses, 2015/16-2016/17.

Primary Diagnosis	Finished consultant episodes	Admissions	Male	Mean age	Age 0	Age 1-4	Age 5-9	Age 10-14	Age 15	Age 16	Age 17	Age 18	Age 19	Age 20-24	Age 25-29	Age 30-34	Age 35-39	Age 40-44	Age 45-49	Age 50-54	Age 55-59	Age 60-64	Age 65-69	Age 70-74	Age 75-79	Age 80-84	Age 85-89	Age 90+
M20.2 Hallux rigidus	4,393	4,386	1,375	57	-	-	-	1	-	1	3	4	4	19	51	96	135	328	517	582	578	689	707	371	202	82	15	4
M17 Gonarthrosis [arthrosis of knee]	116,078	112,460	50,217	67	-	6	3	2	1	7	15	21	22	159	317	560	973	2,117	4,299	7,800	11,105	14,973	20,625	19,484	16,867	10,484	4,630	1,522
M16 Coxarthrosis [arthrosis of hip]	89,612	86,885	35,170	68	-	1	1	3	5	8	13	18	18	160	234	455	770	1,694	3,282	5,439	7,693	10,386	14,827	15,118	14,094	9,541	4,405	1,359
M18 Arthrosis of first carpometacarpal joint	8,374	8,338	2,178	63	-	-	1	-	-	-	2	-	1	8	9	13	50	162	498	1,090	1,442	1,418	1,574	1,123	641	251	74	16

Table A-17. Raw HES data for joint-specific OA diagnoses, 2016/17-2017/18.

Primary Diagnosis	Finished consultant episodes	Admissions	Male	Mean age	Age 0	Age 1-4	Age 5-9	Age 10-14	Age 15	Age 16	Age 17	Age 18	Age 19	Age 20-24	Age 25-29	Age 30-34	Age 35-39	Age 40-44	Age 45-49	Age 50-54	Age 55-59	Age 60-64	Age 65-69	Age 70-74	Age 75-79	Age 80-84	Age 85-89	Age 90+
M20.2 Hallux rigidus	4,362	4,347	1,401	58	-	-	-	2	2	1	1	2	1	16	40	66	123	292	532	675	579	649	672	414	200	73	16	2
M17 Gonarthrosis [arthrosis of knee]	119,120	115,423	51,665	68	-	3	3	2	3	11	9	9	19	140	312	538	859	1,833	4,159	7,969	11,587	15,068	20,783	20,780	16,992	10,962	4,933	1,617
M16 Coxarthrosis [arthrosis of hip]	93,609	90,710	36,833	68	-	1	-	5	5	4	10	20	21	167	287	447	845	1,696	3,363	5,795	8,139	10,932	15,383	16,160	14,157	9,686	4,532	1,544
M18 Arthrosis of first carpometacarpal joint	9,244	9,209	2,292	63	-	-	-	-	-	-	-	-	1	7	10	35	43	162	540	1,192	1,600	1,532	1,743	1,242	688	322	84	14

Table A-18. Raw HES data for joint-specific OA diagnoses, 2017/18-2018/19.

Primary Diagnosis	Finished consultant episodes	Admissions	Male	Mean age	Age 0	Age 1-4	Age 5-9	Age 10-14	Age 15	Age 16	Age 17	Age 18	Age 19	Age 20-24	Age 25-29	Age 30-34	Age 35-39	Age 40-44	Age 45-49	Age 50-54	Age 55-59	Age 60-64	Age 65-69	Age 70-74	Age 75-79	Age 80-84	Age 85-89	Age 90+
M20.2 Hallux rigidus	4,083	4,068	1,395	58	0	0	0	0	4	1	1	0	0	18	29	83	91	243	463	613	575	618	577	449	211	69	22	0
M17 Gonarthrosis [arthrosis of knee]	112,429	108,398	48,553	68	0	4	8	2	2	6	3	16	12	122	255	434	823	1,519	3,736	7,248	10,758	14,792	18,416	21,028	16,185	10,469	4,705	1,545
M16 Coxarthrosis [arthrosis of hip]	90,293	87,244	35,703	68	0	2	0	11	6	7	5	17	17	154	249	490	833	1,638	3,349	5,713	7,863	10,640	13,819	16,448	13,423	9,413	4,376	1,528
M18 Arthrosis of first carpometacarpal joint	9,254	9,191	2,329	63	0	0	0	0	0	0	0	1	0	8	10	30	58	165	517	1,125	1,644	1,623	1,606	1,313	713	313	95	13

Table A-19. Raw ONS population data for people 18-years-old and over in England, 2012-2017.

Year	2000	2001	2002	2003	2004	2005	2006	2007	2008	2009	2010	2011	2012	2013	2014	2015	2016	2017
Population	49,230,000	49,450,000	49,680,000	49,930,000	50,190,000	50,610,000	50,970,000	51,380,000	51,820,000	52,200,000	52,640,000	53,010,000	53,490,000	53,870,000	54,320,000	54,790,000	55,270,000	55,620,000

Table A.1-20. Raw ONS population data for England stratified by age-group, 2012-2017.

Year	25-34	35-44	45-54	55-64	65-74	75+
2012	7,266,794	7,266069	7,445,129	6,066,563	4,141,171	4,212,018
2013	7,367,357	7,159067	7,543,287	6,053,995	4,382,363	4,281,606
2014	7,425,591	7,103408	7,635,651	6,100,512	4,560,930	4,374,835
2015	7,485,996	7,107372	7,700,360	6,183,043	4,703,160	4,425,817
2016	7,561,210	7,092,277	7,756,174	6,308,633	4,846,866	4,469,497
2017	7,589,024	7,085,401	7,757,304	6,461,954	4,936,563	4,535,330

Appendix B. Additional Data for Testing and Reliability of MAP1st

As part of the background to Chapter 4 and 5, documentation was prepared and submitted to the IRB at HSS. This appendix details the supplementary information required to organise the human subjects testing as well as additional data not reported in the main text of Chapter 4.

B.1 CITI Program Certification

In order to conduct clinical research at HSS, it was necessary to complete the following CITI Program modules for Human Research as part of the IRB Reference Resource.

CITI PROGRAM

Completion Date 20-Jun-2019
Expiration Date N/A
Record ID 32098988

This is to certify that:

Oliver Morgan

Has completed the following CITI Program course:

Human Research (Curriculum Group)
IRB Reference Resource (Course Learner Group)
1 - Basic Course (Stage)

Under requirements set by:

Hospital for Special Surgery - New York

CITI
Collaborative Institutional Training Initiative

Verify at www.citiprogram.org/verify/?w1c808a76-c927-466e-8d6e-8caa95edf06b-32098988

B.2 Hospital for Special Surgery Institutional Review Board Submission

HOSPITAL FOR SPECIAL SURGERY electronic Clinical Application Portal (eCAP)

Date: Thursday, September 13, 2018 10:26:07 AM
ID: 2018-0754

Print | Close

Help
VIEW000072

Study Identification Information

This is the first step in your Human Research Application. You will automatically be guided to the appropriate forms needed to complete your submission.

1.0 Title: (please do not use initials)
Reliability of a First Ray Mobility Jig: A Pilot Study

* **Short Title for EPIC:**
First Ray Mobility (If Not Applicable, please enter N/A)

2.0 Description:
The research team will determine the reliability of a new jig to measure first ray mobility in partial and full weight-bearing, as well as a handheld first ray measurement device (FRMD), in a cohort of 20 healthy subjects (40 feet) which will encompass 10 bilateral planus subjects (20 feet) and 10 bilateral rectus subjects (20 feet). In addition,10 subjects diagnosed with unilateral metatarsus primus elevatus (10 feet) will also be included for a total of 50 feet. The purpose of this study is to establish the reliability of the new 1st ray mobility jig and the FRMD for measuring superior translation and position.

Glossary of Terms:
First ray: a collective anatomical unit of the bones comprising the medial aspect of the forefoot, including the medial cuneiform, first metatarsal, hallucial sesamoids, and proximal and distal phalanges of the hallux.
First ray mobility: the collective motion between the medial cuneiform and first metatarsal.
First ray hypermobility: an overly flexible first ray, defined by a dorsal/plantar translation of the first metatarsal ≥10 mm
Metatarsus primus elevatus: ≥5 mm elevation of the first metatarsal bone, which is often associated with moderate to end-stage first metatarsophalangeal joint osteoarthritis.
FRMD: handheld first ray measurement device
1st MTP joint: First Metatarsophalangeal joint
Healthy 1st MTP joint: (>60° dorsiflexion) necessary for efficient transfer of body-weight during propulsive gait
Hallux limitus: (<40° dorsiflexion) partially restricted sagittal plane motion, and at the end-stage
Hallux rigidus: (<20° dorsiflexion) severely restricted sagittal plane motion

3.0 * **Principal Investigator:**
Howard Hillstrom, Ph.D.

4.0 Study Contact:
Ibadete Thaqi

5.0

Co-Investigators:

First Name	Last Name	Organization
Jonathan	Deland, MD	Foot and Ankle
Scott	Ellis, MD	Foot and Ankle
Howard	Hillstrom, Ph.D.	Rehabilitation
Jennifer	Jezequel	Motion Analysis
Mehnaz	Shahid	Motion Analysis
Ibadete	Thaqi	Rehabilitation
Robert	Turner, DPT OCS MS OM	Rehabilitation

If a name does not appear in Co-Investigators directory, please contact castelc@hss.edu to have an eCAP account created.

6.0 Other Study Staff/Collaborators:

FirstName	LastName	Organization	Email	Role
Rajshree	Hillstrom	Anglia Ruskin University	Rajshree.Hillstrom@Anglia.ac.uk	co-investigator
Oliver	Morgan	Anglia Ruskin University	Oliver.Morgan@Anglia.ac.uk	co-investigator

7.0 Type of Application:

- (●) **Clinical Research Proposal**
- ( ) Expedited Retrospective Chart Review
- ( ) Request for Exemption
- ( ) New Registry
- ( ) Existing Approved Registry

Please click *here* to preview Exempt Categories.

Click *here* to preview Study Designs.

8.0 Select appropriate funding sources for this study:
Name
Foundation

Name Funding Sources:
British Orthopaedic Foot and Ankle Society (BOFAS)
Chelmsford Medical Education Research Trust (CMERT)

Note: If the funding source of the study is 'Industry Funded Support', Clinical Research Administration (CRA) will be notified.

If your study requires CRA review, please upload applicable documents, including sponsor protocol, drug brochure, etc :
Name Version
There are no items to display

Help

ID: 2018-0754

Help

CRP Information

1.0 **The proposal should be submitted to the appropriate Clinical Review Panel (CRP) for scientific review. If you are unsure of which Clinical Review Panel to select, please contact Barbara Bosco at 212.606.1914**

Name
Rehabilitation

Help

ID: 2018-0754

Help

Regulatory Status of Drugs and Devices

1.0 **The regulatory status of the drugs or devices in this research proposal is:**
Name
Does not apply to this study

Help

ID: 2018-0754

Help

Pharmacy Involvement

1.0 Is this an inpatient study?
○ Yes ◉ **No**

2.0 * Will this study have Investigational Drug Service involvement? (Pharmacy will be purchasing/dispensing any medications being used and/or study requires placebo and patient randomization)
○ Yes ◉ **No**

3.0

If the answer to either question is yes, please explain briefly below AND contact Mylinh Duong at 646.797.8410 (duongm@hss.edu) or Nicole Oliva at 646.797.8324 (OlivaN@hss.edu).

Help

ID: 2018-0754

Help

Study Locations

1.0 Select the Research Facilities where this study will be conducted:

Facility
HSS

1.1 If Other, please specify:

2.0 * Is this a multi-Center study?

No

ID: 2018-0754

This section will be reviewed by the appropriate Clinical Review Panel. Each of the headings in this section must be addressed.

Help

Specific Aims or Research Questions

1.0 What is the condition or intervention to be studied?

Please click Here for example.

We are studying the reliability of measuring (1) superior translation (mobility) and (2) position of the 1st ray, using a new **1st Ray Mobility Jig**. The 1st ray mobility jig is a measurement device that quantifies the global motion of the 1st ray although the vast majority of the motion is expected to occur at the 1st metatarsocuneiform joint. The 1st ray mobility jig is designed to make these measurements while seated (partial weight-bearing) and standing (weight-bearing). In addition, we will be studying the reliability of measuring

1st ray mobility using a hand-held non-weight-bearing device (humanlocomotion.org) while in the prone position.

2.0 What is/are the research question(s)/specific aim(s)? Pose very specific questions that can be addressed within the proposed design of the study. Prioritize them in order of importance.

1. Estimate the ICCs for the **pooled** intra and inter-rater reliability of the new **1st Ray Mobility Jig** for: (1) healthy individuals with rectus feet, (2) healthy individuals with planus feet, and (3) individuals with physician-diagnosed metatarsus primus elevatus.

2. Estimate the ICCs for the intra and inter-rater reliability of the new **1st Ray Mobility Jig** for **each of the following groups**: (1) healthy individuals with rectus feet, (2) healthy individuals with planus feet, and (3) individuals with physician-diagnosed metatarsus primus elevatus.

Note: these specific aims **will** be conducted for both seated and standing conditions.

The aforementioned pooled and individual group reliability estimates will also be performed for a hand-held **FRMD**

3.0 What is/are the hypothesis(es)?

Task 1: First ray mobility in *non-weight-bearing* (prone) subjects with rectus, planus, and metatarsus primus elevatus foot structures **will** exhibit remove-replace reliability (ICC(2,1)>0.7) within and between raters using an existing hand-held **FRMD** (humanlocomotion.org).

Task 2: First ray mobility in *partial weight-bearing* (seated) subjects with rectus, planus, and metatarsus primus elevatus foot structures will exhibit test-retest and remove-replace reliability (ICC(2,1)>0.7) within and between raters as measured by the new **1st Ray Mobility Jig**.

Task 3: First ray mobility in *weight-bearing* (standing) subjects with rectus, planus, and metatarsus primus elevatus foot structures will exhibit test-retest and remove-replace reliability (ICC(2,1)>0.7) within and between raters as measured by the new **1st Ray Mobility Jig**.

4.0 Identify and <u>define</u> the primary outcome and when the outcome will be measured. If measuring change in post-operative function is the most important, that will be your primary outcome.

The primary outcome was defined as the reliability (ICC) for measuring first ray superior translation for non-weight-bearing (prone)*, partial weight-bearing (seated)* and weight-bearing (standing)* conditions in response to a 50-N vertically applied load. Note that first ray mobility is a global measure of superior translation which may occur predominantly in the 1st metatarsal-cuneiform joint.

*while the subject's foot is either in subtalar joint neutral or resting calcaneal stance position.

Note: maximum values recorded will be expressed in millimetres (mm).

5.0 Identify and define the secondary outcome(s) and when they will be measured (list additional goals one at a time with their corresponding outcomes).

The secondary outcome was defined as the reliability (ICC) for measuring first ray superior position in partial weight-bearing (seated) and weight-bearing (standing) conditions.

Note: the maximum value for 1st ray position, in response to a 5-N vertically oriented preload, will be recorded and expressed in millimeters (mm).

Help

ID: 2018-0754

Help

BACKGROUND - Be sure to answer each question individually

1.0 Explain why these research questions are being asked:

Comparisons of foot type showed a lower plantar pressure magnitude beneath the first metatarsal head and a higher plantar pressure magnitude beneath the hallux in planus versus rectus feet (Hillstrom et al., 2013). One plausible explanation is that the 1st ray of planus individuals has greater superior translation (hypermobility) than rectus feet. Such pressure distributions indicate an interaction between superior translation of the metatarsal and hallucial dorsiflexion in individuals with pes planus. Many authors have independently theorized that first ray hypermobility may be present in asymptomatic individuals with planus feet, supporting the finding of a hypermobile load transfer phenomenon associated with foot structure. (Cooper et al., 2009; King & Toolan, 2004; Doty et al., 2014; Rao & Bell, 2013). The biomechanical influence of the flexor muscle-tendon systems and plantar fascia are shown to be fundamental in, both, the passive laxity (hypermobility) and a flexion contracture of the first ray (Kirane, 2008). It is also likely that, over time, an extensive contracture of the 1st ray develops, causing MPE and further increasing joint reaction forces within the 1st MTP joint, which is associated with 1st MTP joint OA (Horton et al., 1994; Bouaicha et al., 2010; Cheung et al., 2018). However, without a reliable standardized method of measuring 1st ray mobility and position, it will be difficult to investigate the pathomechanics of these structures.

To address this need, the investigational team designed a new jig to measure 1st ray mobility and position in partial weight-bearing and weight-bearing conditions (Figure 1a, 1b, and 1c). The heel is seated in an articulating cup, while the medial aspect of the 1st metatarsal head is seated within an anterior delve of the 1st MTP joint mobility jig (Figure 1a). The 2nd metatarsal head is then immobilized by lowering a clamp placed superiorly upon the 2nd MTP joint. A linear actuator will apply (1) a 5-N pre-load to measure 1st ray position from the inferior aspect of the 1st metatarsal head and (2) a 50-N load (Glasoe (2002)) will be applied to measure 1st ray mobility from the superior aspect of the 1st metatarsal head, using an etched graticule. Finally, a hand-held FRMD will be used to measure first ray mobility in non-weight-bearing (Figure 1d).

2.0 What is the background of the topic that you believe is important for the reviewer to know in considering this protocol, including prior studies by this research team. Describe strengths and deficiencies of prior studies; explain how this study fits in. Include references.

Over time, repetitive jamming of the proximal phalanx base into the metatarsal head during sagittal plane motion (*1st ray hypermobility followed by MPE)* may cause excessive joint force and stress, damaging the tissues within the diarthrodial joint (e.g. cartilage and subchondral bone). However, investigating the role of 1st ray hypermobility and MPE in OA pathogenesis is hindered by the absence of an objective standardized measurement device for quantifying mobility and position in the sagittal plane. Although MPE is typically estimated with a weight-bearing X-ray ((Horton, 1999), (Bouaicha, 2010), (Cheung, 2018)) to assess the difference in vertical position between the 1st and 2nd metatarsal heads, there is currently no jig for making this measurement directly. In the absence of such a jig, longitudinal assessments require repeated X-rays which add exposure to ionizing radiation and cost.

Qualitatively, clinicians can manually estimate the amount of 1st ray mobility (Voellmicke and Deland, 2002) or use the Coleman block test (Faber et al, 2001). Glasoe et al. (Glasoe et al, 2002) developed a jig to assess 1st ray mobility and found substantial differences between experienced and inexperienced clinicians using the clinical method. Their jig was reliable but overly complicated and bulky so it has limited use in a clinical setting. Previously Cavanagh et al. (Cavanagh et al, 1986) also developed a 1st ray mobility jig which had electronic controls. This design was prone to include 'fat pad' compression within the results which could yield an overestimation of the actual mobility. Finally, Klaue et al. (Klaue et al, 1994) developed a completely mechanical device, but was devoid of a standardized applied force which could potentially add variability to the results. To date, no one has developed a jig to measure position. The new 1st ray mobility and position jig (Figures 1a, 1b, and 1c) is designed to address these previous shortcomings in a relatively small form factor and, hence, could be used by clinicians as well as researchers.

3.0 Identify specific gaps in current knowledge that this study is intended to fill.

The following gaps in knowledge will be addressed by this study: (1) intra and inter rater reliability for measuring 1st ray mobility in **non-weight-bearing** with a hand held FRMD, (2) intra and inter rater reliability for measuring 1st ray mobility and position in **partial weight bearing** with the new 1st ray mobility device, (3) intra and inter rater reliability for measuring 1st ray mobility and position in **weight bearing** with the new 1st ray mobility device.

4.0 How will answering these questions change clinical practice, change concepts about the topic or confirm the work of other investigators?

Establishing a simple means of accurately measuring 1st ray mobility and position, that is accessible to physicians, physical therapists, podiatric physicians, and biomechanists will permit assessment of the longitudinal process associated with 1st MTP joint OA, hence, improving the precision of clinical

2.0 What is the background of the topic that you believe is important for the reviewer to know in considering this protocol, including prior studies by this research team. Describe strengths and deficiencies of prior studies; explain how this study fits in. Include references.

Over time, repetitive jamming of the proximal phalanx base into the metatarsal head during sagittal plane motion (*1st ray hypermobility followed by MPE)* may cause excessive joint force and stress, damaging the tissues within the diarthrodial joint (e.g. cartilage and subchondral bone). However, investigating the role of 1st ray hypermobility and MPE in OA pathogenesis is hindered by the absence of an objective standardized measurement device for quantifying mobility and position in the sagittal plane. Although MPE is typically estimated with a weight-bearing X-ray ((Horton, 1999), (Bouaicha, 2010), (Cheung, 2018)) to assess the difference in vertical position between the 1st and 2nd metatarsal heads, there is currently no jig for making this measurement directly. In the absence of such a jig, longitudinal assessments require repeated X-rays which add exposure to ionizing radiation and cost.

Qualitatively, clinicians can manually estimate the amount of 1st ray mobility (Voellmicke and Deland, 2002) or use the Coleman block test (Faber et al, 2001). Glasoe et al. (Glasoe et al, 2002) developed a jig to assess 1st ray mobility and found substantial differences between experienced and inexperienced clinicians using the clinical method. Their jig was reliable but overly complicated and bulky so it has limited use in a clinical setting. Previously Cavanagh et al. (Cavanagh et al, 1986) also developed a 1st ray mobility jig which had electronic controls. This design was prone to include 'fat pad' compression within the results which could yield an overestimation of the actual mobility. Finally, Klaue et al. (Klaue et al, 1994) developed a completely mechanical device, but was devoid of a standardized applied force which could potentially add variability to the results. To date, no one has developed a jig to measure position. The new 1st ray mobility and position jig (Figures 1a, 1b, and 1c) is designed to address these previous shortcomings in a relatively small form factor and, hence, could be used by clinicians as well as researchers.

3.0 Identify specific gaps in current knowledge that this study is intended to fill.

The following gaps in knowledge will be addressed by this study: (1) intra and inter rater reliability for measuring 1st ray mobility in **non-weight-bearing** with a hand held FRMD, (2) intra and inter rater reliability for measuring 1st ray mobility and position in **partial weight bearing** with the new 1st ray mobility device, (3) intra and inter rater reliability for measuring 1st ray mobility and position in **weight bearing** with the new 1st ray mobility device.

4.0 How will answering these questions change clinical practice, change concepts about the topic or confirm the work of other investigators?

Establishing a simple means of accurately measuring 1st ray mobility and position, that is accessible to physicians, physical therapists, podiatric physicians, and biomechanists will permit assessment of the longitudinal process associated with 1st MTP joint OA, hence, improving the precision of clinical

2.2 If Randomized Controlled Clinical Trial is selected, please choose one of the following:
Name
There are no items to display

If other, please list name or indicate N/A below:

ID: 2018-0754

Help

Recruitment

1.0 **Check all that apply to describe your study population:**

Population
Patients
Normal Healthy Volunteers

Vulnerable Populations
There are no items to display

1.1 If Other, please specify:

Note that the rectus *(n=10 subjects, 20 feet)* and planus *(n=10 subjects, 20 feet)* groups will be recruited from normal healthy volunteers. The MPE cohort is based upon a physician diagnosis of an elevated 1st ray *(n=10 subjects, presenting unilaterally, n=10 feet)*. Physicians are trying to determine when the dorsal head of the 1st MTP joint is more than 4 mm elevated with respect to the 2nd MTP joint - this is typically estimated either with the aid of an X-ray or by eye.

2.0 **Inclusion Criteria:** *list characteristics that potential subjects and controls need to have. Use a bullet format, if applicable.*

Planus and Rectus Subjects

- Healthy adults over the age of 21 years old
- No current foot and ankle pathology,
- No pain within the lower extremity that could affect gait
- Male or female
- Planus: $AHI_{standing} < 0.365$
- Rectus: $0.365 \leq AHI_{standing} \leq 0.39$

MPE Subjects

- Adults over the age of 21 years old
- The 1st ray exhibits an >4mm elevated position (contracture) under the physician's exam

- May exhibit signs of hallux limitus or rigidus including pain or discomfort,
- Male or female

3.0 **Exclusion Criteria:** *list characteristics that would cause you to exclude potential subjects and controls.*

Justify any age, ethnicity, language, or gender-based exclusion criteria. *Use a bullet format, if applicable.*

- Individuals without the capacity to consent and/or understand procedures of the study
- Hallux valgus or hallux rigidus (in planus and rectus subjects)
- Rheumatoid arthritis, osteoporosis, osteoarthritis or any other degenerative disease involving the lower limb (in planus and rectus subjects) – MPE may have signs of OA.
- Participants with arthroplasty (excision, hemiarthroplasty and total joint replacement), capsular interposition, osteochondral transplantation, joint distraction, osteotomy, arthrodesis, or any other surgical intervention will be excluded.
- Current pathology within the foot and ankle (in planus and rectus subjects)
- Limb length discrepancy greater than 1 cm
- Inability to walk without assistive devices or any pathology that impacts one's ability to walk independently.

4.0 **Age Range:**
>21

5.0 **Describe how you will identify and recruit potential subjects for participation in the study.**

Potential subjects will be recruited from any willing participant that meets the inclusion/exclusion criteria of the study. The goal is to recruit approximately 50% male and 50% female participants in each group. Foot and ankle surgeons, Drs. Scott Ellis, MD, and Jonathan Deland, MD will assist with test subject recruitment, especially the MPE group.

The test subjects will be consented by the project study coordinator, co-Investigators, or PI. A flyer inviting participation from perspective test subjects will also be prepared. After signing informed consent, each subject will have their AHI measured to determine their static foot structure.

AHI will be measured by placing the subject's feet within a pair of custom made anodized aluminum jigs, with their heels seated within each heel cup (Figure 2a). The most anterior adjustable bar will be set to maximum foot length (FL). A small adjustable cup will be positioned at the 1st MTP joint to denote truncated foot length (TFL). Finally, a vertical bar, which is positioned at one half of FL, will be lowered upon the dorsal aspect of the foot to measure arch height (AH). Linear graticules, scaled in cm, are laminated to the jig for visual measurement of

each parameter. Arch height index (AHI) is defined as the dorsal arch height (AH) at one-half of FL normalized by the TFL (Hillstrom et al, 2013) while sitting ($AH_{sitting}$) and standing ($AH_{standing}$). AHI sitting and standing (Figure 2b) are calculated according to the following formulae:

$AHI_{sitting} = ((AH_{sitting})/TFL) \times 100$

$AHI_{standing} = ((AH_{standing})/TFL) \times 100$

AHI can objectively distinguish planus, rectus, and cavus foot types in asymptomatic healthy individuals, according to thresholds previously established (Hillstrom et al, 2013). AHI will be measured immediately after consenting to determine whether a subject is in the asymptomatic rectus or planus groups. Note: that asymptomatic cavus individuals will not be included in this study because this foot type is rarely involved in 1st ray pathologies.

MPE subjects are considered pathologic and will be diagnosed by their physicians. The standard of care for physician based diagnosis of MPE is by lateral weight-bearing radiographs. Each study physician will refer patients who have recently been diagnosed with MPE into this study. Note that MPE typically presents unilaterally.

We will attempt to have even numbers of males and females and will halt recruitment of a gender when that quota is achieved.

6.0 * **Please select enrollment type from following drop down list:**
Over Course of Study

Help

ID: 2018-0754

Help

Target Enrollment

1.0 * **What is the maximum number of subject you plan to enroll in this study at HSS?(Please enter a number)**
30

2.0 **If this is a multi-center study, indicate the projected total subject accrual across all sites.**

Help

ID: 2018-0754

Help

Patients

1.0 **Please check the box(es) below that best reflect how patients will be identifed and recruited for participation.**

How subjects will be identified

- [x] **Potential subjects will be identified after a review of medical records of patients under the care of one or more of the study investigators**
- [ ] Medical records and/or other Institution sources (databases,registries,billing records,pathology reports,admission logs) will be reviewed to identify potential participants. May involve access of records by individuals not involved in the patient's care.
- [x] **Potential subjects will be identified by their treating physicians and referred to the researchers. Patients' private and identifiable information will not be shared prior to receiving permission from the patient to do so.**
- [ ] Potential subjects will be identified from a registry of individuals interested in research opportunities.
- [ ] Subjects will roll-over from another research study.
- [x] **Potential subjects will self-refer in response to advertisements.**

ID: 2018-0754

Help

Normal Healthy Volunteers

1.0 If this research involves a medical procedure(s), provide a justification for involving normal volunteers in research.

n/a

ID: 2018-0754

Help

Interventions and Observations

1.0 Be specific and describe the Interventions or Observations that will be part of this research project. Include a detailed description of the treatment arms, if applicable.

n/a

2.0 Will you be collecting human fluid or tissue? ○ Yes ◉ **No**

If yes, what will you be collecting? ☐ **Fluid** ☐ **Tissue**
(Intraoperative and/or outpatient collection)

Help

ID: 2018-0754

Help

Data Collection

1.0 Indicate what data will be collected.

We will be measuring 1st ray mobility and position in standing and seated postures (Figure 3) in the Leon Root, MD Motion Analysis Laboratory (LRMALab). Two independent raters (one experienced physical therapist (RT) and one biomedical engineer (HJH)) will each perform **three measurements** (baseline, test-retest, and remove-replace), permitting computation of intra-rater and inter-rater reliability for the test-retest (i.e. successive trials while in the test jig) and remove-replace (i.e. successive trials before and after having the foot removed and replaced into the test jig). Note: the measurements will be performed in two foot positions: subtalar joint neutral and resting calcaneal stance position. The experienced physical therapist represents who is likely to be making such measurements in the clinic while the biomedical engineer may be more likely to make the measurements in a research protocol. Non weight bearing will refer to measurements made in the prone position. Partial weight bearing refers to the seated posture. Weight bearing refers to standing with arms to both sides looking straight ahead in ~50% BW on each limb. Each rater will read their own results for each trial. The order of rater measurements will be randomized by the study biostatistician (JN). It will not be possible to blind the raters to foot type. Pain should be of limited effect: the healthy rectus and planus subjects won't have any while the MPE subjects may have some but the testing should not invoke any more pain than standing. The raters will provide one minute of rest between mobility and position measurements. Given the viscoelastic nature of soft tissues it is possible that stretching during each trial may affect successive trials but this phenomenon is difficult to measure and may differ among subjects. By having a standardized time (one minute) between the trials we will, at least, be controlling the recent strain history of the tissues. The rectus and planus subjects data will be acquired bilaterally. The MPE subjects will be acquired unilaterally. Analyses will be performed by limb. An outcome table illustrates (Figure 4) the intra and inter rater reliability ICC calculations that will be acquired for each condition.

Measurements of 1st ray mobility will be taken from the dorsal aspect of the metatarsal head. The subject will be seated on an adjustable chair with their hip and knee at 90 degrees. Each foot will be positioned within the mobility jig which, essentially, grounds the 2nd ray while permitting vertical translation (superior) of the 1st ray with respect to the 2nd. Two foot positions will be assessed: (1) subtalar joint neutral (where the talar head begins to bulge medially or laterally when the foot is pronated or supinated) and (2) resting calcaneal stance position (natural weight-bearing hindfoot alignment). Each tester (Rater 1:Howard J Hillstrom, PhD and Rater 2: Robert Turner, PT, DPT) will view the graticule with their aiming eye in a perpendicular orientation to avoid parallax error and record the superior displacement in millimeters. All measurements will be replicated while seated and standing. The primary and secondary outcomes will be measured in each of the aforementioned conditions. First ray mobility will also be assessed in non-weight-bearing using a hand-held device while the subjects are prone.

Primary outcomes:

- ICCs for 1st ray superior translation in non-weight-bearing, partial weight-bearing* and weight-bearing* conditions

*while the subject's foot is in subtalar joint neutral and natural-alignment (resting calcaneal stance position).

Secondary outcomes:

- ICCs for 1st ray superior position in partial and full weight-bearing conditions

*while the subject's foot is in subtalar joint neutral and natural-alignment (resting calcaneal stance position).

2.0 Who will collect the data:

Howard	Hillstrom, Ph.D.	Director of Motion Analysis Lab
Robert	Turner, DPT OCS MS OM	Rehabilitation

3.0 When the data will be collected? Include timing of visits(either SOC or specifically for the study).
During regularly scheduled visits (~30 min - 1hr)

4.0 From what source:
Patient

No Private Office Charts Please specify which private office:

No Registries Please specify which registry:

☐ Other Please specify:

Help

ID: 2018-0754

Help

General Methods and Procedures

1.0 * **Are controls included in the study?** No

1.1 If yes, describe how they will be matched with the study subjects; state whether the controls will have identical data recorded, or describe any differences compared to the intervention subjects.

This is a reliability study so no controls are required. First ray mobility and position will be measured on all feet (planus, rectus, MPE). Healthy rectus and planus individuals will be recruited with the aid of a recruitment flyer (Figure 5). MPE subjects will be referred by physician diagnosis only.

2.0 * **Are all tests Standard of care?** No

If not, identify which tests are not standard of care. What source of funds will be used to pay for them (text box below):

This is a research protocol based on a new prototype device designed to measure 1st ray mobility and position. First ray mobility and position measurements are not standard of care.

Development and prototyping of the device is a collaboration between Anglia Ruskin University and the Hospital for Special Surgery. The new test jig is paid for by a British Orthopaedic Foot and Ankle Society (BOFAS) grant. The doctoral student's time for data collection and analysis is paid for by a Chelmsford Medical Education and Research Trust (CMERT) grant.

A data collection sheet has been added (Figure 3) as well as a ICC outcome sheet (Figure 4).

3.0 * **Will surveys/questionnaires be used?** No

4.0 * **Does the study involve randomization?** Yes

5.0 * **Does your study included Placebo or No-Treatment Arm?** No

6.0 * **Does your study included Washout of Previous Medication?** No

7.0 **Data collection sheet should be created for the study and uploaded:**

Name	Version
Figure 3 - Data Collection Sheet	0.01
Figure 4 - ICC Outcomes	0.01
Figure 5 - Recruitment Flyer	0.01

Help

ID: 2018-0754

Help

Randomization

1.0 **Please state who will do the Randomization:**

Randomization will be performed by the study statistician (JN). The order of rater testing will be randomized.

2.0 **Please state when the Randomization will be done:**

The randomization will be performed prior to testing the 1st subject.

3.0 **Please state how the Randomization will be performed:**

The statistician will use a random number generator within SAS.

4.0 Please state who will insure that the Randomization is carried out and if anyone will be blinded to the Randomization group:

The biostatistician will insure that the randomization is carried out. The raters will be informed of the order of testing immediately prior to testing.

Help

ID: 2018-0754

Help

Sample Size and Data Analysis

If you are uncertain about how to calculate your sample size and determine appropriate data analysis, please contact the Epidemiology and Biostatistics Core at biostats@hss.edu for assistance in completing this section.

1.0 Is this is a case series based only on the patients available using descriptive statistics in lieu of a sample size calculation?

* Yes

Help

ID: 2018-0754

Help

Statistical Analysis

1.0 **Descriptive Statistics** are summary statistics that describe your study population rather than testing hypotheses. Examples include means, medians, standard deviations, frequency counts, and percentages. If you intend to test a hypothesis (calculate a p-value) then you need a sample size calculation in order to determine your statistical power.

Two older and bulkier, but similar devices for assessing 1st ray mobility, were able to establish reliability with similar sample sizes to the proposed study of the new 1st Ray Mobility Jig (Jones et al (2005) - n=16 subjects; ICC = 0.9; Glasoe et al (2000) - n=20 subjects; ICC = 0.98)). In this study, we will have n=20 rectus feet, n=20 planus feet, and n=10 MPE feet, which will provide a pooled group of n=50 feet.

Using SPSS v22, we will compute intra and inter-class correlation coefficients (ICC(2,1)) for two raters for test-retest and remove-replace reliability. All data will

be pooled for the reliability assessments, as well as evaluated by the individual foot structures. In specific, the following three analysis tasks will be performed:

Task 1: Remove-replace reliability (ICC(2,1) and 95% confidence intervals) within and between raters for first ray mobility in *non-weight-bearing* (prone) subjects with rectus, planus, and metatarsus primus elevatus foot structures will be summarized (hand held device).

Task 2: Test-retest and remove-replace reliability (ICC(2,1) and 95% confidence intervals) within and between raters for first ray mobility and position in *partial weight-bearing* (seated) subjects with rectus, planus, and metatarsus primus elevatus foot structures will be summarized. (new 1st Ray Mobility Jig)

Task 3: Test-retest and remove-replace reliability (ICC(2,1) and 95% confidence intervals) within and between raters for first ray mobility and position in *weight-bearing* (standing) subjects with rectus, planus, and metatarsus primus elevatus foot structures will be summarized (new 1st Ray Mobility Jig).

Effect sizes will be computed for distinguishing the three groups (rectus, planus, and MPE) for the two parameters of interest: 1st ray mobility and 1st ray position to be used in future research.

Help

ID: 2018-0754

Help

Consent Information

1.0 Describe how, when, and where the consent process will be initiated:

The study will be explained at the beginning of the visit by the study coordinator. Once a test subject has asked all of their questions and has agreed to participate, they will sign informed consent and be enrolled into the study. All data collection will proceed immediately and be completed with 30 minutes to 1 hour.

2.0 Who will obtain informed consent from subjects for this research?

First Name	Middle Name	Last Name	Title
Ibadete		Thaqi	

Help

ID: 2018-0754

You have completed the Clinical Research Proposal for this study. Click FINISH button to save and exit the proposal.

When you are ready to submit your proposal for pre-review, hit the SUBMIT STUDY link on your study homepage. The appropriate Clinical Review Panel (CRP) will receive and review your proposal.

B.3 Arduino Code: Recent Strain History

```
int EnablePin1 = 8; // pins for megamoto
int PWMPinA1 = 11; // selects jumper signal for PWMPinA (retract stroke)
int PWMPinB1 = 3;  // selects jumper signal for PWMPinB (extend stroke)
int LoadReading;
int MaxLoad1 = 250;
int A=1;
int strain = 10;
const int LoadPin = A1;

void setup() {

  Serial.begin(115200);
  pinMode(EnablePin1,OUTPUT); // enables to megamoto board
  pinMode(PWMPinA1,OUTPUT);
  pinMode(PWMPinB1,OUTPUT);
  pinMode(LoadPin,INPUT);

}

void loop() {

 Serial.println("Recent Strain History");
  while (A<=strain) {
   Serial.print("Recent Strain Excitation #: ");
   Serial.println(A);

   digitalWrite(EnablePin1,HIGH); // enable the board
   analogWrite(PWMPinB1,0); //Set pinB to 0, when speed is written to pinA the motor will retract
   analogWrite(PWMPinA1,102);

   LoadReading = analogRead(LoadPin);

   if (LoadReading >= MaxLoad1) {
    digitalWrite(EnablePin1,LOW); // enable the board
    analogWrite(PWMPinB1,0); //Set pinB to 0, when speed is written to pinA the motor will retract
    analogWrite(PWMPinA1,0);
    delay(100);
    digitalWrite(EnablePin1,HIGH); // enable the board
    analogWrite(PWMPinB1,102); //Set pinB to 0, when speed is written to pinA the motor will retract
    analogWrite(PWMPinA1,0);
    delay(2000);
    digitalWrite(EnablePin1,LOW); // enable the board
    analogWrite(PWMPinB1,0); //Set pinB to 0, when speed is written to pinA the motor will retract
    analogWrite(PWMPinA1,0);
    A=A+1;
  }
 }
}
```

B.4 Arduino Code: First Ray Elevation and Mobility

```
int EnablePin1 = 8; // pins for megamoto
int PWMPinA1 = 11; // selects jumper signal for PWMPinA (retract stroke)
int PWMPinB1 = 3;  // selects jumper signal for PWMPinB (extend stroke)
int LoadReading;
int MaxLoad2 = 125;
int MaxLoad3 = 314;
int B=1;
int pos = 1;
int C=1;
int mob =1;
const int LoadPin = A1;

void setup() {

  Serial.begin(115200);
  pinMode(EnablePin1,OUTPUT); // enables to megamoto board
  pinMode(PWMPinA1,OUTPUT);
  pinMode(PWMPinB1,OUTPUT);
  pinMode(LoadPin,INPUT);

}

void loop() {

  Serial.println("Position");
   while (B<=pos) {
     Serial.print("Position Excitation #: ");
     Serial.println(B);

    digitalWrite(EnablePin1,HIGH); // enable the board
    analogWrite(PWMPinB1,0); //Set pinB to 0, when speed is written to pinA the motor will retract
    analogWrite(PWMPinA1,102);

  LoadReading = analogRead(LoadPin);
 if (LoadReading >= MaxLoad2) {
    digitalWrite(EnablePin1,LOW); // enable the board
    analogWrite(PWMPinB1,0); //Set pinB to 0, when speed is written to pinA the motor will retract
    analogWrite(PWMPinA1,0);
    delay(4000);
    digitalWrite(EnablePin1,HIGH); // enable the board
    analogWrite(PWMPinB1,102); //Set pinB to 0, when speed is written to pinA the motor will retract
    analogWrite(PWMPinA1,0);
    delay(1500);
    digitalWrite(EnablePin1,LOW); // enable the board
    analogWrite(PWMPinB1,0); //Set pinB to 0, when speed is written to pinA the motor will retract
    analogWrite(PWMPinA1,0);
     B=B+1;
  }
 }
{
 Serial.println("Mobility");
  while (C<=mob) {
   Serial.print("Mobility Excitation #: ");
   Serial.println(C);
   digitalWrite(EnablePin1,HIGH); // enable the board
   analogWrite(PWMPinB1,0); //Set pinB to 0, when speed is written to pinA the motor will retract
   analogWrite(PWMPinA1,102);
```

```
  LoadReading = analogRead(LoadPin);
 if (LoadReading >= MaxLoad3) {
   digitalWrite(EnablePin1,LOW); // enable the board
   analogWrite(PWMPinB1,0); //Set pinB to 0, when speed is written to pinA the motor will retract
   analogWrite(PWMPinA1,0);
   delay(4000);
   digitalWrite(EnablePin1,HIGH); // enable the board
   analogWrite(PWMPinB1,102); //Set pinB to 0, when speed is written to pinA the motor will retract
   analogWrite(PWMPinA1,0);
   delay(1500);
   digitalWrite(EnablePin1,LOW); // enable the board
   analogWrite(PWMPinB1,0); //Set pinB to 0, when speed is written to pinA the motor will retract
   analogWrite(PWMPinA1,0);
    C=C+1;
  }
 }
}
}
```

Table B-1. Subject information.

ID	Sex	Group	Race	Ethnicity	Age (Years)	Height (cm)	Weight (kg)	BMI	Side
1	Male	Healthy	White	Non-hispanic	32	187.9	99	28.01	Bilateral
2	Female	Healthy	Asian	Non-hispanic	50	154.9	62	25.81	Bilateral
4	Male	Healthy	Asian	Non-hispanic	27	180.3	84.8	26.23	Bilateral
5	Male	Healthy	White	Non-hispanic	25	180.3	86.2	26.5	Bilateral
6	Female	Healthy	Asian	Non-hispanic	23	152.4	55.3	23.8	Bilateral
7	Male	Healthy	White	Non-hispanic	26	177.8	65.8	20.8	Bilateral
8	Male	Healthy	White	Non-hispanic	36	180.3	82.6	25.6	Bilateral
9	Male	Healthy	Asian	Non-hispanic	30	177.8	79.4	24.9	Bilateral
10	Male	Healthy	Asian	Non-hispanic	27	185.4	72.6	21.3	Bilateral
11	Male	Healthy	White	Non-hispanic	44	179.5	78.5	24.4	Bilateral
12	Male	Healthy	White	Non-hispanic	25	190	77	21.3	Bilateral
13	Female	Healthy	White	Non-hispanic	23	177	68	21.7	Bilateral
14	Male	Healthy	White	Non-hispanic	55	176	95	30.7	Bilateral
15	Female	Healthy	White	Non-hispanic	23	185	71.6	21	Bilateral
16	Male	Healthy	White	Non-hispanic	59	182.8	92.9	27.8	Bilateral
17	Female	Healthy	White	Hispanic	44	160	68	26.6	Bilateral
18	Male	Healthy	White	Non-hispanic	26	182.9	77.1	23	Bilateral
19	Male	Healthy	Asian	Non-hispanic	27	175.3	77	25	Bilateral
21	Female	Healthy	White	Non-hispanic	23	165	58.8	21.5	Bilateral
22	Male	Patient	White	Non-hispanic	55	177	70	22.3	R affected
23	Female	Patient	White	Non-hispanic	59	151.1	74.8	32.8	L affected
24	Female	Patient	White	Non-hispanic	49	153.7	66.7	28.1	R affected
26	Female	Healthy	White	Non-hispanic	22	172.7	90.7	30.3	Bilateral
27	Male	Healthy	White	Non-hispanic	57	185.4	97.5	28.5	Bilateral
31	Female	Healthy	White	Non-hispanic	32	167.6	53.1	18.8	Bilateral

Table B-2. First ray mobility measurements with the FRMD and AHI system calculations (Rater 1).

	FRMD						AHI System							
	Hand held (right) [mm]			Hand held (left) [mm]			Sitting				Standing			
	STJN (Trial)													
ID	1	2	3	1	2	3	TFL (right) [cm]	TFL (left) [cm]	Metatarsal height (right) [mm]	Metatarsal height (left) [mm]	TFL (right) [cm]	TFL (left) [cm]	Metatarsal height (right) [mm]	Metatarsal height (left) [mm]
1	3	4	4	4	5	5	20.9	21	41	37	21.7	21.1	36	37
2	5	4	5	5	5	5	16.3	16.1	36	36	16.7	16.6	35	36
4	6	5	7	10	11	10	19.3	19.5	43	40	20.2	19.8	36	36
5	7	8	7	8	9	8	20.3	20.4	44	41	20.5	20.3	41	40
6	9	10	10	10	10	10	16.4	16.5	34	31	16.6	16.6	33	33
7	3	3	4	5	4.5	4	18.1	18	36	37	18.8	19.5	36	35
8	4	4.5	4	3	3	3	20.5	20.4	43	41	21.2	21	40	40
9	5	6	5	5	5	5	19.4	19.3	39	37	19.4	19.3	39	43
10	4	5	4	6	7	7	19.2	19.1	35	33	19.1	19	36	35
12	6	7	6	5	5.5	6	20.2	20.4	40	38	20.4	20.6	40	38
13	5	5	4	5	5	5.5	18	18.4	36	35	17.9	17.7	36	37
14	5	4	5	4	4	5	18.3	18.4	40	39	18.6	19.6	37	34.5
15	6	7	7	6.5	7	7.5	19.3	18.9	37	36	18.7	18.7	40	34
16	6	6	6.5	5	5	4.5	18.6	18.6	39	37	19.1	19	39	37
18	5	5.5	5	5	5	5	18.8	18.6	37	39	19.5	20	38	36
21	5	5	5.5	7	5	5.5	17.5	17.9	39	37	17.6	18	37.5	37
22	9.5	10	11	9	10	10	20.8	19.8	39	39.8	20.5	20.8	4.23	38.7
23	7	7	6	7	8	8.5	16.2	17	38	39	16.2	17	36.6	39
24	5	5	5.5	5	4	5	16.1	16.6	38.5	34	16.4	16.6	37.5	32.8
26	8	10	11	9	8	8	18	18	33.5	38.7	18.1	18.4	36	36
27	5	4	5	5	5	5	19.6	19.75	43.3	44.3	19.6	19.9	42.6	43.6
31	6	5.5	6	5	5	5.5	16.7	16.6	34	36.7	17.3	17.1	36.7	35.7

Table B-3. First ray mobility measurements with the FRMD and AHI system calculations (Rater 2).

	FRMD						AHI System							
	Hand held (right) [mm]			Hand held (left) [mm]			Sitting				Standing			
	STJN (Trial)													
ID	1	2	3	1	2	3	TFL (right) [cm]	TFL (left) [cm]	Metatarsal height (right) [mm]	Metatarsal height (left) [mm]	TFL (right) [cm]	TFL (left) [cm]	Metatarsal height (right) [mm]	Metatarsal height (left) [mm]
1	2.5	4	4	4	4	3	20.4	21	37	38	21.5	21	36	37
2	2	2	2	1	1	1.5	16.2	16.2	36	36	16.4	16.5	35	36
4	4	5	5	1.5	1.5	2	20	19.6	39	38	20.4	20.5	35	39
5	5	5	5	4.5	5	5	20	20.5	45	40	20.5	20.5	42	39
6	6	6	6	6.5	6	5	16	16.3	33	32	16.4	16.5	33	31
7	4	5	4	4	4	5	19	18.8	37	36	19.1	19.4	37	35
8	6.5	6.5	6.5	7	7	7.5	20.8	20.2	41	41	21.8	22.6	39	38
9	5	5	5.5	6	7	5.5	19.4	19.4	40	39	19.8	19.4	39	40
10	6	5	6	5	5.5	5	19.6	19.5	34	33	19.4	19.2	34	33
12	7.5	7	7.5	4	2.5	2.5	20.5	20.7	40	38	20.6	21	40	37
13	2	4	4	4	4	5	18	18	36	36	18.1	18.4	35	35
14	6	6	6	5	4.5	5	19.6	18.8	34	37	20.3	19.3	33	36
15	6	5.5	5.5	4	4	3.5	18.8	19.1	39	35.5	20.2	19.9	36	35.5
16	5	5	5	4	4	5	19.3	18.9	38	37	19.7	19.4	36	36
18	6	5.5	6	5.5	5	5	19.3	19.1	35	36	19.7	19.1	36	37
21	6	6	6	6	5	5	17.5	17.9	37.5	35.6	17.6	18	37.6	40
22	5	5	5	6	6	6	20.8	19.8	41.6	39.6	20.8	20.5	41	37.6
23	6.5	7	7	3	5	4	16.2	17	38.6	40	16.2	17	38.6	39
24	4	5	5	3	4	4	16.1	16.6	38.2	34.3	16.4	16.6	36.7	34
26	5.5	6.5	6.5	4.5	5	5	18	18	37.3	37	18.1	18.4	39	37
27	5	5	5	5	5.5	5	19.6	19.75	44	44.8	19.6	19.9	42	43.7
31	3.5	4	4.5	3	3	3.5	16.7	16.6	34	36.7	17.3	17.1	33.7	34

Table B-4. First ray mobility measurements (raw) with MAP1st in STJN and RCSP (Rater 1).

	First Ray Mobility (Raw)																							
	MAP1st seated (right) [mm]			MAP1st seated (left) [mm]			MAP1st seated (right) [mm]			MAP1st seated (left) [mm]			MAP1st standing (right) [mm]			MAP1st standing (left) [mm]			MAP1st standing (right) [mm]			MAP1st standing (left) [mm]		
	STJN						RCSP						STJN						RCSP					
ID	1	2	3	1	2	3	1	2	3	1	2	3	1	2	3	1	2	3	1	2	3	1	2	3
1	9	9	10	16	16	14	7	7	7	9	9	11	4	5	2	10	9	10	2	2	2	1	0	1
2	10	10	10	8	9	8	7	8	7	6	7	5	8	9	6	5	4	4	9	8	9	5	5	5
4	5	5	5	10	10	10	4	4	1	6	6	5	4	3	6	8	10	10	2	2	2	2	2	2
5	8	8	6	9	10	9	5	5	3	7	7	7	7	7	7	7	7	7	5	5	4	3	4	3
6	15	15	10	15	15	15	11	11	12	12	13	12	15	15	14	10	11	6	9	9	12	7	6	6
7	14	14	13	9	10	11	6	7	6	8	8	7	7	7	7	10	10	9	9	9	7	9	9	8
8	12	12	8	9	9	10	6	6	6	10	10	12	9	9	6	9	9	7	5	4	4	5	4	4
9	11	11	16	13	13	13	10	11	10	11	11	11	6	6	11	4	3	3	11	11	4	4	4	3
10	20	20	16	15	16	15	5	6	10	12	12	9	9	8	8	9	8	7	5	5	1	3	3	3
12	6	6	6	8	8	7	6	7	4	6	6	6	0	0	1	3	3	2	3	0	1	2	5	2
13	9	9	9	11	11	11	8	8	8	9	9	10	4	3	2	2	2	2	3	2	1	2	3	1
14	7	7	6	10	10	6	8	8	5	7	7	6	7	6	1	4.5	3.5	3.5	3	3	1	1.5	1.5	1.5
15	13	13	13	11	11	10	11	12	12	11	10	11	9	8	8	2	4	4	5	5	3	5	6	6
16	7	7	7	8	8	8	6	6	6	8	8	6	2	2	2	2	2	4	2	2	2	1	1	1
18	7	7	8	7	7	6	7	8	5	7	7	6	3	3	3	5	5	5	2	2	5	5	4	3
21	11.5	11.5	13.5	10.5	11	11	11.5	12	10	10	10	9.5	11.5	11.5	9.5	3	3	2	7.5	8.5	5.5	5	4.5	2
22	4.1	4.1	4.3	4.05	4.05	3.7	3.8	3.8	4.1	3.45	3.45	4	4	4	4.1	3.4	3.4	3.25	4.25	4.25	4.15	3.95	3.95	3.5
23	4	4	4	3.9	3.9	3.9	3.9	3.9	3.9	3.8	3.8	3.8	3.7	3.7	3.7	4	4	4	3.7	3.6	3.6	3.9	3.9	3.9
24	4.3	4.3	3.9	3.35	3.35	3.35	3.9	3.9	3.8	3.45	3.45	3.35	3.8	3.8	3.75	3.4	3.43	3.4	3.8	3.8	3.9	3.25	3.25	3.3
26	13	13.5	14.5	9.3	9.3	8.3	5.5	5.5	8	4.3	5.3	5.3	1	1.5	1	6.5	6.5	7.5	0	0	0	2	1	4
27	4.2	9.2	5.7	7.7	7.7	5.7	2.7	2.7	6.7	4.7	5.7	4.2	4.4	3.9	3.4	1.4	1.4	3.4	1.4	1.4	3.4	1.4	1.4	1.9
31	9	9	10	8.3	8.3	7.3	9	9	7	9.3	9.3	8.3	3.3	5.3	4.3	5.3	5.3	4.3	5.3	5.3	3.3	5.3	6.3	5.3

Table B-5. First ray mobility measurements (raw) with MAP1st in STJN and RCSP (Rater 2).

	First Ray Mobility (Raw)																							
	MAP1st seated (right) [mm]			MAP1st seated (left) [mm]			MAP1st seated (right) [mm]			MAP1st seated (left) [mm]			MAP1st standing (right) [mm]			MAP1st standing (left) [mm]			MAP1st standing (right) [mm]			MAP1st standing (left) [mm]		
	STJN						RCSP						STJN						RCSP					
ID	1	2	3	1	2	3	1	2	3	1	2	3	1	2	3	1	2	3	1	2	3	1	2	3
1	8	8	8	8	8	8	10	10	7	10	8	8	5	5	6	7	7	7	3	2	2	1	1	1
2	8	8	9	9	7	9	9	9	9	8	8	10	8	8	8	4	2	3	5	5	8	3	3	2
4	11	12	12	9	11	8	6	6	6	8	8	7	11	12	9	1	2	0	5	5	3	0	0	0
5	5	5	6	9	9	10	8	8	4	7	8	7	4	4	8	7	8	7	3	4	4	4	4	5
6	12	13	15	11	11	10	12	13	13	10	11	10	7	6	9	9	9	9	6	7	9	8	8	8
7	9	10	10	10	10	9	9	9	9	8	8	10	5	6	7	10	10	8	6	6	2	6	6	5
8	10	10	10	4	5	8	10	10	10	8	9	8	9	7	12	5	7	9	3	3	3	3	3	2
9	11	12	11	10	11	9	10	10	10	9	10	10	7	7	7	6	6	3	5	5	4	4	5	5
10	12	12	11	13	13	11	6	6	8	10	9	10	2	2	2	2	2	2	8	8	7	11	11	7
12	3	3	0	0	0	0	9	10	9	8	8	8	6	6	6	6	6	6	2	2	3	2	2	2
13	7	7	6	6	7	6	8	8	8	8	8	8	5	5	4	5	5	3	3	2	2	2	2	2
14	9	9	9	6	6	7	11	11	8	8	8	7	4	5	5	4	4	2	2	2	1	1	1	1
15	5	5	5	5.5	5.5	7.5	5	5	5	7.5	7.5	6	5	6	6	3.5	4.5	2.5	2	2	3	3.5	3.5	3.5
16	6	7	6	5	6	5	5	5	7	9	8	7	3	3	5	3	3	1	1	1	2	1	1	3
18	10	10	9	5	6	6	8	8	10	2	2	8	7	7	8	4	4	4	6	6	4	5	5	3
21	10.5	10.5	4.5	3.4	3.4	3.4	5.5	5.5	9.5	3.4	3.4	0.4	8.4	8.4	11.4	5	5	6	5.4	5.4	5.4	7	7	4
22	4.1	4.1	4.1	3.9	3.9	3.9	4.2	4.2	4.1	4	4	3.9	3.9	3.9	4.2	3.8	3.8	3.6	4.1	4.1	4.1	3.7	3.7	3.8
23	4	4.3	4	4.2	4.1	4.1	3.8	3.8	3.9	3.95	4	4.1	3.7	3.7	3.5	4	4	4	3.85	3.9	3.5	3.9	3.9	3.9
24	4	3.95	3.95	3.4	3.4	3.4	3.85	3.85	3.8	3.9	3.5	3.9	3.85	3.9	3.75	3.5	3.8	3.6	3.6	3.65	3.75	3.3	3.3	3.5
26	10.7	10.7	11.2	7	8	9	5.7	5.7	7.2	5	5	5	6	3	3	11	10.5	8	4	4	0	1	1	2
27	5	5	5	10.2	10.2	9.2	3.5	3.5	3	7.2	7.2	9.7	5.5	5.5	4.5	3.3	3.3	1.3	0.5	0.5	5	2.8	2.8	2.3
31	8.5	8.5	8.5	7.3	7.3	5.3	8	8.5	8.5	9.3	9.3	8.3	7.3	8.3	5.3	5	5	4	4.8	5.3	6.3	6	6	5

Table B-6. First ray mobility measurements (normalised) with MAP1st in STJN and RCSP (Rater 1).

	First Ray Mobility (Normalised)																							
	MAP1st seated (right) [mm]			MAP1st seated (left) [mm]			MAP1st seated (right) [mm]			MAP1st seated (left) [mm]			MAP1st standing (right) [mm]			MAP1st standing (left) [mm]			MAP1st standing (right) [mm]			MAP1st standing (left) [mm]		
	STJN						RCSP						STJN						RCSP					
ID	1	2	3	1	2	3	1	2	3	1	2	3	1	2	3	1	2	3	1	2	3	1	2	3
1	0.431	0.431	0.478	0.762	0.762	0.667	0.335	0.335	0.335	0.429	0.429	0.524	0.184	0.230	0.092	0.474	0.427	0.474	0.092	0.092	0.092	0.047	0.000	0.047
2	0.613	0.613	0.613	0.497	0.559	0.497	0.429	0.491	0.429	0.373	0.435	0.311	0.479	0.539	0.359	0.301	0.241	0.241	0.539	0.479	0.539	0.301	0.301	0.301
4	0.259	0.259	0.259	0.513	0.513	0.513	0.207	0.207	0.052	0.308	0.308	0.256	0.198	0.149	0.297	0.404	0.505	0.505	0.099	0.099	0.099	0.101	0.101	0.101
5	0.394	0.394	0.296	0.441	0.490	0.441	0.246	0.246	0.148	0.343	0.343	0.343	0.341	0.341	0.341	0.345	0.345	0.345	0.244	0.244	0.195	0.148	0.197	0.148
6	0.915	0.915	0.610	0.909	0.909	0.909	0.671	0.671	0.732	0.727	0.788	0.727	0.904	0.904	0.843	0.602	0.663	0.361	0.542	0.542	0.723	0.422	0.361	0.361
7	0.773	0.773	0.718	0.500	0.556	0.611	0.331	0.387	0.331	0.444	0.444	0.389	0.372	0.372	0.372	0.513	0.513	0.462	0.479	0.479	0.372	0.462	0.462	0.410
8	0.585	0.585	0.390	0.441	0.441	0.490	0.293	0.293	0.293	0.490	0.490	0.588	0.425	0.425	0.283	0.429	0.429	0.333	0.236	0.189	0.189	0.238	0.190	0.190
9	0.567	0.567	0.825	0.674	0.674	0.674	0.515	0.567	0.515	0.570	0.570	0.570	0.309	0.309	0.567	0.207	0.155	0.155	0.567	0.567	0.206	0.207	0.207	0.155
10	1.042	1.042	0.833	0.785	0.838	0.785	0.260	0.313	0.521	0.628	0.628	0.471	0.471	0.419	0.419	0.474	0.421	0.368	0.262	0.262	0.052	0.158	0.158	0.158
12	0.297	0.297	0.297	0.392	0.392	0.343	0.297	0.347	0.198	0.294	0.294	0.294	0.000	0.000	0.049	0.146	0.146	0.097	0.147	0.000	0.049	0.097	0.243	0.097
13	0.500	0.500	0.500	0.598	0.598	0.598	0.444	0.444	0.444	0.489	0.489	0.543	0.223	0.168	0.112	0.113	0.113	0.113	0.168	0.112	0.056	0.113	0.169	0.056
14	0.383	0.383	0.328	0.543	0.543	0.326	0.437	0.437	0.273	0.380	0.380	0.326	0.376	0.323	0.054	0.230	0.179	0.179	0.161	0.161	0.054	0.077	0.077	0.077
15	0.674	0.674	0.674	0.582	0.582	0.529	0.570	0.622	0.622	0.582	0.529	0.582	0.481	0.428	0.428	0.107	0.214	0.214	0.267	0.267	0.160	0.267	0.321	0.321
16	0.376	0.376	0.376	0.430	0.430	0.430	0.323	0.323	0.323	0.430	0.430	0.323	0.105	0.105	0.105	0.105	0.105	0.211	0.105	0.105	0.105	0.053	0.053	0.053
18	0.372	0.372	0.426	0.376	0.376	0.323	0.372	0.426	0.266	0.376	0.376	0.323	0.154	0.154	0.154	0.250	0.250	0.250	0.103	0.103	0.256	0.250	0.200	0.150
21	0.657	0.642	0.346	0.284	0.625	0.615	0.657	0.686	0.571	0.559	0.559	0.531	0.653	0.653	0.540	0.167	0.167	0.111	0.426	0.483	0.313	0.278	0.250	0.111
22	0.197	0.207	0.110	0.102	0.198	0.187	0.183	0.183	0.197	0.174	0.174	0.202	0.195	0.195	0.200	0.163	0.163	0.156	0.207	0.207	0.202	0.190	0.190	0.168
23	0.247	0.235	0.105	0.100	0.241	0.229	0.241	0.241	0.241	0.224	0.224	0.224	0.228	0.228	0.228	0.235	0.235	0.235	0.228	0.222	0.222	0.229	0.229	0.229
24	0.267	0.259	0.101	0.099	0.204	0.202	0.242	0.242	0.236	0.208	0.208	0.202	0.232	0.232	0.229	0.205	0.207	0.205	0.232	0.232	0.238	0.196	0.196	0.199
26	0.722	0.750	0.433	0.240	0.514	0.461	0.306	0.306	0.444	0.239	0.294	0.294	0.055	0.083	0.055	0.353	0.353	0.408	0.000	0.000	0.000	0.109	0.054	0.217
27	0.214	0.466	0.132	0.174	0.393	0.289	0.138	0.138	0.342	0.238	0.289	0.213	0.224	0.199	0.173	0.070	0.070	0.171	0.071	0.071	0.173	0.070	0.070	0.095
31	0.539	0.542	0.294	0.226	0.480	0.440	0.539	0.539	0.419	0.560	0.560	0.500	0.191	0.306	0.249	0.310	0.310	0.251	0.306	0.306	0.191	0.310	0.368	0.310

Table B-7. First ray mobility measurements (normalised) with MAP1st in STJN and RCSP (Rater 2).

	First Ray Mobility (Normalised)																							
	MAP1st seated (right) [mm]			MAP1st seated (left) [mm]			MAP1st seated (right) [mm]			MAP1st seated (left) [mm]			MAP1st standing (right) [mm]			MAP1st standing (left) [mm]			MAP1st standing (right) [mm]			MAP1st standing (left) [mm]		
	STJN						RCSP						STJN						RCSP					
ID	1	2	3	1	2	3	1	2	3	1	2	3	1	2	3	1	2	3	1	2	3	1	2	3
1	0.392	0.392	0.392	0.381	0.381	0.381	0.490	0.490	0.343	0.476	0.381	0.381	0.233	0.233	0.279	0.333	0.333	0.333	0.140	0.093	0.093	0.048	0.048	0.048
2	0.494	0.494	0.556	0.556	0.432	0.556	0.556	0.556	0.556	0.494	0.494	0.617	0.488	0.488	0.488	0.242	0.121	0.182	0.305	0.305	0.488	0.182	0.182	0.121
4	0.550	0.600	0.600	0.459	0.561	0.408	0.300	0.300	0.300	0.408	0.408	0.357	0.539	0.588	0.441	0.049	0.098	0.000	0.245	0.245	0.147	0.000	0.000	0.000
5	0.250	0.250	0.300	0.439	0.439	0.488	0.400	0.400	0.200	0.341	0.390	0.341	0.195	0.195	0.390	0.341	0.390	0.341	0.146	0.195	0.195	0.195	0.195	0.244
6	0.750	0.813	0.938	0.675	0.675	0.613	0.750	0.813	0.813	0.613	0.675	0.613	0.427	0.366	0.549	0.545	0.545	0.545	0.366	0.427	0.549	0.485	0.485	0.485
7	0.474	0.526	0.526	0.532	0.532	0.479	0.474	0.474	0.474	0.426	0.426	0.532	0.262	0.314	0.366	0.515	0.515	0.412	0.314	0.314	0.105	0.309	0.309	0.258
8	0.481	0.481	0.481	0.198	0.248	0.396	0.481	0.481	0.481	0.396	0.446	0.396	0.413	0.321	0.550	0.221	0.310	0.398	0.138	0.138	0.138	0.133	0.133	0.088
9	0.567	0.619	0.567	0.515	0.567	0.464	0.515	0.515	0.515	0.464	0.515	0.515	0.354	0.354	0.354	0.309	0.309	0.155	0.253	0.253	0.202	0.206	0.258	0.258
10	0.612	0.612	0.561	0.667	0.667	0.564	0.306	0.306	0.408	0.513	0.462	0.513	0.103	0.103	0.103	0.104	0.104	0.104	0.412	0.412	0.361	0.573	0.573	0.365
12	0.146	0.146	0.000	0.000	0.000	0.000	0.439	0.488	0.439	0.386	0.386	0.386	0.291	0.291	0.291	0.286	0.286	0.286	0.097	0.097	0.146	0.095	0.095	0.095
13	0.389	0.389	0.333	0.333	0.389	0.333	0.444	0.444	0.444	0.444	0.444	0.444	0.276	0.276	0.221	0.272	0.272	0.163	0.166	0.110	0.110	0.109	0.109	0.109
14	0.459	0.459	0.459	0.319	0.319	0.372	0.561	0.561	0.408	0.426	0.426	0.372	0.197	0.246	0.246	0.207	0.207	0.104	0.099	0.099	0.049	0.052	0.052	0.052
15	0.266	0.266	0.266	0.288	0.288	0.393	0.266	0.266	0.266	0.393	0.393	0.314	0.248	0.297	0.297	0.176	0.226	0.126	0.099	0.099	0.149	0.176	0.176	0.176
16	0.311	0.363	0.311	0.265	0.317	0.265	0.259	0.259	0.363	0.476	0.423	0.370	0.152	0.152	0.254	0.155	0.155	0.052	0.051	0.051	0.102	0.052	0.052	0.155
18	0.518	0.518	0.466	0.262	0.314	0.314	0.415	0.415	0.518	0.105	0.105	0.419	0.355	0.355	0.406	0.209	0.209	0.209	0.305	0.305	0.203	0.262	0.262	0.157
21	0.600	0.600	0.257	0.190	0.190	0.190	0.314	0.314	0.543	0.190	0.190	0.022	0.477	0.477	0.648	0.278	0.278	0.333	0.307	0.307	0.307	0.389	0.389	0.222
22	0.197	0.197	0.197	0.197	0.197	0.197	0.202	0.202	0.197	0.202	0.202	0.197	0.188	0.188	0.202	0.185	0.185	0.176	0.197	0.197	0.197	0.180	0.180	0.185
23	0.247	0.265	0.247	0.247	0.241	0.241	0.235	0.235	0.241	0.232	0.235	0.241	0.228	0.228	0.216	0.235	0.235	0.235	0.238	0.241	0.216	0.229	0.229	0.229
24	0.248	0.245	0.245	0.205	0.205	0.205	0.239	0.239	0.236	0.235	0.211	0.235	0.235	0.238	0.229	0.211	0.229	0.217	0.220	0.223	0.229	0.199	0.199	0.211
26	0.594	0.594	0.622	0.389	0.444	0.500	0.317	0.317	0.400	0.278	0.278	0.278	0.331	0.166	0.166	0.598	0.571	0.435	0.221	0.221	0.000	0.054	0.054	0.109
27	0.255	0.255	0.255	0.516	0.516	0.466	0.179	0.179	0.153	0.365	0.365	0.491	0.281	0.281	0.230	0.166	0.166	0.065	0.026	0.026	0.255	0.141	0.141	0.116
31	0.509	0.509	0.509	0.440	0.440	0.319	0.479	0.509	0.509	0.560	0.560	0.500	0.422	0.480	0.306	0.292	0.292	0.234	0.277	0.306	0.364	0.351	0.351	0.292

Appendix C. Additional Data for Foot Type Biomechanics

This appendix details the supplementary information including raw data for the subject information, rotational flexibility, and plantar loading not reported in the main text of Chapter 5.

Table C-1. Subject information.

ID	Sex	Group	Race	Ethnicity	Age (Years)	Height (cm	Weight (Kg)	BMI	Tested Side
1	Male	Healthy	White	Non-hispanic	32	187.9	99	28.01	Bilateral
4	Male	Healthy	Asian	Non-hispanic	27	180.3	84.8	26.23	Bilateral
5	Male	Healthy	White	Non-hispanic	25	180.3	86.2	26.5	Bilateral
6	Female	Healthy	Asian	Non-hispanic	23	152.4	55.3	23.8	Bilateral
7	Male	Healthy	White	Non-hispanic	26	177.8	65.8	20.8	Bilateral
8	Male	Healthy	White	Non-hispanic	36	180.3	82.6	25.6	Bilateral
9	Male	Healthy	Asian	Non-hispanic	30	177.8	79.4	24.9	Bilateral
10	Male	Healthy	Asian	Non-hispanic	27	185.4	72.6	21.3	Bilateral
11	Male	Healthy	White	Non-hispanic	44	179.5	78.5	24.4	Bilateral
12	Male	Healthy	White	Non-hispanic	25	190	77	21.3	Bilateral
13	Female	Healthy	White	Non-hispanic	23	177	68	21.7	Bilateral
14	Male	Healthy	White	Non-hispanic	55	176	95	30.7	Bilateral
16	Male	Healthy	White	Non-hispanic	59	182.8	92.9	27.8	Bilateral
17	Female	Healthy	White	Hispanic	44	160	68	26.6	Bilateral
18	Male	Healthy	White	Non-hispanic	26	182.9	77.1	23	Bilateral
19	Male	Healthy	Asian	Non-hispanic	27	175.3	77	25	Bilateral
21	Female	Healthy	White	Non-hispanic	23	165	58.8	21.5	Bilateral
26	Female	Healthy	White	Non-hispanic	22	172.7	90.7	30.3	Bilateral
27	Male	Healthy	White	Non-hispanic	57	185.4	97.5	28.5	Bilateral
31	Female	Healthy	White	Non-hispanic	32	167.6	53.1	18.8	Bilateral

Table C-2. First MTP joint flexibility measurements.

Planus						
Subject	Early Flexibility	Late Flexibility	Maximum Dorsiflexion	Laxity	Bilinear Angle	Bilinear Torque
1 L	0.22	0.087	72.8	53.7	59	285
1 R	0.16	0.071	65.4	50.3	58	260
4 L	0.29	0.076	70	44.3	49	205.7
4 R	0.37	0.058	65.6	33	44	115
5 L	0.26	0.058	65.8	34	42	181
5 R	0.2	0.029	63.3	39.3	47.7	205.3
6 L	1.22	0.11	95.9	58	73.7	76.3
6 R	1.33	0.117	89.7	48.3	67.3	51
7 L	0.66	0.088	86.8	56.3	66.7	106
7 R	0.52	0.063	71.9	38.7	51	96.3
8 L	0.1	0.054	66.4	63	63	596
8 R	0.26	0.059	66.7	39.3	48.3	183.7
9 L	0.26	0.082	62.1	47.3	48.7	213
9 R	0.51	0.054	80.9	49.3	61.3	96
10 L	0.62	0.096	78.8	43.7	53.7	97
10 R	0.97	0.1	86	44.7	59.7	72.7
11 L	0.18	0.05	85.02	62	66	316
11 R	0.29	0.05	71.6	45	49	188.7
13 L	0.34	0.086	84.24	54	63.7	120.7
13 R	0.61	0.081	62.1	42	45.7	114
19 L	0.33	0.03	77.5	52.3	56.3	185.3
Average	0.46	0.071	74.6	47.5	55.8	179.2
SD	0.34	0.024	10.2	8.4	8.8	120.1

Rectus						
Subject	Early Flexibility	Late Flexibility	Maximum Dorsiflexion	Laxity	Bilinear Angle	Bilinear Torque
2 L	0.23	0.05	56.8	27	35	195.7
2 R	1.9	0.13	82.1	34.7	56	35.3
12 L	0.28	0.063	74	50.7	60	215.3
12 R	0.28	0.061	49.8	26	36.3	173.3
14 L	0.34	0.145	87.7	74.7	74.7	228
14 R	0.51	0.065	82.9	56	63	143
15 L	0.151	0.066	66.6	56.3	58.3	389.3
15 R	0.26	0.131	57.2	52.7	52.7	273
16 L	0.84	0.11	104.8	69.3	82.7	113.7
16 R	0.7	0.14	98.5	65	73.7	119
18 L	0.3	0.049	73.8	52.3	58	207.7
18 R	0.98	0.053	92.4	48	72	79.7
19 R	0.35	0.06	100.7	50.3	70.3	76.7
Average	0.54	0.086	79.0	51.0	60.9	173.0
SD	0.47	0.038	17.8	14.7	14.2	94.6

Table C-3. Means for CPEIH, IPI, total PP, CA, MF, FTI, PTI, and ratios of PP, MF, PTI, and FTI.

SubjectID	CPEIH	IPI	PPTO	CTO	MFTO	FTITO	PTITO	RatioPP	RatioMF	RatioPTI	RatioFTI
1 L	20.83	4.3426	820	162.25	1030.326	517.5602	327.12	0.82	0.75	0.81	0.63
4 L	17.40	9.969	549.1667	158.50	885.4817	447.4545	183.33	0.47	0.85	0.48	0.68
5 L	21.70	9.619	814.1667	142.75	848.9817	489.8115	249.77	0.57	0.55	0.53	0.50
6 L	21.30	6.8615	325	113.33	561.6483	254.6845	117.52	0.54	0.91	0.62	0.87
7 L	15.80	3.220167	454.1667	121.83	670.4617	351.9607	187.73	0.56	0.66	0.53	0.56
8 L	21.00	14.771	820	127.83	879.5017	402.4335	266.95	0.31	0.35	0.40	0.37
9 L	22.10	10.9484	454	137.45	781.776	447.9692	187.44	0.55	0.70	0.57	0.68
10 L	18.90	7.159667	754.1667	132.13	771.98	415.312	279.08	0.57	0.87	0.65	0.80
11 L	13.00	5.525833	636.6667	144.83	832.2717	449.3847	220.73	0.49	0.62	0.48	0.52
12 L	13.92	4.79	505	138.11	786.9671	430.1423	234.80	1.38	1.61	1.49	1.62
13 L	13.15	0.929	643	118.85	722.852	386.5642	240.38	0.96	1.14	1.04	1.07
14 L	21.48	6.145	405.7143	151.06	950.6957	578.8453	203.81	0.74	1.06	0.83	0.99
16 L	14.67	6.745286	760	114.71	892.6271	468.6957	324.63	1.69	1.13	1.56	1.09
17 L	14.41	7.659	635	129.79	728.795	384.7032	199.25	0.30	0.58	0.42	0.58
18 L	29.89	4.7074	888.3333	114.88	824.1283	436.9205	313.50	1.03	0.84	1.09	0.88
19 L	29.46	7.3744	456.6667	154.96	803.6067	401.0078	198.82	0.71	0.75	0.65	0.69
21 L	18.58	4.947667	1221	111.85	739.278	376.4402	306.03	1.05	1.20	1.08	1.24
26 L	17.28	11.783	893	138.10	1024.802	497.9722	294.63	0.31	0.61	0.39	0.59
27 L	30.04	11.37217	615	156.21	1072.44	571.7438	210.13	0.47	1.01	0.64	1.00
31 L	17.30	3.286	483.3333	85.25	548.19	264.0417	197.43	0.78	0.83	0.72	0.74
1 R	25.70	6.1244	787	168.50	1006.828	521.8168	257.38	0.43	0.74	0.47	0.60
4 R	8.90	5.363667	440.8333	156.54	889.4	441.5702	171.08	0.40	0.80	0.50	0.69
5 R	25.70	6.198833	463.3333	146.50	831.98	486.7308	199.77	0.70	0.49	0.69	0.46
6 R	18.90	6.1236	390	117.08	572.94	247.9462	121.00	0.42	0.77	0.45	0.62
7 R	19.70	1.9082	575.8333	126.21	651.7517	351.2367	214.83	0.53	0.66	0.52	0.55
8 R	28.10	13.5282	1091	126.25	867.752	398.0028	298.64	0.18	0.34	0.27	0.33
9 R	21.80	9.089667	712	135.50	780.402	455.2808	261.11	0.55	0.54	0.51	0.49

10 R	19.30	9.08125	795.8333	128.67	775.565	391.9643	254.58	0.58	0.89	0.57	0.77
11 R	14.98	7.055143	497.1429	151.07	843.4857	445.4553	189.01	0.62	0.61	0.59	0.56
12 R	18.00	5.601286	748.5714	139.25	767.6986	409.0429	276.47	0.59	0.75	0.55	0.69
13 R	13.15	0.9824	502	117.60	714.978	393.6698	214.74	0.74	0.99	0.83	0.97
14 R	22.02	7.5855	502.1429	145.58	948.1414	560.5296	234.81	0.91	1.17	0.96	1.11
16 R	17.35	9.155	670	119.17	926.9617	495.9657	295.42	1.23	1.16	1.30	1.14
17 R	10.84	3.469167	508.3333	136.71	712.21	390.9433	186.52	0.36	0.49	0.45	0.47
18 R	27.15	7.096833	921.6667	122.58	812.2333	438.5457	324.10	0.54	0.73	0.71	0.73
19 R	30.20	4.338167	475.8333	152.71	800.4	404.0285	180.23	1.40	1.09	1.00	0.94
21 R	25.67	5.468	1025	112.58	735.1283	378.6965	313.38	0.82	0.90	0.83	0.89
26 R	14.01	15.6784	730	134.95	1004.652	512.1814	258.54	0.88	1.00	0.97	0.91
27 R	26.54	15.5395	555.8333	156.04	1130.047	571.9128	217.97	0.52	1.00	0.69	1.03
31 R	23.87	7.3714	483	92.55	557.502	266.735	191.08	0.95	0.97	0.75	0.77

Table C-4. Means for PP across the twelve-segment foot mask.

SubjectID	PPhallux	PPtoe2	PPtoe345	PPmh1	PPmh2	PPmh3	PPmh4	PPmh5	PPlathindfoot	PPmedhindfoot	PPlatmidfoot	PPmedmidfoot
1 L	559.00	342.00	197.00	606.00	742.00	800.00	518.00	387.00	362.00	497.00	140.00	92.00
4 L	536.67	212.50	130.83	160.00	341.67	357.50	311.67	126.67	299.17	306.67	93.33	89.17
5 L	801.67	115.00	120.83	221.67	390.83	357.50	286.67	181.67	277.50	293.33	102.50	102.50
6 L	213.33	193.33	40.00	174.17	323.33	300.00	260.00	105.00	226.67	232.50	114.17	116.67
7 L	368.33	255.00	120.00	176.67	315.00	303.33	209.17	226.67	311.67	320.00	69.17	62.50
8 L	450.83	220.83	182.50	256.67	820.00	501.67	246.67	156.67	345.83	357.50	50.83	37.50
9 L	422.00	73.00	47.00	194.00	354.00	346.00	305.00	221.00	261.00	259.00	106.00	114.00
10 L	321.67	89.17	56.67	377.50	665.00	705.83	218.33	614.17	291.67	312.50	207.50	69.17
11 L	635.83	90.00	91.67	214.17	437.50	437.50	247.50	86.67	243.33	257.50	80.83	84.17
12 L	315.00	103.57	57.14	320.71	232.14	442.86	383.57	406.43	339.29	385.00	54.29	50.71
13 L	423.00	91.00	31.00	422.00	440.00	406.00	278.00	458.00	310.00	351.00	101.00	57.00
14 L	195.00	138.57	95.71	302.14	405.71	364.29	230.71	133.57	320.71	316.43	132.14	107.86
16 L	381.43	157.86	52.14	589.29	349.29	375.71	309.29	340.00	511.43	544.29	108.57	68.57
17 L	163.33	77.50	57.50	188.33	627.50	366.67	244.17	135.83	230.00	236.67	144.17	144.17
18 L	264.17	53.33	29.17	375.00	363.33	521.67	796.67	603.33	316.67	320.00	59.17	57.50
19 L	275.00	75.83	47.50	224.17	315.83	348.33	350.83	176.67	391.67	437.50	104.17	99.17
21 L	1221.00	152.00	66.00	353.00	335.00	334.00	248.00	97.00	338.00	398.00	74.00	77.00
26 L	592.00	194.00	143.00	259.00	832.00	532.00	364.00	619.00	344.00	357.00	116.00	109.00
27 L	332.50	60.00	56.67	181.67	383.33	615.00	415.00	335.00	375.83	350.83	163.33	102.50
31 L	411.67	200.83	132.50	309.17	395.00	350.00	231.67	115.83	356.67	416.67	65.83	70.83
1 R	531.00	335.00	129.00	340.00	787.00	441.00	372.00	406.00	489.00	509.00	130.00	122.00
4 R	409.17	184.17	126.67	145.83	363.33	368.33	297.50	164.17	278.33	285.00	113.33	103.33
5 R	361.67	101.67	115.83	320.00	455.00	409.17	279.17	187.50	290.00	287.50	120.00	120.00
6 R	172.50	148.33	37.50	154.17	370.00	373.33	235.83	94.17	240.00	248.33	117.50	116.67
7 R	512.50	419.17	210.00	235.00	440.00	330.00	220.00	239.17	304.17	295.00	87.50	58.33
8 R	465.00	288.00	297.00	192.00	1091.00	436.00	218.00	153.00	367.00	384.00	57.00	27.00
9 R	654.00	112.00	89.00	194.00	350.00	372.00	343.00	167.00	290.00	295.00	90.00	78.00
10 R	332.50	225.00	86.67	415.00	714.17	495.00	204.17	431.67	339.17	354.17	190.00	63.33

11 R	269.29	151.43	111.43	230.71	370.00	436.43	444.29	153.57	247.86	252.14	83.57	79.29
12 R	328.33	40.83	49.17	246.43	417.86	702.86	220.00	292.86	305.00	318.33	70.83	67.50
13 R	484.00	107.00	68.00	306.00	411.00	432.00	224.00	296.00	281.00	280.00	72.00	61.00
14 R	359.29	115.00	70.71	412.86	455.00	356.43	192.86	122.14	316.43	312.86	147.86	118.57
16 R	216.67	145.83	70.83	463.33	376.67	404.17	353.33	368.33	575.00	602.50	102.50	60.83
17 R	147.50	205.83	125.83	183.33	508.33	351.67	277.50	185.00	210.83	208.33	154.17	115.83
18 R	212.50	165.83	92.50	471.67	871.67	381.67	510.83	401.67	305.00	327.50	86.67	51.67
19 R	210.83	65.00	27.50	466.67	333.33	316.67	244.17	119.17	279.17	298.33	115.00	102.50
21 R	1025.00	150.00	68.33	266.67	325.83	316.67	231.67	122.50	363.33	400.83	76.67	74.17
26 R	706.00	119.00	59.00	501.00	569.00	504.00	388.00	462.00	319.00	325.00	122.00	122.00
27 R	365.83	35.00	21.67	218.33	420.83	553.33	453.33	510.00	357.00	349.00	138.00	154.00
31 R	329.00	225.00	210.00	309.00	324.00	340.00	227.00	156.00	386.00	465.00	81.00	83.00

Table C-5. Means for CA across the twelve-segment foot mask.

SubjectID	CAhallux	CAtoe2	CAtoe345	CAmh1	CAmh2	CAmh3	CAmh4	CAmh5	CAlathindfoot	CAmedhindfoot	CAlatmidfoot	CAmedmidfoot
1 L	12.50	3.35	5.10	14.85	11.65	14.25	10.95	6.75	21.25	21.80	31.40	8.40
4 L	13.54	4.38	8.21	17.08	12.67	12.71	10.00	5.79	19.54	19.33	24.33	10.88
5 L	10.46	2.96	6.63	12.79	10.54	12.50	9.92	6.88	20.75	20.33	24.46	4.54
6 L	8.04	2.75	2.58	11.29	8.79	10.46	8.46	5.29	14.58	14.54	20.88	5.67
7 L	8.46	4.04	7.54	11.13	10.00	11.46	9.38	5.75	18.46	18.08	15.17	2.38
8 L	12.33	5.38	10.00	12.46	9.46	9.63	9.25	6.46	20.33	19.96	12.00	0.58
9 L	11.20	2.95	4.05	12.85	10.60	12.75	10.40	6.60	18.60	18.65	22.90	5.90
10 L	9.38	2.92	3.08	13.25	10.04	12.54	10.54	6.75	16.50	16.33	27.29	3.50
11 L	16.29	3.46	6.54	14.00	11.42	12.29	10.63	6.21	19.79	20.58	20.83	2.79
12 L	11.64	4.61	7.25	13.29	9.39	13.04	11.82	8.39	20.39	20.29	16.11	1.89
13 L	8.10	2.75	2.05	12.15	9.30	11.40	9.30	6.35	15.50	15.50	23.70	2.75
14 L	10.77	4.24	7.42	15.78	12.71	14.44	11.66	6.98	18.63	18.80	26.16	3.35
16 L	10.18	4.46	4.25	12.46	9.82	11.21	9.68	6.32	16.96	16.64	11.68	1.04
17 L	7.92	3.04	5.42	12.50	10.83	12.13	10.17	6.08	15.63	15.63	24.42	6.04
18 L	10.67	2.58	2.42	12.21	8.67	10.54	10.42	7.67	17.83	17.38	13.13	1.38
19 L	12.25	2.79	2.88	15.83	11.88	14.42	11.71	7.17	19.33	19.29	30.58	6.75
21 L	11.20	4.10	5.30	11.45	8.90	9.30	7.70	4.40	15.40	15.05	16.30	2.75
26 L	11.05	3.50	4.10	14.30	12.45	12.50	9.75	6.05	16.95	17.05	25.60	4.80
27 L	10.63	2.50	3.83	16.63	13.08	15.08	11.71	7.29	20.92	20.83	31.46	4.13
31 L	7.75	3.63	6.67	8.46	6.46	7.92	7.33	4.38	13.54	13.88	3.67	1.54
1 R	11.85	4.75	5.05	16.10	13.50	14.35	11.20	6.80	21.30	21.70	30.95	10.85
4 R	12.21	3.88	5.46	16.63	12.46	13.67	10.63	6.71	19.54	19.54	25.46	10.33
5 R	10.63	3.38	7.67	13.58	11.46	12.21	9.54	6.50	19.71	19.71	28.33	3.79
6 R	7.42	3.13	3.08	11.50	9.71	10.88	8.13	4.46	14.75	15.00	23.00	5.96
7 R	7.21	3.25	7.13	10.92	8.92	11.67	9.38	6.21	18.33	18.42	22.29	2.50
8 R	12.30	5.30	10.15	11.20	9.40	9.70	9.10	6.15	20.35	19.50	12.75	0.30
9 R	12.45	3.50	5.00	11.50	9.95	12.15	10.10	6.70	19.40	19.05	23.20	2.50
10 R	7.54	3.42	4.21	12.96	9.67	11.92	10.42	6.38	16.67	16.04	25.29	4.17

11 R	12.61	4.32	8.00	13.32	12.11	12.93	11.50	7.11	19.07	20.04	27.68	2.39
12 R	12.50	2.46	5.83	12.32	9.71	12.89	12.11	8.25	20.42	20.67	23.88	2.83
13 R	9.85	3.20	5.50	11.80	9.00	10.80	9.35	6.15	15.30	15.65	19.10	1.90
14 R	10.94	3.45	5.92	15.71	12.55	13.58	11.66	6.73	18.62	18.59	24.68	3.10
16 R	10.25	4.54	5.75	13.00	10.04	11.83	9.79	6.08	17.58	17.54	11.54	1.21
17 R	9.79	4.50	9.38	11.67	10.46	11.42	9.88	5.92	16.04	16.29	26.54	4.79
18 R	9.75	3.88	7.00	11.42	8.92	10.92	10.92	8.00	18.25	18.08	13.83	1.54
19 R	10.00	2.71	1.88	16.71	13.00	14.92	12.08	7.46	18.54	19.04	31.00	5.96
21 R	10.50	3.79	6.46	10.54	8.83	10.13	8.17	5.21	15.13	15.46	16.50	1.88
26 R	10.65	3.15	3.05	15.10	12.05	12.60	10.30	6.40	16.95	16.65	23.60	4.40
27 R	10.96	1.85	0.58	17.25	13.29	14.96	11.79	7.21	20.55	20.40	32.80	5.50
31 R	8.75	3.85	8.05	9.00	6.75	8.00	7.50	4.95	13.35	13.45	7.10	1.70

Table C-6. Means for MF across the twelve-segment foot mask.

SubjectID	MFhallux	MFtoe2	MFtoe345	MFmh1	MFmh2	MFmh3	MFmh4	MFmh5	MFlathindfoot	MFmedhindfoot	MFlatmidfoot	MFmedmidfoot
1 L	173.08	30.88	20.40	151.95	202.70	304.10	163.93	69.80	273.60	384.28	202.35	32.05
4 L	217.56	27.65	30.21	139.17	163.96	225.10	134.44	39.13	279.92	328.29	123.58	39.46
5 L	148.81	15.60	23.44	118.19	214.19	209.10	132.08	57.50	276.33	326.31	97.40	21.19
6 L	72.98	17.58	5.83	104.25	114.23	148.02	94.77	26.60	157.69	193.35	107.83	29.00
7 L	111.63	31.38	32.46	103.38	155.79	168.81	95.60	48.04	257.58	248.94	51.75	9.56
8 L	183.10	43.96	43.96	102.77	292.04	190.44	89.56	48.40	269.13	353.35	36.96	2.19
9 L	134.13	10.90	10.20	112.95	161.23	204.20	139.48	65.68	212.83	259.20	99.18	27.70
10 L	75.19	14.77	8.79	165.42	189.56	195.56	96.96	100.83	199.92	238.33	187.19	10.90
11 L	177.10	16.38	24.08	153.35	247.02	208.23	80.46	30.85	241.54	298.69	49.15	12.92
12 L	110.23	20.59	21.23	132.84	82.30	207.16	161.38	105.82	257.04	333.27	42.45	5.63
13 L	91.20	12.35	3.83	179.60	157.00	171.05	92.30	66.28	222.05	252.00	120.35	8.23
14 L	92.77	26.89	30.82	247.35	233.49	218.94	129.11	60.93	291.35	303.99	172.52	15.41
16 L	104.34	24.91	9.73	196.45	173.45	201.66	137.25	84.93	291.88	290.71	43.86	4.32
17 L	52.58	12.25	17.48	121.67	209.46	168.17	112.85	50.40	185.25	221.88	160.23	33.23
18 L	82.79	7.50	3.27	124.35	148.92	217.92	195.06	116.40	274.19	252.83	36.77	5.25
19 L	137.33	11.17	7.75	132.92	178.06	215.10	143.17	52.56	232.27	277.06	135.25	28.81
21 L	227.65	24.75	14.13	184.98	154.05	148.43	82.13	22.25	196.33	234.20	52.88	11.40
26 L	155.68	20.70	17.33	168.85	276.75	259.70	143.05	78.50	278.68	306.88	137.23	22.68
27 L	89.56	10.40	10.29	185.38	183.81	262.71	200.02	104.33	286.71	400.38	226.54	21.19
31 L	100.73	27.71	27.71	101.63	122.44	128.79	71.94	25.50	184.08	200.42	10.38	6.44
1 R	148.93	46.63	19.25	169.23	227.50	223.33	137.60	77.50	316.50	341.15	208.88	48.05
4 R	172.48	26.79	24.06	130.69	163.60	240.00	141.79	51.29	260.90	299.15	143.10	39.13
5 R	119.38	14.71	20.96	126.50	257.08	213.81	122.90	59.54	284.85	279.50	140.52	19.63
6 R	56.88	17.92	5.88	96.69	126.21	170.98	89.27	24.23	167.54	206.06	117.54	27.08
7 R	91.48	33.50	37.13	103.06	156.44	185.02	91.25	51.21	264.46	226.73	95.46	8.44
8 R	178.40	48.08	63.83	95.93	284.10	151.93	86.00	42.50	315.65	341.13	35.78	0.75
9 R	142.85	18.18	21.25	88.25	162.48	213.45	146.50	54.98	254.68	287.08	100.05	10.38
10 R	74.54	28.38	14.52	166.77	187.23	186.88	97.13	73.06	210.02	273.96	161.48	10.83

11 R	106.79	24.29	33.34	128.59	211.54	232.32	154.30	55.98	242.13	276.79	91.18	9.73
12 R	101.67	6.35	11.52	110.30	146.93	222.43	114.57	75.23	259.23	308.98	80.81	10.27
13 R	117.83	14.60	18.20	144.33	145.23	170.70	87.60	64.18	212.90	233.23	79.15	7.18
14 R	133.47	17.68	21.00	302.58	258.64	187.39	117.37	54.71	293.49	304.41	148.41	16.27
16 R	71.52	21.54	14.75	202.67	174.67	238.15	162.19	90.29	276.67	297.33	36.40	4.65
17 R	70.54	29.40	49.79	86.83	178.48	170.04	127.71	58.92	157.04	174.40	196.73	26.10
18 R	82.71	25.02	25.92	137.38	187.90	181.90	183.29	110.98	263.21	284.81	46.58	5.17
19 R	77.13	10.38	2.63	207.08	189.29	193.04	132.13	47.44	220.63	228.19	149.17	20.94
21 R	229.69	26.06	20.67	135.48	150.02	154.73	85.04	33.25	224.21	261.88	68.17	7.94
26 R	134.90	13.75	7.40	233.15	232.08	246.08	152.33	79.85	252.15	301.05	117.63	22.55
27 R	104.67	4.78	1.04	201.29	200.90	269.63	224.77	123.63	284.88	426.08	222.95	37.53
31 R	94.73	33.53	48.23	111.13	114.00	116.25	76.50	36.08	160.03	195.58	24.05	8.58

Table C-7. Means for FTI across the twelve-segment foot mask.

SubjectID	FTIhallux	FTItoe2	FTItoe345	FTImh1	FTImh2	FTImh3	FTImh4	FTImh5	FTIlathindfoot	FTImedhindfoot	FTIlatmidfoot	FTImedmidfoot
1 L	35.04	5.14	4.80	38.00	60.40	90.75	47.66	20.08	63.86	89.30	56.07	6.46
4 L	35.40	5.11	6.23	29.10	42.51	61.94	41.62	13.64	75.31	84.16	43.57	8.85
5 L	27.65	2.91	3.66	28.40	56.42	62.99	42.36	18.09	96.11	113.99	30.13	7.10
6 L	12.39	2.77	0.84	28.10	32.20	41.01	25.84	7.38	32.76	39.48	26.66	5.27
7 L	19.78	6.13	6.10	23.17	41.41	48.18	28.92	13.90	74.84	76.08	11.13	2.32
8 L	35.56	10.92	6.45	34.19	92.77	65.34	32.27	14.70	47.78	57.76	4.45	0.24
9 L	32.22	2.63	2.53	41.10	60.36	76.72	52.55	22.75	54.19	66.01	29.96	6.95
10 L	16.67	1.86	1.44	47.63	59.88	58.33	34.18	30.45	50.47	56.22	55.71	2.49
11 L	37.90	3.19	3.43	43.59	84.02	74.68	30.69	9.95	66.33	81.02	10.92	3.68
12 L	25.62	3.87	3.18	47.30	29.15	69.69	59.22	32.55	68.58	81.24	8.41	1.33
13 L	23.34	2.10	0.34	48.65	45.49	48.38	27.39	14.30	59.28	78.02	37.62	1.65
14 L	15.34	5.55	8.18	80.91	82.01	79.68	52.73	23.65	81.64	82.52	61.98	4.57
16 L	23.33	4.57	0.84	61.15	56.23	65.99	46.25	25.31	85.31	86.13	12.43	1.15
17 L	11.96	2.99	3.33	38.65	66.59	57.33	39.23	15.97	43.79	50.96	46.21	7.68
18 L	15.69	1.09	0.52	28.53	32.29	62.99	61.67	35.93	94.34	94.93	7.77	1.16
19 L	22.40	1.07	1.00	31.67	46.14	62.24	42.58	14.16	61.84	75.96	34.61	7.33
21 L	46.81	5.46	3.22	64.60	52.00	50.53	27.52	6.55	45.97	59.60	11.99	2.18
26 L	31.65	4.51	3.34	47.62	81.34	80.78	47.55	24.30	64.12	70.75	37.17	4.85
27 L	16.39	1.64	2.16	55.97	56.17	82.61	66.99	33.99	76.46	97.11	78.11	5.19
31 L	20.94	6.34	5.95	26.42	35.77	40.93	22.90	6.66	43.80	50.59	2.49	1.23
1 R	30.63	9.71	4.51	38.32	63.83	62.51	40.28	22.32	82.69	96.24	59.81	10.93
4 R	33.87	5.50	5.37	32.23	46.40	64.50	40.05	14.52	65.62	74.22	48.62	10.67
5 R	21.37	2.90	3.46	34.38	74.09	73.13	47.51	23.45	76.43	78.27	46.11	5.64
6 R	7.61	2.25	0.64	18.80	30.18	41.15	22.24	5.92	37.21	44.94	31.20	5.79
7 R	17.83	6.96	5.73	23.13	42.34	53.76	26.51	13.12	71.38	66.71	21.72	2.04
8 R	37.79	10.88	9.25	28.47	86.43	52.52	28.95	13.67	60.84	63.20	5.91	0.09
9 R	34.39	4.03	5.14	28.05	56.73	81.85	56.53	19.59	68.22	73.72	24.68	2.34
10 R	15.66	4.29	3.06	42.72	55.76	51.82	29.74	22.16	53.18	60.47	50.28	2.81

11 R	17.84	3.91	5.24	35.82	63.84	74.56	49.49	17.25	70.27	80.50	23.84	2.89
12 R	23.81	1.10	1.93	35.93	51.89	79.24	44.02	24.83	61.43	69.27	17.39	2.16
13 R	31.43	2.84	3.24	45.62	46.98	56.03	31.83	17.95	60.01	70.59	25.37	1.78
14 R	22.70	3.21	4.43	102.74	92.30	71.94	46.44	18.99	75.19	73.13	45.77	3.68
16 R	19.77	5.09	2.18	72.10	63.49	79.07	51.89	25.26	79.11	87.89	9.08	1.03
17 R	14.31	6.67	11.37	30.67	64.91	64.49	47.06	19.45	36.18	39.46	51.81	4.54
18 R	17.45	3.91	4.28	32.01	43.78	56.42	67.96	41.71	75.51	84.44	10.19	0.87
19 R	13.65	0.88	0.12	48.85	51.98	60.14	42.05	13.69	57.91	64.73	43.98	6.07
21 R	49.30	5.47	4.80	43.65	49.01	52.70	30.55	10.88	51.42	63.79	15.62	1.51
26 R	25.00	3.40	1.33	67.32	74.00	83.02	56.35	27.55	63.62	71.00	34.07	5.50
27 R	17.97	0.47	0.13	65.85	64.04	85.82	71.05	33.74	66.35	92.37	70.91	8.17
31 R	19.23	6.93	11.80	25.46	32.93	38.65	25.50	10.74	40.24	48.74	4.87	1.63

Table C-8. Means for PTI across the twelve-segment foot mask.

SubjectID	PTIhallux	PTItoe2	PTItoe345	PTImh1	PTImh2	PTImh3	PTImh4	PTImh5	PTIlathindfoot	PTImedhindfoot	PTIlatmidfoot	PTImedmidfoot
1 L	112.40	55.54	47.64	132.88	164.50	229.00	134.50	85.60	85.18	107.32	39.84	23.82
4 L	94.00	38.65	30.93	40.12	82.78	90.68	81.38	42.18	83.47	84.03	38.35	31.58
5 L	148.80	23.18	17.78	56.63	107.02	105.23	85.58	58.98	100.43	105.43	42.13	36.53
6 L	42.92	29.12	9.25	46.83	75.45	78.22	66.62	28.72	48.30	49.57	30.75	24.73
7 L	70.62	49.53	28.35	44.68	83.77	90.17	65.93	59.07	92.15	94.22	23.38	19.48
8 L	114.10	64.28	32.35	87.93	217.85	151.68	85.13	51.31	62.95	64.74	9.59	4.62
9 L	106.54	21.78	16.60	68.39	119.91	122.00	104.87	74.48	69.47	70.39	38.93	29.65
10 L	75.60	13.60	12.25	109.78	169.02	197.85	71.10	141.95	73.53	76.13	55.77	18.13
11 L	143.65	21.73	18.30	69.80	146.90	150.93	84.10	31.47	71.58	74.77	26.10	25.85
12 L	84.30	22.09	13.03	109.46	73.56	119.54	116.74	120.77	86.24	95.01	19.69	14.54
13 L	111.70	18.02	4.39	113.89	109.92	103.60	73.15	74.95	91.96	104.22	33.19	16.45
14 L	41.79	32.04	33.41	105.47	127.08	116.49	82.60	63.01	94.15	91.94	58.65	32.23
16 L	84.06	31.74	6.97	177.27	113.97	120.71	99.89	93.24	141.77	144.61	36.70	20.69
17 L	36.55	21.70	13.85	65.32	154.18	105.82	74.42	46.55	58.92	59.75	49.23	34.18
18 L	49.08	9.77	5.60	85.35	77.97	182.25	233.28	172.35	115.82	119.67	24.68	18.02
19 L	59.27	8.70	7.30	55.97	86.13	98.85	92.78	43.57	98.87	112.97	36.50	28.62
21 L	219.55	37.22	20.21	118.48	109.90	109.58	81.24	31.83	81.05	89.31	20.33	16.96
26 L	126.71	40.73	31.71	74.91	191.59	136.88	104.89	134.71	83.10	85.57	40.05	31.34
27 L	57.78	10.56	14.48	59.82	93.22	139.84	109.08	87.09	94.16	94.22	61.37	28.75
31 L	88.88	45.69	29.63	79.47	110.15	105.28	73.53	34.16	85.30	90.58	17.28	16.77
1 R	106.32	68.58	31.38	72.26	153.44	106.28	81.90	79.76	117.10	123.50	49.32	36.78
4 R	95.48	40.25	29.68	43.22	86.72	89.52	70.87	45.97	73.85	76.17	46.03	32.12
5 R	65.52	22.32	23.73	87.98	128.32	124.97	95.08	74.28	82.38	82.42	47.18	34.13
6 R	26.13	20.52	6.40	34.17	75.77	76.87	56.13	25.85	55.55	57.12	33.18	27.12
7 R	94.95	78.38	36.75	53.65	103.72	100.92	67.02	55.97	86.68	85.20	27.43	18.22
8 R	119.80	69.78	48.47	65.27	238.56	128.53	72.73	50.39	73.75	75.35	12.43	3.36
9 R	165.12	26.91	27.52	62.32	123.16	132.27	122.85	66.18	80.03	81.30	33.84	21.28
10 R	70.98	33.95	20.63	100.15	175.90	139.70	60.80	101.97	79.87	81.08	56.35	18.20

11 R	50.99	26.56	23.83	65.44	111.06	126.06	122.07	48.34	77.36	77.67	30.91	24.81
12 R	90.07	9.02	12.53	74.61	136.63	213.63	77.84	84.34	73.58	75.70	24.32	16.28
13 R	134.58	25.07	14.77	93.93	113.76	122.18	71.15	77.26	86.01	87.98	27.20	17.66
14 R	66.84	23.81	21.02	140.79	147.01	119.94	74.85	52.91	86.89	84.40	51.50	28.56
16 R	63.43	38.95	12.95	154.52	119.08	125.90	107.97	92.95	146.28	149.62	30.28	16.27
17 R	36.17	47.62	33.80	64.82	144.30	114.65	92.97	63.10	46.67	46.32	53.17	24.47
18 R	49.78	28.25	19.53	101.38	142.93	138.55	184.92	159.70	92.50	99.13	29.73	12.47
19 R	40.62	6.72	1.63	98.13	97.97	100.08	80.63	38.35	77.30	83.25	39.82	29.55
21 R	221.11	34.86	21.21	86.85	104.55	105.56	78.18	44.38	87.15	94.83	22.42	16.34
26 R	123.13	31.69	16.82	136.57	140.26	139.26	120.19	115.34	81.92	82.59	41.30	31.16
27 R	52.96	4.54	2.90	74.71	108.86	143.38	129.16	127.15	84.16	84.82	54.14	33.50
31 R	71.61	45.91	52.20	69.93	93.10	99.80	75.15	51.52	78.53	89.93	21.36	19.76

Appendix D. Additional Data for Finite Element Modelling

This appendix details the supplementary information including von Mises and maximum principal stress distributions at the first metatarsal head cartilage not shown in the main text of Chapter 7.

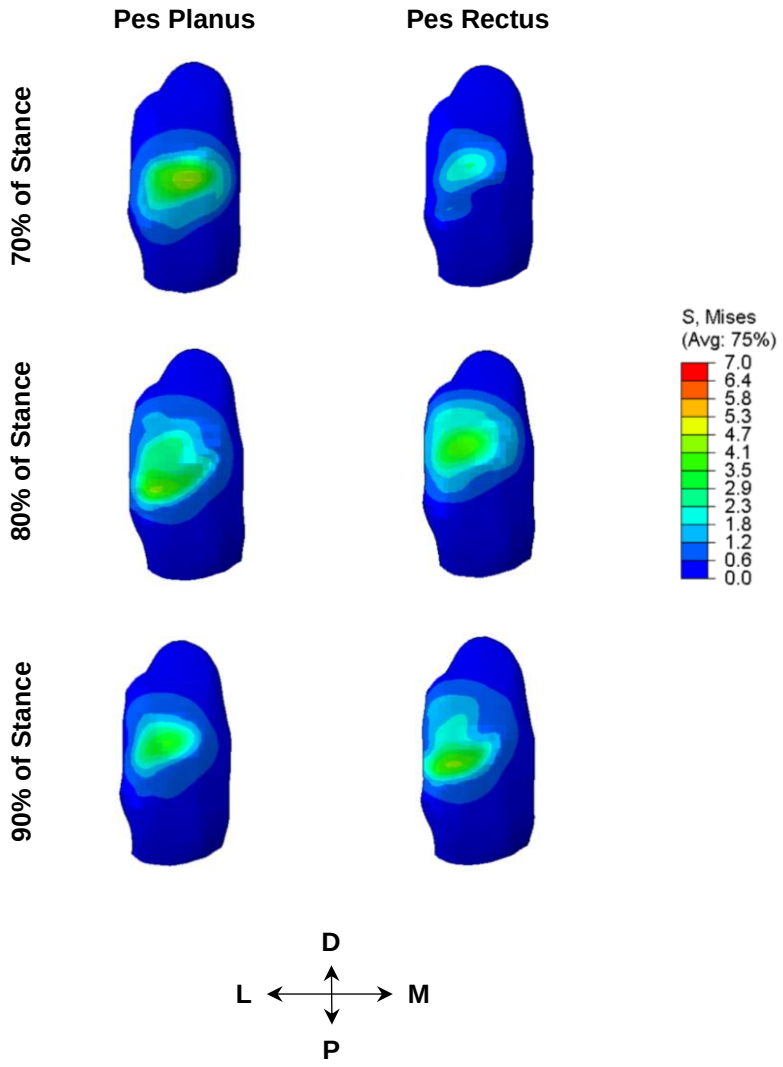

Figure D-1. von Mises stress distributions at the articular surface of the second metatarsal head. The FE images are separated by planus and rectus simulations across the late stance phase of gait.

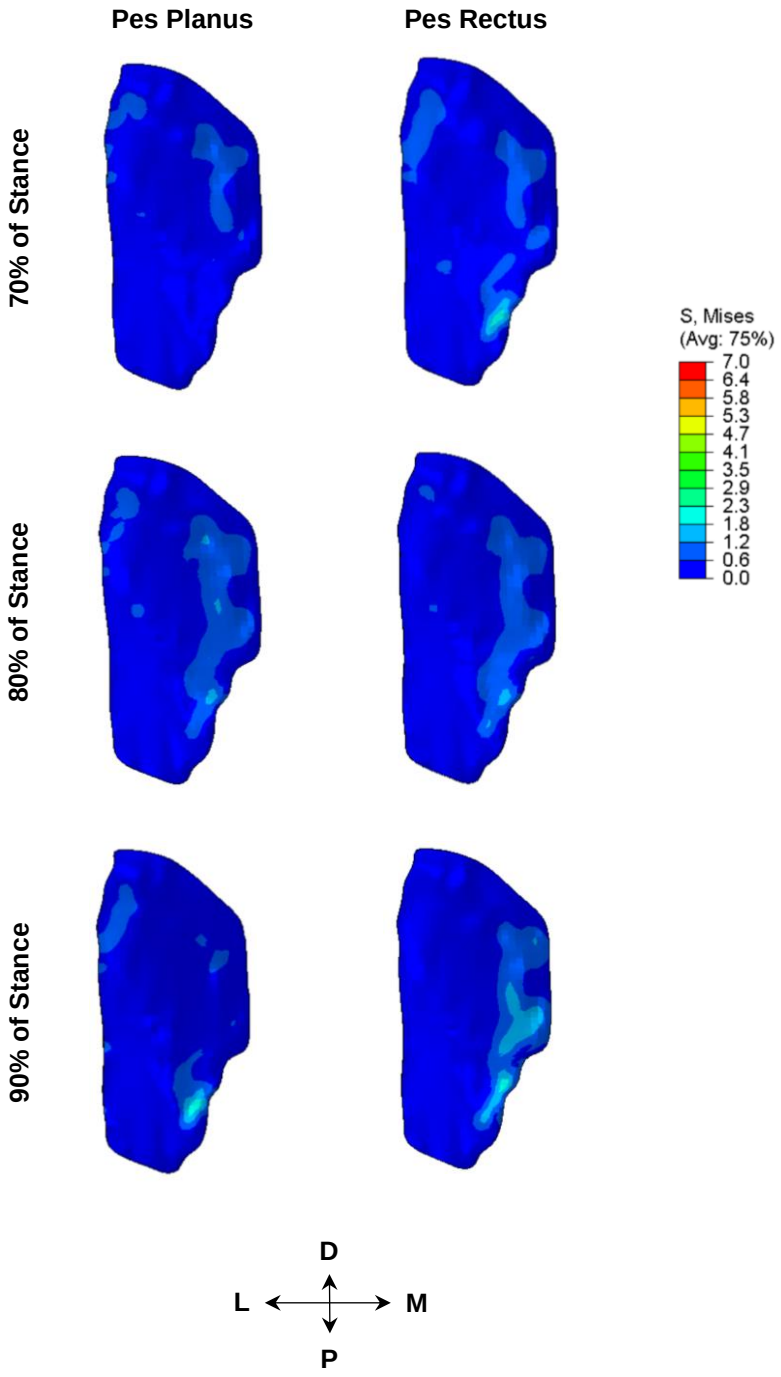

Figure D-2. von Mises stress distributions at the articular surface of the medial cuneiform. The FE images are separated by planus and rectus simulations across the late stance phase of gait.

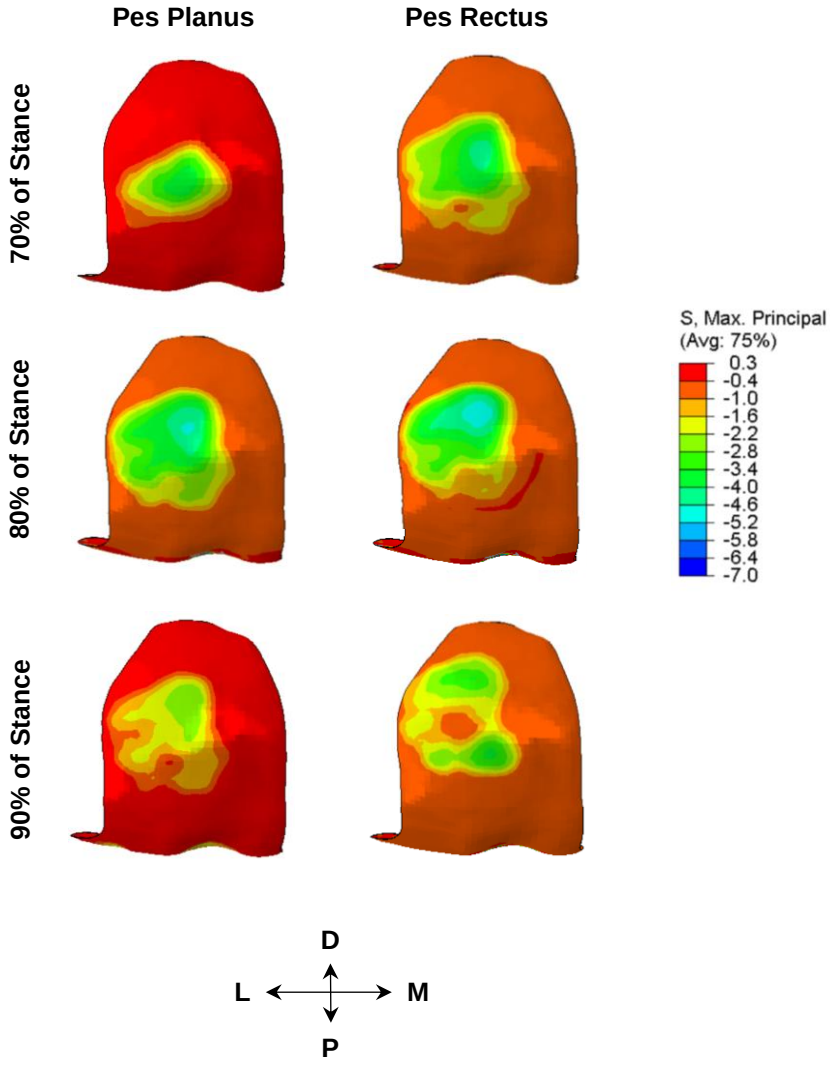

Figure D-3. Maximum principal stress distributions at the articular surface of the first metatarsal head. The FE images are separated by planus and rectus simulations across the late stance phase of gait.

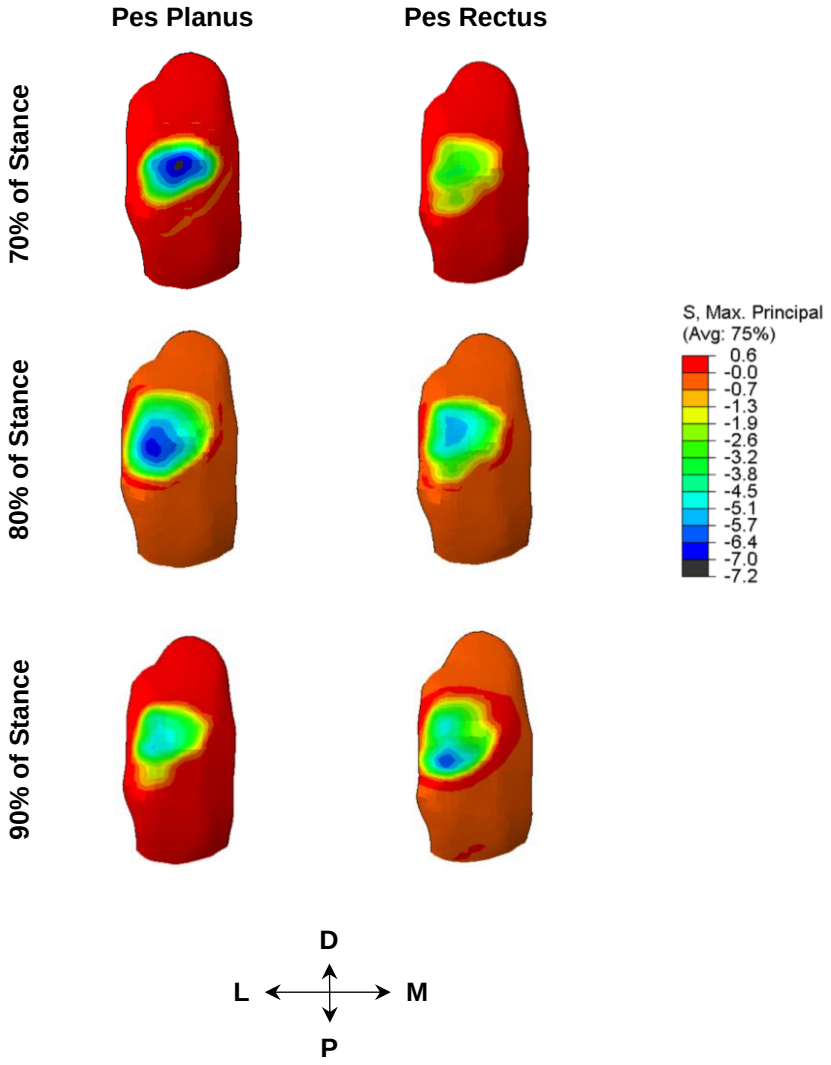

Figure D-4. Maximum principal stress distributions at the articular surface of the second metatarsal head. The FE images are separated by planus and rectus simulations across the late stance phase of gait.

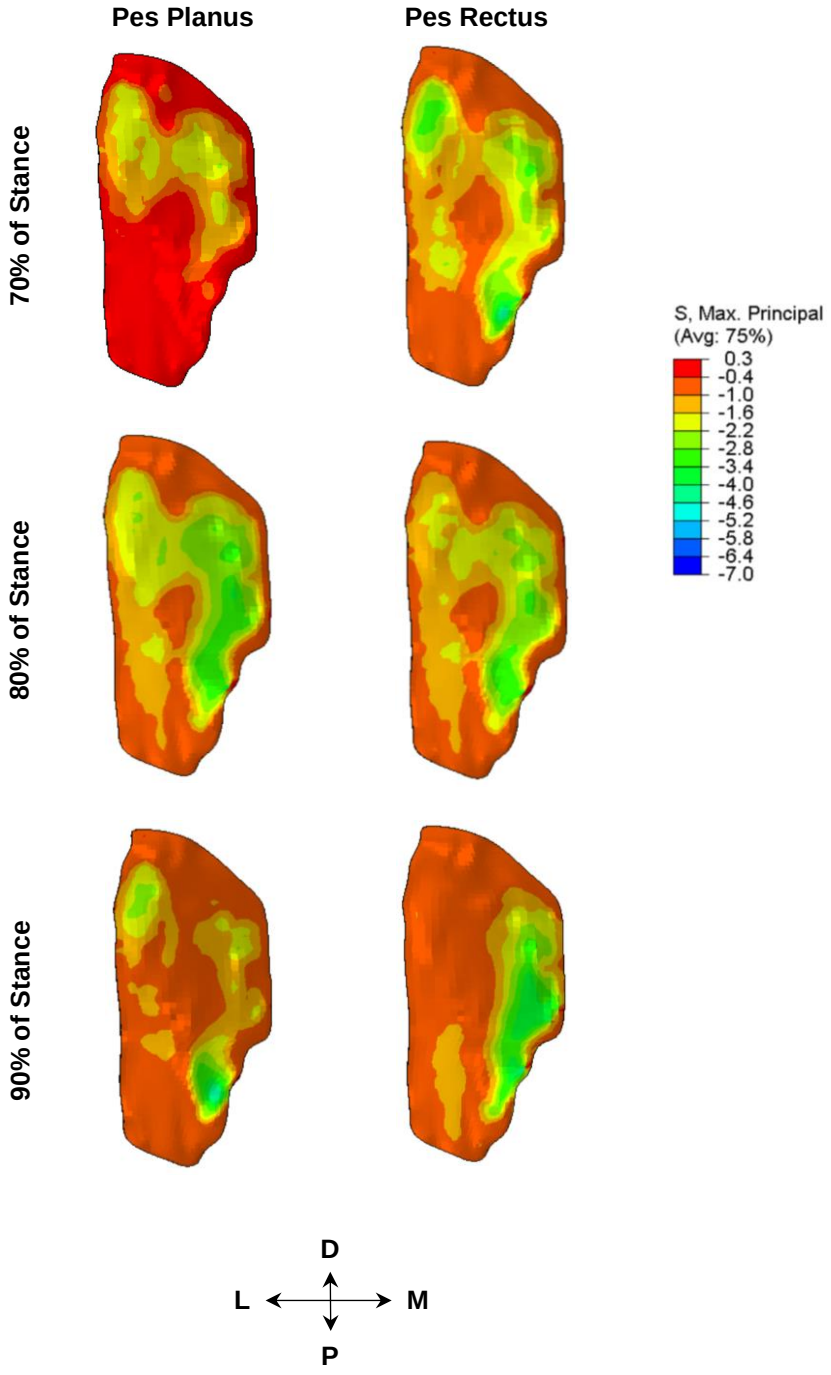

Figure D-5. Maximum principal stress distributions at the articular surface of the medial cuneiform. The FE images are separated by planus and rectus simulations across the late stance phase of gait.

Table D-1. Means and SD for contact force (N) of the first MTC, first MTP, and second MTP joints between the non-hypermobile rectus and hypermobile planus simulations. Contact forces are expressed in the three primary anatomical planes of motion.

Stance (%)	**Contact Force (N)**					
	Planus			Rectus		
	L(+)/M(-)	I(+)/S(-)	C(+)/D(-)	L(+)/M(-)	I(+)/S(-)	C(+)/D(-)
First MTC Joint						
70	-4	151	218	-6	174	254
80	-22	250	318	-21	235	257
90	-6	120	152	-32	189	157
First MTP Joint						
70	9	35	215	5	43	258
80	16	59	357	21	44	360
90	5	38	183	2	54	216
Second MTP Joint						
70	9	47	173	15	30	113
80	38	78	253	18	41	189
90	18	37	152	33	60	170

L, lateral; M, medial; I, inferior; S, superior; C, compression; D, distraction.

Table D-2. Contact area of each joint during late stance.

Stance (%)	**Contact Area (mm^2)**	
	Planus	Rectus
First MTC Joint		
70	190	188
80	223	222
90	158	115
First MTP Joint		
70	93	108
80	119	116
90	104	99
Second MTP Joint		
70	34	38
80	47	40
90	34	36

Table D-3. Peak von Mises (MPa) stress throughout late stance at the articular and osteochondral interfaces. The first MTP, MTC, and second MTP joints are shown.

	von Mises Stress (MPa)			
Stance (%)	Planus		Rectus	
	Articular	Osteochondral	Articular	Osteochondral
First MTC Joint				
70	1.3	1.6	2.4	4.2
80	1.9	2.9	1.9	2.9
90	**2.4**	**4.2**	**2.6**	**4.6**
First MTP Joint				
70	**2.4**	3.2	1.7	2.6
80	2.1	**6.5**	2.6	**4.0**
90	1.5	2.0	**2.8**	3.1
Second MTP Joint				
70	**4.8**	**6.8**	2.6	3.1
80	4.6	6.3	4.4	**6.5**
90	3.8	4.9	**4.5**	5.6

Table D-4. Peak maximum principal stress (MPa) stress throughout late stance at the articular and osteochondral interfaces. The first MTP, MTC, and second MTP joints are shown.

	Maximum Principal Stress (MPa)			
Stance (%)	Planus		Rectus	
	Articular	Osteochondral	Articular	Osteochondral
First MTC Joint				
70	-2.9	-2.2	**-4.5**	**-5.2**
80	-3.8	-3.6	-4.2	-3.5
90	**-4.9**	**-5.3**	-4.3	-4.6
First MTP Joint				
70	-3.9	-4.7	-4.0	-4.4
80	**-4.6**	**-4.9**	**-4.7**	**-5.6**
90	-2.7	-3.1	-3.3	-4.3
Second MTP Joint				
70	**-7.5**	**-9.2**	-3.8	-4.6
80	-7.1	-8.1	-5.8	-7.3
90	-5.5	-6.8	**-6.6**	**-7.9**